Investigations on Voltage Stability Assessment and FACTS Modeling Approaches

Ph.D. Thesis

PRADEEP SINGH

ID No. 2014REE9532

DEPARTMENT OF ELECTRICAL ENGINEERING

MALAVIYA NATIONAL INSTITUTE OF TECHNOLOGY JAIPUR

August 2019

Investigations on Voltage Stability Assessment and FACTS Modeling Approaches

Submitted in

fulfillment of the requirements for the degree of

Doctor of Philosophy

by

Pradeep Singh

ID: 2014REE9532

Under the Supervision of

Prof. Rajive Tiwari

DEPARTMENT OF ELECTRICAL ENGINEERING

MALAVIYA NATIONAL INSTITUTE OF TECHNOLOGY JAIPUR

August 2019

Declaration

I, **Pradeep Singh**, declare that this thesis titled, ***"Investigations on Voltage Stability Assessment and FACTS Modeling Approaches"*** and the work presented in it, are my own. I confirm that:

- This work was done wholly or mainly while in candidature for a research degree at this university.
- Where any part of this thesis has previously been submitted for a degree or any other qualification at this university or any other institution, this has been clearly stated.
- Where I have consulted the published work of others, this is always clearly attributed.
- Where I have quoted from the work of others, the source is always given. With the exception of such quotations, this thesis is entirely my own work.
- I have acknowledged all main sources of help.
- Where the thesis is based on work done by myself, jointly with others, I have made clear exactly what was done by others and what I have contributed myself.

Date:

Pradeep Singh

(2014REE9532)

Certificate

This is to certify that the thesis entitled ***"Investigations on Voltage Stability Assessment and FACTS Modeling Approaches"*** being submitted by ***Pradeep Singh (ID: 2014REE9532)*** is a bonafide research work carried out under my supervision and guidance in fulfillment of the requirement for the award of the degree of **Doctor of Philosophy** in the Department of Electrical Engineering, Malaviya National Institute of Technology, Jaipur, India. The matter embodied in this thesis is original and has not been submitted to any other University or Institute for the award of any other degree.

Prof. Rajive Tiwari

Supervisor
Department of Electrical Engineering
Malaviya National Institute of Technology Jaipur

Place: *Jaipur*

Date:

The thesis is dedicated to

My respected teachers and beloved brothers

Acknowledgements

I am indebted to all, who directly or indirectly played the role of steroids in the prolonged exercise of my agonies. This work is an outcome of evitable suffering, sacrifices and is achieved by firmness, dedication, hope, adamant nature and constant hard work. Perhaps, I may exempt myself from debt of casual readers, but those owe me .... Who support, motivate, and encourage me.

First of all, I would like to convey my heartfelt gratitude to my supervisor Professor Rajive Tiwari for his constant prudent supervision, patience and politeness during my PhD research work. His doors are always open for my interest and new ideas.

I am grateful to my DREC members, Prof. H. P. Tiwari, Dr. Nikhil Gupta, and Dr. Anil Swarnkar for their encouraging words and tremendous support during various stages of my PhD research work.

I am beholden to Prof. K. R. Niazi and Dr. Nikhil Gupta for their continuous feedback, constructive comments and prudent suggestions. Discussions with them illuminate my understanding, thoughts and vision.

My sincere thanks to Prof. Udaykumar R Yaragatti, Director, MNIT, and staff members of MNIT for providing adequate fellowship and timely laboratory facilities. My warm thanks to Prof. Rajesh Kumar, Head of the Department and Prof. Manoj Fozdar, Convener, DPGC for their continuous encouragement and motivation to maintain mental and physical fitness simultaneously.

With great pleasure, I thank to my friends at MNIT, Dr. Narayanan K., Dr. Ajeet Kumar Singh, Dr. Nand Kishor Meena, Dr. Saurabh Ratra, Dr. Sujil A., Rayees Ahmad Thokar, Abhilash Kumar Gupta, Pranda Prashnata Gupta, Jay Prakash Keshri, Sachin Sharma, and other fellow researchers for their valuable help, continuous encouragement and ambiguous jokes which made my stay enjoyable. My heartiest thanks to Dr. Ajeet Kumar Singh for his wonderful discussion on ethics, morals and values of life from dusk to dawn.

I sincerely thank Dr. Shruti Rao, Application Engineer at GE Power, New York, for suggesting appropriate materials, technical assistance and valuable remarks to my queries.

I am privileged to have stayed with my brothers, Sunny Nashier, Jitender Nashier and Vikas Nashier. I have learnt several things from them. Their continuous help and appreciation have been extremely valuable to me.

I have no words to express my gratitude to my family members. The inspiration from my father and the infinite love of my mother act as a crutch which make my walk smooth during a difficult time.

I acknowledge several friends and well-wishers, whom I haven't mentioned above and whose best wishes always encouraged me. Above all, I thank the Almighty God who is being with me and showers his blessings and benevolence towards me in all phases of my life.

Last but not the least, I am highly thankful to those who gave me the opportunity to procure a particular set of skills .... You know who you are.

(Pradeep Singh)

Abstract

During the past few decades, the demand of electrical energy is drastically increased because the electricity is the plinth of life, research, national economy, defence and industrial growth. But due to limited transmission line expansion, the power system continuously operates at highly stressed condition in the present time. This stressed condition of the modern power system can lead to poor voltage profile and voltage instability. The continuous assessment of voltage stability state of power system plays a vital role in the reliable operation as well as uninterrupted power supply. It also assists the system operator to undertake improved preventive actions before system collapse.

In the literature, various voltage stability state indicators have been developed for the assessment of the current voltage stability state to identify the weak nodes/lines and to estimate the available active/reactive power margin in the power system. Considering the approximate transmission line model and neglecting line charging capacitance; the accuracy of existing indices has been compromised in detection of voltage instability. Considering these limitations, a Distributed Parameter-based Voltage Stability Index ($DPVSI$) has been developed for assessment of voltage stability of the power system. The proposed index incorporates the effects of distributed parameters of transmission line to predict voltage collapse. The proposed index is capable to identify critical lines and reactive power margin.

Flexible control of power flow is the need of modern power system. The Flexible Alternating Current Transmission System (FACTS) devices attract the researchers due to their capability of flexible control of stressed power network. The mechanical power flow controllers are replaced by power electronics power flow controllers. The Unified Power Flow Controller (UPFC), Distributed Power Flow Controller (DPFC) and Hybrid Electromagnetic Unified Power Flow Controller (HEUPFC) are considered as most versatile power flow controllers. But these FACTS devices are not widely used in the power system due to their high cost and low reliability as compared to the rest of power flow controllers. Thus, another goal of this research work is to develop a new FACTS device which has higher reliability, low cost, and control capabilities similar to a UPFC. Therefore, a new member to FACTS family named as Amalgam Power Flow Controller (APFC) is proposed in this thesis. APFC is the amalgamation of electromagnetic and Voltage Source Converter (VSC) based devices. The key feature of the model is that it inherits the characteristics of both the devices. APFC is an economical FACTS device which not only controls power flow in a network but also increases the reliability and security of the power systems. The

viability and flexibility of APFC can be investigated using its mathematical model. The popular modeling approaches such as Voltage Source Model (VSM) and Power Injection Model (PIM) suffer from asymmetry of admittance matrix and poor convergence characteristics respectively. Also, the line current is not treated as a state variable in these modeling approaches. The line current must be considered as one of the state variables since the capability of UPFC is limited by its current constraints. Considering the merits and demerits of existing modeling approaches, this thesis proposes a new Hybrid Approach Based Modeling (HABM) technique to develop a steady-state mathematical model of APFC. Converter losses of APFC are also incorporated in mathematical modeling. The proposed APFC can regulate the bus voltage, active and reactive power flows through the transmission line simultaneously or independently to the specified values with excellent convergence characteristics.

Various line based voltage stability indices have been developed in the literature. But when the performance of line based indices is investigated under topological changes of the power system, it is observed that these indices do not identify the weak nodes of the power system. It is also found that the performance of the node based indices is unaffected by topological changes. The values of these voltage stability indices have been calculated from the power flow results obtained using traditional iterative numerical methods *e.g.* Newton-Raphson (N-R), Gauss-Seidal (GS), Fast Decoupled Load-Flow (FDLF) method *etc.* But these traditional iterative methods mainly suffer from two problems *viz.*; need of better initial conditions and poor convergence particularly when the power system is operated close to its maximum loading condition. These problems can be resolved if Holomorphic Embedding Load-Flow Method (HELM) is used for power flow calculation. The inherent properties of this method are non-iterative process and deterministic initial seeds. The incentive of this method lies in the fact that the method is guaranteed to converge, if the solution exists. In the literature of HELM, all power system buses have been modeled holomorphically. But the shunt conductance of Voltage Regulating Transformer (VRT) is neglected and shunt power injection at buses is also not included. The shunt conductance of VRT is significant and can not be neglected. So some modifications are needed to enhance its practicability. Therefore, in this research work existing Holomorphic Embedding (HE) formulation is extended to incorporate the shunt conductance of VRT and reactive power injections at the buses. The assessment of distance between the current operating state of the power system and its Saddle Node Bifurcation (SNB) point is essential for identification of the critical bus. Therefore, a new node based voltage stability index for evaluation of equivalent distance to voltage collapse has been proposed. Power flow solution obtained

from the proposed HE formulation are used to evaluate the equivalent distance from SNB point.

Convergence characteristics of the existing N-R load-flow method based FACTS devices models are affected by the choice of initial conditions. Many a time, solution is either spurious or fails to converge. To overcome the problem of convergence, HELM modeling of thyristor based FACTS controllers have been presented in the literature. But during embedding, FACTS devices are represented as a variable reactance/tap ratio, which can't represent the actual characteristics of VSC based FACTS devices. Considering the modeling of VSC based FACTS devices using HE as a new area of research, this thesis proposes HELM model of Static synchronous Compensator (STATCOM). Initial conditions of the proposed model are deterministic and therefore the solution of the model is always unique. The model always converges if solution exists. The proposed model can be operated in various control modes to regulate different parameters of the power system.

The research work in this thesis also emphasized to improve the existing optimization technique to solve formulated optimization problem of STATCOM. The existing Sine Cosine Algorithm (SCA) is modified to overcome its limitations. The multi-objective problem is formulated by considering three different techno-economic objectives of conflicting nature and converting them into single objective problem using fuzzy logic.

Contents

List of Tables

List of Figures

Nomenclature

Acronyms

AC	Alternating current
AHP	Analytic hierarchy
ALO	Ant lion optimizer
$APFC$	Amalgam power flow controller
$AVSI$	Area based voltage stability index
$BPEE$	Bus power equilibrium equation
CBM	Current based model
$CIGRE$	International Council on Large Electric Systems
CPF	Continuation power flow
CSC	Convertible static compensator
DC	Direct current
$DPFC$	Distributed power flow controller
$DPVSI$	Distributed parameter based voltage stability index
$DSSC$	Distributed static series compensator
$ENVSI$	Equivalent node voltage collapse index
ESM	Equivalent system model
$FACTS$	Flexible alternating current transmission system
$FDLF$	Fast decoupled load-flow

$FVSI$	Fast voltage stability index
GA	Genetic algorithm
GS	Gauss-Seidal
$GUPFC$	Generalized unified power flow controller
GWO	Grey wolf optimization
$HABM$	Hybrid approach based model
HE	Holomorphic embedding
$HELM$	Holomorphic embedded load-flow method
$HEUPFC$	Hybrid electromagnetic unified power flow controller
HV	High voltage
$HVDC$	High-voltage, direct current
$IEEE$	Institute of electrical ande electronics engineers
$IPFC$	Interline power flow controller
$ISCA$	Improved sine cosine Algorithm
$LCPI$	Line collapse proximity index
LLV	Lower limit violation
LV	Low voltage
$MATLAB$	Matrix laboratory
MFO	Moth-flame optimization
MLI	Maximum loadability index
$N-R$	Newton-Raphson
NA	Not applicable
$NCOSI$	Network composite overall severity index
NI	Number of iteration
$NLSI$	Novel line stability index

NP	Nose point
$NRLF$	Newton-raphson load-flow
NT	Number of terms
$OLTC$	On-load tap changing transformer
PAR	Phase angle regulator
PBE	Active power balance equation
PCP	Active power flow control constraint
PCQ	Reactive power flow control constraint
PCV	Bus voltage magnitude control constraint
PIM	Power injection model
PMU	Phasor measurement unit
POR	Line's porosity coefficient index
PSO	Particle swarm optimization
PST	Phase shifting transformer
QBE	Reactive power balance equation
RED	Relative electrical distance
$RPLI$	Reactive power loss index
$SAEP$	Self-adaptive evolutionary programming
SCA	Sine cosine Algorithm
SNB	Saddle node bifurcation
$SSSC$	Static synchronous series compensator
ST	SEN transformer
$STATCOM$	Static synchronous compensator
SVC	Static var compensation
SVD	Singular value decomposition

SVS	Synchronous voltage source
$SVSI$	Simplified voltage stability index
$TCPAR$	Thyristor controlled phase angle regulator
$TCPST$	Thyristor controlled phase shifting transformer
TCR	Thyristor controlled reactor
$TCSC$	Thyristor controlled switched capacitor
$TCVR$	Thyristor controlled voltage regulator
$TISEM$	Transfer impedance based system equivalent modal
$TPSI$	Transmission path stability index
TSC	Thyristor switched capacitor
$TSSC$	Thyristor switched series capacitor
UEP	Unstable equilibrium point
ULV	Upper limit violation
$UPFC$	Unified power flow controller
VRT	Voltage regulating transformer
VSC	Voltage source converter
VSM	Voltage source model
WOA	Whale optimization algorithm

Symbols

$\bar{\gamma}$	Propagation constant
$\bar{Y}$	Line charging admittance of the transmission line
$\bar{Z}$	Transmission line impedance
$\bar{Z}_0$	Characteristics impedance of transmission line
δ	Phase angle of bus voltage
$\eth$	Operating range of STATCOM in $MVAR$
$\Im$	Imaginary part
λ	Loading multiplier
ϕ	Phase angle of current
ψ_{SE}	Phase angle of series voltage injected by SSSC
ψ_{SH}	Phase angle of shunt voltage injected by shunt converter
ψ_T	Phase angle of series voltage injected by ST
$\Re$	Real part
θ	Impedance angle
I	Current phasor
I_{pq}	Magnitude of series line pq current
I_{SH}	Magnitude of shunt current injected by shunt converter
I_T	Magnitude of shunt current injected by ST
J	Power flow jacobian matrix
l	Length of transmission line
L_{mn}	Line stability index
L_s	Line loadability index
N	Total number of buses
n	Index number

N_A	Number of APFC connected in the system
nt	Total number of transmission line
P	Active power
P^{h3}	Active power at 3^{rd} harmonic frequency
P_{SL}	Switching loss of converter
PQ	Set of load buses
PV	Set of generator buses
Q	Reactive power
R_C^{SE}	Resistance represents switching loss across SSSC
R_C^{SH}	Resistance represents switching loss across shunt converter
S	Complex power
s	Complex-valued embedding parameter
SB	Slack bus
ST	Set of STATCOM connected buses
T	Tap setting of ST
U	Adimensional voltage
V	Magnitude of bus voltage
V^{SP}	Specified bus voltage
V_{SE}	Magnitude of series voltage injected by SSSC
V_{SH}	Magnitude of shunt voltage injected by shunt converter
V_T	Magnitude of series voltage injected by ST
Y_{SH}	Coupling admittance of shunt transformer

Chapter 1

Introduction

In last few decades, the load demand is drastically increased which led to overloading of transmission lines and transmission system is forced to operate at high stressed condition. Therefore, the power systems are more prone to voltage instability [1–4]. Excessive reactive power absorption by the load and system itself is identified as primary cause of voltage collapse. Voltage collapse is the process by which the sequence of events accompanying voltage instability leads to a blackout or abnormally low voltages in a significant part of the power system [5–12]. The voltage instability problem had got more attention during past decades due to the proliferate blackouts that occurred in some of the countries [4]. Such blackouts directly result in socio-economic deprivation. Simultaneously, the power network is continuously becoming more and more complex due to the introduction of micro-grids and various power electronic devices *etc.* Therefore, the problem related to voltage stability in a power system is one of the influential criteria in power system planning and operation.

The voltage stability analysis can be broadly classified as dynamic and static. The static voltage stability methods depend upon the steady-state model; such as power flow model or a linearized dynamic model described by the steady-state operation. The dynamic analysis implies the use of a model, characterized by non-linear differential and algebraic equations which include generators dynamics, tap changing transformers *etc.* using time-domain simulations [13–15].

In the literature significant effort has been done to develop suitable methods for assessment of voltage instability and counter measures for its mitigation. For identification of weak nodes/lines and margin available; several approaches such as Jacobian matrix based approaches [16, 17], PV and QV curves [8, 18], continuation power flow [4], node and line

based voltage stability indices [19–41], and Thevenin's equivalent based [42] *etc.* have been developed. The voltage stability indices based approaches provide fast and adequate results about the current state of the systems. From the literature survey it has been observed that most of the voltage stability indices are based upon the approximate model of transmission line where line capacitance and resistance have been neglected. In [34], the transmission line is considered as an equivalent pi-model where line parameters were assumed as lumped parameters. Prediction of the current state of a power system based on these indices is erroneous due to the assumptions considered during development of these indices. Moreover, the accurate loading margins can't be estimated by [29, 41], due to negligence of various parameters. Considering these limitations and shortcomings of the existing indices, a new voltage stability index is proposed in this thesis to accurately predict the proximity of the actual system's operating point to the point of instability.

Advances in the high power solid-state switches have led to the development of Flexible Alternating Current Transmission System (FACTS) controllers that provide capability of flexible control of stressed power network [43–68]. Various devices have been proposed and modeled by the researchers but Unified Power Flow Controller (UPFC) is the most versatile power flow controller which can simultaneously control all the parameters of the system; *i.e.* the line impedance, the transmission angle and bus voltage. But the cost of UPFC is very high owing to higher rating required for handling line voltage and line current. Another disadvantage of UPFC is that if any converter fails then it affects the whole system due to common DC-link interconnection. Therefore, to increase the reliability of the power network, Distributed Power Flow Controller (DPFC) has been developed in [46] which eliminates the common DC-link interconnection and the real power flow between the series and shunt converter is transferred through the transmission line at the third-harmonic frequency. To mitigate the cost problem, a transformer less UPFC has been presented in [69] which does not require zigzag transformer although the cost of inverter is not reduced. For the cost effective solution of power flow control, SEN Transformer (ST) has been developed by [70] which is composed of two traditional and well developed devices, *i.e.*, Phase Angle Regulator (PAR) and Voltage Regulating Transformer (VRT). The main disadvantages of the ST are slow time response and inability to generate reactive power. In [71], a Hybrid Electromagnetic Unified Power Flow Controller (HEUPFC) has been developed which is the combination of ST and UPFC. But this combination also doesn't offer higher reliability and cost effectiveness owing to problem of common DC-link interconnection and higher cost of UPFC. Considering the limitations of different FACTS devices as discussed above, there is a pressing need to develop a new FACTS device which

can increase the reliability and reduce the cost simultaneously. Therefore, research work is carried out to develop a new FACTS device which can mitigate the aforesaid problems.

The incorporation of FACTS devices in power system has numerous benefits such as improvement in voltage and transient stability *etc.* To investigate the possible benefits of a FACTS device, its mathematical model is required. In the literature, various mathematical models of the FACTS devices have been developed to investigate their capability, characteristics and effects on power system network. The existing steady-state model of the UPFC can be categorized as coupled and decoupled approach based models [66]. Decoupled approach is simple but it can only work when UPFC is used to control all three variables simultaneously, otherwise this approach fails [55]. Additionally, in this approach UPFC parameters are evaluated after the load-flow has converged, *i.e.* there is no way to know whether UPFC parameters are within range or not during iterative process [55]. Coupled approach based model can be further bifurcated into two category *i.e.* Voltage Source Model (VSM) and Power Injection Model (PIM) [57, 58, 67, 68]. VSM has good convergence property but it destroys the symmetry of admittance matrix [66]. PIM keeps the symmetry of the admittance matrix and block-diagonal property of Jacobian matrix, but has poor convergence [66]. In [65], the UPFC has been modeled as an ideal transformer and variable shunt susceptance. In [61], the UPFC is modeled as a combination of passive elements by augmenting an extra bus in the power network to reduce coding complexity. In these modeling approaches, the current is not treated as a state variable. It is convenient to consider the line current as one of the state variables because the capability of UPFC is mainly limited by current constraints. Pereira *et al.* [63] considered the current as a state variable and proved that Current Based Model (CBM) of UPFC has better convergence property as compared to PIM of UPFC especially with narrower current limit. But, the shunt element of UPFC was not modeled in [63], therefore this model does not provides valuable information about the shunt variables. In the models of FACTS devices [44–46, 53, 55, 57, 58, 61–64, 66, 67, 71, 72] developed so far, converter losses [73, 74] are not accounted. Considering merits and demerits of existing approaches to model FACTS devices, the research work is carried out to develop a new methodology to model the FACTS devices. The proposed approach inherits the benefits of both CBM and PIM based methods.

Load-flow study is a numerical technique to evaluate the steady-state numerical value of all unknown variables of the power system. It plays a vital role in the power system planning and the results obtained are used for the power system operation, protection and control [75–93]. The power system can be represented by a set of non-linear algebraic

equations. The traditional iterative numerical techniques are the core to solve these non-linear algebraic equations. Lots of iterative methods have been developed so far in the literature *e.g.*; Newton-Raphson (N-R), Gauss-Sedial (GS), Fast Decoupled Load-Flow (FDLF) method *etc.* Existing iterative methods have following drawbacks:

- They have multiple solutions of state variables and only one of them corresponds to the real operating state of the power system.
- There is no guarantee of convergence.
- Convergence characteristics depend upon the choice of initial conditions.
- May converge to a spurious solution.

Many variants of these methods and heuristic techniques have been developed to circumvent these problems but still it is not known that when the solution is not obtained by these iterative techniques then what is the pivotal reason behind that. Recently, to circumvent the aforesaid problems, a new load-flow technique known as Holomorphic Embedded Load-Flow Method (HELM) has been developed by Trias to solve the Bus Power Equilibrium Equations (BPEEs) [77]. The key advantages of HELM are the non-iterative process, deterministic initial seed, and clear indication if solution doesn't exists. The HELM converges either to a high voltage-low angle or low voltage-high angle solution depends on the formulation of BPEEs. The BPEEs are developed for high voltage-low angle because it is the feasible solution, and if the HELM is diverges it means the solution doesn't exist. Rao *et al.* [78] presented different ways to embed the BPEEs, each with distinct numerical properties and precision. The generator bus has also been modeled holomorphically in [78]. To eliminate the reactive power term of PV bus from BPEE, type-2 model of generator bus has been developed without considering the shunt conductance [80, 81]. Normally, the shunt conductance of the transmission line is negligible but when the voltage regulating transformer is represented by its pi-model in steady-state analysis, the total shunt conductance becomes significant. Therefore, the existing formulation of HELM requires suitable modifications. Considering these aspects, this thesis presents a more practical holomorphic embedded BPEEs for the ZIP type load model where shunt conductance and fixed shunt reactive power injection at the buses are properly accommodated in the power balance equations. In the voltage stability studies, non-uniform load increase in the system is more pragmatic for voltage stability assessment. Therefore, research work is carried out to develop a new HE formulation where loading of different buses are corresponding to their criticality.

The non-linear algebraic equations become more complex when FACTS devices are integrated in the power flow program. It may diverge the solution if proper initial conditions are not chosen. So far no efforts have been made to develop the models of FACTS devices which are unaffected by the choice of initial conditions. The reason may be that under normal operating conditions, the problem of convergence doesn't appear often, and even the flat profile provides a good initial solution. But the solutions may be spurious or model may not converge under heavy loading conditions. Therefore, there is a pressing need to develop a model of FACTS device which is reliable, deterministic and converges under all the operating/system conditions. The problem can be resolved if models based upon iterative methods can be redeveloped using HELM. In [92], HELM modeling of Thyristor based FACTS controllers, *i.e.* Static Var Compensator (SVC), Thyristor Controlled Switched Capacitor (TCSC), Thyristor Controlled Voltage Regulator (TCVR) and Thyristor Controlled Phase Angle Regulator (TCPAR) have been presented. In these models, FACTS devices are represented as variable reactance/tap ratio that modifies the bus power balance equations. Models presented in [92] are extension of existing holomorphic based load-flow equations with a minor change in the coefficient-matrix of linear algebraic equations. Moreover, various control modes of FACTS devices have not been explored in [92]. A variable reactance/tap ratio based model can't represent the actual characteristics of Voltage Source Converter (VSC) based FACTS devices. A voltage source converter model is quite complex which requires a large number of equations to be incorporated in load-flow, modification in coefficient-matrix and representation of different control modes *etc.* But so far HELM has not been employed to develop the models of VSC based FACTS devices. Considering the modeling of VSC based devices using HELM as a new area of research, this thesis proposes a HELM model of Static synchronous Compensator (STATCOM).

The FACTS devices have been utilized for adequate operation of existing system infrastructures by controlling the power flow over designated transmission routes. FACTS devices are also used to enhance voltage stability margin and system security. Therefore, the FACTS devices should be optimally allocated to extract the maximum possible benefits. The optimal allocation of FACTS devices can improve the power system performance in terms of better node voltage profile, reduce system losses and power flows, and better power quality and reliability of power supply [94–110]. Considering these aspects, a optimization framework is presented in this thesis to optimally allocate the FACTS devices for diversified objectives. The optimal allocation problem of FACTS devices involve the determination of its optimal number, location and size in the power system. This is a non-linear complex combinatorial optimization problem which is subjected to various equality and non-equality constraints. In the literature, various approaches have been developed to

optimally allocate the FACTS devices in power system which can be classified into three broad categories: classical optimization approaches, evolutionary computation approaches, and index based approaches. Analytical approaches fail to determine optimal solution in an efficient manner. The evolutionary and swarm optimization, *e.g.* Genetic Algorithm (GA), Particle Swarm Optimization PSO *etc.* have already proven their potential to solve highly complex engineering problems. A number of successful attempts have been made in the literature to solve the optimal allocation problem of FACTS devices. Each optimization technique has its own advantages and weaknesses in terms of computational time, accuracy and simplicity. But the challenging task is to tune the parameters which guide the algorithm to reach the solution and care should be taken to avoid a local minima and slow convergence. For an enormous large search space, these algorithms show premature convergence as they stuck into a local minima. Several researchers have made attempt to squeeze the search space by fixing or restricting the optimal candidate node location for STATCOM using indices based approaches. However, these approaches offer a rough idea about the optimal candidate node locations which can lead to a sub-optimal solution. The Sine Cosine Algorithm (SCA) has proved its potential in solving complex optimization problem but the exploration and exploitation potential of SCA needs to be enhanced. In this thesis, modifications are suggested for this algorithm to enhance its exploration and exploitation capability, and its application potential for formulated optimization problem has been explored. As the formulated optimization problem is a multi-objective optimization problem, therefore, the fuzzy approach is used to transform multiple objectives into a single objective function. Fuzzy framework [111, 112] offers a means to combine the objectives which are conflicting in nature and also ensures maximum degree of satisfaction among the different objectives.

Chapter 2

Literature Review

This chapter reviews the technical literature and it is identified that the following contents are relevant to cover the scope of the work:

- Review on voltage stability assessment
- Review on FACTS devices and their modeling approaches
- Review on holomorphic embedding approach
- Review on optimal allocation of FACTS devices

2.1 Voltage Stability

At present, the power system is highly stressed and operates near to stability limits due to enormous increase in electrical energy demand and various impediment of concomitant existing power system infrastructure. Conversely, the complexity of power system is increased due to various factors *i.e.* incorporation of various FACTS devices, interconnection of existing power systems *etc.* Therefore, it is very arduous to plan, analyze and operate the interconnected power system [2]. As the power system operates under stressed conditions, it becomes more prone to voltage instability issues [3]. Therefore, the information of current state of the power system is indispensable for its reliable and secure operation. The voltage instability problem has got more attention during past decades due to the proliferate blackouts that occurred in many countries [4, 7]. The problem related to voltage stability in a power system is one of the influential criteria in power system planning and operation.

According to IEEE/CIGRE, the power system voltage stability and its related terms can be defined as follows [1]:

"Voltage stability refers to the ability of a power system to maintain steady voltages at all buses in the system after being subjected to a disturbance from a given initial operating condition". It depends on the ability to maintain/restore equilibrium between load demand and load supply from the power system. Voltage instability may result in the form of a progressive fall or rise of voltages at some buses. A possible outcome of voltage instability is loss of load in an area, or tripping of transmission lines and other elements by their protective systems leading to cascading outages. The voltage collapse is the process by which the sequence of events accompanying voltage instability leads to a blackout or abnormally low voltages in a significant part of the power system.

The time frame of interest for voltage stability problems may vary from a few seconds to tens of minutes. Therefore, voltage stability is bifurcated in two categories such as a short-term voltage stability and a long-term voltage stability [1].

- Short-term voltage stability involves dynamics of fast acting load components such as induction motors, electronically controlled loads and HVDC converters. Its analysis requires solution of suitable system differential equations. Dynamic modeling of loads and analysis of short circuit near loads are important.
- Long-term voltage stability involves slower acting equipment such as tap-changing transformers, thermostatically controlled loads, and generator current limiters. Long-term voltage stability is determined by the resulting outage of devices. This instability mainly occurs when loads try to restore their power beyond the capability of the transmission network and connected generation.

The voltage instability arises due to insufficient reactive power support. This can be overcome considerably by proper allocation of adequate reactive power sources at appropriate locations [19]. To achieve this a robust and reliable approach is required. The voltage stability analysis can be broadly classified as dynamic and static analysis. The static voltage stability methods depend mainly on the steady state model in the analysis, such as power flow model or a linearized dynamic model described by the steady-state operation. The dynamic analysis implies the use of a model, characterized by non-linear differential and algebraic equations, which include generators dynamics, tap changing transformers *etc.* through transient stability simulations [13–15]. Dynamic analysis needs time domain simulation, which involves complex computation and large amount of computation time.

In addition to that this analysis doesn't provide degree of voltage instability. Therefore, dynamic analysis is not suitable to take corrective action for larger power system in context of online application because the system conditions vary continuously due to addition/removal of load or occurrence of contingencies. On the other hand, the static approaches are fast and provide much insight into problem of voltage stability. Static approaches can also provide the distance to voltage collapse. Therefore, this thesis addresses the static approaches for assessment of voltage stability and presents a brief literature survey on static approaches in the following sections.

2.1.1 Voltage Stability Margin Assessment

The basic concepts of the voltage stability have been presented by Kimbark [5] in his book. The relationship between load and generator terminal voltage, and reactive power is used as the voltage stability criterion. Thereafter, Venikov *et al.* [6] suggested the use of convergence and divergence property of the NRLF method to estimate the voltage stability limit. To obtain the divergence point, the loading factor is increased in finite steps till the load-flow will not diverge. But the NRLF may diverge either due to voltage instability or due to numerical problems [7]. Also, this is time consuming approach. Further, Abe [8] used sensitivity matrices to determine the voltage collapse criterion, and presented stability and controllability concepts based on PQ and PV curves. These PQ and PV curves provide useful insight into basic concept of voltage instability but these methods require large computation time as it requires repeated power flow calculations and NRLF method diverges near nose point. In [9], a continuation power flow method is presented to eliminate the divergence problem of NRLF method near maximum loading point. But this method requires large computation time, therefore, it can't be used in real time operation of power system. These problems encouraged the researchers to develop the static voltage stability indices, which are fast, reliable and quantitative measures of available voltage stability margin. These indices are used to identify critical buses, lines, available margin to voltage collapse, contingency ranking, and load shedding *etc.* Therefore, the voltage stability indices can be used as a supplementary criterion in power system planning, operation and protection. In the literature, various voltage stability indices have been proposed and can be categorized in three categories: Jacobian matrix based indices, node based voltage stability indices, and line based voltage stability indices. In Jacobian matrix based approaches; the singularity of Jacobian matrix [6], minimum singular value of Jacobian matrix [10], sign of the determinant of Jacobian matrix [6], and minimum eigen value [16] *etc.* are used as an indicator for voltage instability. The Jacobian matrix based approaches

mainly suffer from increase in computation time with increase in network size. There is numerical difficulties due to the singularity of the Jacobian matrix near the maximum loading point and it doesn't offer relative voltage stability determination. In addition to that, these indices are global voltage stability indices, therefore, they don't provide any information about point of origin of voltage instability. Therefore, it becomes difficult to take corrective action for avoiding voltage collapse. To sidestep these problems, node and line based voltage stability indices have been developed. A brief literature survey related to voltage stability indices is presented in the following sections.

2.1.1.1 Node based Voltage Stability Indices

As discussed earlier, to avoid voltage collapse, it is essential to identify the weakest bus from where voltage instability instigates. The weakest buses can be identified using node based voltage stability indices.

Lots of work have been carried out on node based voltage stability indices in the literature. *L*-index is proposed by Kessel [19], to identify the voltage weak nodes or areas. *L*-index is based on the mathematical equation of the desired node and it varies in the range of 0 (no-load) to 1 (voltage collapse). After the voltage collapse incident in Tokyo [7], it was recognised that the system load-model has influence on power system voltage stability. When all loads are assumed constant-power type load, the Nose Point (NP) and Saddle Node Bifurcation (SNB) point overlap each other. But if the loads are different from constant-power load, they don't overlap each other, and SNB point is referred as voltage collapse point. Therefore, the effect of load-model is necessary to consider for accurate prediction of system's state. During the development of *L*-index, it is assumed that all loads are constant-power type. Consequently, the *L*-index is not suitable for all types of load models. Therefore, Hongjie *et al.* [20] presented an improved voltage stability index (L_I) to account the influence of the load characteristics for accurate prediction of power system voltage instability. A new stability index (Z ratio), which is the ratio of Thevenin's impedance to load impedance is proposed by Chebbo *et al.* [42]. The Z ratio is calculated using the Thevenin's voltage and load voltage. But when the power system approaches towards instability, its sharp declining voltage level gives a high value of Z ratio. The Z ratio index provides inconsistent result because it is highly sensitive near to critical zone. Wang *et al.* [21] proposed an Equivalent Node Voltage Collapse Index (ENVCI) based on Equivalent System Model (ESM), which includes the effect of rest of the system outside the local network. The ENVCI requires only the information of local voltage phasors which can be obtained by PMU. The identification of the most dominant

generator(s) related to the weakest node(s) in the system is useful for designing an appropriate reactive power reservation strategy and taking an appropriate control to avoid system voltage collapse. Using superposition theorem, the whole network is converted into Transfer Impedance based System Equivalent Model (TISEM) in [22], to obtain the i^{th} generator contribution on k^{th} node voltage. This technique requires lesser time as compared to eigen value calculation. Moger *et al.* [23] proposed a new Reactive Power Loss Index (RPLI) for identification of weak nodes and to provide reactive power compensation devices at the suitable location in the power system for additional voltage support. Due to the incorporation of Network Composite Overall Severity Index (NCOSI) in RPLI, there is no need to load the system upto its critical loading point, *i.e.* identification of weak load buses is completely a non-iterative process. Gubina *et al.* [24] presented a Transmission Path Stability Index (TPSI) to identify the critical node and endangered transmission path. This index automatically provides the network transmission paths to the load nodes which are subjected to voltage collapse due to additional real or reactive loading. This index only requires voltage phasor values. But this index has high computational cost due to the iterative process involved in determination of paths between the generator and load under the changing operating conditions of the power system. So it is necessary to improve the path determination methodology. Therefore, a Simplified Voltage Stability Index (SVSI) is proposed in [25]. In SVSI, Relative Electrical Distance (RED) is used for path determination to avoid iterative process and correction factor (β) is used to increase sensitivity. But voltage deviation at load buses is not a reliable measure of voltage instability. Kamel *et al.* [26] proposed a new normalized voltage stability indicator (P-index) which is used to estimate voltage stability margin for load shedding purpose. This index is based on active power flow increment at a bus.

The node based voltage stability indices provide only the information of critical node or area. But many a times, the identification of critical line is necessary since the line outages are an important cause of voltage collapse. Therefore, in the literature, various line based voltage stability indices have been developed. A brief literature of line based voltage stability indices is presented in the following section.

2.1.1.2 Line based Voltage Stability Indices

In the literature, numerous line based voltage stability indices have been proposed. The main differences among them is due to different assumptions and procedures adopted during their development stages.

Lee and Jasmon [27] proposed a system stability criterion denoted as (L_{eq}) by reducing the whole network into a single line. This index provides information about the overall system stability. The key deficiency of this index is that it doesn't provide any information about the origin of voltage instability. In [28], a new line stability index (L_{ij}) is proposed which is based on the real power transfer. But during formulation stage of this index, the shunt admittances are not considered. Since only real power flow through the transmission line is not an adequate indicator to identify the voltage instability, this index is erroneous. Moghavvemi *et al.* [29] proposed voltage stability index (L_{mn}) but this index includes only the effect of reactive power flow through a transmission line. Therefore, this index is not suitable for voltage stability assessment purpose because when reactive power flow is less than or equal to zero, it indicates the respective line and thus the system is always secure at this particular situation. Also, the line resistance and charging capacitance have not been considered. Musirin *et al.* [30] presented a Fast Voltage Stability Index (FVSI). This index also suffers from same problem as L_{mn} index. Mohamed *et al.* [31] presented a line stability factor (LQP) index but the line resistance and charging capacitance have been not accounted during formulation of this index. A Novel Line Stability Index (NLSI) is presented in [32]. It is fast but suffers from same problem as LQP index. Moghavvemi and Faroque [33] used the concept of maximum power transfer through a line to predict the voltage instability of the power system and proposed two Voltage Collapse Proximity Indicators *i.e.* VCPI(power) and VCPI(loss) [33]. The point of voltage collapse is reached when both indicators are equal to unity. Rajive *et al.* [34] proposed a Line Collapse Proximity Index (LCPI) by considering the exact model of transmission line and accounting the effect of relative direction of real and reactive power flows in the transmission line.

Venkatesh *et al.* [35] proposed a Maximum Loadability Index (MLI). This index doesn't provide accurate results, if the power factor angle is nearly equal to the line impedance angle. At this condition this index loses its robustness mathematically because denominator becomes zero. Conversely, the loadability index (L_p) [36] doesn't work properly when the power factor angle is not equal to the line impedance angle. In addition to that, it can be observed that when active power flow through a transmission line is less than or equal to zero, this index becomes zero or negative, which indicates that the line is always secure. Therefore, Yu *et al.* [37] proposed an alternative line loadability index (L_s) to mitigate the problem in [35, 36] for radial distribution system. In this index, shunt admittance has been ignored. The effect of various load models on the voltage stability index (SI(m2)) is examined by Rajan and Das [38] using modified load-flow method. Ref. [38] concluded that a constant impedance load model can be used for voltage stability analysis without losing the effect of load models. A novel static voltage stability index (L_{ij}) is proposed

in [39] which is based on equilibrium solution region of branch power flow. Halilčević *et al.* [40] proposed a line's porosity coefficient index known as POR index. The main problem of this index is that its upper limit is not fixed, therefore, available loading margin can not be computed on the basis of POR index.

2.1.1.3 Critical Review on Voltage Stability Indices

From the literature survey, it has been observed that most of the voltage stability indices are based upon the approximate model of transmission line where line capacitance and resistance have been neglected. In [34], the transmission line is considered as an equivalent pi-model where line parameters were assumed as lumped parameters. Prediction of the state of a system based on these approaches was erroneous due to the assumptions considered during the development of these indices. Some indices got attention as they used only post power flow solutions, but due to some theoretical assumptions accuracy has been compromised in detection of voltage instability. A transmission system can be best represented by distributed parameters model. No efforts has been made so far to develop a voltage stability index considering distributed parameters of a transmission system. It is also observed from [34] that the voltage stability of line is affected by relative direction of active and relative power flow in the line. Therefore, the effect of the relative direction of active and reactive power flow must be considered in developing an effective index. Moreover, the accurate loading margins can't be estimated by [29, 41], due to negligence of various parameters as discussed above.

Considering these limitations and shortcomings of the existing indices, a new voltage stability index needs to be developed to accurately predict the proximity of the actual system's operating point to the point of instability. In addition to that voltage stability index must be fast, computationally efficient and capable to identify the location from where voltage instability instigates.

2.2 FACTS Devices

As discussed in Section 2.1, the power system network operates under stressed condition due to lots of constraints like economic operation, right of way, *etc.* These constraints necessitate the control of power flow through the transmission network. To achieve this, special devices are needed. The power flow controlling devices attracted the researchers

due to their capability of flexible control of stressed power network [44, 45]. In the literature, lots of power flow controlling devices have been proposed and modeled by the researchers. Advances in power flow controllers' configuration and their modeling approaches are discussed in the following sections.

2.2.1 Configuration Perspective

The power flow controllers can be broadly classified into two categories based on technology involved: mechanical and power electronics based power flow controllers. Due to slow response and non-continuous control (stepwise adjustment) of parameters, the mechanical power flow controllers have been replaced by power electronics based power flow controllers [43, 46]. The power flow controllers can also be divided into three categories based on their placement: shunt, series and combined devices. The idea behind the shunt devices is to supply/absorb reactive power locally to the load. The shunt devices can vary the bus voltage magnitude by varying their impedance. The three well known shunt devices are: switched shunt inductor/capacitor, Static Var Compensation (SVC), and Static synchronous Compensator (STATCOM). The switched shunt inductor/capacitor are mechanical power flow controllers which have only turn on and turn off facility. A SVC is a bank of Thyristor-Switched Capacitors (TSC) along-with a Thyristor-Controlled Reactor (TCR). SVC has anti-parallel thyristors in place of mechanical switches to provide fast response. SVC acts as a controllable reactor (or capacitor), and the supplied/absorbed reactive power is proportional to the square of the bus voltage magnitude. Therefore, the SVC is less effective to supply/absorb reactive power when the bus voltage is low [43]. Moreover, the injected current by SVC contains large amount of harmonics so a low-cut off frequency filter is required to improve quality of waveform [46]. STATCOM is a Voltage Source Converter (VSC) which is connected between a grid and the ground through a coupling inductance and acts as an AC voltage source. STATCOM has characteristics similar to a synchronous condenser, but it is faster and has no inertia. STATCOM is better than the SVC as it causes less harmonics and it can independently supply/absorb reactive power to bus voltage magnitude [46]. However, STATCOM is more costly and complex than the SVC due to incorporation of a VSC.

The series devices are mainly used to improve system stability and loadability of transmission network. Using these devices line impedance is varied to control the power flow through the transmission line. In the literature, various series devices have been presented; mechanical switched compensators, thyristor controlled series compensators, and VSC-based series compensators. The Thyristor Switched Series Capacitor (TSSC) is a

segment of the series capacitor bank in parallel with anti-parallel thyristors. It can rapidly add or remove the capacitor in discrete steps. As the TCSC is composed of only capacitors, it can't limit the line current [46]. Thyristor Controlled Series Capacitor (TCSC) is comprised of a series capacitor bank in parallel with a TCR to provide a smoothly variable series capacitive reactance. TCSC injects small amount of harmonics into the transmission line [46]. But the voltage injected by the TSSC and TCSC is proportional to the line current, therefore, these are not effective in case of low loading condition. The Static synchronous Series Compensator (SSSC) is a voltage source converter which is connected in series with the transmission line [43]. SSSC is better than TSSC and TCSC as it contains fewer harmonics and independently inject series voltage to line current. During both low and high load conditions, SSSC is effective. Although, SSSC and STATCOM are very much similar but SSSC is more complicated. It needs platform mounting for high-voltage isolations and complex bypass protection in case of failures [47]. The Distributed Static Series Compensator (DSSC) is a distributed SSSC, which has similar control capability as SSSC but at lower cost and higher reliability [46]. It uses larger number of VSC units with low power rating. As the VSC units in DSSC are single-phase devices, high voltage isolation is not required. Since these devices floats on the lines, additional land is not required. The redundancy of DSSC provides uninterrupted operation during a single module failure. Therefore, DSSC offers higher reliability at lower cost.

To increase the degree of freedom various combined shunt and series devices also have been proposed in the literature. The Phase Shifting Transformer (PST) is a special arrangement of transformers used to control the active power flow of transmission network. PST is the combination of shunt transformer with a tap changer and a series transformer. It injects series voltage which is obtained from the other phases of shunt transformer. PST has slow response due to inertia of mechanical tap changer. The time response can be improved by using thryrisor switches but this configuration is not widely used due to complex short circuit current protection scheme requirement. Other disadvantages of PST are frequent maintenance requirement and limited lifetime due to mechanical wear and oil deterioration. The Unified Power Flow Controller (UPFC) consists of a STATCOM and a SSSC coupled via a common DC link for bi-directional flow of active power between STATCOM and SSSC [43, 47]. Each converter can independently generate/absorb reactive power. The UPFC can control concurrently active and reactive power flow through the line. Therefore, in the literature, UPFC is considered as the most versatile power flow controller, which can simultaneously control all the parameters of the system; *i.e.* the line impedance, the transmission angle and bus voltage [53, 55]. But due to requirement of high rating VSC to handle line voltage and line current, and their protection, UPFC is very costly which limits

its practical application [46]. Another disadvantage of UPFC is that if any converter fails then it affects the whole system due to common DC-link interconnection. To mitigate the cost problem, a transformerless UPFC has been presented in [69], which does not require zigzag transformer although the cost of inverter is not reduced. The Interline Power Flow Controller (IPFC) is composed of two SSSCs in different transmission lines coupled with a common DC-link [47]. IPFC can control the power flow in multi-line of transmission network. In IPFC active power delivered to one line is taken from another line. STATCOM coupled with IPFC is called Generalized Unified Power Flow Controller (GUPFC). The Distributed Power Flow Controller (DPFC) [46] has been proposed to mitigate the high cost and reliability problem of UPFC. DPFC consists of a STATCOM and a number of DSSCs. It eliminates the common DC-link interconnection and the real power between the series and shunt converter is transferred through the transmission line at the third-harmonic frequency. But DPFC injects an extra third harmonic current in the transmission line which limits the current carrying capacity of the transmission line and increases line losses [46]. For the cost effective solution to power flow control, SEN Transformer (ST) has been developed by [70], which is composed of two traditional and well developed devices *i.e.* Phase Angle Regulator (PAR) and Voltage Regulating Transformer (VRT). The main disadvantage of the SEN transformer is that it can't generate reactive power. In [71], the Hybrid Electromagnetic Unified Power Flow Controller (HEUPFC) has been developed which is the combination of ST and UPFC. But this combination doesn't offer higher reliability and cost effectiveness owing to problem of common DC-link interconnection and higher cost of UPFC.

2.2.1.1 Critical Review on FACTS Configuration

The previous section reviewed the configuration of power flow controllers. DSSC offers high reliability at low cost, but its control capabilities are limited as it can only inject/ absorb reactive power. It is found that the combined FACTS devices offer best control capabilities. Therefore, the combined FACTS devices are the most appropriate devices for the future grids. However, their complexity and high cost restrict their use in practical power system. Ref. [71] presented a HEUPFC device, but it does not offer higher reliability and cost effectiveness owing to problem of common DC-link interconnection and higher cost of UPFC. Considering the limitations of different FACTS devices as discussed previously, there is an imperative need to develop a new FACTS device which offers controlling capability as UPFC at a lower cost and higher reliability.

2.2.2 Modeling Perspective

To investigate the effects of FACTS devices on the power network, load-flow calculations are integrated with FACTS devices. To incorporate FACTS devices in load-flow calculation, their suitable steady-state mathematical model are required, which can represent their all control capabilities without affecting the convergence property of the load-flow method. In the literature, various dynamic and steady-state mathematical models of FACTS devices have been developed to investigate their characteristics. The dynamic models of FACTS devices are beyond the scope of this research work, therefore, their dynamic models are not discussed in this section. A brief literature survey related to the steady-state modeling perspective of FACTS devices is presented below:

Noroozian *et al.* [52] modeled the UPFC as an additional complex nodal power injections at both ends of the transmission line. In this model, magnitude and angle of the series voltage source are adjusted by trial and error to achieve a power flow solution which, it is hoped, will match the target power flow. The drawback of this formulation is that the automatic UPFC parameters adjustment has not been addressed. Niaki and Irvani [53] presented the steady-state, dynamic and large signal models of UPFC, which are suitable for power-flow studies, eigen-value analysis and transient stability studies respectively. The developed steady-state model was based on the decoupled modeling approach, in which sending and receiving ends of UPFC are transformed into PQ and PV buses and then standard N-R method is used for power flow calculations. This model works well when someone desire to control voltage magnitude, real and reactive power flow simultaneously. But, if someone desire to control one or two variables, this model is no longer applicable. Another disadvantage of this model is that UPFC parameters were calculated after the load-flow has been conversed, so during the iterative process there is no way to know whether the UPFC parameters are within the limits or not. Gotham and Heydt [54] presented a model of UPFC by assuming fictitious bus to control active and reactive power flow in the transmission line. The main disadvantage of this model is that the bus voltage magnitude control flexibility has not been incorporated. Esquivel and Acha [55] suggested two UPFC's model based on voltage source modeling approach. First model is general UPFC model and in second model, shunt converter is assumed to be operated at unity power factor named as Synchronous Voltage Source (SVS) UPFC model. In [55], the control parameters are directly treated as state variables, therefore, it has a good convergence property. But the disadvantage of this approach is that augmented admittance matrix is asymmetrical and thus it can't be used in a decoupled power flow analysis. This approach requires appropriate estimation of UPFC series voltage parameters but there is

a possibility of ill conditioned Jacobian matrix. In [56], UPFC has been modeled using d-q transformation but this model is not suitable for large scale power system networks. Ref. [57] suggested that if the UPFC state-variables are corrected simultaneously along-with the nodal network state-variables to achieve the specified control target; the interaction between the network and the UPFC can be a better representation. Therefore, Ref. [57] presented a comprehensive model of UPFC by incorporating UPFC state-variables inside the Jacobian matrix and mismatch vector. But the presented model destroyed the symmetry of admittance matrix. Almoush [58] presented an exact pi-model of UPFC. In [58], the shunt and series variable voltage sources of UPFC are converted as equivalent shunt current sources. Then, the UPFC were modeled as the complex power injected by these sources with modified shunt and line admittance of transmission line. Zarghami and Crow [59] show that Power Injection Model (PIM) of UPFC provides a multiple equilibrium point, therefore, the PIM of UPFC may lead to inaccurate estimates of the stability and dynamic behavior of the system. Moreover, the PIM approach also suffers from poor convergence. Radman and Raje [60] proposed a model of UPFC by modifying the existing Jacobian matrix to investigate the effect of UPFC in the power network. However, the switching losses and thermal limits of device were not accounted in the presented model. Bhowmick *et al.* [61] introduced an indirect model of UPFC by converting 'N' bus power system along with 'p' UPFCs to an equivalent 'N+2p' bus system without UPFC to reduce the complexity of N-R method coding. Thermal limits of converters are also considered in this model. But the switching losses of VSC were neglected. Tiwari *et al.* [62] proposed a decoupled power exchange model of the UPFC with thermal limits, in which susceptance of the series transformer was used as a new state variable. But this model also did not accommodate the switching losses. Percira *et al.* [63] presented a Current Based Model (CBM) of UPFC by considering series converter current as a state-variable to improve the convergence property of the model. Current Based Model (CBM) of UPFC has better performance where current limits are narrower. Joe *et al.* [64], modeled the Convertible Static Compensator (CSC) and integrated it in N-R power flow algorithm to solve all the state-variables simultaneously. In this model, sensitivities of the control variables are calculated w.r.t the network variables, and used to control bus voltages, line flows and maximize power transfer. But sensitivity analysis approach is not suitable when the size of Jacobian matrix is larger. Therefore, Seungwon *et al.* [65] suggested the first-order sensitivity analysis approach to reduce computation, where UPFC is modeled in terms of ideal transformer with complex turns ratio and a variable shunt admittance.

2.2.2.1 Critical Review on FACTS Modeling

In the literature, various steady-state mathematical models of the UPFC have been developed which can be categorized as coupled and decoupled approach based models [66]. Decoupled approach is simple but it can only work when UPFC is used to control all three variables simultaneously, otherwise this approach fails [55]. Additionally, in this approach UPFC parameters are evaluated after the load-flow has converged, *i.e.* there is no way to know whether UPFC parameters are within range or not during iterative process [55]. Coupled approach based model can be further bifurcated into two categories *i.e.* Voltage Source Model (VSM) and Power Injection Model (PIM) [57, 58, 67, 68]. VSM has good convergence property but it destroys the symmetry of admittance matrix [66]. PIM keeps the symmetry of the admittance matrix and block diagonal property of Jacobian matrix but has poor convergence [66]. In [65], the UPFC has been modeled as ideal transformer and variable shunt susceptance. In [61], the UPFC is modeled as a combination of passive elements by augmenting an extra bus in the power network to reduce coding complexity. In these modeling approaches, the current is not treated as a state variable. It is convenient to consider the line current as one of the state variable because the capability of UPFC is mainly limited by the current constraints. Pereira *et al.* [63] considered the current as a state variable and proved that CBM of UPFC has better convergence property as compared to PIM of UPFC, especially with narrower current limit. But shunt element of UPFC was not modeled in [63], therefore this model does not provide valuable information of the shunt variables. In the model of FACTS devices [44–46, 53, 55, 57, 58, 61–64, 66, 67, 71, 72] developed so far, converter losses [73, 74] are not accounted. Considering merits and demerits of current and power injection based models, there is pressing need to develop a new approach which inherits the benefits of both CBM and PIM approach.

2.3 Power Flow Methods

The power flow calculations include the non-linear Power Balance Equations (PBEs) of the network. In the literature, various numerical techniques have been introduced to solve power flow equations. However, the pursuit to search the best method is still in process, which can handle power flow problem of all sizes and types with minimum computation efforts and has better convergence property. A brief literature survey on power flow methods of iterative and non-iterative is presented in the following section:

2.3.1 Iterative Methods to solve Power Flow Problem

The most popular iterative methods to solve power flow problems are Gauss-Seidal (GS), Newton-Raphson (N-R) and Fast Decoupled Load-Flow (FDLF) method. The GS method is the oldest method. It is simple, reliable, and usually tolerant to poor voltage conditions. It has low computer memory requirements. However, the computation time increases rapidly with increase in system size. This method has a slow convergence rate (*i.e.* linear) and exhibits convergence problems when the system is stressed due to high levels of active power transfer. N-R method has a very good convergence rate (*i.e.* quadratic). The computation time increases only linearly with system size. This method has convergence problems when the initial voltages are significantly different from their true values, it is therefore not suited for bad estimate of initial conditions. Once the voltage solution is near to the true solution, the convergence is very rapid. FDLF method is basically approximations to the N-R method. In the N-R method, Jacobian matrix is required for computing $\triangle V$ and $\triangle\theta$. Therefore, the Jacobian matrix has an impact on the convergence of the iterative solution but does not directly affect the final solution. The approximation made in the FDLF methods generally results in a small increase in the number of iterations. However, the computation effort is significantly reduced since the Jacobian matrix doesn't have to be recalculated and refactorized in each iteration. The computer memory requirements are also reduced. The convergence rate of the FDLF method is linear. The FDLF method is less sensitive to the initial voltage conditions than the N-R method. For most system conditions, the FDLF method provides rapid solution with good accuracy. However, for system conditions with very large angles across lines and with special control devices that strongly influence active and reactive power-flows, full N-R formulation may be required.

Mathematically, for an N-bus power system with one slack bus, there are upto 2^{N-1} possible voltage solutions. Out of all possible solutions, only one solution corresponds to feasible solution referred as High Voltage (HV) solution. The N-R and FDLF methods converge to the HV solution if estimated initial conditions are reasonably good. Although, several factors such as high R/X ratio, poor initial condition and operation close to maximum loading condition can lead to ill-conditioned Jacobian matrix resulting in convergence issues. Therefore, it can be concluded that the common pitfalls of iterative methods are dependency on initial estimate and problem of convergence, especially when the power system operates close to its maximum loading condition.

2.3.2 Need of Non-iterative Methods

The main objective of power flow problem is to find out the bus voltages magnitude and angles by satisfying the complex power balance equations at each bus. The solution of the power flow problem is core stage to study and investigates the planning, operation and protection of the power system. These calculations are also used in voltage stability assessment. The primary goal of voltage stability assessment is to estimate the available margin. For this, determination of Saddle Node Bifurcation (SNB) point is necessary. The three conventional iterative power flow methods work well when the power system operates near to nominal conditions. But, when the power system operates far away from its nominal voltage profile, these iterative methods are not robust. As discussed earlier, iterative methods need better initial guess of variables. Therefore, continuation method [9] is developed to find out SNB point as in this method the modified Jacobian matrix doesn't become singular near to the SNB point. But in Continuation Power Flow (CPF) method, new power flow problem has to be solved at each step, which increases its complexity as compared to N-R method. So the execution time is also increased and become more problematic when system is larger. In the literature, many modifications have been suggested to reduce computation time but still CPF suffers from dependency on estimation of initial condition.

2.3.3 Non-iterative Methods to solve Power Flow Problem

This section presents the literature survey on non-iterative methods: Series Load-Flow method [75], Homotopy Continuation method, [76] and the Holomorphic Embedded Load-Flow Method [77]. Although, the Series Load-Flow method is non-iterative in nature. But this method is also depends on initial guess because the initial operating point is evaluated through iterative process. If one continuous function can be deformed into the other one, the deformation is called a homotopy between the two functions [76]. The Homotopy Continuation method is capable to solve power flow problem even when power system is ill-conditioned. But the major disadvantage of this method is that the initial values are arbitrarily chosen. Another disadvantage is larger execution time due to computational complexity and larger storage requirement.

A new non-iterative technique is developed by Trias in [77] to solve power flow problem, which eliminates the convergence problem and the need of initial conditions estimation as in conventional iterative methods. This method clearly provide signal if solution doesn't exist. HELM also guarantees to find HV solution if solution exists [77]. Both the High

Voltage (HV) and Low Voltage (LV) solutions can be obtained through HELM that depends upon the way of BPEEs embedding. In [77], the holomorphic embedded equations have been developed only for load buses. Rao *et al.* [78] presented different ways to embed the BPEEs, each with distinct numerical properties and precision. The generator buses have been modeled holomorphically in [78]. Four different Holomorphic Embedding (HE) based methods are proposed to estimate SNB point of a power system in [79]. Moreover, the formulation which allows the user to scale load at different buses by different amounts has also been presented. The HE equation of generator bus presented in [78, 79] includes the reactive power term and it is treated as a variable in left hand side of the coefficient matrix. Subramanian *et al.* [80, 81] presented an alternative HE equation for generator bus by eliminating unknown reactive power term from the PBE of generator bus. The key disadvantage of this method is that it involves triple convolution of voltage power series in PV bus HE equation and neglects the shunt conductance term. Wallace *et al.* [82] presented a different generator bus modeling to mitigate the problem of precision due to double and triple convolution of voltage power series. Ref. [83] briefly illustrates the advantages of HELM over conventional iterative methods.

Feng and Tylavsky [84] embedded the power balance equation of load bus to calculate the Unstable Equilibrium Point (UEP) for two-bus system. The presented embedding technique guaranteed to find the UEP solution but the HE equation is developed only for load bus. The multi-bus formulation is missing, therefore, presented HE equation is not suitable for a larger system. Sarnari *et al.* [85] presented a robust Padé approximation using Singular Value Decomposition (SVD) for HELM to circumvent the degeneracy problem of voltage power series. Wang *et al.* [86] presented a multi-stage holomorphic embedding method to accurately trace the PV curve. This method reduces the round-off errors caused by the limited digits used in computation.

Baghsorkhi *et al.* [87] presented a method to embed the power flow problem with voltage magnitude constraints in the complex plane. This paper demonstrates the superiority of HELM over conventional N-R and semi-definite methods of power flow problems. The limitation of methods developed in [77–82,84,86,87] is that these are suitable only when the load/generation profile is scaled in proportion. Zhu *et al.* [88] presented a bivariate HELM to incorporate the two scaling parameters. In this method, the two scaling parameters allow the operator to scale the loads of the buses separately. Standard HE method can calculate the solutions only when the load/generation profile is scaled as a whole. Chiang *et al.* [89] proposed a Fast and Flexible Holomorphic Embedding (FFHE) method. The flexibility of this method lies in the fact that it can support any initial guess to speed

up the computation. The initial guess is obtained by GS or N-R method to reduce the number of terms which are used to obtain convergence. Liu *et al.* [90] presented a multi-dimensional holomorphic embedding method using two stage Padé approximation. The key advantage of this method is that it uses physical germ solution instead of virtual germ solution to solve power flow problem. The extension of HELM to DC based systems has been proposed and investigated by Trias in [91]. Basiri *et al.* [92] presented a HELM modeling of Thyristor–based FACTS controllers, *i.e.* Static Var Compensator (SVC), Thyristor Controlled Switched Capacitor (TCSC), Thyristor Controlled Voltage Regulator (TCVR), and Thyristor Controlled Phase Angle Regulator (TCPAR). In these models, FACTS devices are represented as a variable reactance/tap ratio that modifies the power balance equation.

2.3.4 Critical Review on Power Flow Methods

In the literature, various voltage stability indices have been developed to extract the information about the current state of the power system. The values of voltage stability indices have been calculated from the power flow results obtained from the iterative numerical methods *e.g.* N-R, FDLF *etc.* These iterative numerical methods are the core for the solution of non-linear Bus Power Equilibrium algebraic Equations (BPEEs) in the available commercial software. But these iterative methods mainly suffer from two problems *viz.* need of better initial conditions and poor convergence, particularly when power system is operated close to its maximum loading condition. The estimation of initial conditions of variables introduced becomes more complicated due to addition of FACTS devices. Moreover, the iterative methods are highly sensitive to the initial estimation. Therefore, the numerical technique to solve non-linear BPEEs is the area of interest for the researchers. A new power flow solution technique known as HELM has been developed by Trias in [77]. The inherent properties of this method are non-iterative process, deterministic initial seed and elimination of non-convergence problem (*i.e.* clear indication if solution doesn't exist). The convergence of the HELM is guaranteed if the solution exists. In [81], the shunt conductance of the transmission line has not been considered, but when the voltage regulating transformer is represented by its pi-model in steady-state analysis, the total shunt conductance becomes significant. In most of the papers [78, 79, 82, 84, 86–90, 92], the fixed shunt reactive power injection at a bus is also not considered. In [92], HELM is explored for the SVC, TCSC, TCVR and TCPAR by assuming a variable susceptance/tap ratio. But the HE equations for the FACTS devices based on voltage source converters are still not developed. Moreover, the characteristics of FACTS devices based on VSC technology

can't be accurately represented by variable susceptance/tap ratio. Also, various control modes of FACTS devices have not been explored so far. Considering the limitation of HELM, there is a need to modify the HELM and modified HELM can be used to develop the accurate model of VSC based FACTS devices.

2.4 Optimal Allocation of FACTS devices

As discussed in Section 2.1, nowadays the electrical power system is experiencing new challenges due to various Technical, Economical and Environmental (TEE) constraints, which led to stressed operating conditions. The stressed operating conditions may lead the system to voltage instability, poor voltage profile and loss of economy, if corrective control actions are not taken [19, 93]. Numerous incidents associated to voltage instability have been reported globally [7, 19, 34]. The insufficient reactive power, heavy loading on the transmission line and power shipping across long distances play a vital role in consequent blackouts and voltage collapse. The incorporation of the FACTS devices not only overcomes the aforesaid problems but also provides flexible control of the power system, *i.e.* releases the overflow through the transmission lines from prevailing overload conditions [94,97,98,106]. FACTS devices are also used to enhance voltage stability margin and the system security. As suggested in [95], the most effective use of FACTS devices depends on the location and optimal parameter setting of these devices. Therefore, the FACTS devices should be optimally allocated to extract the maximum possible benefits. The optimal allocation of FACTS devices can improve the performance of power system in terms of better node voltage profile, reduce system losses and power flows, and better power quality and reliability of power supply [98, 105, 106]. The optimal allocation problem of FACTS devices involves the determination of its optimal number, location and size in the power system. This is a non-linear complex combinatorial optimization problem which is subjected to various equality and non-equality constraints. Each device has its own advantages and limitations, and zone of application.

In literature, various techniques have been used to optimally allocate FACTS devices in transmission system which can be classified into three broad categories: classical optimization methods, evolutionary computation techniques, and index based methods. Yang *et al.* [96] used mixed-integer programming for optimal allocation of TCSC. In their work, the objective function is formulated to enhance system loadability limit, voltage profile and to minimize the investment cost. The key problems with mixed-integer programming formulation are the convexity and size, which depend upon the system parameters. Index based

methods such as sensitivity index [97], extended voltage phasors approach [98], bus participation factor [99] and residue method [100] identify the weak nodes in the system. The placement of FACTS devices at these locations benefits in terms of increased voltage stability margin, reduced losses, and optimized loading of transmission network [101, 102, 105]. Singh *et al.* [103] presented a sensitivity based approach for optimal location of TCSC and TCPAR in deregulated environment. But index based methods don't provide a true picture of whole power system, it can only offer a rough idea about the optimal candidate node location which can lead to a sub-optimal solution. Analytical methods sometimes fail to determine optimal solution in an efficient manner and also suffer from slow convergence.

On the other hand, meta-heuristic methods can determine optimal solution of complex optimization problems. Some well-established algorithms such as Genetic Algorithm (GA) [104], Particle Swarm Optimization (PSO) [105], Sparse Optimization [106], Self-adaptive Fire-Fly Algorithm [107] have been used for optimal allocation of FACTS devices. In [104], a fuzzified-GA algorithm is presented to optimally place four different types of FACTS devices. In their work, three parameters, the location, type (*i.e.* TCSC, TCPST, TCVR and SVC) and sizing of FACTS devices, are optimized by considering minimization of line loading and bus voltage deviation as an objective function. But the cost of FACTS devices are not considered. Ippolito *et al.* [108] considered TCPST for optimal allocation using GA approach. In [108], the objective function comprises of the cost of generation, installation and maintenance of TCPST; the line overload and the transmission losses. But voltage stability enhancement objective is not considered. Hao *et al.* [109] used Self-Adaptive Evolutionary Programming (SAEP) for optimal location and parameter setting of given number of UPFCs to maximize the loadability limit by satisfying the thermal and voltage limits of the power system. Huang *et al.* [110] used hybrid optimization method which constitutes of harmony search and ant algorithm for optimal power flow. The optimal locations and sizes are evaluated by considering three different objectives such as minimization of active power loss, performance index of active power flow and the voltage difference between buses. The weighting values of different objectives are selected on the basis of Analytic Hierarchy Process (AHP). Duan *et al.* [106] formulated the optimal allocation problem for SVC, TCSC, and TCPS FACTS devices and solved using sparse optimization. In practice, power systems have to achieve more than one objective. Therefore, in the literature various techno-economic objectives such as minimization of active and reactive power losses, minimization of node voltage deviation, enhancement in voltage stability margin, improvement in loadability limit, minimization of transmission line flows, minimization of investment cost, *etc.* have been considered to improve the power system performance and to defend the cost of FACTS devices. As the FACTS devices

optimal allocation problem is multi-objective optimization problem, the fuzzy approach is used to transform multiple objectives into a single objective function. Fuzzy framework [111,112] offers a means to combine the objectives which are conflicting in nature and also ensures minimum degree of satisfaction among the different objectives.

2.4.1 Critical Review on Optimal Allocation of FACTS devices

From the literature survey, it is clear that the FACTS devices should be optimally allocated to extract the maximum possible benefits. In the literature, various approaches have been proposed to optimally allocate the different FACTS devices by considering different objectives. It is also clear that to investigate the effects of FACTS devices one should needs to consider multiple objectives. Therefore, the optimal allocation of proposed FACTS device needs to be investigate by considering diverse objectives.

On the other hand, the evolutionary and swarm optimization, *e.g.* GA, PSO *etc.* have already proven their potential to solve highly complex engineering problems. A number of successful attempts have been made in the literature to solve the optimal allocation problem of FACTS devices. Each optimization technique has its own advantages and weaknesses in terms of computational time, accuracy, and simplicity. But the challenging task is to tune the parameters which guide the algorithm to reach the solution, and care should be taken to avoid a local minima and slow convergence. For an enormously large search space, these algorithms show premature convergence since they stuck into local minima. Several researchers have made attempts to squeeze the search space by fixing or restricting the optimal candidate node location for FACTS devices using indices based approaches. However, these approaches don't provide a true picture of whole power system but only offer a rough idea about the optimal candidate node location which can lead to a sub-optimal solution. The Sine Cosine Algorithm (SCA) has proved its potential in solving complex optimization problem, however the exploration and exploitation potential of SCA still needs to be enhanced. Improved SCA must be investigated to explore its potential to find optimum location of FACTS devices.

2.5 Research Objectives

In view of critical reviews, the following research objectives have been framed:

1. To develop new voltage stability indices to predict the voltage stability state of the power systems.
2. To propose a new flexible and cost effective FACTS device.
3. To develop mathematical model of the proposed FACTS device and study its impact on voltage stability.
4. To modify the standard HELM so as to incorporate the practical load models and system parameters.
5. To develop a non-iterative model of FACTS device using HELM.
6. To improve an existing optimization algorithm to solve the multiobjective FACTS allocation problem.
7. To formulate the FACTS allocation problem considering techno-economic benefits.

Chapter 3

Distributed Parameter-based Voltage Stability Index

3.1 Introduction

Currently, the demand for electric power is rapidly increasing, which requires continuous addition of new transmission lines, new components and interconnection between power systems *etc.* Therefore, monitoring, operation and control of power systems are becoming more complex. Additionally, the power system expansion is restricted by right of way and economic constraints. Consequently, to meet such enormous demand of electrical power, the power system continuously operates under stressed conditions and it becomes more prone to voltage instability issues [3]. Therefore, it is very arduous to plan, analyze and operate an interconnected power systems. The voltage instability problem has got more attention during past decades due to the proliferate blackouts that occurred in some of the countries [4, 7]. The problem related to voltage instability in a power system is one of the influential criteria in power system planning and operation [11, 22]. A number of researchers have devised various approaches for assessment of voltage instability. The indices devised from algebraic equations for voltage stability assessment got more attention due to their simple, fast and straightforward nature. These indices use the elements of the bus admittance matrix and system variables such as bus voltages, bus angles and complex power flow through transmission lines.

As discussed in Chapter 2, most of the voltage stability indices are based upon the approximate model of transmission line where line capacitance and resistance have been neglected.

In [34] the transmission line is considered as equivalent pi-model where line parameters were assumed as lumped parameters. Prediction of the current state of a power system based on these approaches was erroneous due to the assumptions considered during development of these indices. Moreover, the accurate loading margins can't be estimated by [29, 41], due to negligence of various parameters. A transmission system can be best represented by distributed parameters model. It is also observed from [34] that voltage stability of line is affected by relative direction of active and relative power flow in the line. Therefore, the effect of the relative direction of active and reactive power flow must be considered in developing an effective index. Considering the limitations and shortcomings of the existing indices, a new index is proposed in this chapter to accurately predict the proximity of the actual system's operating point to the point of voltage instability. The effectiveness of the proposed index has been tested on IEEE 30-bus and 118-bus test systems under various operating conditions and compared with existing voltage stability indices. Some of the established line voltage stability indices *viz.* L_{mn} [29], *FVSI* [41] and *POR* [40] are briefly discussed in Appendix A to enlighten the potential of proposed Distributed Parameter-based Voltage Stability Index (*DPVSI*). The following paper has been accepted from this chapter:

- Pradeep Singh and Rajive Tiwari, "Distributed Parameter-based Voltage Stability Index for Identification of Critical Lines and Voltage Stability Margin in Power System", *Cogent Engineering, Taylor & Francis*, vol. 5, no. 1, pp. 1-20, 2018.

3.2 Proposed Distributed Parameter-based Voltage Stability Index (*DPVSI*)

The indices proposed by [29, 31, 41] used the model of a medium transmission line. The line charging reactance and shunt conductance in deriving equations of indices are neglected and the parameters are assumed to be lumped by [29, 31, 41]. However, the line charging reactance may support the voltage stability of the system. In the developed indices [29, 31, 41], the effect of distributed parameters was also neglected. As a result, the methods which utilize approximate model may not provide a precise prediction of voltage stability. Consequently, a Distributed Parameter-based Voltage Stability Index based upon distributed parameters of transmission line, considering the effect of the relative direction of real and reactive power flow through the transmission line of the system has been proposed. An exact model of long length transmission line is usually described by

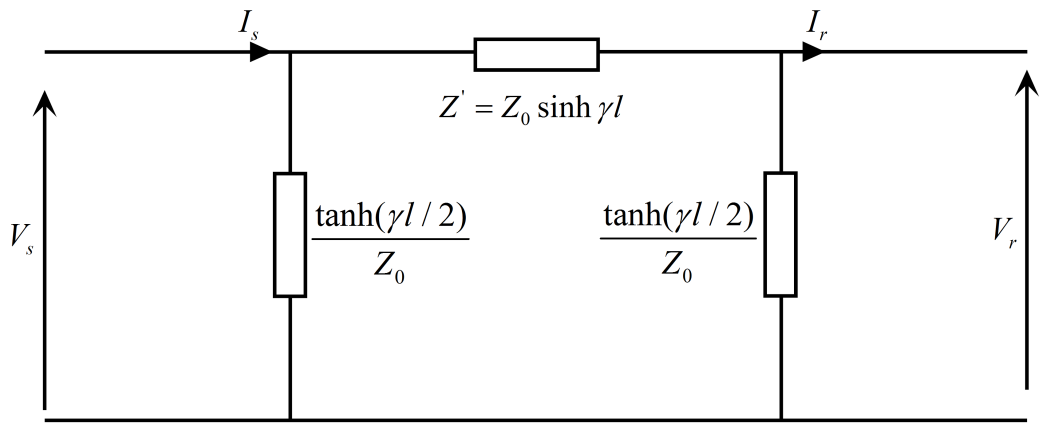

FIGURE 3.1: Typical one-line diagram of long transmission line

two-port equivalent pi-model. Therefore, the proposed index is derived using distributed parameters of pi-model of a long length transmission line. The pi-model of a long length transmission line of a two bus system is shown in Figure 3.1. The voltage and current relationship can be expressed as follows:

$$\bar{V}_s = cosh(\bar{\gamma}l)\bar{V}_r + \bar{Z}_0 sinh(\bar{\gamma}l)\bar{I}_r \tag{3.1}$$

$$\bar{I}_s = \frac{sinh(\bar{\gamma}l)}{\bar{Z}_0}\bar{V}_r + cosh(\bar{\gamma}l)\bar{I}_r \tag{3.2}$$

Where, $\bar{Z}_0$ and $\bar{\gamma}$ are known as the characteristic impedance and propagation constant respectively and they can be expressed as:

$$\bar{Z}_0 = \sqrt{\frac{\bar{Z}}{\bar{Y}}} \tag{3.3}$$

$$\bar{\gamma} = \sqrt{\bar{Z}\bar{Y}} \tag{3.4}$$

Where, $\bar{Z}$ and $\bar{Y}$ denote the impedance and line charging admittance of the transmission line respectively. The current at the receiving end of the line is expressed as:

$$\bar{I}_r = \frac{P_r - jQ_r}{\bar{V}_r^*} \tag{3.5}$$

Where, P_r, Q_r and $\bar{V}_r$ are the active power, reactive power and voltage at the receiving end respectively. The sending end voltage $\bar{V}_s$ of the line can be written from (3.1) as follows:

$$V_s\angle\delta_s = cosh(\alpha_l + j\beta_l)V_r\angle\delta_r + (Z_{0x} + jZ_{0y})sinh(\alpha_l + j\beta_l)I_r\angle 0^\circ \tag{3.6}$$

Where, δ_s is the sending end phase angle. $\sqrt{(Z_{0x}^2 + Z_{0y}^2)}$ and $\sqrt{\alpha_l^2 + \beta_l^2}$ are magnitudes while $tan^{-1}\frac{Z_{0y}}{Z_{0x}}$ and $tan^{-1}\frac{\beta_l}{\alpha_l}$ are phase angles of parameters $\bar{Z}_0$ and $\bar{\gamma}l$ respectively. Substituting, the value of $\bar{I}_r$ from (3.5) into (3.6), we get

$$V_s\angle\delta_s = cosh(\alpha_l + j\beta_l)V_r\angle\delta_r + (Z_{0x} + jZ_{0y})sinh(\alpha_l + j\beta_l)\left(\frac{P_r - jQ_r}{\bar{V}_r\angle - \delta_r}\right) \tag{3.7}$$

Rearranging (3.7), yields

$$V_sV_r\angle\delta = cosh(\alpha_l + j\beta_l)V_r^2 + (Z_{0x} + jZ_{0y})sinh(\alpha_l + j\beta_l)(P_r - jQ_r) \tag{3.8}$$

Where, $\delta = (\delta_s - \delta_r)$. Separating (3.8) into real and imaginary parts, we obtain the following quadratic equation from the real part.

$$V_r^2 - \left[\frac{V_scos\delta}{cos(\beta_l)cosh(\alpha_l)}\right]V_r + \left[H_r^{'}tanh(\alpha_l) - H_r^{''}tan(\beta_l)\right] = 0 \tag{3.9}$$

Where,

$$H_r^{'} = P_rZ_{0x} + Q_rZ_{0y}$$

$$H_r^{''} = P_rZ_{0y} - Q_rZ_{0x}$$

$$V_s^{'} = V_scos\delta/\left[2cos(\beta_l)cosh(\alpha_l)\right]$$

The roots of quadratic equation (3.9) will be

$$V_r = V_s^{'}\sqrt{\left(2V_s^{'}\right)^2 - 4\left[H_r^{'}tanh(\alpha_l) - H_r^{''}tan(\beta_l)\right]} \tag{3.10}$$

To find real and non-zero values of V_r, equation (3.10) must have real and non-zero roots, which can be obtained by setting the discriminant of (3.10) greater than zero, *i.e.*

$$\left[\frac{V_scos\delta}{cos(\beta_l)cosh(\alpha_l)}\right]^2 - 4\Big[H_r^{'}tanh(\alpha_l) - H_r^{''}tan(\beta_l)\Big] > 0 \tag{3.11}$$

On the basis of (3.11), it is concluded that the following condition must be satisfied to avoid voltage collapse of the system.

$$\frac{2\Big[H_r^{'}cos^2(\beta_l)sinh(2\alpha_l) - H_r^{''}cosh^2(\alpha_l)sin(2\beta_l)\Big]}{(V_scos\delta)^2} \leq 1 \tag{3.12}$$

DPVSI for line 'sr' can be described as:

$$DPVSI_{sr} = \frac{2}{(V_s cos\delta)^2}\Big[H_r^{'} cos^2(\beta_l) sinh(2\alpha_l) - H_r^{''} cosh^2(\alpha_l) sin(2\beta_l)\Big] \tag{3.13}$$

To maintain the voltage stability of the system the proposed index must be less than unity, *i.e.*

$$DPVSI_{sr} < 1;\ \forall\ (s,r) \in \{1,2,....nt\}\ \&\ s \neq\ r \tag{3.14}$$

Where, nt denotes the total number of transmission lines. The proposed index $DPVSI_{sr}$ has an indeterminate form when the shunt admittance is zero and the term $\frac{sinh(2\sqrt{ZY}cos\frac{\theta}{2})}{\sqrt{\bar{Y}}}$ will be equal to unity. Therefore, the $DPVSI_{sr}$ can be modified as shown in (3.15).

$$DPVSI_{sr}\ |_{Y=0} = \frac{4Z}{(V_s cos\delta)^2}\left[H_r^{+} cos\frac{\theta_+}{2} cos^2\left(\sqrt{ZY} sin\frac{\theta_+}{2}\right) - H_r^{-} sin\frac{\theta_+}{2} cosh^2\left(\sqrt{ZY} cos\frac{\theta_+}{2}\right)\right] \tag{3.15}$$

Where,

$$\theta_+ = \angle\bar{Z} + \angle\bar{Y}$$

$$\theta_- = \angle\bar{Z} - \angle\bar{Y}$$

$$H_r^{+} = P_r cos\frac{\theta_-}{2} + Q_r sin\frac{\theta_-}{2}$$

$$H_r^{-} = P_r sin\frac{\theta_-}{2} - Q_r cos\frac{\theta_-}{2}$$

$$DPVSI = \max_{(s,r)=1}^{nt}\Big(DPVSI_{sr}\Big) \tag{3.16}$$

$DPVSI_{sr}$ of all the transmission lines are computed simultaneously and voltage stability state of different lines are measured on the basis of index value. If a transmission line is at the brink of voltage instability then the value of $DPVSI_{sr}$ of the line will be close to unity. The highest value of $DPVSI_{sr}$ is denoted as $DPVSI$ which shows global voltage stability state of the system. The proposed index incorporates the effect of relative direction of active and reactive power flow in a line. If P_r and Q_r flow in the same direction, index value is high, conversely index value is low if active and reactive power flow in opposite direction. This proves that voltage stability condition of a line is a function of both magnitude and relative direction of real and reactive powers. Moreover, $DPVSI_{sr}$ is based upon distributed parameters of a long transmission line which improves the accuracy in measurement of voltage stability. In (3.13) and (3.15), the parameters α_l, β_l, Z_{0x}, and Z_{0y} are known for a given transmission network and P_r, Q_r, and δ can be obtained on-line. Therefore, the proposed index is also a valuable tool for on-line voltage stability

monitoring and prediction. The effectiveness of the proposed index has been investigated in the next section.

3.3 Test Results and Discussions

The IEEE 30-bus and 118-bus test systems are considered with the different loading combination and topology (*i.e.* contingency analysis) to appraise the potential of the proposed index. The line and bus data of both systems are taken from [114] and given in Appendix B. A MATLAB code is developed to perform the test and tolerance value of 10^{-12} is considered for mismatch of power [115]. The results are also compared with other indices *viz.* L_{mn} [29], *FVSI* [41] and *POR* [40] to prove its feasibility. The transmission lines whose *DPVSI* index are found too close to unity are denoted as critical lines.

3.3.1 IEEE 30-Bus Test System

As mentioned, the IEEE 30-bus test system [114] has been considered to examine different voltage stability indices under different loading patterns. The loading patterns considered are stated below:

- Base case loading
- Single load change
- Multiple load change

3.3.1.1 Base case loading

This loading denotes that at all the nodes, the loads are fixed at base load values. The voltage stability indices L_{mn}, *FVSI* and *POR* are evaluated and compared with proposed index *DPVSI*. Lines with smaller values of *DPVSI* are expected to have adequate stability margin, whereas larger values of *DPVSI* indicate that lines are critical and further any addition of load may lead to voltage instability. The test results are presented in Table 3.1 for base case loading of IEEE 30-bus test system. The observation of Table 3.1 reveals that for some lines the indices [29, 41] offer lower values in comparison to proposed index for branches 1-3, 6-2, 6-7 and 25-27 and for branches 6-4 and 25-24 other indices [29, 41] offer higher values in comparison to proposed index. The dissimilarity between the values

of proposed index and L_{mn} and $FVSI$ is due to the fact that index L_{mn} and $FVSI$ have neglected the effect of distributed parameters, line resistance and relative direction of active and reactive power flows. Equation (3.13) reveals that the value of proposed index is higher if the direction of active and reactive power flows are same. On the other hand, if the direction is different then the value of the index is low. It is also observed from Table 3.1, that when the resistances and shunt capacitance of branches (like 6-9, 6-10) are zero, then the value of indices L_{mn} and $DPVSI_{sr}$ are consistent with each other because the direction of active power flow relative to reactive power flow has negligible effect. The results obtained by proposed index ($DPVSI$) are in agreement with the another voltage stability assessment index POR. Therefore, the proposed index works as an unerring tool for prediction of voltage collapse under all circumstances.

TABLE 3.1: Voltage stability indices with base case loading (30-bus)

(Line) From-To	L_{mn} [29]	$FVSI$ [41]	POR [40]	Proposed Index ($DPVSI_{sr}$)
1-3	0.042173	0.038565	3.18302	0.183055
6-2	0.007918	0.007310	4.76506	0.134563
6-4	0.031247	0.030677	22.5914	0.004254
25-24	0.026763	0.026979	42.8403	0.010695
6-7	0.004654	0.004557	17.2050	0.034613
6-9	0.072628	0.072424	12.2029	0.072628
6-10	0.013675	0.013586	5.94850	0.013675
25-27	0.008401	0.008479	60.0046	0.027305
28-8	0.020420	0.020433	62.5243	0.019876

3.3.1.2 Single load change

In this case, the load has been changed at one particular node at a time and all other nodes are fixed at their base values. Various combinations are considered to accomplish this [29]:

- Single load change with real load only
- Single load change with reactive load only
- Single load change with real and reactive load

TABLE 3.2: Single load change with real load only (30-bus)

Node Loading ($p.u.$)	(Line) from-to	L_{mn} [29]	$FVSI$ [41]	POR [40]	Proposed Index ($DPVSI_{sr}$)	Proposed Index $DPVSI$	Most Stressed Line
P=6.487 at node 6	7-5	0.5902	0.4950	1.3359	0.8404	0.8404	7-5
	1-2	3.4247	1.2451	1.9011	0.7739		
	4-6	1.5040	1.0839	2.7166	0.7492		
	2-5	2.0928	1.0211	1.6931	0.7354		
	6-8	0.7333	0.6916	54.776	0.6152		
	6-9	0.5607	0.5597	64.420	0.5607		
	2-4	0.2202	0.1001	71.439	0.5453		
P=1.134 at node 27	1-3	0.3577	0.3005	1.4164	0.5779	0.5779	1-3
	25-24	0.0476	0.0332	2.4204	0.5128		
	30-27	0.2132	0.1899	2.9828	0.4182		
	24-22	0.2210	0.1988	3.4234	0.4133		
	27-28	0.3937	0.2482	3.9463	0.3937		
	2-6	0.1225	0.1033	4.0901	0.3885		

Single load change with real load only:

An exhaustive analysis is performed at all nodes and only two representative cases at nodes 6 and 27 are discussed. The voltage stability indices [29, 40, 41] and proposed index values are calculated and presented in Table 3.2. A heavy real load of value 6.487 $p.u.$ at node 6 increases the index $DPVSI$ to 0.8404. It shows that the transmission line 7-5 is the most critical line. The line 1-2 is the second most critical line. The results are confirmed by other indices but L_{mn} and $FVSI$, in some cases cross unity. On the particular occasion, the indices L_{mn} and $FVSI$ show very less value of the index for some transmission lines. Therefore, indices L_{mn} and $FVSI$ show pessimistic results. The index POR also shows that the transmission line 7-5 is the most stressed line. The heavy real load of value 1.134 $p.u.$ at node 27 makes the line 1-3 most stressed and the results are confirmed by all indices. From the test results, it may be concluded that indices [29, 41] don't provide actual assessment of voltage stability near the voltage collapse in certain cases. But the proposed index provides promising information regarding the voltage stability status of a transmission line.

Single load change with reactive load only:

In this pattern of loadability, the reactive load at a single node is increased at a time. The value of voltage stability indices increases with the increase in reactive loading. The maximum reactive loading point at any selected node is identified as the reactive load for which $DPVSI$ is close to unity. The load-flow solution will diverge for any further augmentation in loading. The results of simulation are presented in Table 3.3. A heavy reactive load of value 10.434 $p.u.$ at node 6 increases the index $DPVSI$ to 0.9821. It

TABLE 3.3: Single load change with reactive load only (30-bus)

Node Loading ($p.u$)	(Line) from-to	L_{mn} [29]	$FVSI$ [41]	POR [40]	Proposed Index ($DPVSI_{sr}$)	Proposed Index ($DPVSI$)	Most Critical Line
Q=10.434 at node 6	2-6	0.9538	0.7700	1.1747	0.9821	0.9821	2-6
	8-6	1.3357	1.0711	47.126	0.9680		
	8-28	0.9293	1.0002	1.0954	0.8842		
	4-2	0.8082	0.7263	1.3092	0.8555		
	6-9	0.7904	0.7790	24.044	0.7904		
	5-7	0.8045	0.8280	1.3784	0.7829		
	6-28	0.9534	0.8925	71.598	0.7692		
Q=2.207 at node 10	6-10	0.9993	0.9908	0.9943	0.9993	0.9993	6-10
	17-16	0.9479	0.9724	1.1999	0.9098		
	9-6	0.9005	0.8982	1.0943	0.9005		
	16-12	0.8797	0.8970	1.3296	0.8502		
	10-9	0.7585	0.7571	1.3117	0.7585		
	27-28	0.7043	0.6910	1.2311	0.7043		
	12-4	0.6816	0.6544	1.1322	0.6816		
Q=0.7129 at node 27	28-27	0.9998	0.9960	0.9973	0.9998	0.9998	28-27
	27-25	0.7845	0.8128	1.5407	0.7281		
	24-25	0.6734	0.6987	1.8398	0.6380		
	30-27	0.3057	0.2639	2.2683	0.5558		
	24-22	0.3668	0.3660	3.5034	0.3705		
	1-3	0.2334	0.2129	2.2292	0.3691		
	27-30	0.1361	0.1175	3.4573	0.3507		

shows that line 2-6 is the most critical line. The criticality of line 2-6 is confirmed by L_{mn}. For the line 8-6, the indices L_{mn} and $FVSI$ crosses unity which denotes that voltage collapse had occurred. Therefore, these indices present the erroneous prediction of voltage instability. In some cases, a difference is observed in the identification of most critical line by proposed index and other indices. This is due to fact that these indices are based upon approximation and therefore the indices values are not correct representation of actual voltage stability of line. Studies of results reveal that the proposed index provide promising information of system state during heavy reactive loading.

Single load change with real and reactive load:

In a practical electric power system, the real and reactive load change simultaneously. In this case, the real and reactive load at a particular node are varied in same proportion. The loads at all other nodes are fixed at base values. As shown in Table 3.4, when both real and reactive loads are augmented gradually at node 6 upto a level of very close to voltage collapse then it is observed that the line 5-2 is the most critical line with an index value of 0.9230. The indices L_{mn} and $FVSI$ show very less value in this case. The index POR also indicates the transmission line 5-2 as the most critical line but the value 0.8587 (for stable system $POR > 1$) indicates that the system has already collapsed, but actually the system is still voltage stable. Therefore, the index POR is also not able to represent

TABLE 3.4: Single load change with real and reactive load (30-bus)

Node Loading ($p.u$)	(Line) from-to	L_{mn} [29]	*FVSI* [41]	*POR* [40]	Proposed Index		Most Critical Line
					($DPVSI_{sr}$)	($DPVSI$)	
P=Q=4.864 at node 6	5-2	0.3501	0.1930	0.8587	0.9230	0.9230	5-2
	6-10	0.8614	0.8555	21.400	0.8614		
	8-6	1.0454	0.9351	119.78	0.8344		
	2-4	0.3832	0.2228	1.3753	0.7402		
	8-28	0.7743	0.8157	1.3473	0.7226		
	6-7	0.5247	0.5549	6.3756	0.7181		
	7-5	0.5185	0.4610	1.8496	0.6270		
	6-9	0.5843	0.5824	68.156	0.5843		
P=Q=0.524 at node 27	28-27	0.9722	0.8594	0.9547	0.9722	0.9722	28-27
	27-25	0.6440	0.5875	1.6291	0.7868		
	24-25	0.5607	0.4984	1.9913	0.6701		
	30-27	0.3646	0.3093	1.9895	0.6375		
	3-1	0.2807	0.2475	1.7913	0.4539		
	24-22	0.3353	0.3202	3.3341	0.4176		
	27-29	0.1984	0.1821	3.5581	0.3532		
	2-6	0.1503	0.1335	2.5335	0.3426		

voltage stability of the system accurately in some cases. Therefore, these indices fail to provide accurate results. Similarly, for a load P=Q=0.524 *p.u.* at node 27, the line 28-27 is the most critical line. Thus, the proposed index provides promising information regarding the voltage stability status of a transmission line.

3.3.1.3 Multiple load change

A practical electric power system consist of hundreds of nodes and loads changes simultaneously at several nodes. To prove the suitability of the proposed index, the loads are varied uniformly at all nodes upto the level of voltage instability. For the load level of 3.2 times of system's real load, the line 4-12 is the most stressed line as shown in Table 3.5.

TABLE 3.5: Multiple load change with real load only (30-bus)

Loading Multiplier ($p.u.$)	(Line) from-to	L_{mn} [29]	*FVSI* [41]	*POR* [40]	Proposed Index		Most Stressed Line
					($DPVSI_{sr}$)	($DPVSI$)	
$\lambda = 3.2$	4-12	0.7857	0.6172	1.2195	0.7857	0.7857	4-12
	29-27	0.4389	0.3615	1.6978	0.7497		
	27-30	0.0868	0.0573	2.0948	0.5720		
	10-6	0.5351	0.4600	0.9609	0.5351		
	8-28	0.5078	0.5178	2.1262	0.4809		
	30-29	0.1901	0.1621	2.5931	0.4689		
	6-8	0.5948	0.5631	47.010	0.4623		

TABLE 3.6: Multiple load change with reactive load only (30-bus)

Loading Multiplier ($p.u.$)	(Line) from-to	L_{mn} [29]	*FVSI* [41]	*POR* [40]	Proposed Index		Most Stressed Line
					($DPVSI_{sr}$)	($DPVSI$)	
	10-9	0.9318	0.9290	1.0556	0.9318	0.9318	10-9
	12-4	0.9124	0.8815	1.4378	0.9124		
	28-27	0.8486	0.8324	1.1320	0.8486		
$\lambda = 5.7$	6-10	0.7704	0.7564	1.2282	0.7704		
	25-26	0.7693	0.8445	1.6853	0.6914		
	27-29	0.6534	0.6405	1.8005	0.6857		
	12-15	0.6986	0.7045	1.7069	0.6848		

TABLE 3.7: Multiple load change with real and reactive load (30-bus)

Loading Multiplier ($p.u.$)	(Line) from-to	L_{mn} [29]	*FVSI* [41]	*POR* [40]	Proposed Index		Most Critical Line
					($DPVSI_{sr}$)	($DPVSI$)	
	29-27	0.7355	0.6135	1.3019	0.9986	0.9986	29-27
	6-2	0.4646	0.3026	2.0043	0.9821		
	4-2	0.6077	0.4762	1.1046	0.9143		
$\lambda = 2.73$	10-6	0.9140	0.8132	1.3530	0.9140		
	27-30	0.3217	0.2132	1.8339	0.7030		
	2-5	1.8444	0.9487	1.7225	0.6378		
	30-29	0.3503	0.2961	2.0029	0.6299		

It is observed from Table 3.6 that the line 10-9 is the most critical line for load level of 5.7 times of system's reactive load. Results of simulation for combined active and reactive loading are shown in Table 3.7. For the load level of 2.73 times of both real and reactive system's load, the line 29-27 is the most critical line. Index L_{mn} and *FVSI* are not able to detect the voltage collapse under this condition as their values are much less than one. The results are also supported by index *POR*. Therefore, the proposed index is a versatile index which is able to detect the voltage instability under all types of conditions.

Figures 3.2–3.4 display the variation of the voltage stability indices namely L_{mn}, *FVSI*, *POR* and *DPVSI* of the weakest node with an increase in loading factor (λ) (w.r.t. only real or only reactive or both real and reactive power loading for the constant power load model) in the IEEE 30-bus test system. It can be easily observed that when the loading is increased the value of index *POR* decline, while the values of indices L_{mn}, *FVSI* and *DPVSI* rise, and at the bifurcation point, indices approaches to unity value.

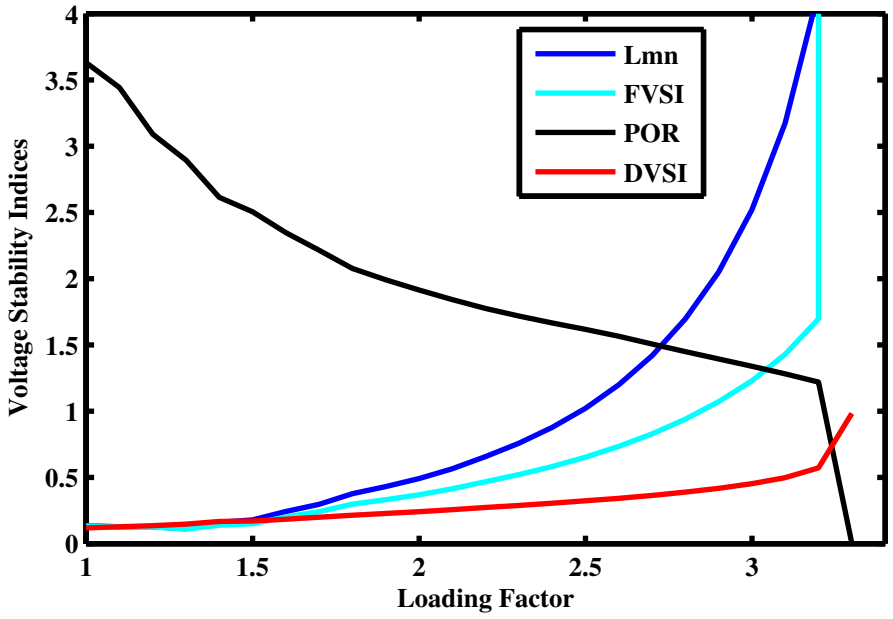

FIGURE 3.2: Variation of voltage stability indices with real load for IEEE 30-bus test system

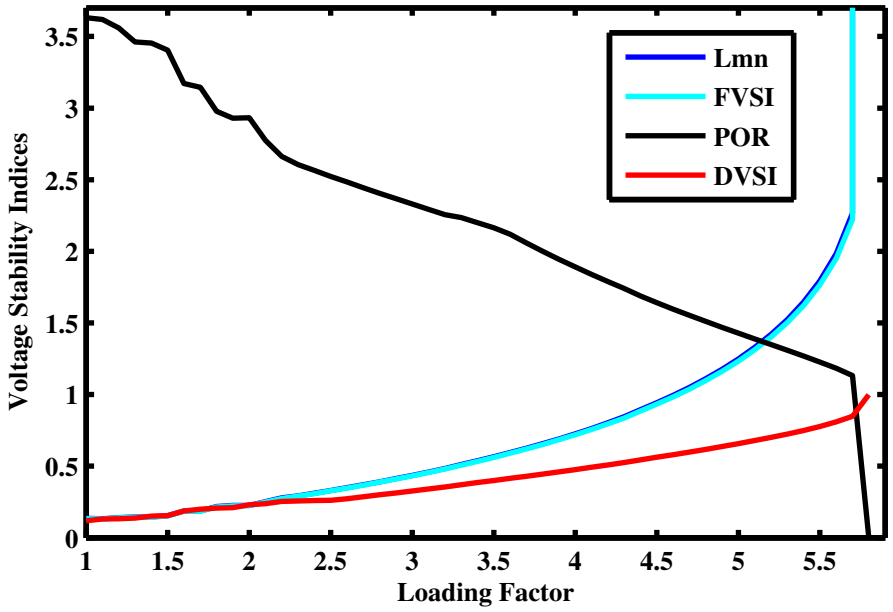

FIGURE 3.3: Variation of voltage stability indices with reactive load for IEEE 30-bus test system

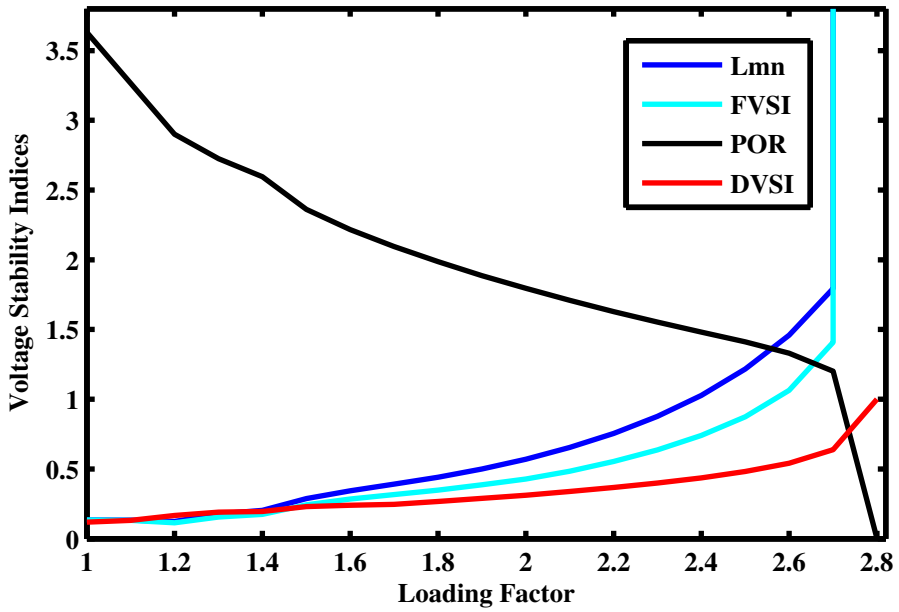

FIGURE 3.4: Variation of voltage stability indices with real and reactive load for IEEE 30-bus test system

3.3.2 IEEE 118-Bus Test System

To prove the effectiveness of the proposed index, the tests are also performed on a larger IEEE 118-bus test system for different operating conditions. The results of simulation are presented below.

3.3.2.1 Base case loading

The results of the base case are illustrated in Table 3.8. It is observed from the table that the highest value of *DPVSI* is 0.406332 for the line 27-25. The indices L_{mn} [29] and *FVSI* [41] show higher values as compared to proposed index *DPVSI* for the lines connected between nodes 80-99, 92-100, 100-101 *etc.*, where active and reactive powers flow in opposite direction. The direction of power flows is not considered in these indices and the effect of distributed parameters is also neglected. The proposed index value is almost consistent with values of other indices [29, 41] for lines 37-38, 59-63 *etc.*, where lines have zero value of line resistance and shunt admittance. The results obtained by the proposed index are also supported by the index *POR*.

TABLE 3.8: Voltage stability indices with base case loading (118-bus)

(Line) From-To	L_{mn} [29]	*FVSI* [41]	*POR* [40]	Proposed Index ($DPVSI_{sr}$)
3-5	0.059389	0.061063	7.332066	0.131312
23-32	0.021461	0.020150	5.124336	0.120560
27-25	0.246559	0.216315	1.671721	0.406332
26-30	0.132346	0.123515	2.371836	0.184164
37-38	0.166235	0.165271	3.832773	0.166235
65-38	0.259556	0.261474	7.088009	0.285923
54-49	0.176056	0.164677	3.005861	0.285942
59-63	0.107970	0.107604	5.414449	0.107970
65-66	0.103402	0.103402	9.670279	0.103402
77-80	0.056490	0.058577	8.867690	0.142908
80-99	0.179022	0.183594	4.303939	0.124007
92-100	0.228067	0.213611	7.471049	0.111095
100-101	0.132684	0.134510	6.791953	0.105017
105-107	0.079521	0.078233	9.389853	0.106616
101-102	0.055375	0.056515	7.623743	0.009725
98-100	0.093496	0.096204	4.965965	0.025887
95-96	0.079335	0.078095	61.94438	0.047679
94-96	0.082556	0.079340	13.44302	0.007748
93-94	0.087608	0.084473	15.19913	0.018233
86-85	0.040747	0.040172	34.93888	0.012463
84-83	0.137418	0.146118	5.338816	0.012638
83-82	0.064680	0.066084	9.726264	0.020119
77-82	0.174639	0.182169	4.652905	0.088191
44-45	0.024169	0.024409	19.09432	0.003487
20-21	0.024605	0.024850	16.66352	0.003640

3.3.2.2 Single load change

In this case, the load has been changed at one particular node at a time and all other loads are fixed at their base values. Literature reveals that the voltage stability is very sensitive to the flow of reactive power [2,7,19,34]. Therefore, the results for single load change with the reactive load only is illustrated in Table 3.9. The reactive load at node 28 is increased gradually upto a level of 4.128 *p.u.* where the value of proposed index *DPVSI* reaches to 0.9987 for line 27-28. Therefore, the transmission line 27-28 is the most critical line, the value of index *POR* for this case is 1.0219. Therefore, the results are supported by the index *POR*. For the same loading, both the indices L_{mn} and *FVSI* exceed unity. The load-flow solution diverged for further addition of load at node 28, which confirms that the loading is critical and very close to voltage collapse point. Near-unity value of the proposed index at the critical point confirms that it is able to detect the maximum loading point. It

TABLE 3.9: Single load change with reactive load only (118-bus)

Node Loading ($p.u$)	(Line) from-to	L_{mn} [29]	*FVSI* [41]	*POR* [40]	Proposed Index ($DPVSI_{sr}$)	Proposed Index ($DPVSI$)	Most Critical/Stressed Line
	27-28	1.0007	1.0256	1.0219	0.9987	0.9987	27-28
	29-28	1.1055	1.0287	93.728	0.9735		
	27-25	0.5883	0.5003	1.1121	0.7509		
Q=4.128 at node 28	29-31	0.7618	0.7517	160.59	0.7222		
	76-77	0.1433	0.1515	4.7472	0.3047		
	49-54	0.1851	0.1732	3.3427	0.2713		
	65-38	0.2200	0.2204	4.1726	0.2673		
	43-44	0.9446	0.9810	1.0818	0.9189	0.9189	43-44
	45-44	0.9327	0.9140	47.901	0.8891		
	49-45	0.7189	0.7442	8.6502	0.7952		
Q=1.956 at node 44	46-45	0.7264	0.7256	32.856	0.7214		
	43-34	0.6778	0.6759	1.5411	0.6766		
	27-25	0.2468	0.2164	1.6672	0.4072		
	65-38	0.2822	0.2840	6.5787	0.3112		
	100-94	1.1953	1.0700	24.028	0.9984	0.9984	100-94
	92-94	1.0010	1.0003	1.0679	0.9964		
	96-97	0.9273	0.9250	168.12	0.9183		
Q=8.688 at node 94	97-80	0.8614	0.8579	1.1913	0.8662		
	94-96	1.0437	0.9423	333.24	0.8421		
	96-80	0.8367	0.8354	1.2298	0.8322		
	94-93	0.8252	0.8290	1.2941	0.8216		

is also observed that line 29-28 connected with the same node 28 is also close to instability. The same results are obtained for other critically loaded buses where the proposed index approaches to unity while indices L_{mn} and *FVSI* exceed unity. Therefore, indices L_{mn} and *FVSI* do not provide accurate estimation of voltage stability. The difference in values of *DPVSI* is on account of distributed parameters modeling approach. In some cases, a difference is observed in the identification of most critical line by proposed index and other indices as shown in Table 3.9. This is due to fact that these indices are based upon approximation and therefore the indices values are not correct representation of actual voltage stability of line. It is observed that the proposed index provides consistent results in all the cases.

3.3.2.3 Multiple load change

In this case, the total load at each bus of a system is increased upto the level of voltage collapse. As shown in Table 3.10, for a loading factor 1.97, the index *DPVSI* of line 38-37 reaches at 0.9877, which shows that this line is in the critical state. The result is also confirmed by the other indices.

TABLE 3.10: Multiple load change with real and reactive load (118-bus)

Loading Multiplier ($p.u$)	(Line) from-to	L_{mn} [29]	*FVSI* [41]	*POR* [40]	Proposed Index ($DPVSI_{sr}$)	Proposed Index ($DPVSI$)	Most Critical Line
	38-37	0.9877	0.9533	4.7294	0.9877	0.9877	38-37
	45-46	0.5171	0.5511	4.3262	0.7645		
	49-66	0.2326	0.2326	1.3989	0.6346		
$\lambda = 1.97$	27-25	0.3253	0.2407	1.0681	0.6190		
	75-77	0.7207	0.6890	180.40	0.5991		
	30-26	0.4938	0.4379	1.1490	0.5566		
	96-80	0.3980	0.3501	1.4535	0.5494		

3.3.3 Line Reactive Power Margin Estimation

The proposed index is also capable of measuring the reactive power margin of a line. Margin of reactive power can be measured by multiplying $(1 - DPVSI)$ with maximum reactive loading. Maximum reactive loading is the permissible loading at which index reaches near unity value. Case studies for IEEE 30-bus and 118-bus test systems are presented below.

IEEE 30-Bus: To estimate the line reactive power margin, line 27-28 is chosen randomly. At the node 27, reactive load is slowly varied till maximum reactive loading. The actual reactive power margin at any point is the difference between the maximum reactive load and the reactive load at that point. The maximum possible reactive load at bus 27 is 0.72 *p.u.* The estimated reactive power margin is the multiplication of maximum reactive load and $(1 - DPVSI)$. The results are presented in Table 3.11. From the table, it is observed that for reactive load 0.5 *p.u.*, the actual reactive power margin is 0.22 *p.u.* The estimated margin is 0.25 *p.u.* which is nearly equal to actual available reactive loading margin.

TABLE 3.11: Actual vs Estimated reactive power margin of line 27-28 when reactive load at bus 27 is varied (30-bus)

$Q_{max} = 0.72$ *p.u.*			
Reactive Load at Bus 27 ($p.u.$) (A)	Proposed Index ($DPVSI$) (B)	Actual Reactive Power Margin of Line 28-27 ($p.u.$) $= Q_{max} - A$	Estimated Reactive Power Margin of Line 28-27 ($p.u.$) $= (1 - B) * Q_{max}$
0.2	0.2800	0.52	0.52
0.3	0.3912	0.42	0.44
0.4	0.5106	0.32	0.35
0.5	0.6447	0.22	0.25
0.7	0.9590	0.02	0.02

TABLE 3.12: Actual vs Estimated reactive power margin of line 117-12 when reactive load at bus 117 is varied (118-bus)

$Q_{max} = 1.53\ p.u.$			
Reactive Load at Bus 117 ($p.u.$) (A)	Proposed Index ($DPVSI$) (B)	Actual Reactive Power Margin of Line 117-12 ($p.u.$) $= Q_{max} - A$	Estimated Reactive Power Margin of Line 117-12 ($p.u.$) $= (1 - B) * Q_{max}$
1.08	0.6826	0.45	0.48
1.18	0.7433	0.35	0.39
1.28	0.8210	0.25	0.27
1.38	0.8832	0.15	0.17
1.48	0.9456	0.05	0.08

IEEE 118-Bus: To verify the consistency of results, proposed index is also tested on IEEE 118-bus test system. Here to estimate the line reactive power margin, line 117-12 is chosen randomly. At the node 117, reactive load is slowly varied until power flow diverges and *DPVSI* for line 117-12 is measured. The maximum possible reactive load at bus 117 is 1.53 *p.u.* The results are presented in Table 3.12 and from these results it is verified that proposed index is capable to measure reactive power margin.

3.3.4 Contingency Analysis

To investigate the suitability of proposed *DPVSI* index for predicting the voltage collapse during line outage of the system, single line contingency analysis is performed under base loading by removing one line at a time [12]. The proposed index *DPVSI* and other indices are calculated from the solution of power flow. The critical lines are identified on the basis of *DPVSI* value, whose outage may instigate the voltage collapse. The outage of a line from the power system, overloads other lines. The most stressed line can be identified by the maximum value of *DPVSI*. The results of contingency analysis of IEEE 30-bus test system at the base case are presented in Table 3.13. An outage of line 6-7 leads to the highest value of *DPVSI* equal to 0.4000 for branch 5-2. The results are also confirmed by the index *POR*. The indices [29,41] don't count the relative direction effect and distributed parameters effect, therefore they have shown inaccurate value. Conversely, the proposed index provides accurate results under all the conditions.

TABLE 3.13: Various contingency for IEEE 30-bus test system

(Line) From-To	L_{mn} [29]	*FVSI* [41]	*POR* [40]	Proposed Index ($DPVSI_{sr}$)	Most Stressed Line
6-7	0.1648	0.1379	1.6858	0.4000	5-2
27-29	0.1455	0.1341	4.1974	0.2957	30-27
28-27	0.1675	0.1578	4.7541	0.2784	25-24
2-5	0.0712	0.0629	2.4072	0.2538	1-3
2-4	0.0670	0.0597	2.5461	0.2393	1-3
2-6	0.0569	0.0506	2.5526	0.2325	1-3
29-30	0.0911	0.0853	5.6808	0.2148	30-27
9-10	0.0639	0.0584	3.0160	0.2058	1-3
6-9	0.0633	0.0578	3.0213	0.2051	1-3
27-30	0.0991	0.0939	6.1807	0.2004	29-27
6-28	0.0603	0.0551	3.0585	0.2011	1-3
1-3	0.0088	0.0078	2.5268	0.1997	5-2

3.4 Summary

In this chapter, a new voltage stability index namely *DPVSI* has been proposed for voltage stability assessment. This index is based on distributed parameters of the transmission line. The novelty of the index lies in the fact that it accounts the effect of distributed parameters of a transmission line as well as the magnitude and direction of active and reactive powers for assessment of voltage stability of the system. Stressed condition of a line can be monitored and reactive loading margin can be calculated online using the proposed index. Since distributed parameters model approach has been considered for developing the index, therefore it is capable of providing more promising results in comparison to other indices. The value of index reaches unity near the voltage collapse condition. The difference of index with unity indicates the loading margin. The suitability of the proposed index has been investigated and compared with other existing indices under various operating conditions on IEEE 30-bus and IEEE 118-bus test systems. The proposed index has following features:

- It is based on the distributed parameters of the transmission line and also take into accounts the effect of the relative direction of active and reactive powers flow through the transmission line. The line resistance and shunt admittance is also considered during the development stage of proposed index. Therefore, the proposed index provides more accurate and promising results.

- The proposed index is capable to indicate the local as well as global voltage stability of the power system.
- The proposed index is suitable to identify the weak lines in the power system and it can estimate the available reactive loading margin.
- Assessment of viability of new lines from voltage stability point of view at the planning stage can be done using proposed index.
- It is also suitable for online assessment of voltage stability state of power system. Therefore, it can assists the system operator to undertake improved preventive actions before system collapse.

Chapter 4

Amalgam Power Flow Controller

4.1 Introduction

As discussed in previous Chapters, the power system network operates under stressed condition due to various constraints like economic operation, right of way, *etc.* These constraints necessitate the control of power flow through transmission network. The FACTS device family attracted the researchers due to its capability of flexible control of stressed power network [44, 45]. Due to the high control capability of VSC based FACTS devices, especially UPFC, IPFC, DPFC, and HEUPFC are worthy for the future power system. But due to the high cost and proneness to failures, these devices are still not in practice. Although, a electromagnetic device *i.e.* SEN transformer provides cost effective solution but it can't generate reactive power. Therefore, there is a pressing need to develop a new FACTS device which increases the reliability and reduces the cost simultaneously. Considering the limitations of different FACTS devices as discussed in Chapter 2, this chapter proposes a new member to FACTS family, namely an Amalgam Power Flow Controller (APFC) which is more reliable and cost-effective.

FACTS devices are also very useful tool in improvement of transient stability, load sharing by parallel lines and voltage stability *etc.* Simulation studies are carried out to investigate the possible benefits. Therefore, an accurate steady-state or dynamic model is required, which can represent all the operational and functional features of the device. At the same time, model should not deteriorate the convergence characteristics of load-flow method. The well recognized modeling approaches, especially VSM and PIM for FACTS devices have their own pros and cons. VSM has good convergence property but it destroys the

symmetry of admittance matrix [66]. Although, PIM keeps the symmetry of the admittance matrix and block diagonal property of Jacobian matrix but it has poor convergence characteristics [66]. Furthermore, the current is not treated as a state variable in these modeling approaches. It is convenient to consider the line current as one of the state variables because the capability of UPFC is mainly limited by current constraints. Pereira *et al.* [63] considered the current as a state variable and proved that the Current Based Model (CBM) of UPFC has better convergence property as compared to PIM of UPFC especially with narrower current limit. But the shunt element of UPFC was not modeled in [63], therefore this model does not provide valuable information of the shunt variables. In the model of FACTS devices [44–46, 53, 55, 57, 58, 61–64, 66, 67, 71, 72, 116] developed so far, converter losses [73, 74] are also not accounted. Therefore, this chapter also focuses on the formulation of a new approach to develop a steady-state mathematical model of APFC. Considering merits and demerits of current and power injection based models, this research work utilizes the inherit benefits of two different type approaches to model the proposed APFC, which is referred as Hybrid Approach Based Model (HABM). In this approach series devices are modeled as CBM and shunt devices are modeled as PIM. The following paper has been accepted from this chapter:

- Pradeep Singh and Rajive Tiwari, "Amalgam Power Flow Controller: A Novel Flexible, Reliable, and Cost-Effective Solution to Control Power Flow", *IEEE Transactions on Power Systems*, vol. 33, no. 3, pp. 2842-2853, May 2018.

4.2 Amalgam Power Flow Controller (APFC)

The APFC circuit topology, which is composed of large capacity SEN Transformer (ST) [70] and small capacity Distributed Power Flow Controller (DPFC) [46], is shown in Figure 4.1. The basic operating principle of the ST and DPFC is well documented in the literature [46, 48, 50, 51, 70, 72]. The DPFC is composed of independent Static synchronous Compensator (STATCOM) and Static Synchronous Series Compensators (SSSC). All the converters have their own capacitors and separate DC links. The real power is exchanged between series and shunt converters through the transmission line at the 3^{rd} harmonic frequency. To circulate the real power of 3^{rd} harmonic frequency between the converters, star-delta transformers are connected at each side of the transmission line as shown in Figure 4.2. HPF is the acronym of high pass filter and it can be used to block fundamental frequency component and allows 3^{rd} harmonic component to pass, thereby providing a return path for the 3^{rd} harmonic component. Except this, the working principle of DPFC

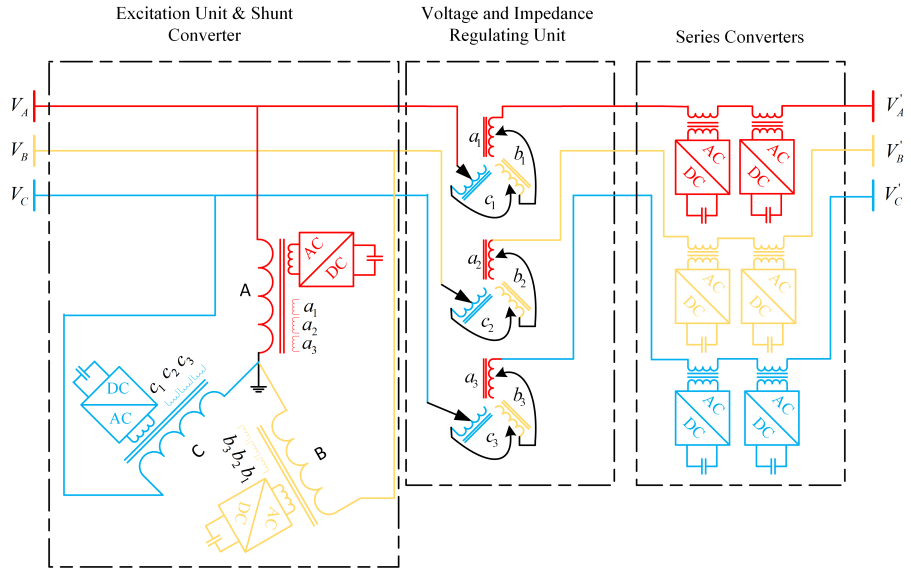

FIGURE 4.1: Proposed APFC configuration

is similar to UPFC. SEN transformer is a three-phase transformer with a star connected primary winding and nine secondary windings. The excitation winding for ST and shunt converter of DPFC is same, thereby eliminating the need of additional transformer and thus reducing the cost. The voltage and impedance-regulating unit constitute of nine secondary windings (a1, a2, and a3 on the core of A-phase; b1, b2, and b3 on the core of B-phase; c1, c2, and c3 on the core of C-phase) along-with the provision of tap changers. Therefore, the compensating voltage injected by ST in phase A, is the phasor sum of the voltages across the secondary windings a1, b1, and c1. Similarly, the voltages injected in phase B and C are also derived from all the phases. Variation in the magnitude and phase-angle of the compensating voltage can be accomplished by varying the tap-settings. The SEN transformer is composed of conventional Phase Angle Regulator (PAR) and Voltage Regulating Transformer (VRT). It can exchange both active and reactive power. As reactive power can be exchanged through series and shunt transformer of ST, the size of DC battery/capacitor required in series converter of DPFC is reduced. The single-phase schematic diagram of the proposed APFC is shown in Figure 4.2. The resistances R_{C1}^{SE}, R_{C2}^{SE}, and R_{C}^{SH} shown across the capacitors of SSSC1, SSSC2, and shunt converter are representatives of their switching losses. Equivalent circuit of APFC is shown in Figure 4.3. R_{C1}^{SEeq}, R_{C2}^{SEeq}, and R_{C}^{SHeq} in parallel with $\bar{V}_{SE1}$, $\bar{V}_{SE2}$ and $\bar{V}_{SH}$ are the equivalent effective resistances to account the switching losses of SSSC1, SSSC2, and shunt converter on the line side of the coupling transformers respectively, where $\bar{V}_{SE1} = V_{SE1}\angle\Psi_{SE1}$, $\bar{V}_{SE2} = V_{SE2}\angle\Psi_{SE2}$ and $\bar{V}_{SH} = V_{SH}\angle\Psi_{SH}$ are the voltage injected by SSSC1, SSSC2 and shunt converter respectively. The mathematical relationship between the R_{C1}^{SE} and R_{C1}^{SEeq}

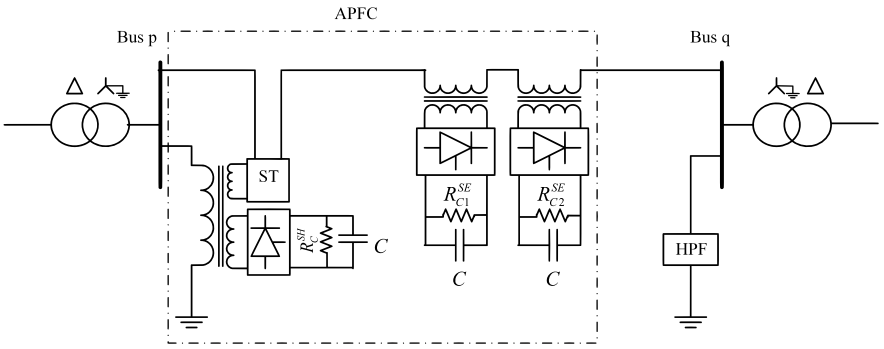

FIGURE 4.2: APFC schematic single line diagram

can be developed as follows:
As we know

$$\bar{V}_{SE1} = m_{SE1} V_{DC} \tag{4.1}$$

Where, m_{SE1} is a constant that depends on the type of the converter used. Then, the switching losses can be written as:

$$P_{SL} = \frac{V_{DC}^2}{R_{C1}^{SE}} \tag{4.2}$$

From (4.1) and (4.2), we obtain

$$P_{SL} = \frac{\bar{V}_{SE1(rms)}^2}{R_{C1}^{SEeq}}; \quad \text{Where } R_{C1}^{SEeq} = \left(\frac{R_{C1}^{SE}}{m_{SE1}^2} \right) \tag{4.3}$$

Similarly, the relationship between $R_{C2}^{SE}, R_{C2}^{SEeq}$, and R_C^{SH}, R_C^{SHeq} can be obtained.

4.3 Hybrid Approach Based Model

The proposed APFC model is an amalgamation of PIM and CBM models which is developed to inherit the merits of both the models. The proposed modeling approach is appreciated in the following sections. In the existing PIM model, the series injected voltage is selected as a state variable. One of the main restrictions of FACTS converter is imposed by its current rating. Therefore, alike CBM model, series line current is considered as state variable in place of the series injected voltage. Tap setting of SEN transformer is also proposed as a new state variable. Power flow of line is controlled by controlling the line current using SEN transformer and series elements of DPFC. On the basis of required line current, the series voltage injected in line by ST and DPFC may be computed

indirectly. The existing bus admittance matrix is modified to include the effect of SEN transformer and DPFC. All the power balance equations, power exchange equations, and control constraint equations are derived in terms of series current, phase angle of the series current, tap ratio of ST, and other existing state variables. Equations are also derived for shunt power injected by ST and shunt element of DPFC which were neglected by CBM model [63]. Converter losses are also included in the developed equations. The new entries of Jacobian matrix are developed in terms of new and existing state variables and incorporated in the existing Jacobian matrix. The detailed modeling procedure is presented in the following section:

The APFC equivalent circuit is shown in Figure 4.3 to derive the steady-state load-flow model. To develop the steady-state model of APFC, it is assumed that the power network is symmetrical and operates under 3-phase balanced condition. In hybrid approach, the current phasor is considered as a state-variable for series devices and the voltage phasor is considered as a state-variable for shunt devices. In Figure 4.3,
$\bar{V}_p = V_p \angle \delta_p$ is the voltage of bus p
$\bar{V}_k = V_k \angle \delta_k$ is the voltage of bus k
$\bar{V}_q = V_q \angle \delta_q$ is the voltage of bus q
$\bar{V}_T = V_T \angle \Psi_T$ is the series voltage injected by ST
$\bar{I}_{pq} = I_{pq} \angle \Phi_{pq}$ is the series line current
$\bar{I}_T$ is the shunt current injected by the ST
$\bar{I}_{SH}$ is the shunt current injected by the shunt converter
$\bar{Y}_{SH} = Y_{SH} \angle \theta_{SH}$ is the coupling admittance of shunt transformer

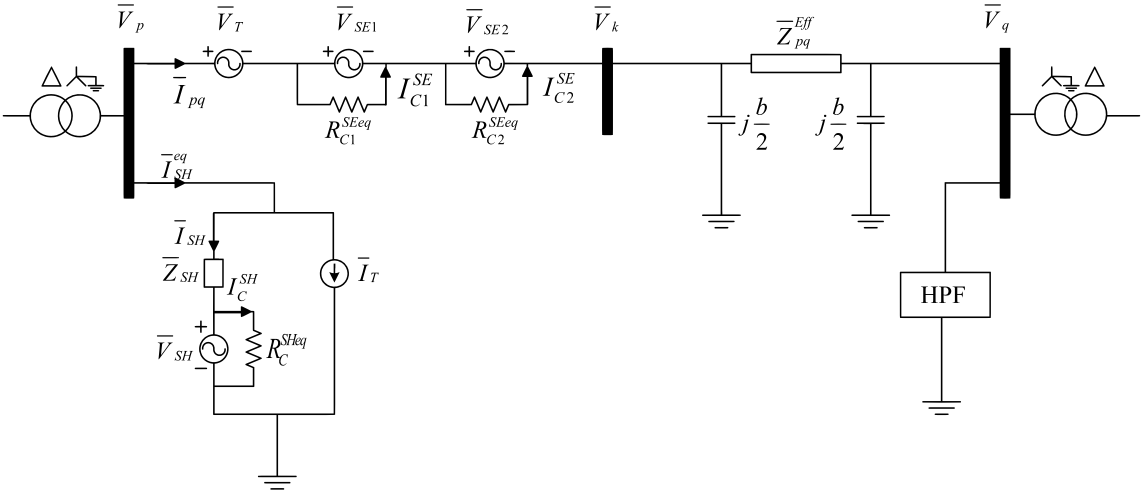

FIGURE 4.3: APFC equivalent circuit at fundamental frequency

To describe the modeling procedure, let us consider that APFC is connected between the buses p and q. The impedance of series transformers of ST, SSSC1, and SSSC2 are denoted as $\bar{Z}_T^{TF}$, $\bar{Z}_T^{SE1}$, and $\bar{Z}_T^{SE2}$ respectively. $\bar{Z}_{SH}$ denote impedance of the shunt transformer. A fictitious bus k is considered to model the APFC. The effective line impedance $\bar{Z}_{pq}^{Eff}$ is the sum of transmission line impedance and impedances of series coupling transformers; *i.e.* $\bar{Z}_{pq}^{Eff} = \bar{Z}_{pq} + \bar{Z}_T^{TF} + \bar{Z}_T^{SE1} + \bar{Z}_T^{SE2}$. The $\bar{Z}_{pq}^{Eff}$ is connected between the fictitious bus k and bus q. On the basis of Figure 4.4, new elements corresponds to bus k are added in existing bus admittance matrix and elements of bus admittance matrix corresponding to buses p and q are modified. New and modified elements of bus admittance matrix are shown by matrix Y_{Bus}^m in (4.4). Now, the admittance matrix of modified network as shown in Figure 4.4 can be calculated as:

$$Y_{Bus}^m = \begin{bmatrix} Y_{pp}^{'} & Y_{pq}^{'} & Y_{pk}^{'} \\ Y_{qp}^{'} & Y_{qq}^{'} & Y_{qk}^{'} \\ Y_{kp}^{'} & Y_{kq}^{'} & Y_{kk}^{'} \end{bmatrix} \tag{4.4}$$

$$Y_{Bus}^m \in \mathbb{R}^{(N+N_A)\times(N+N_A)} \tag{4.5}$$

Where, N_A is the number of APFC connected in the system and N is the number of existing buses. From Figure 4.4, real and reactive power injected at bus p can be obtained as:

$$P_p = P_p^m + P_p^{SE} + P_p^{SH} \tag{4.6}$$

$$Q_p = Q_p^m + Q_p^{SE} + Q_p^{SH} \tag{4.7}$$

Where, P_p^m and Q_p^m are the injected real and reactive power in the absence of APFC. P_p^{SE}, Q_p^{SE}, and P_p^{SH}, Q_p^{SH} are the injected real and reactive powers by series and shunt devices respectively.

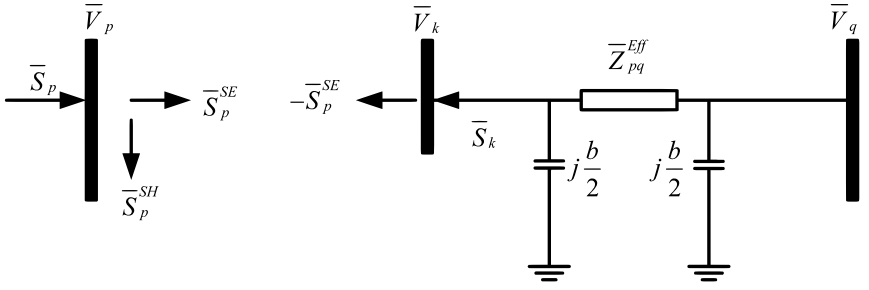

FIGURE 4.4: Injected complex power at buses with inclusion of APFC

4.3.1 Complex Power Injected by Series Current

The supplementary series complex powers $\bar{S}_p^{SE}$ and $\bar{S}_k^{SE}$, due to current $\bar{I}_{pq}$ can be obtained from Figure 4.4. According to network theory principle, the supplementary complex power $\bar{S}_p^{SE}$ can be written as:

$$\bar{S}_p^{SE} = \bar{V}_p \bar{I}_{pq}^* \tag{4.8}$$

The injected real and reactive power at bus p can be expressed in terms of two new state variables; *i.e.* magnitude of series current I_{pq} and its phase angle Φ_{pq} in following way:

$$P_p^{SE} = V_p I_{pq} cos(\delta_p - \Phi_{pq}) \tag{4.9}$$

$$Q_p^{SE} = V_p I_{pq} sin(\delta_p - \Phi_{pq}) \tag{4.10}$$

Similarly, for the bus k the injected complex power can be written as:

$$\bar{S}_k^{SE} = -\bar{V}_k \bar{I}_{pq}^* \tag{4.11}$$

The injected real and reactive power at bus k can also be expressed in terms of new state variables as shown in (4.12) and (4.13) respectively.

$$P_k^{SE} = -V_k I_{pq} cos(\delta_k - \Phi_{pq}) \tag{4.12}$$

$$Q_k^{SE} = -V_k I_{pq} sin(\delta_k - \Phi_{pq}) \tag{4.13}$$

4.3.2 Complex Power Injected by Shunt Current

The supplementary shunt complex powers $\bar{S}_p^{SH}$ due to current $\bar{I}_{SH}^{eq}$, can be expressed as:

$$\bar{S}_p^{SH} = \bar{V}_p \bar{I}_{SH}^{eq*} \tag{4.14}$$

From Figure 4.3, we have

$$\bar{S}_p^{SH} = \bar{V}_p (\bar{I}_T + \bar{I}_{SH})^* \tag{4.15}$$

Putting the value of $\bar{I}_T$ and $\bar{I}_{SH}$

$$\bar{S}_p^{SH} = \bar{V}_p \left[\frac{\bar{V}_T}{\bar{V}_p} \bar{I}_{pq} \right]^* + \bar{V}_p \left[\frac{\bar{V}_p - \bar{V}_{SH}}{\bar{Z}_{SH}} \right]^* \tag{4.16}$$

Where,

$$\bar{V}_T = \bar{T}V_p \tag{4.17}$$

$$\bar{T} = T_A + \alpha^2 T_B + \alpha T_C \tag{4.18}$$

Where, T_A, T_B, and T_C are the tap setting of the ST on secondary side of phase A, B, and C respectively. By rearranging (4.16), we obtain

$$\bar{S}_p^{SH} = TV_pI_{pq}\angle(2\delta_p - \Psi_T - \Phi_{pq}) + V_p^2 Y_{SH}\angle(-\Theta_{SH}) - V_pV_{SH}Y_{SH}\angle(\delta_p - \Phi_{SH} - \Theta_{SH}) \tag{4.19}$$

Separating (4.19) into real and imaginary parts, we obtain

$$\bar{P}_p^{SH} = TV_pI_{pq}cos(2\delta_p - \Psi_T - \Phi_{pq}) + V_p^2 Y_{SH}cos\Theta_{SH} - V_pV_{SH}Y_{SH}cos(\delta_p - \Phi_{SH} - \Theta_{SH}) \tag{4.20}$$

$$\bar{Q}_p^{SH} = TV_pI_{pq}sin(2\delta_p - \Psi_T - \Phi_{pq}) - V_p^2 Y_{SH}sin\Theta_{SH} - V_pV_{SH}Y_{SH}sin(\delta_p - \Phi_{SH} - \Theta_{SH}) \tag{4.21}$$

4.3.3 Series Voltage Equation

Due to the consideration of series current as a state-variable, the injected series voltages must be incorporated inside the Jacobian matrix. The voltage equation between the bus p and k can be written as:

$$\bar{V}_k - \bar{V}_p = -(\bar{V}_T + \bar{V}_{SE1} + \bar{V}_{SE2}) \tag{4.22}$$

We know,

$$\begin{aligned} \bar{V}_T &= TV_p\angle\Psi_T \\ \bar{V}_{SE1} &= r_1^{SE}V_p\angle\Psi_{SE1} \\ \bar{V}_{SE2} &= r_2^{SE}V_p\angle\Psi_{SE2} \end{aligned} \tag{4.23}$$

Where T, r_1^{SE}, and r_2^{SE} are the fractional factors of series voltages and Ψ_T, Ψ_{SE1}, and Ψ_{SE2} represents phase angles of $\bar{V}_T$, $\bar{V}_{SE1}$, and $\bar{V}_{SE2}$ respectively. Putting the values of $\bar{V}_T, \bar{V}_{SE1}$ and $\bar{V}_{SE2}$ in (4.22), we can write

$$V_k\angle\delta_k - V_p\angle\delta_p = -TV_p\angle\Psi_T - r_1^{SE}V_p\angle\Psi_{SE1} - r_2^{SE}V_p\angle\Psi_{SE2} \tag{4.24}$$

Separating (4.24) into the real and imaginary parts, we obtain

$$G_1 = V_kcos\delta_k - V_pcos\delta_p + V_p(Tcos\Psi_T + r_1^{SE}cos\Psi_{SE1} + r_2^{SE}cos\Psi_{SE2}) \tag{4.25}$$

$$G_2 = V_ksin\delta_k - V_psin\delta_p + V_p(Tsin\Psi_T + r_1^{SE}sin\Psi_{SE1} + r_2^{SE}sin\Psi_{SE2}) \tag{4.26}$$

Equations (4.25) and (4.26) will be incorporated inside the existing Jacobian matrix of the power system.

4.3.4 Power Exchange Equations

To accomplish the APFC steady-state model, the real and reactive power exchange equations due to the DPFC and ST must be considered in the mathematical modeling. ST can exchange both real and reactive powers, while DPFC exchanges only real power. DPFC has the ability to generate or absorb reactive power. The total active power required at the fundamental frequency by the series converters of DPFC can be expressed as:

$$P_{SE} = \Re\Big[(\bar{V}_{SE1} + \bar{V}_{SE2})I^*_{pq}\Big] \tag{4.27}$$

The independency of the active power at different frequencies gives the possibility that a converter without power source can generate active power at one frequency and absorb this power from other frequencies. In [46, 117], the active power between the shunt and series converters within the DPFC system has been exchanged using the 3^{rd} harmonics. Therefore, the amount of active power generated at fundamental frequency by the series converter is equal to the amount of active power consumed by the series converter at 3^{rd} harmonics (*i.e.* $P^{h_3}_{SE}$). Mathematically,

$$P^{h_3}_{SE} = -P_{SE} \tag{4.28}$$

The real power supplied by the shunt converter (*i.e.* STATCOM and shunt transformer of ST) can be expressed as:

$$PBE^{SH} = \Re\Big[\bar{V}_{SH}(\bar{I}_{SH} - \bar{I}^{SH}_{C})^* + \bar{V}_p\bar{I}^*_T\Big] \tag{4.29}$$

Putting all the values, we obtain

$$PBE^{SH} = V_pV_{SH}Y_{SH}cos(\Psi_{SH}-\delta_p-\Theta_{SH})-V^2_{SH}Y_{SH}cos\Theta_{SH}+TV_pI_{pq}cos(2\delta_p-\Psi_T-\Phi_{pq}) - \frac{V^2_{SH}}{R^{SHeq}_C} \tag{4.30}$$

Similarly, the real power demanded by the series converters of DPFC and series transformer of ST can be expressed as:

$$PBE^{SE} = \Re\Big[-\bar{V}_TI^*_{pq} + \bar{V}_{SE1}(\bar{I}^{SE*}_{C1} - \bar{I}^*_{pq}) + \bar{V}_{SE2}(\bar{I}^{SE*}_{C2} - \bar{I}^*_{pq})\Big] \tag{4.31}$$

Putting all the values, we obtain

$$PBE^{SE} = -TV_pI_{pq}cos(\Psi_T - \Phi_{pq}) - \frac{(r_1^{SE}V_p)^2}{R_{C1}^{SEeq}} - r_1^{SE}V_pI_{pq}cos(\Psi_{SE1} - \Phi_{pq}) + \frac{(r_2^{SE}V_p)^2}{R_{C2}^{SEeq}} - r_2^{SE}V_pI_{pq}cos(\Psi_{SE2} - \Phi_{pq}) \quad (4.32)$$

As we know, the DPFC and ST can only transfer the real power. Therefore, the real power exchange equation can be expressed as:

$$PBE = PBE^{SE} - PBE^{SH} = 0 \quad (4.33)$$

Putting values of PBE^{SE} and PBE^{SH} from (4.32) and (4.30) respectively, we obtain

$$PBE = -TV_pI_{pq}cos(\Psi_T - \Phi_{pq}) + V_{SH}^2Y_{SH}cos\Theta_{SH} - r_1^{SE}V_pI_{pq}cos(\Psi_{SE1} - \Phi_{pq}) + \frac{V_{SH}^2}{R_C^{SHeq}} - r_2^{SE}V_pI_{pq}cos(\Psi_{SE2} - \Phi_{pq}) + \frac{(r_2^{SE}V_p)^2}{R_{C2}^{SEeq}} - TV_pI_{pq}cos(2\delta_p - \Psi_T - \Phi_{pq}) - V_pV_{SH}Y_{SH}cos(\Psi_{SH} - \delta_p - \Theta_{SH}) - \frac{(r_1^{SE}V_p)^2}{R_{C1}^{SEeq}} \quad (4.34)$$

Reactive power can be exchanged between series and shunt transformers of ST. The reactive power supplied by shunt part of ST can be expressed as:

$$QBE^{SH} = \Im\big[\bar{V}_p\bar{I}_T^*\big] \quad (4.35)$$

Putting all the values, we obtain

$$QBE^{SH} = TV_pI_{pq}sin(2\delta_p - \Psi_T - \Phi_{pq}) \quad (4.36)$$

The reactive power demanded by series part of ST can be expressed as:

$$QBE^{SE} = -\Im\big[\bar{V}_T\bar{I}_{pq}^*\big] \quad (4.37)$$

Putting all the values, we obtain

$$QBE^{SE} = -TV_pI_{pq}sin(\Psi_T - \Phi_{pq}) \quad (4.38)$$

Similarly to the real power exchange (4.33), the reactive power exchange equation can be expressed as:

$$QBE = QBE^{SE} - QBE^{SH} = 0 \quad (4.39)$$

Therefore, the reactive power exchange equation can be written as shown in (4.40).

$$QBE = -TV_pI_{pq}sin(\Psi_T - \Phi_{pq}) - TV_pI_{pq}sin(2\delta_p - \Psi_T - \Phi_{pq}) \tag{4.40}$$

4.3.5 Power Flow and Voltage Control Constraints of APFC

The APFC presented in Figure 4.2 can control active and reactive power flow in the transmission line, and voltage of the bus independently/simultaneously. The active and reactive power flow constraints in the transmission line kq can be expressed as:

$$\Delta PCP = P_{kq}^{SP} - P_{kq} = 0 \tag{4.41}$$

$$\Delta PCQ = Q_{kq}^{SP} - Q_{kq} = 0 \tag{4.42}$$

Where, P_{kq}^{SP} and Q_{kq}^{SP} are the specified real and reactive powers of the line kq. From Figure 4.4, we know $\bar{S}_{kq} = -\bar{S}_k$. Therefore,

$$P_{kq} = V_kI_{pq}cos(\delta_k - \Phi_{pq}) \tag{4.43}$$

$$Q_{kq} = V_kI_{pq}sin(\delta_k - \Phi_{pq}) \tag{4.44}$$

The voltage control constraints of the sending end of transmission line *i.e.* at bus p is:

$$\Delta PCV = V_p^{SP} - V_p = 0 \tag{4.45}$$

Where, V_p^{SP} is the specified voltage of bus p.

4.3.6 APFC Jacobian Equations

The linearized Jacobian matrix of the modified power network without APFC is:

$$J^m = \begin{bmatrix} H^m & N^m \\ M^m & L^m \end{bmatrix} \tag{4.46}$$

To account the supplementary shunt and series injected powers at the bus p and k, the additional shunt and series Jacobian matrices are added to matrix described by (4.46) in following way:

$$\left[J^{MS}\right] = \left[J^m\right] + \left[J^{SE}\right] + \left[J^{SH}\right] \tag{4.47}$$

The elements of the series Jacobian matrix $[J^{SE}]$ are:

$$L_{pp}^{SE} = -H_{pp}^{SE} = H_{p,\hbar+1}^{SE} = L_{p,\hbar+2}^{SE} = V_p I_{pq} sin(\delta_p - \Phi_{pq}) \tag{4.48}$$

$$N_{pp}^{SE} = M_{pp}^{SE} = N_{p,\hbar+2}^{SE} = -M_{p,\hbar+1}^{SE} = V_p I_{pq} cos(\delta_p - \Phi_{pq}) \tag{4.49}$$

$$L_{kk}^{SE} = -H_{kk}^{SE} = H_{k,\hbar+1}^{SE} = L_{k,\hbar+2}^{SE} = -V_k I_{pq} sin(\delta_k - \Phi_{pq}) \tag{4.50}$$

$$N_{kk}^{SE} = M_{kk}^{SE} = N_{k,\hbar+2}^{SE} = -M_{k,\hbar+1}^{SE} = -V_k I_{pq} cos(\delta_k - \Phi_{pq}) \tag{4.51}$$

The elements of the shunt Jacobian matrix $[J^{SH}]$ are:

$$H_{p,\hbar+1}^{SH} = TV_p I_{pq} sin(2\delta_p - \Psi_T - \Phi_{pq}) \tag{4.52}$$

$$N_{p,\hbar+2}^{SH} = TV_p I_{pq} cos(2\delta_p - \Psi_T - \Phi_{pq}) \tag{4.53}$$

$$H_{p,\hbar+3}^{SH} = -V_p V_{SH} Y_{SH} sin(\delta_p - \Psi_{SH} - \Theta_{SH}) \tag{4.54}$$

$$N_{p,\hbar+4}^{SH} = -V_p Y_{SH} cos(\delta_p - \Psi_{SH} - \Theta_{SH}) \tag{4.55}$$

$$H_{p,\hbar+5}^{SH} = TV_p I_{pq} sin(2\delta_p - \Psi_T - \Phi_{pq}) \tag{4.56}$$

$$N_{p,\hbar+6}^{SH} = V_p I_{pq} cos(2\delta_p - \Psi_T - \Phi_{pq}) \tag{4.57}$$

$$M_{p,\hbar+1}^{SH} = -TV_p I_{pq} cos(2\delta_p - \Psi_T - \Phi_{pq}) \tag{4.58}$$

$$L_{p,\hbar+2}^{SH} = TV_p I_{pq} sin(2\delta_p - \Psi_T - \Phi_{pq}) \tag{4.59}$$

$$M_{p,\hbar+3}^{SH} = V_p V_{SH} Y_{SH} cos(\delta_p - \Psi_{SH} - \Theta_{SH}) \tag{4.60}$$

$$L_{p,\hbar+4}^{SH} = -V_p Y_{SH} sin(\delta_p - \Psi_{SH} - \Theta_{SH}) \tag{4.61}$$

$$M_{p,\hbar+5}^{SH} = -TV_p I_{pq} cos(2\delta_p - \Psi_T - \Phi_{pq}) \tag{4.62}$$

$$L_{p,\hbar+6}^{SH} = V_p I_{pq} sin(2\delta_p - \Psi_T - \Phi_{pq}) \tag{4.63}$$

$$H_{pp}^{SH} = -2TV_p I_{pq} sin(2\delta_p - \Psi_T - \Phi_{pq}) + V_p V_{SH} Y_{SH} sin(\delta_p - \Psi_{SH} - \Theta_{SH}) \tag{4.64}$$

$$M_{pp}^{SH} = 2TV_p I_{pq} cos(2\delta_p - \Psi_T - \Phi_{pq}) - V_p V_{SH} Y_{SH} cos(\delta_p - \Psi_{SH} - \Theta_{SH}) \tag{4.65}$$

$$N_{pp}^{SH} = TV_p I_{pq} cos(2\delta_p - \Psi_T - \Phi_{pq}) + 2V_p^2 Y_{SH} cos\Theta_{SH} - V_p V_{SH} Y_{SH} cos(\delta_p - \Psi_{SH} - \Theta_{SH}) \tag{4.66}$$

$$L_{pp}^{SH} = TV_p I_{pq} sin(2\delta_p - \Psi_T - \Phi_{pq}) - 2V_p^2 Y_{SH} sin\Theta_{SH} - V_p V_{SH} Y_{SH} sin(\delta_p - \Psi_{SH} - \Theta_{SH}) \tag{4.67}$$

The voltage equations (4.25), (4.26), power exchange equations (4.34), (4.40) and control constraints equations (4.41), (4.42), (4.45) are also included in the Jacobian matrix to complete the formation. Therefore, a sub-matrix J^{CC} is inserted into J^{MS} to accommodate all these equations. The flexibility of the developed formulation is that all the control

constraints (*i.e.* voltage, real and reactive power of specified line) can be controlled simultaneously or each one can be controlled independently. The complete Jacobian matrix is:

$$J = \begin{bmatrix} J^{MS} \\ \dots \\ J^{CC} \end{bmatrix} \tag{4.68}$$

The structure of series $[J^{SE}]$, shunt $[J^{SH}]$ and control constraints $[J^{CC}]$ Jacobian matrices are given in (4.110), (4.111) and (4.112) respectively. Also, the partial derivatives terms of control constraints are as follows:

$$J^{CC}_{1,p} = V_p sin\delta_p \tag{4.69}$$
$$J^{CC}_{1,p+1} = -V_p cos\delta_p + V_p(T cos\Psi_T + r_1^{SE} cos\Psi_{SE1} + r_2^{SE} cos\Psi_{SE2}) \tag{4.70}$$
$$J^{CC}_{1,k} = -V_k sin\delta_k \tag{4.71}$$
$$J^{CC}_{1,k+1} = V_k cos\delta_k \tag{4.72}$$
$$J^{CC}_{1,\hbar+5} = -TV_p sin\Psi_T \tag{4.73}$$
$$J^{CC}_{1,\hbar+6} = V_p cos\Psi_T \tag{4.74}$$
$$J^{CC}_{1,\hbar+7} = -r_1^{SE} V_p sin\Psi_{SE1} \tag{4.75}$$
$$J^{CC}_{1,\hbar+8} = V_p cos\Psi_{SE1} \tag{4.76}$$
$$J^{CC}_{1,\hbar+9} = -r_2^{SE} V_p sin\Psi_{SE2} \tag{4.77}$$
$$J^{CC}_{1,\hbar+10} = V_p cos\Psi_{SE2} \tag{4.78}$$
$$J^{CC}_{2,p} = -V_p cos\delta_p \tag{4.79}$$
$$J^{CC}_{2,p+1} = -V_p sin\delta_p + V_p(T sin\Psi_T + r_1^{SE} sin\Psi_{SE1} + r_2^{SE} sin\Psi_{SE2}) \tag{4.80}$$
$$J^{CC}_{2,k} = V_k cos\delta_k \tag{4.81}$$
$$J^{CC}_{2,k+1} = V_k sin\delta_k \tag{4.82}$$
$$J^{CC}_{2,\hbar+5} = TV_p cos\Psi_T \tag{4.83}$$
$$J^{CC}_{2,\hbar+6} = V_p sin\Psi_T \tag{4.84}$$
$$J^{CC}_{2,\hbar+7} = r_1^{SE} V_p cos\Psi_{SE1} \tag{4.85}$$
$$J^{CC}_{2,\hbar+8} = V_p sin\Psi_{SE1} \tag{4.86}$$
$$J^{CC}_{2,\hbar+9} = r_2^{SE} V_p cos\Psi_{SE2} \tag{4.87}$$
$$J^{CC}_{2,\hbar+10} = V_p sin\Psi_{SE2} \tag{4.88}$$
$$J^{CC}_{3,p} = -V_p V_{SH} Y_{SH} sin(\Psi_{SH} - \delta_p - \Theta_{SH}) + 2TV_p I_{pq} sin(2\delta_p - \Psi_T - \Phi_{pq}) \tag{4.89}$$

$$J^{CC}_{3,p+1} = - TV_pI_{pq}cos(\Psi_T - \Phi pq) + \frac{2(r_1^{SE}V_p)^2}{R_{C1}^{SEeq}} - r_1^{SE}V_pI_{pq}cos(\Psi_{SE1} - \Phi_{pq}) + \frac{2(r_2^{SE}V_p)^2}{R_{C2}^{SEeq}} - r_2^{SE}V_pI_{pq}cos(\Psi_{SE2} - \Phi_{pq}) - V_pV_{SH}Y_{SH}cos(\Psi_{SH} - \delta_p - \Theta_{SH}) - TV_pI_{pq}cos(2\delta_p - \Psi_T - \Phi_{pq}) \quad (4.90)$$

$$J^{CC}_{3,\hbar+1} = - TV_pI_{pq}sin(\Psi_T - \Phi pq) - r_1^{SE}V_pI_{pq}sin(\Psi_{SE1} - \Phi_{pq}) - r_2^{SE}V_pI_{pq}sin(\Psi_{SE2} - \Phi_{pq}) - TV_pI_{pq}sin(2\delta_p - \Psi_T - \Phi_{pq}) \quad (4.91)$$

$$J^{CC}_{3,\hbar+2} = - TV_pI_{pq}cos(\Psi_T - \Phi pq) - r_1^{SE}V_pI_{pq}cos(\Psi_{SE1} - \Phi_{pq}) - r_2^{SE}V_pI_{pq}cos(\Psi_{SE2} - \Phi_{pq}) - TV_pI_{pq}cos(2\delta_p - \Psi_T - \Phi_{pq}) \quad (4.92)$$

$$J^{CC}_{3,\hbar+3} = V_pV_{SH}Y_{SH}sin(\Psi_{SH} - \delta_p - \Theta_{SH}) \quad (4.93)$$

$$J^{CC}_{3,\hbar+4} = - V_pY_{SH}cos(\Psi_{SH} - \delta_p - \Theta_{SH}) + 2\frac{V_{SH}}{R_C^{SHeq}} + 2V_{SH}Y_{SH}cos\Theta_{SH} \quad (4.94)$$

$$J^{CC}_{3,\hbar+5} = TV_pI_{pq}sin(\Psi_T - \delta_p - \Phi_{pq}) - TV_pI_{pq}sin(2\delta_p - \Psi_T - \Phi_{pq}) \quad (4.95)$$

$$J^{CC}_{3,\hbar+6} = - V_pI_{pq}cos(\Psi_T - \delta_p - \Phi_{pq}) - V_pI_{pq}cos(2\delta_p - \Psi_T - \Phi_{pq}) \quad (4.96)$$

$$J^{CC}_{3,\hbar+7} = - r_1^SEV_pI_{pq}sin(\Psi_{SE1} - \Phi_{pq}) \quad (4.97)$$

$$J^{CC}_{3,\hbar+8} = 2\frac{r_1^{SE}V_p^2}{R_{C1}^{SEeq}} - V_pI_{pq}cos(\Psi_{SE1} - \Phi_{pq}) \quad (4.98)$$

$$J^{CC}_{3,\hbar+9} = r_2^{SE}V_pI_{pq}sin(\Psi_{SE2} - \Phi_{pq}) \quad (4.99)$$

$$J^{CC}_{3,\hbar+10} = 2\frac{r_2^{SE}V_p^2}{R_{C2}^{SEeq}} - V_pI_{pq}cos(\Psi_{SE2} - \Phi_{pq}) \quad (4.100)$$

$$J^{CC}_{4,p} = - 2TV_pI_{pq}cos(2\delta_p - \Psi_T - \Phi_{pq}) \quad (4.101)$$

$$J^{CC}_{4,p+1} = - TV_pI_{pq}sin(\Psi_T - \Phi_{pq}) - TV_pI_{pq}sin(2\delta_p - \Psi_T - \Phi_{pq}) \quad (4.102)$$

$$J^{CC}_{4,\hbar+1} = TV_pI_{pq}cos(\Psi_T - \Phi_{pq}) + TV_pI_{pq}cos(2\delta_p - \Psi_T - \Phi_{pq}) \quad (4.103)$$

$$J^{CC}_{4,\hbar+2} = - TV_pI_{pq}sin(\Psi_T - \Phi_{pq}) - TV_pI_{pq}sin(2\delta_p - \Psi_T - \Phi_{pq}) \quad (4.104)$$

$$J^{CC}_{4,\hbar+5} = - TV_pI_{pq}cos(\Psi_T - \Phi_{pq}) + TV_pI_{pq}cos(2\delta_p - \Psi_T - \Phi_{pq}) \quad (4.105)$$

$$J^{CC}_{4,\hbar+6} = - V_pI_{pq}sin(\Psi_T - \Phi_{pq}) - V_pI_{pq}sin(2\delta_p - \Psi_T - \Phi_{pq}) \quad (4.106)$$

$$J^{CC}_{5,\hbar+1} = - J^{CC}_{5,k} = J^{CC}_{6,k+1} = J^{CC}_{6,\hbar+2} = V_kI_{pq}sin(\delta_k - \Phi_{pq}) \quad (4.107)$$

$$J^{CC}_{5,k+1} = J^{CC}_{5,\hbar+2} = -J^{CC}_{6,\hbar+1} = J^{CC}_{6,k} = V_kI_{pq}cos(\delta_k - \Phi_{pq}) \quad (4.108)$$

$$J^{CC}_{7,p+1} = V_p \quad (4.109)$$

$$\begin{bmatrix} \Delta P_p^{SE} \\ \Delta Q_p^{SE} \\ \dots \\ \Delta P_k^{SE} \\ \Delta Q_k^{SE} \end{bmatrix} = \begin{bmatrix} \dots & H_{pp}^{SE} & N_{pp}^{SE} & \dots & \dots & \dots & \dots & \dots & H_{p,\hbar+1}^{SE} & N_{p,\hbar+2}^{SE} & \dots & \dots & \dots & \dots & \dots & \dots & \dots & \dots \\ \dots & M_{pp}^{SE} & L_{pp}^{SE} & \dots & \dots & \dots & \dots & \dots & M_{p,\hbar+1}^{SE} & L_{p,\hbar+2}^{SE} & \dots & \dots & \dots & \dots & \dots & \dots & \dots & \dots \\ \dots & \dots & \dots & \dots & \dots & \dots & \dots & \dots & \dots & \dots & \dots & \dots & \dots & \dots & \dots & \dots & \dots & \dots \\ \dots & \dots & \dots & \dots & H_{kk}^{SE} & N_{kk}^{SE} & \dots & \dots & H_{k,\hbar+1}^{SE} & N_{k,\hbar+2}^{SE} & \dots & \dots & \dots & \dots & \dots & \dots & \dots & \dots \\ \dots & \dots & \dots & \dots & M_{kk}^{SE} & L_{kk}^{SE} & \dots & \dots & M_{k,\hbar+1}^{SE} & L_{k,\hbar+2}^{SE} & \dots & \dots & \dots & \dots & \dots & \dots & \dots & \dots \end{bmatrix} \begin{bmatrix} \Delta X \end{bmatrix} \tag{4.110}$$

$$\begin{bmatrix} \Delta P_p^{SH} \\ \Delta Q_p^{SH} \end{bmatrix} = \begin{bmatrix} \dots & H_{pp}^{SH} & N_{pp}^{SH} & \dots & \dots & \dots & \dots & \dots & H_{p,\hbar+1}^{SH} & N_{p,\hbar+2}^{SH} & H_{p,\hbar+3}^{SH} & N_{p,\hbar+4}^{SH} & H_{p,\hbar+5}^{SH} & N_{p,\hbar+6}^{SH} & \dots & \dots & \dots & \dots \\ \dots & M_{pp}^{SH} & L_{pp}^{SH} & \dots & \dots & \dots & \dots & \dots & M_{p,\hbar+1}^{SH} & L_{p,\hbar+2}^{SH} & M_{p,\hbar+3}^{SH} & L_{p,\hbar+4}^{SH} & M_{p,\hbar+5}^{SH} & L_{p,\hbar+6}^{SH} & \dots & \dots & \dots & \dots \end{bmatrix} \begin{bmatrix} \Delta X \end{bmatrix} \tag{4.111}$$

$$\begin{bmatrix} \Delta G_1 \\ \Delta G_2 \\ \Delta PBE \\ \Delta QBE \\ \Delta PCP \\ \Delta PCQ \\ \Delta PCV \end{bmatrix} = \begin{bmatrix} \dots & J_{1,p}^{CC} & J_{1,p+1}^{CC} & \dots & J_{1,k}^{CC} & J_{1,k+1}^{CC} & \dots & \dots & \dots & \dots & \dots & \dots & J_{1,\hbar+5}^{CC} & J_{1,\hbar+6}^{CC} & J_{1,\hbar+7}^{CC} & J_{1,\hbar+8}^{CC} & J_{1,\hbar+9}^{CC} & J_{1,\hbar+10}^{CC} \\ \dots & J_{2,p}^{CC} & J_{2,p+1}^{CC} & \dots & J_{2,k}^{CC} & J_{2,k+1}^{CC} & \dots & \dots & \dots & \dots & \dots & \dots & J_{2,\hbar+5}^{CC} & J_{2,\hbar+6}^{CC} & J_{2,\hbar+7}^{CC} & J_{2,\hbar+8}^{CC} & J_{2,\hbar+9}^{CC} & J_{2,\hbar+10}^{CC} \\ \dots & J_{3,p}^{CC} & J_{3,p+1}^{CC} & \dots & \dots & \dots & J_{3,\hbar+1}^{CC} & J_{3,\hbar+2}^{CC} & J_{3,\hbar+3}^{CC} & J_{3,\hbar+4}^{CC} & J_{3,\hbar+5}^{CC} & J_{3,\hbar+6}^{CC} & J_{3,\hbar+7}^{CC} & J_{3,\hbar+8}^{CC} & J_{3,\hbar+9}^{CC} & J_{3,\hbar+10}^{CC} & & \\ \dots & J_{4,p}^{CC} & J_{4,p+1}^{CC} & \dots & \dots & \dots & J_{4,\hbar+1}^{CC} & J_{4,\hbar+2}^{CC} & \dots & \dots & \dots & \dots & \dots & \dots & \dots & \dots & & \\ \dots & \dots & \dots & \dots & J_{5,k}^{CC} & J_{5,k+1}^{CC} & J_{5,\hbar+1}^{CC} & J_{5,\hbar+2}^{CC} & \dots & \dots & \dots & \dots & \dots & \dots & \dots & \dots & \dots & \dots \\ \dots & \dots & \dots & \dots & J_{6,k}^{CC} & J_{6,k+1}^{CC} & J_{6,\hbar+1}^{CC} & J_{6,\hbar+2}^{CC} & \dots & \dots & \dots & \dots & \dots & \dots & \dots & \dots & \dots & \dots \\ \dots & \dots & \dots & \dots & \dots & J_{7,k+1}^{CC} & \dots & \dots & \dots & \dots & \dots & \dots & \dots & \dots & \dots & \dots & \dots & \dots \end{bmatrix} \begin{bmatrix} \Delta X \end{bmatrix} \tag{4.112}$$

$$[\Delta X] = [\dots \quad \Delta\delta_p \quad \frac{\Delta V_p}{V_p} \quad \dots \quad \Delta\delta_k \quad \frac{\Delta V_k}{V_k} \quad \dots \quad \dots \quad \Delta\Phi_{pq} \quad \frac{\Delta I_{pq}}{I_{pq}} \quad \Delta\Psi_{SH} \quad \Delta V_{SH} \quad \Delta\Psi_T \quad \Delta T \quad \Delta\Psi_{SE1} \quad \Delta r_1^{SE} \quad \Delta\Psi_{SE2} \quad \Delta r_2^{SE}]' \tag{4.113}$$

4.4 Results and Model Verification

Based upon the developed HABM mathematical model, this section presents feasibility of APFC to control parameters of power systems and its adaplibility in N-R load-flow method. Study is also carried out to find the effect of impedance of coupling transformer and switching losses of converter on convergence characteristics. The linearized equations of HABM model of APFC is incorporated into NRLF method. The proposed model of APFC is tested on IEEE 30-bus and 118-bus test systems and their system data are given in Appendix A. A convergence tolerance of 10^{-12} *p.u.* has been chosen for all the cases. The coupling transformer impendances $\bar{Z}_T^{TF} = \bar{Z}_T^{SE1} = \bar{Z}_T^{SE2} = \bar{Z}_{SH} = 0.1 + j0.1$ *p.u.* have been chosen according to [49]. To represent the shunt and series voltage source converter switching losses, $R_{C1}^{SEeq} = R_{C2}^{SEeq} = R_C^{SHeq} = 50$ *p.u.* have been chosen [116]. The feasibility of the proposed load-flow model of APFC is validated through the obtained results using MATLAB coding [115]. The APFC location, real and reactive power flow and bus voltage control constraints are chosen according to [62]. Case study on IEEE 30 and 118-bus test systems are presented below.

4.4.1 IEEE 30-Bus Test System

For this test system, the three APFC locations and specified control constraints have been chosen on the basis of [62]; *i.e.* between buses 3-4 (APFC 1), 12-15 (APFC 2), and 25-27 (APFC 3). At a time, one APFC is considered to be connected in the network with different control functions. The studies have been carried out for two cases; *i.e.* APFC with and without device limit constraints. Specified control constraint chosen for APFC 1 are; $V_3^{SP} = 1.06$ *p.u.*, $P_{3-4}^{SP} = 78.012$ MW, and $Q_{3-4}^{SP} = -3.63$ MVAR respectively. The unconstrained solution of APFC parameters for specified voltage, real and reactive power control is shown in Table 4.1. These results show that specified values are met in 14 iterations.

The convergence characteristics of the proposed model has been examined with different values of transformer impedance. The convergence characteristics of the developed load-flow model of UPFC in the literature is found to be affected by the value of impedance of series coupling transformer [64]. It is observed from the literature survey that smaller the impedance, more is the number of iteration required [64]. Conversely, in the proposed model, the number of iterations is not affected when impedance of series transformer is varied in the range of $0.0001 + j0.0001$ to $0.1 + j0.1$ *p.u.* as shown in Table 4.2.

TABLE 4.1: APFC test results for IEEE 30-bus test system

Unconstrained solution of APFC parameters			
Base case power flow solution $V_3 = 1.0217, V_4 = 1.0131, V_{12} = 1.058, V_{15} = 1.0217, V_{25} = 1.0201, V_{27} = 1.0217,$ $P_{3-4} = 78.02\ MW, P_{12-15} = 17.82\ MW, P_{25-27} = -4.84\ MW,$ $Q_{3-4} = -3.25\ MVAR, Q_{12-15} = 6.69\ MVAR, Q_{25-27} = -0.63\ MVAR$			
Specified parameters $V_3^{SP} = 1.06, P_{3-4}^{SP} = 78.012\ MW, Q_{3-4}^{SP} = -3.63\ MVAR$ $V_{12}^{SP} = 1.06, P_{12-15}^{SP} = 17.857\ MW, Q_{12-15}^{SP} = 6.947\ MVAR$ $V_{25}^{SP} = 1.02, P_{25-27}^{SP} = -4.877\ MW, Q_{25-27}^{SP} = -0.778\ MVAR$			
Parameters	APFC 1	APFC 2	APFC 3
T	0.2768	0.1813	0.1537
Ψ_T (Degree)	98.56	74.29	72.60
r_1^{SE}	0.1914	0.1359	0.0413
Ψ_{SE1} (Degree)	98.45	-150.56	-151.44
r_2^{SE}	0.1265	0.1208	0.1348
Ψ_{SE2} (Degree)	113.97	-87.44	-86.99
V_{SH} $(p.u.)$	1.0792	1.058	1.0194
Ψ_{SH} (Degree)	-10.38	-15.80	-17.62
I_{pq} $(p.u.)$	0.6633	0.1708	0.0493
Φ_{pq} (Degree)	5.31	-35.35	153.68
P_{Line} (MW)	78.012	17.857	-4.877
Q_{Line} $(MVAR)$	-3.63	6.947	-0.778
V_{Bus} $(p.u.)$	1.06	1.06	1.02
δ_{Bus} (Degree)	-8.56	-15.71	-17.39
NI	14	9	7
Time (sec)	0.094802	0.278341	0.230689

TABLE 4.2: Effect of the coupling transformer impedance on the convergence property of the proposed model (30-bus)

$\bar{Z_T}^{TF} = \bar{Z_T}^{SE1} = \bar{Z_T}^{SE2}$ $(p.u.)$	NI
0.1+j0.1	7
0.01+j0.01	7
0.001+j0.001	7
0.0001+j0.0001	7

The impact of variation of switching losses on convergence characteristic of proposed model has also been investigated. The switching losses for all VSCs devices are considered equal for simplification. As shown in Table 4.3, the solution converged in same number of iterations (NI=7) when resistance representing the converter's switching losses is varied from 30 $p.u.$ to 500 $p.u.$

TABLE 4.3: Effect of the switching losses on the convergence property of the proposed model (30-bus)

$R_{C1}^{SEeq} = R_{C2}^{SEeq} = R_{C}^{SHeq}$ $(p.u.)$	NI
30	7
40	7
50	7
60	7
70	7
90	7
100	7
200	7
500	7

TABLE 4.4: APFC test results for IEEE 30-bus test system (constrained solution)

Constrained solution of APFC parameters			
Hard Constraints $(p.u.)$ $I_{3-4} \leq 0.3, I_{12-15} \leq 0.1, I_{25-27} \leq 0.04$			
Specified parameters $V_3^{SP} = 1.06, Q_{3-4}^{SP} = -3.63\ MVAR$ $V_{12}^{SP} = 1.06, Q_{12-15}^{SP} = 6.947\ MVAR$ $V_{25}^{SP} = 1.02, Q_{25-27}^{SP} = -0.778\ MVAR$			
Parameters	APFC 1	APFC 2	APFC 3
T	0.3188	0.1408	0.2664
Ψ_T (Degree)	87.71	74.94	72.19
r_1^{SE}	0.0847	0.0336	0.1833
Ψ_{SE1} (Degree)	83.18	95.86	102.73
r_2^{SE}	0.0864	0.0335	0.1020
Ψ_{SE2} (Degree)	83.13	95.84	109.09
V_{SH} $(p.u.)$	1.0564	1.0595	1.0201
Ψ_{SH} (Degree)	-2.29	-15.21	-18.08
I_{pq} $(p.u.)$	0.1770	0.067	0.04
Φ_{pq} (Degree)	0.28	99.71	152.09
P_{Line} (MW)	18.11	1.18	-3.95
Q_{Line} $(MVAR)$	-3.63	6.947	-0.778
V_{Bus} $(p.u.)$	1.06	1.06	1.02
δ_{Bus} (Degree)	-2.29	-15.06	-17.81
NI	9	8	6
Time (sec.)	0.062169	0.056020	0.051010

Robustness of the proposed model is also investigated for device limit constraint violation. Current limit constraint is imposed for series converter while relaxing some of the control constraints. A case study for IEEE 30-bus test system while imposing current limit

constraints and relaxing real power flow constraint is shown in Table 4.4. For APFC 3, the current limit constraint is chosen as 0.04 *p.u.* [62]. The N-R load-flow converged in six iterations. Reactive power flow in the line 25-27 is -0.778 MVAR, voltage of bus 25 is 1.02 *p.u.*, and line current is 0.04 *p.u.* These results shows that current, reactive power and voltage constraints are still imposed while real power constraints is relaxed. Similar results are obtained for APFC 1 and APFC 2. The computation time is less than 0.5 sec. These results show that model is robust and adaptable to different operating conditions.

The response of any FACTS device is very crucial under heavy loading conditions as the power systems are more prone to voltage instability under heavy loading conditions. Therefore, the proposed FACTS device is tested under heavy loading conditions. A case (*i.e.* APFC 3) of heavy MVA loading (1.4 times of the base case) is presented in Table 4.5 to investigate the effect of APFC on voltage stability of the power system. The results shows top ten stressed buses in decreasing order of their criticality. It is proved that the value of L-index of different buses decreases with the integration of APFC. This shows that the overall voltage stability margin of the power system is increased when APFC is integrated in the system. The node voltage profile with and without APFC is shown in Figure 4.5. From this figure, it can be observed that the node voltage profile is significantly improved after installation of APFC.

TABLE 4.5: Values of L-index with and without APFC for IEEE 30-bus test system (at $\lambda = 1.4$)

Without APFC		With APFC	
Bus No.	L-index	Bus No.	L-index
30	0.6639	26	0.2693
26	0.6223	25	0.2476
29	0.6176	5	0.2113
24	0.5960	24	0.1963
19	0.5954	30	0.1774
18	0.5858	19	0.1696
20	0.5840	23	0.1665
23	0.5806	20	0.1630
25	0.5805	22	0.1604
21	0.5698	18	0.1603

4.4.2 IEEE 118-Bus Test System

For this test system, the three APFC locations have been chosen on the basis of [62]; *i.e.* between buses 20-21 (APFC 1), 45-44 (APFC 2) and 94-95 (APFC 3). The voltage, real

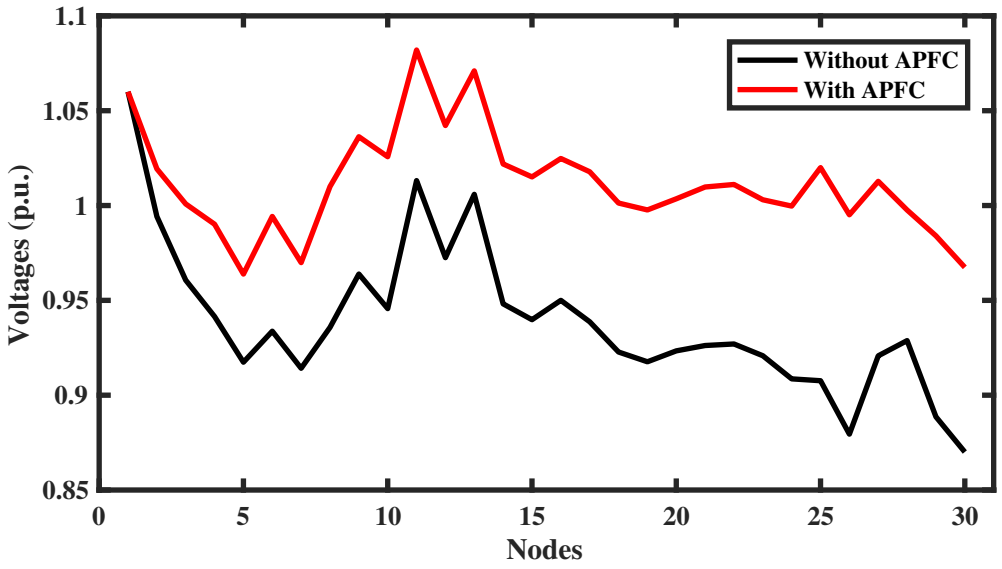

FIGURE 4.5: Node voltage profile with and without APFC for IEEE 30-bus test system

and reactive power control constraints are shown in Table 4.6. The values of coupling transformer impedance and switching loss have been considered as in previous case. For APFC 1 the real power, reactive power and voltage of bus are specified as 3.08 MW, -2.501 MVAR, 1.02 *p.u.* [62]. The results of Table 4.6 show that all targeted values are met in ten iterations. For APFC 2 and APFC 3, specified control parameters are also attained in reasonable number of iterations. These results validate the feasibility of the proposed model. For the IEEE 118-bus test system, the computation time is less than 5 sec. The effect of different values of transformer impedance on convergence characteristic of proposed model has been also investigated and presented in Table 4.7. From Table 4.7, it is observed that in the proposed model, the number of iterations is not affected when impedance of series transformer is varied in the range of $0.0001 + j0.0001$ to $0.1 + j0.1$ *p.u.* Also, the solution converged in same number of iteration (NI=12) when switching losses is varied from 30 *p.u.* to 500 *p.u.* as shown in Table 4.8.

Robustness of the proposed model is also investigated on IEEE 118-bus test system for device limit constraint violation. Current limit constraint is imposed for series converter while relaxing some of the control constraints. A case study for IEEE 118-bus test system while imposing current limit constraints and relaxing real power flow constraint is shown in Table 4.9. For APFC 3, the current limit constraint is chosen as 0.05 *p.u.*. The N-R load-flow converged in ten iterations. Reactive power flow in the line 94-95 is 1.77 MVAR, voltage of bus 94 is 1.01 *p.u.*, and line current is 0.0469 *p.u.* These results show that current, reactive power and voltage constraints are still imposed while real power constraints is

TABLE 4.6: APFC test results for IEEE 118-bus test system

Unconstrained solution of APFC parameters			
Base case power flow solution $V_{20} = 0.9570, V_{21} = 0.9583, V_{44} = 0.9865, V_{45} = 0.9883, V_{94} = 0.9857, V_{95} = 0.9751,$ $P_{20-21} = -26.37\ MW, P_{45-44} = 20.11\ MW, P_{94-95} = 75.93\ MW,$ $Q_{20-21} = 3.64\ MVAR, Q_{45-44} = -3.96\ MVAR, Q_{94-95} = 1.66\ MVAR$			
Specified parameters $V_{20}^{SP} = 1.02, P_{20-21}^{SP} = 3.08\ MW, Q_{20-21}^{SP} = -2.501\ MVAR$ $V_{45}^{SP} = 1.02, P_{45-44}^{SP} = 26\ MW, Q_{45-44}^{SP} = -7.09\ MVAR$ $V_{94}^{SP} = 1.01, P_{94-95}^{SP} = 76.93\ MW, Q_{94-95}^{SP} = 1.766\ MVAR$			
Parameters	APFC 1	APFC 2	APFC 3
T	0.24	0.1655	0.2081
Ψ_T (Degree)	-100.73	-97.90	-80.22
r_1^{SE}	0.0572	0.0113	0.068
Ψ_{SE1} (Degree)	7.12	28.78	-160.91
r_2^{SE}	0.0172	0.0103	0.0596
Ψ_{SE2} (Degree)	9.58	28.74	-160.26
V_{SH} $(p.u.)$	1.0672	1.058	1.0873
Ψ_{SH} (Degree)	-13.68	-10.27	3.95
I_{pq} $(p.u.)$	0.0408	0.2657	0.6631
Φ_{pq} (Degree)	41.46	16.18	19.98
P_{Line} (MW)	3.08	26	76.93
Q_{Line} $(Mvar)$	-2.501	-7.09	1.766
V_{Bus} $(p.u.)$	1.02	1.02	1.01
δ_{Bus} (Degree)	-10.73	-7.90	9.78
NI	10	12	15
Time (sec.)	3.088689	1.496003	4.720697

TABLE 4.7: Effect of the coupling transformer impedance on the convergence property of the proposed model (118-bus)

$\bar{Z_T}^{TF} = \bar{Z_T}^{SE1} = \bar{Z_T}^{SE2}$ $(p.u.)$	NI
0.1+j0.1	12
0.01+j0.01	12
0.001+j0.001	12
0.0001+j0.0001	12

TABLE 4.8: Effect of the switching losses on the convergence property of the proposed model (118-bus)

$R_{C1}^{SEeq} = R_{C2}^{SEeq} = R_{C}^{SHeq}$ $(p.u.)$	NI
30	12
40	12
50	12
60	12
70	12
90	12
100	12
200	12
500	12

TABLE 4.9: APFC test results for IEEE 118-bus test system (constrained solution)

Constrained solution of APFC parameters			
Hard Constraints $(p.u.)$ $I_{20-21} \leq 0.027, I_{45-44} \leq 0.14, I_{94-95} \leq 0.05$			
Specified parameters $V_{20}^{SP} = 1.02, Q_{20-21}^{SP} = -2.501\ MVAR$ $V_{45}^{SP} = 1.02, Q_{45-44}^{SP} = -7.09\ MVAR$ $V_{94}^{SP} = 1.01, Q_{94-95}^{SP} = 1.77\ MVAR$			
Parameters	APFC 1	APFC 2	APFC 3
T	0.1000	0.0457	0.1142
Ψ_T (Degree)	-132.26	-96.64	102.36
r_1^{SE}	-0.0438	0.0333	0.0158
Ψ_{SE1} (Degree)	43.03	28.86	-19.01
r_2^{SE}	0.0410	0.0323	0.0156
Ψ_{SE2} (Degree)	33.87	28.82	-18.98
V_{SH} $(p.u.)$	1.0524	1.0595	1.0774
Ψ_{SH} (Degree)	-12.28	-8.63	8.14
I_{pq} $(p.u.)$	0.1400	0.067	0.0469
Φ_{pq} (Degree)	66.19	25.46	-15.77
P_{Line} (MW)	0.62	11.51	4.29
Q_{Line} $(MVAR)$	-2.501	-7.09	1.77
V_{Bus} $(p.u.)$	1.02	1.02	1.01
δ_{Bus} (Degree)	-10.36	-6.64	12.36
NI	12	11	10
Time (sec.)	0.343249	0.366328	0.327730

relaxed. Similar results are obtained for APFC 1 and APFC 2. The computation time is less than 0.5 sec. These results show that the proposed model is robust and adaptable to different operating conditions.

The effect of the proposed FACTS device on voltage stability is also tested for IEEE 118-bus test system under heavy loading conditions. A case (*i.e.* APFC 3) for heavy real and reactive loading (1.4 times of the base case) is presented in Table 4.10. It is observed that the value of L-index of different buses decreases with the reactive power support of APFC. This shows that the APFC is capable to improve voltage stability margin of the power system. The node voltage profile with and without APFC is shown in Figure 4.6. From this figure, it is observed that the node voltage profile is improved with installation of APFC.

TABLE 4.10: Values of L-index with and without APFC for IEEE 118-bus test system (at $\lambda = 1.4$)

Without APFC		With APFC	
Bus No.	L-index	Bus No.	L-index
76	0.2584	76	0.2305
118	0.2379	118	0.2035
74	0.2056	74	0.1875
75	0.1833	75	0.1603
20	0.1735	1	0.1366
43	0.1703	3	0.1082
21	0.1594	117	0.1071
33	0.1582	44	0.1023
19	0.1558	2	0.0982
36	0.1467	70	0.0882

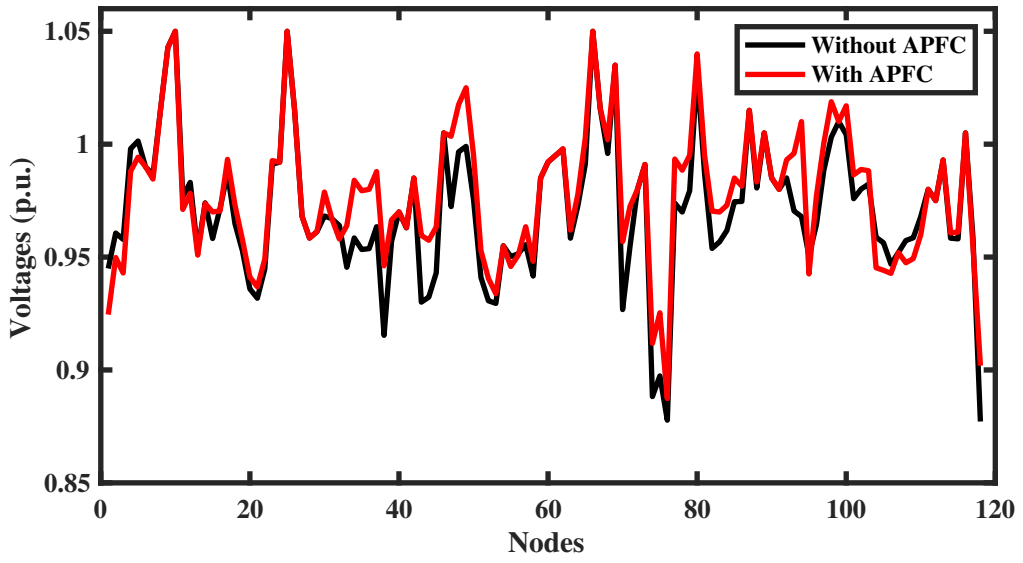

FIGURE 4.6: Node voltage profile with and without APFC for IEEE 118-bus test system

4.5 Comparison among APFC, DPFC and UPFC

The merit of APFC is that it allows independent control of real and reactive power flow in the line similar to a DPFC and UPFC. Power flow control is the function of phasor voltage injected in series. In DPFC, series voltage is injected by a group of small rating series converters and by one large rating converter in UPFC. Conversely in APFC, series voltage is injected by SEN transformer (ST) and series converters. Where, major portion (90%) is injected by ST and remaining 10% is injected by series converter for fine tuning (*i.e.* for continuous control). Therefore, the VA rating of series converters of APFC will be approximately 10% to that of required in DPFC and 5% that required in UPFC for same working range of operation. Again ST is a robust and economical device while converter is delicate and costly device. Lower dependency on series converters offers lower cost, increased reliability, and easy control making it a commercially viable device. The absence of common dc link also offers additional opportunity to operate the APFC as an independent STATCOM or SSSC depending upon situations.

The difference in characteristics of UPFC, DPFC, and APFC is elaborated by voltage phasors in Figures 4.7, 4.8, and 4.9 respectively. The variation range of receiving end voltage $V_A^{'}$ is a standard circle in case of UPFC whose center is at the apex of sending end voltage V_A. The locus of series injected voltage is represented by a circle.

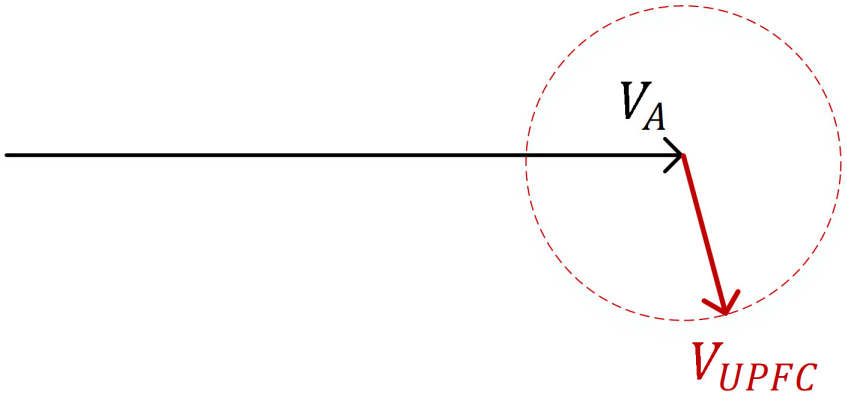

FIGURE 4.7: Output voltage phasor of UPFC

In case of DPFC, variation range of receiving end voltage is also a circle which is obtained by phasor sum of the series voltages injected by the series converters as shown in Figure 4.8. The characteristics of APFC are amalgamation of the characteristics of ST and DPFC. The series injected voltage by ST can reach any point within the hexagon. A circle at the

vertex of hexagon represents the locus of series voltage injected by DPFC. The APFC series injected voltage can reach any arbitrary point within the area enclosed by the combination of hexagonal and circles as shown in Figure 4.9. For phases B and C, same principle can be applied. Real power is exchanged through common dc link in UPFC at fundamental

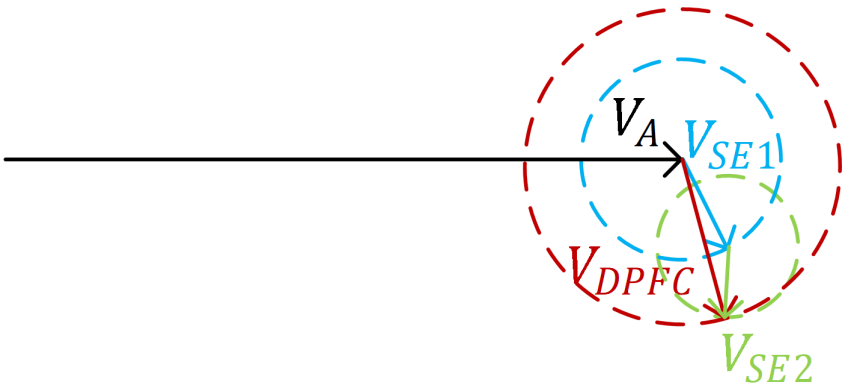

FIGURE 4.8: Output voltage phasor of DPFC

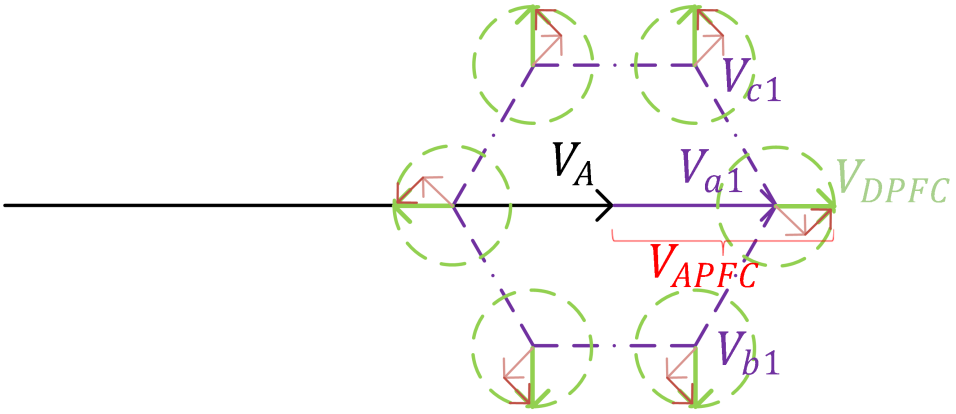

FIGURE 4.9: Output voltage phasor of APFC

frequency while in DPFC it is exchanged through transmission line at third harmonic frequency. In APFC, series converter exchange real power at third harmonic frequency while ST exchanges real power at fundamental frequency. Since real power exchange is mainly due to ST, percentage of third harmonics in line due to APFC will be lower in comparison to DPFC. It also lowers the third harmonic line losses. Moreover, APFC can be operated at much higher power level than UPFC and DPFC owing to higher rating of ST. Therefore, it offers merits of both of the devices, *i.e.* increased reliability due to absence of dc link, lower harmonics, and low cost. The basic differences between existing FACTS devices UPFC, DPFC, and the proposed APFC are given in Table 4.11.

TABLE 4.11: Comparison amongst APFC, DPFC and UPFC

Parameters	APFC	DPFC	UPFC
Voltage Regulation	Yes	Yes	Yes
Independent line active and reactive power control	Yes	Yes	Yes
Installation and operating costs	Low	Low	High
Reliability	High	High	Poor
Commercial viability	High	Moderate	Low
Adequate response for utility applications	Yes	Yes	Yes
Cost	Low	High	Very high
3^{rd} harmonic current	Low	High	Negligible
Third harmonic losses	Low	High	Negligible
Operating power level	High	High	High
Independent series or shunt regulator	Yes	Yes	No
Rating of series voltage converter ($p.u.$)	0.005	0.05	0.1
Rating of shunt voltage converter ($p.u.$)	1	1	1
Capability of independent reactive power generation and absorption	Yes	Yes	Yes
Controllable parameters (bus voltage V, transmission angle δ, and line impedance Z)	V, δ, Z	V, δ, Z	V, δ, Z

4.6 Summary

This chapter proposed a new member to FACTS family, termed as Amalgam Power Flow Controller (APFC), for fast, reliable and cost effective solution to power flow control. It is the amalgamation of larger capacity of SEN transformer and small capacity of DPFC. In other words, APFC is amalgamation of attributes of both devices. The proposed APFC can regulate the bus voltage, active and reactive power flow through the transmission line simultaneously as well as independently. The APFC can also be operated as shunt or series compensator independently. The major contributions of APFC are:

- Robustness of ST and elimination of common DC-link, increases reliability and security.
- Cost effectiveness since size of DC battery/capacitor required to supply reactive power is reduced as now reactive power can be exchanged through SEN transformer.
- Fast response and continuous control of power flow.
- Common excitation winding of DPFC and ST, eliminates the need of additional transformer, thereby saving the cost.

This chapter also developed a novel hybrid approach to model the APFC. The proposed model is incorporated into standard Newton-Raphson load-flow method for studying its viability and practicability. The model is tested on standard IEEE 30 and 118-bus test systems, and results of simulation proved its excellent convergence characteristics. The main advantages of the proposed mathematical approach are:

- Symmetry of the admittance matrix is preserved.
- Block diagonal property of Jacobian matrix is maintained.
- Better convergence characteristics.
- Provide valuable information of both series and shunt state variables.
- More precise as converter losses are also incorporated.

Chapter 5

Extended Holomorphic Embedded Load-Flow Method for Voltage Stability Assessment

5.1 Introduction

As discussed in Chapter 3, the online assessment of voltage stability state of power system plays a vital role in the reliable operation as well as uninterrupted supply. It also assists the system operator to undertake improved preventive actions before system collapse. Therefore, various line and node based voltage stability indices have been developed to evaluate the available margin and identify weak nodes in the power system. The values of voltage stability indices have been calculated from the power flow results obtained from the iterative numerical methods *e.g.* N-R, FDLF, *etc.* These iterative numerical methods are the core for the solution of non-linear Bus Power Equilibrium Algebraic Equations (BPEEs) in the available commercial software. But these iterative methods mainly suffer from two problems *viz.* need of better initial conditions and poor convergence, particularly when power system is operated close to its maximum loading condition. Several variants of these methods and heuristic techniques were developed to circumvent these problems. But still it is not guaranteed that when no solution is obtained by these iterative techniques what is the pivotal reason. Sometimes these iterative technique may provide spurious solution especially near the voltage collapse point. Therefore, the numerical techniques to solve non-linear BPEEs is the area of interest for the researchers. Another power flow solution technique known as Holomorphic Embedded Load-Flow Method (HELM)

has been developed by Trias in [77]. The convergence of the HELM is guaranteed if the solution exists.

Therefore, the main focus of this chapter is to develop a proper and suitable HE formulation of the PBEs for all type of system buses considering shunt conductance of the transmission line. The shunt conductance of the transmission line is negligible, but when the voltage regulating transformer is represented by its pi-model in steady-state analysis, the total shunt conductance becomes significant. This chapter presents the more practical holomorphic embedded BPEEs for the ZIP type load model considering the shunt conductance and fixed shunt reactive power injections at the buses. This chapter also proposes the new HE formulation where loading of different buses is corresponding to their criticality.

This chapter also demonstrates intuitive potential of node based indices over line based voltage stability indices. Six well-established line voltage stability indices *viz.* *LCPI*, L_{mn}, *FVSI*, *LQP*, L_p, *MLI* and L_s are investigated under diversified loading conditions and compared with node based L-index. The results indicate that the node based Voltage Stability Index (VSI) is better than line based voltage stability indices for identification of weak nodes. A new node voltage stability index based on load and voltage distance to voltage collapse is also proposed for the accurate assessment of the voltage stability state of the power system. The following papers have been accepted/ under review from this chapter:

- Pradeep Singh and Rajive Tiwari, "Extended Holomorphic Embedded Load-Flow and Voltage Stability Assessment of Power Systems", *Electric Power Systems Research. (Under Review).*
- Pradeep Singh, Jyotsna Singh and Rajive Tiwari, "Performance Evaluation and Quality Analysis of Line and Node based Voltage Stability Indices for the Determination of the Voltage Instability Point", *International Conference on Intelligent Computing Techniques for Smart Energy Systems (2018).*

5.2 Illustrative Example

Let's consider a two bus system as shown in Figure 5.1 with buses 1 and 2. Bus 2 is a load bus with $P_2 + jQ_2 = 0.5 + j1$ *p.u.* These two buses are connected through a transmission line of $r_{12} + jx_{12} = 0.05 + j0.1$ *p.u.* impedance and shunt admittance is assumed to

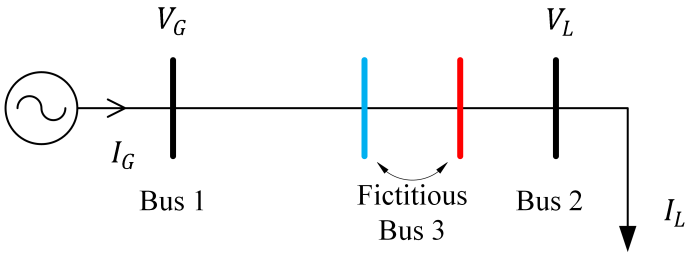

FIGURE 5.1: Two bus system

be zero. In this test system, minimum and maximum reactive power limits of generator have not been accounted. To discriminate the potential of line and node based voltage stability indices, some well developed line based voltage stability indices *viz.* *LCPI* [34], L_{mn} [29], *FVSI* [41], *LQP* [31], L_p [36], *MLI* [35], L_s [37] and most popular node voltage stability index known as L-index [19] are considered for the investigation purpose. A brief description of these indices is included in Appendix A of the thesis. *MLI* index varies from 2 to 1 for no-load to maximum loading point while other indices vary from 0 to 1 for the same situation. At maximum loading point all indices must be equal to 1.

This section investigates and presents simulation results for two bus test system with three different loading conditions, where λ denotes the loading multiplier. Table 5.1 presents the results for increase in both active and reactive load with constant power factor. It is observed that all line stability indices except *MLI* have similar values. for this case power factor angle is equal to impedance angle. From the mathematical formulation of *MLI* as in (A.1.4), it can be observed that for $\phi = \theta$ the denominator of *MLI* becomes zero, therefore, it can't be calculated for this condition.

TABLE 5.1: Comparison of voltage stability indices for two bus system for increase in both active and reactive load with a constant power factor

λ (*p.u.*)	Node	*LCPI* [34]	L_{mn} [29]	*FVSI* [41]	*LQP* [31]	L_p [36]	*MLI* [35]	L_s [37]	L [19]
1.00	2	0.5000	0.5000	0.5000	0.4100	0.5000	*NA*	2.0000	0.1716
1.25	2	0.6250	0.6250	0.6250	0.5156	0.6250	*NA*	1.6000	0.2404
1.50	2	0.7500	0.7500	0.7500	0.6225	0.7500	*NA*	1.3333	0.3333
1.75	2	0.8750	0.8750	0.8750	0.7306	0.8750	*NA*	1.1429	0.4776
2.00	2	1.0000	1.0000	1.0000	0.8400	1.0000	*NA*	1.0000	1.0000

Table 5.2 shows the results for increase in active load only. From Table 5.2, the ineffectiveness of *FVSI* for identifying the voltage collapse condition is observed. For all loading conditions, it always indicates a constant value 0.5 because in the formulation of *FVSI* only reactive power is considered. In this case only *LCPI*, *MLI*, L_s and L indices are capable to identify the voltage collapse condition while remaining indices fail. It is observed

from Tables 5.2 and 5.3 that increase in either active or reactive load ϕ and θ become different, so *MLI* can be calculated and is found to be equal to index L_s.

TABLE 5.2: Comparison of voltage stability indices for two bus system for increase in active load only

λ (*p.u.*)	Node	*LCPI* [34]	L_{mn} [29]	*FVSI* [41]	*LQP* [31]	L_p [36]	*MLI* [35]	L_s [37]	L [19]
2.00	2	0.6023	0.5343	0.5000	0.4400	0.7958	1.6228	1.6228	0.2388
3.00	2	0.7123	0.5835	0.5000	0.4900	0.9539	1.3278	1.3278	0.3475
4.00	2	0.8406	0.6672	0.5000	0.5600	0.9987	1.1111	1.1111	0.5367
4.6601	2	0.9808	0.8465	0.5000	0.6172	0.8835	1.0000	1.0000	0.9909

Table 5.3 shows the results for increase in reactive load only. In this case, *FVSI* prematurely exceeds its critical value *i.e.* 1 indicating that the system had already collapsed. Conversely indices *LQP* and L_p fail to reach their critical value. From the Tables 5.1–5.3, it can be concluded that all indices except L_{mn}, *FVSI*, *LQP* and L_p show actual state of voltage stability for all loading conditions.

TABLE 5.3: Comparison of voltage stability indices for two bus system for increase in reactive load only

λ (*p.u.*)	Node	*LCPI* [34]	L_{mn} [29]	*FVSI* [41]	*LQP* [31]	L_p [36]	*MLI* [35]	L_s [37]	L [19]
1.25	2	0.6001	0.6157	0.6250	0.5100	0.5322	1.6638	1.6638	0.2260
1.50	2	0.7007	0.7271	0.7500	0.6100	0.5722	1.4214	1.4214	0.2958
1.75	2	0.8022	0.8334	0.8750	0.7100	0.6246	1.2392	1.2392	0.3910
2.2132	2	0.9997	0.9982	1.1066	0.8953	0.8838	1.0000	1.0000	0.9976

5.2.1 With One Fictitious Bus in the Middle of the Transmission Line

In this section, a fictitious bus 3 is considered in the middle of the transmission line and the line impedance becomes half. All other network parameters are kept unchanged. Comparison of various voltage stability indices under previously considered scenarios are presented in Tables 5.4–5.6. It can be observed from the Table 5.4, that the performance of all line voltage stability indices is affected. For the same loading level, $\lambda = 2$ the value of *LCPI* changes from 1 to 0.8889 that shows sufficient loading margin is available at maximum loading point. Only node based voltage stability L-index is capable to identify voltage collapse condition in this case. The value of L-index in Table 5.4 is similar to that of in Table 5.1, creation of the fictitious bus results in topological change only while network parameters remain unchanged. It proves that node based index is unaffected by topological change in the system.

TABLE 5.4: Comparison of voltage stability indices for two bus system with one fictitious bus for increase in both active and reactive load with a constant power factor

λ (*p.u.*)	Node	*LCPI* [34]	L_{mn} [29]	*FVSI* [41]	*LQP* [31]	L_p [36]	*MLI* [35]	L_s [37]	L [19]
1.25	3	0.3501	0.3501	0.3501	0.2850	0.3501	*NA*	2.8566	0.1073
	2	0.3832	0.3832	0.3832	0.3124	0.3832	*NA*	2.6098	0.2404
1.50	3	0.4375	0.4375	0.4375	0.3577	0.4375	*NA*	2.2857	0.1429
	2	0.4898	0.4898	0.4898	0.4014	0.4898	*NA*	2.0417	0.3333
1.75	3	0.5420	0.5420	0.5420	0.4453	0.5420	*NA*	1.8451	0.1928
	2	0.6224	0.6224	0.6224	0.5134	0.6224	*NA*	1.6066	0.4776
2.00	3	0.7500	0.7500	0.7500	0.6225	0.7500	*NA*	1.3333	0.3333
	2	0.8889	0.8889	0.8889	0.7427	0.8889	*NA*	1.1250	1.0000

The simulation results for increase in active and reactive load separately are presented in Table 5.5 and Table 5.6 respectively. It is observed that, among all line based voltage stability indices only L_p index detects the collapse condition for increase in active load. When the reactive load is increased all line based voltage stability indices fail but node based L-index still provides promising results.

TABLE 5.5: Comparison of voltage stability indices for two bus system with one fictitious bus for increase in active load only

λ (*p.u.*)	Node	*LCPI* [34]	L_{mn} [29]	*FVSI* [41]	*LQP* [31]	L_p [36]	*MLI* [35]	L_s [37]	L [19]
2.00	3	0.3380	0.2961	0.2878	0.2418	0.4833	2.8986	2.8986	0.1072
	2	0.3655	0.3152	0.3043	0.2582	0.5343	2.6668	2.6668	0.2388
3.00	3	0.4214	0.3402	0.3200	0.2829	0.6630	2.2592	2.2592	0.1506
	2	0.4556	0.3513	0.3236	0.2966	0.7385	2.0514	2.0514	0.3475
4.00	3	0.5385	0.4247	0.3842	0.3588	0.8210	1.7440	1.7440	0.2190
	2	0.4556	0.3513	0.3236	0.2966	0.7385	2.0514	2.0514	0.3475
4.6601	3	0.7245	0.6109	0.5309	0.5084	0.9488	1.3191	1.3191	0.3501
	2	0.7966	0.5886	0.4364	0.5146	0.9999	1.1456	1.1456	0.9909

TABLE 5.6: Comparison of voltage stability indices for two bus system with one fictitious bus for increase in reactive load only

λ (*p.u.*)	Node	*LCPI* [34]	L_{mn} [29]	*FVSI* [41]	*LQP* [31]	L_p [36]	*MLI* [35]	L_s [37]	L [19]
1.25	3	0.3340	0.3442	0.3465	0.2804	0.2920	2.9897	2.9897	0.1016
	2	0.3639	0.3759	0.3790	0.3069	0.3137	2.7435	2.7435	0.2260
1.50	3	0.4024	0.4214	0.4273	0.3455	0.3201	2.4763	2.4763	0.1290
	2	0.4456	0.4688	0.4772	0.3858	0.3428	2.2338	2.2338	0.2958
1.75	3	0.4798	0.5062	0.5171	0.4180	0.3605	2.0726	2.0726	0.1639
	2	0.5408	0.5740	0.5910	0.4773	0.3829	1.8348	1.8348	0.3910
2.2132	3	0.7469	0.7760	0.8064	0.6552	0.5964	1.3322	1.3322	0.3350
	2	0.8793	0.9128	0.9812	0.7929	0.6335	1.1277	1.1277	0.9976

5.2.2 With One Fictitious Bus at $(3/4)^{\text{th}}$ Length of the Transmission Line

Now, a fictitious bus 3 is assumed between the two buses 1 and 2 by dividing the length of transmission line in 3:1 ratio. Therefore, the line impedances become: $r_{13} + jx_{13} = 0.045 + j0.09$ *p.u.*, $r_{32} + jx_{32} = 0.005 + j0.01$ *p.u.* In Table 5.7, the line based indices show that the line 1-3 is critical *i.e.* node 3 is going to collapse for further increase in loading. However, no load has been connected to bus 3. In the considered test system, load is connected at bus 2. Therefore, it is vulnerable to voltage collapse. The value of L-index at bus 2 approaches towards 1, validating the susceptibility of bus 2 to voltage instability. From Tables 5.7–5.9, it can be observed that the line indices provide wrong information about the stressed/critical node. Therefore, the line based voltage stability indices are not reliable and inaccurate in identification of stressed node as well as weak area. In other words, the line indices are not capable to precisely identify the point from where voltage instability instigates. Therefore, the node based indices are more accurate and better than line based indices to identify the weak node area. Line based indices are preferred to find the critical lines of the system.

TABLE 5.7: Comparison of voltage stability indices for two bus system with one fictitious bus at $(3/4)^{th}$ length for increase in both active and reactive load with a constant power factor

λ (*p.u.*)	Node	*LCPI* [34]	L_{mn} [29]	*FVSI* [41]	*LQP* [31]	L_p [36]	*MLI* [35]	L_s [37]	L [19]
1.25	3	0.5760	0.5760	0.5760	0.4741	0.5760	*NA*	1.7360	0.2113
	2	0.0917	0.0917	0.0917	0.0737	0.0917	*NA*	10.905	0.2404
1.50	3	0.6975	0.6975	0.6975	0.5775	0.6975	*NA*	1.4337	0.2903
	2	0.1249	0.1249	0.1249	0.1005	0.1249	*NA*	8.0083	0.3333
1.75	3	0.8251	0.8251	0.8251	0.6873	0.8251	*NA*	1.2120	0.4102
	2	0.1740	0.1740	0.1740	0.1404	0.1740	*NA*	5.7465	0.4776
2.00	3	0.9900	0.9900	0.9900	0.8312	0.9900	*NA*	1.0101	0.8182
	2	0.3306	0.3306	0.3306	0.2688	0.3006	*NA*	3.0250	1.0000

TABLE 5.8: Comparison of voltage stability indices for two bus system with one fictitious bus at $(3/4)^{th}$ length for increase in active load only

λ (*p.u.*)	Node	*LCPI* [34]	L_{mn} [29]	*FVSI* [41]	*LQP* [31]	L_p [36]	*MLI* [35]	L_s [37]	L [19]
2.00	3	0.5552	0.4912	0.4636	0.4043	0.7459	1.7610	1.7610	0.2101
	2	0.0866	0.0727	0.0722	0.0586	0.1402	11.2398	11.2398	0.2388
3.00	3	0.6640	0.5424	0.4752	0.4558	0.9197	1.4257	1.4257	0.3036
	2	0.1137	0.0826	0.0812	0.0673	0.2282	8.1748	8.1748	0.3475
4.00	3	0.7969	0.6332	0.4983	0.5353	0.9978	1.1714	1.1714	0.4629
	2	0.1579	0.1018	0.0986	0.0851	0.3501	5.6353	5.6353	0.5367
4.6601	3	0.9588	0.8289	0.5511	0.6342	0.9392	1.0100	1.0100	0.8276
	2	0.2616	0.1604	0.1505	0.1401	0.5622	3.3220	3.2220	0.9909

TABLE 5.9: Comparison of voltage stability indices for two bus system with one fictitious bus at $(3/4)^{th}$ length for increase in reactive load only

λ $(p.u.)$	Node	*LCPI* [34]	L_{mn} [29]	*FVSI* [41]	*LQP* [31]	L_p [36]	*MLI* [35]	L_s [37]	L [19]
1.25	3	0.5523	0.5672	0.5747	0.4683	0.4883	1.8078	1.8078	0.1989
	2	0.0862	0.0896	0.0898	0.0720	0.0723	11.585	11.585	0.2260
1.50	3	0.6493	0.6751	0.6938	0.5638	0.5272	1.5339	1.5339	0.2586
	2	0.1105	0.1180	0.1184	0.0950	0.0803	9.0006	9.0006	0.2958
1.75	3	0.7502	0.7821	0.8161	0.6621	0.5794	1.3251	1.3251	0.3389
	2	0.1425	0.1548	0.1559	0.1250	0.0916	6.9548	6.9548	0.3910
2.2132	3	0.9875	0.9965	1.0870	0.8813	0.8502	1.0102	1.0102	0.8184
	2	0.3221	0.3540	0.3615	0.2903	0.1786	3.0608	3.0608	0.9976

Results of simulations suggest that node based voltage stability index should be used for planning and monitoring the power system and to take preventive action. It is observed that existing node based indices including L-index does not shows accurate state of voltage stability when the load is other than constant power load. Moreover, all the node based indices measure load distance of a PV curve to estimate the voltage stability margin. Two different shaped PV curve may have same load distance from maximum loading point. Voltage stability state of different shaped PV curve will be different. Although, existing indices measure only load distance from SNB point, therefore, they will show equal voltage stability margin for this case, which is inaccurate. Considering these limitations, a new node based index is proposed that take into account both load distance and voltage distance to accurately assess the voltage stability states of the system. Following section presents the formulation of the proposed index.

5.3 Proposed Node based Voltage Stability Index

Let's consider a simple two bus system shown in Figure 5.1. The load current vector $[I_L]$ using circuit analysis can be written as:

$$\Big[-I_L\Big] = \Big[Y_{LG}\Big]\Big[V_G\Big] + \Big[Y_{LL}\Big]\Big[V_L\Big] \tag{5.1}$$

After rearranging (5.1) for load voltage vector $[V_L]$, we get

$$\Big[V_L\Big] = -\Big[Y_{LL}\Big]^{-1}\Big[Y_{LG}\Big]\Big[V_G\Big] + \Big[Y_{LL}\Big]^{-1}\Big[-I_L\Big] \tag{5.2}$$

Equation (5.2) can also be expressed as:

$$\Big[V_L\Big] = -\Big[V_{eq(G)}\Big] + \frac{\Big[-I_L\Big]}{\Big[Y_{LL}\Big]} \tag{5.3}$$

Where,

$$\Big[V_{eq(G)}\Big] = -\Big[Y_{LL}\Big]^{-1}\Big[Y_{LG}\Big]\Big[V_G\Big] \tag{5.4}$$

For a load bus l, (5.3) can be written as:

$$V_l = V_{eq(g)} + \frac{I_l}{Y_{ll}} \tag{5.5}$$

$$U = 1 + \frac{S_l^*}{Y_{ll}V_l^*V_{eq(g)}\frac{V_{eq(g)}^*}{V_{eq(g)}^*}} \tag{5.6}$$

Where, $U = V_l/V_{eq(g)}$ is a unit less quantity, $S_l = V_l I_l^*$ is the load at the load bus l. Now, let $\sigma_{eq} = S_l^*/(Y_{ll}|V_{eq(g)}|^2)$. So, (5.6) can be rewritten as:

$$|U|^2 = U^* + \sigma_{eq} \tag{5.7}$$

Separating (5.7) into real and imaginary parts, we get

$$|U|^2 = U_{re} + \sigma_{eqre} \tag{5.8}$$

$$0 = -U_{im} + \sigma_{eqim} \tag{5.9}$$

By squaring both sides and adding (5.8) and (5.9), we get

$$f(|U|^2) = |U|^4 - (1 + 2\sigma_{eqre})|U|^2 + |\sigma_{eq}|^2 = 0 \tag{5.10}$$

Equation (5.10) can be viewed as a quadratic equation and Figure 5.2 is the graphical representation of this quadratic equation with vertex (k, h), where $h = -\frac{b}{2a}$ and $k = f(h)$. Where, b and a are the linear and quadratic coefficients of (5.10). The roots of (5.10) are:

$$|U|^2 = \frac{(1 + 2\sigma_{eqre})}{2} \pm \frac{1}{2}\sqrt{\Big[1 - 2\big(|\sigma_{eq}| - \sigma_{eqre}\big)\Big]\Big[1 + 2\big(|\sigma_{eq}| + \sigma_{eqre}\big)\Big]} \tag{5.11}$$

Now for the feasible solution *i.e.* for real roots, the term $\{1-2(|\sigma_{eq}|-\sigma_{eqre})\}$ of (5.11) must be greater than zero (*i.e.* $|\sigma_{eq}| \leq (0.5 + \sigma_{eqre})$) because the other term *i.e.* $\{1 + 2(|\sigma_{eq}| + \sigma_{eqre})\}$ can't be negative. From Figure 5.2, it is observed that the voltage distance (V.D.)

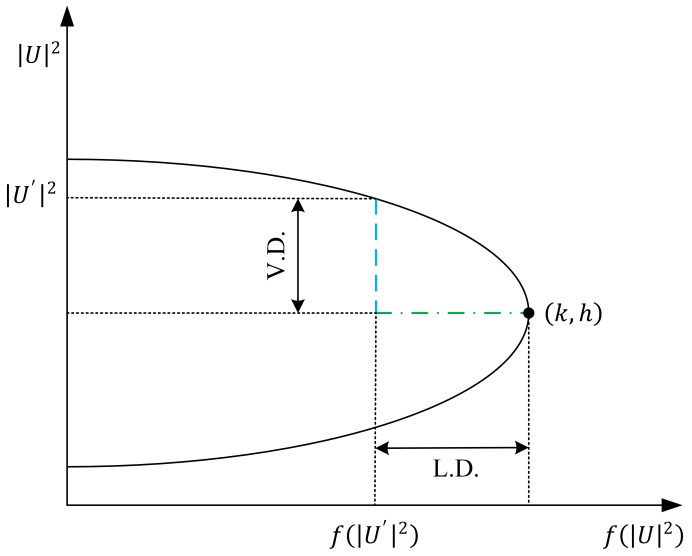

FIGURE 5.2: Graphical representation of distance to SNB point

and load distance (L.D.) are equal to $|U|^2 - 0.5(1 + 2\sigma_{eqre})$ and $(1 - 2(|\sigma_{eq}| - \sigma_{eqre}))/2$ respectively from the SNB point. At the boundary condition, the unit less quantity from (5.11) is $|U|^2 = |\sigma_{eq}|$. At the boundary condition, (*i.e.* $|\sigma_{eq}| = (0.5 + \sigma_{eqre})$, the voltage and load distance are equal to zero. It can be observed that as the system moves towards the voltage collapse, both the voltage and load distance (and consequently their sum) tend to zero. Therefore, the sum of these distances is an indicator of voltage stability state. Hence, the voltage stability index is proposed as sum of load distance and voltage distance. The proposed index *i.e.* Load Voltage Distance Index (LVDI) can be written in the form of equivalent distance from SNB point as follows:

$$LVDI = V.D. + L.D. = |U|^2 - \frac{(1 + 2\sigma_{eqre})}{2} + \frac{(1 - 2|\sigma_{eq}| + 2\sigma_{eqre})}{2} \tag{5.12}$$

For a voltage stable system proposed index must be greater than zero.

$$LVDI = |U|^2 - |\sigma_{eq}| > 0 \tag{5.13}$$

The proposed index is an accurate indicator of voltage stability as it accounts both voltage and load distance aspects of voltage instability. All the buses can be ranked in the order of criticality using proposed index. Mathematically, the most critical bus 'l' can be identified as:

$$\min_{l} LVDI \ ; \ l \in PQ \tag{5.14}$$

Where, PQ is the set of load buses. Proposed index varies from 1 to 0 for no-load to

voltage collapse condition. Accuracy of the proposed index depends upon accuracy of power flow results for ill-conditioned system. To obtain accurate results of power flow, Holomorphic Embedded Load-Flow Method (HELM) is used in place of N-R method. A brief overview of HELM is shown below.

5.4 Overview of HELM

A holomorphic function is a complex-valued analytic function, which has the property that it is infinitely complex differentiable around every point within its domain. Another property of holomorphic functions important for the purpose here is that they can be represented by their Taylor series in the neighborhood of each point in their domain [78]. To address the load-flow problem using holomorphic embedding method, one needs to embed the complex voltage variables as holomorphic functions. For this following procedure is adopted:

For embedding the power balance and voltage constraint equations of the power system buses, first requirement of holomorphic embedding method is that at complex parameter $s = 0$, all injected terms vanish to zero and the system is trivially solvable by linear algebra, and at $s = 1$ original equation must be recovered. So, at $s = 0$ system is considered without load, generation, and shunt elements. Only slack bus maintains voltages at all the buses in the system. The solution of the equations at $s = 0$ is known as the germ solution. Another requirement of the method is that the bus voltage V_i should be holomorphic function in the complex embedding parameter s. To satisfy the Cauchy-Riemann condition of holomorphic function; the term $V_i^*(s^*)$ is used in place of $V_i^*(s)$. The final objective of HELM modeling is to develop the power series for every unknown variable and to compute the numerical values of unknown variable using Padé approximants. As per [77], any holomorphic function (say $V_i(s)$) can be expressed as power series using Maclurin series in the following way:

$$V_i(s) = \sum_{n=0}^{\infty} V[n]s^n \tag{5.15}$$

Where, $V[n]$ is the power series coefficient of the degree n, and n is the index number. A general recurrence formula can be obtained by expressing all unknown variables using power series and comparing the coefficients of powers of s. The coefficients of power series of $V[n]$ are calculated using general recurrence formula and germs solution for any value of n. Afterwards the numerical values of unknown variables at $s = 1$ are to be computed. It requires to perform maximal analytic continuation of the initial solution at $s = 0$ along

the path that ensures single valuedness [118]. Stahl's theorem and [119] describe that the diagonal/near diagonal Padé approximants of the power series are subjected to the maximal analytic continuation. If the Padé approximants converge, then the physical feasible solution will exist and the obtained results are guaranteed to be the analytic continuation of the white branch at $s = 1$. There will not be any solution, if Padé approximants oscillate. The Padé approximants are rational functions of the power series and can be expressed as under:

$$\sum_{n=0}^{\infty} V[n]s^n = \frac{a_0 + a_1 s + a_2 s^2 + ... + a_L s^L}{b_0 + b_1 s + b_2 s^2 + ... + b_L s^M} + O(s^{L+M+1}) \tag{5.16}$$

The set of linear equations can be written in matrix form in the following way:

$$\left[\begin{array}{c} a_0 \\ a_1 \\ \vdots \\ a_M \\ \vdots \\ a_L \\ \hline \\ a_{L+1} \\ \vdots \\ a_{L+M} \end{array}\right] = \left[\begin{array}{cccc} V[0] & & & \\ V[1] & V[0] & & \\ \vdots & \vdots & & \\ V[M] & V[M-1] & \dots & V[0] \\ \vdots & \vdots & & \vdots \\ V[L] & V[L-1] & \dots & V[L-M] \\ \hline & & & \\ V[L+1] & V[L] & \dots & V[L+1-M] \\ \vdots & \vdots & \vdots & \vdots \\ V[L+M] & V[L+M-1] & \dots & V[L] \end{array}\right] \left[\begin{array}{c} b_0 \\ b_1 \\ \vdots \\ b_M \end{array}\right] \tag{5.17}$$

Where, the values of coefficients a_{L+1} to a_{L+M} are equal to zero. Generally, normalization is carried out by assuming $b_0 = 1$. The set of linear equations as per (5.17) may be singular or ill-conditioned. This may be due to degeneracy of the power series or increase in rounding error [85]. Therefore, in this research work singular value decomposition (SVD) based Padé approximants are used to handle the degeneracy of the power series; *i.e.* to eliminate the problem of singularity and ill-conditioning [120]. For this purpose, normalization is carried out using the condition $||b|| = 1$, *i.e.* vector 2-norm of b. If lower part of matrix V is denoted as $\tilde{V}$ then SVD of matrix $\tilde{V}$ can be represented as:

$$\tilde{V} = U\Sigma\nu^T \tag{5.18}$$

Where Σ is an $M \times (M+1)$ real diagonal matrix with diagonal entries $\lambda_1, \lambda_2, ...\lambda_M$. If $\lambda_M > 0$ (*i.e.* $\tilde{V}$ has rank M) then the last column of vector ν provides a unique non-zero null vector b of $\tilde{V}$ up to a scale factor. If $\lambda_M = 0$, rank of $\tilde{V}$ must be less than M. Let ρ

represents the rank of $\tilde{V}$. Now to choose proper L and M, the degree of the denominator polynomial is reduced from M to ρ and the degree of the numerator polynomial is reduced from L to $L-M+\rho$ [120]. Equation (5.17) is reconstructed according to the updated values of L and M. The procedure is repeated until and unless all the singular values λ become larger than the specified tolerance value. Finally, the coefficients a and b can be obtained from (5.17) and the numerical values of unknown variables at $s = 1$ can be evaluated using (5.16). Therefore, the SVD based method provides unique Padé approximants in a minimal degree representation [85].

5.5 Extended HELM Formulation for ZIP type Load

ZIP type load is a more realistic representation of existing load on power systems which requires a proper holomorphic modeling. Therefore, throughout this chapter the ZIP type load model are considered. The conventional ZIP load model can be represented as:

$$P_{Li} = P_{Li}^{0}\big(\alpha_p|V_i|^2 + \beta_p|V_i| + \gamma_p\big) \tag{5.19}$$

$$Q_{Li} = Q_{Li}^{0}\big(\alpha_q|V_i|^2 + \beta_q|V_i| + \gamma_q\big) \tag{5.20}$$

Where, $\alpha_p, \beta_p, \gamma_p$ and $\alpha_q, \beta_q, \gamma_q$ are the constant impedance, current and power components of real and reactive loads respectively.

5.5.1 Slack Bus HE Modeling

The voltage and angle of the slack bus are specified. Therefore, the voltage phasor of the slack bus $'i'$ can be expressed as:

$$V_i = V_i^{SP};\ i \in SB \tag{5.21}$$

Equation (5.21) can be holomorphically embedded as per [78]:

$$V_i(s) = 1 + s(V_i^{SP} - 1);\ i \in SB \tag{5.22}$$

Where, s is a complex-valued embedding parameter. The solution of (5.22) at $s = 0$ offers germ solution which is as follows:

$$V_i[0] = 1;\ i \in SB \tag{5.23}$$

From (5.23), it is observed that the germ solution of slack bus voltage is 1 *p.u.* As discussed in Section 5.4, at $s = 1$ original equation can be recovered (*i.e.* the slack bus voltage is equal to V_i^{SP}).

5.5.1.1 Power series expansion of slack bus HE equation

Since equation (5.22) is holomorphically embedded, the slack bus voltage phasor can be represented by Maclaurin power series using (5.15) and it can be expressed as follows:

$$V_i[0] + V_i[1]s + V_i[2]s^2 + ... = 1 + s(V_i^{SP} - 1);\ i \in SB \tag{5.24}$$

A generalized recurrence relation for (5.24) can be deduced by comparing the coefficients of s^n and it can be expressed as follows:

$$V_i[n] = \eta_{n1}(V_i^{SP} - 1);\ i \in SB;\ \text{for } n \geq 1 \tag{5.25}$$

Where,

$$\eta_{nk} = \begin{cases} 1 & \text{if} n = k \\ 0 & \text{otherwise} \end{cases} \tag{5.26}$$

The function η_{nk} is introduced to represent the recurrence relationship in terms of power series coefficients. The RHS of (5.25) is denoted as RHS_Known_Slack in further analysis. The power series coefficients of $V_i[n]$ for $n \geq 1$ can be evaluated by (5.25).

5.5.2 Load Bus HE Modeling

Any load bus can be described by its active and reactive power balance equation. The loads are assumed to be ZIP type load as given in (5.19) and (5.20). Therefore, the complex power balance equation (PBE) for i^{th} load bus can be expressed as:

$$\sum_{k=1}^{N} Y_{ik}V_k = \frac{P_{Gi} - jQ_{Gi}}{V_i^*} - P_{Li}^0\left[\alpha_p V_i + \frac{\beta_p|V_i| + \gamma_p}{V_i^*}\right] + jQ_{Li}^0\left[\alpha_q V_i + \frac{\beta_q|V_i| + \gamma_q}{V_i^*}\right] - \frac{jQ_i^{Sh}}{V_i^*} \tag{5.27}$$

In (5.27), V_i, $S_i = (P_{Gi} - jQ_{Gi}) - (P_{Li} - jQ_{Li})$, Y_{ik}, and Q_i^{Sh} are the voltage of bus i, injected complex power at bus i, $(i,k)^{th}$ element of bus admittance matrix, and injected shunt reactive power at bus i respectively. Equation (5.27) can be holomorphically embedded as

follows:

$$\sum_{k=1}^{N} Y_{ik}^{tr(SY)} V_k(s) = s(P_{Gi} - jQ_{Gi}) W_i^*(s^*) + jsQ_{Li}^0 \Big[\alpha_q V_i(s) + \big(\beta_q |V_i|(s) + \gamma_q\big) W_i^*(s^*)\Big]$$

$$-sP_{Li}^0 \Big[\alpha_p V_i(s) + \big(\beta_p |V_i|(s) + \gamma_p\big) W_i^*(s^*)\Big] - sY_i^{Shunt} V_i(s) - jsQ_i^{Sh} W_i^*(s^*) - s\sum_{k=1}^{N} Y_{ik}^{tr(Un)} V_k(s);$$

$$i \in PQ \quad (5.28)$$

Where, PQ is the set of load buses. $Y_{ik}^{tr(SY)}$, $Y_{ik}^{tr(Un)}$, and Y_i^{Shunt} are the symmetrical, unsymmetrical, and shunt branch parts of the bus admittance matrix respectively. To fulfill the Wirtinger's derivative condition for holomorphic function [121], $W_i^*(s^*)$ is used in (5.28) in place of $W_i^*(s)$. Solution of (5.28) at $s = 0$ offers germ solutions which is given as follows:

$$\sum_{k=1}^{N} Y_{ik}^{tr(SY)} V_k[0] = 0;\ i \in PQ \quad (5.29)$$

As per (5.29), germ solution for load bus voltage is $1\angle 0°$. $W_i(s)$ is the inverse power series of $V_i(s)$. Therefore, the relationship between $W_i(s)$ and $V_i(s)$ for all buses can be expressed as follows:

$$W_i(s) V_i(s) = 1;\ i \in N \quad (5.30)$$

A general recurrence formula of $W_i[n]$ for all buses can be deduced by comparing the coefficients of s^n after expanding (5.30) using (5.15) and it can be expressed as follows:

$$W_i[n] = -\frac{1}{V_i[0]} \sum_{k=0}^{n-1} W_i[k] V_i[n-k];\ i \in N;\ \text{for } n \geq 1 \quad (5.31)$$

Similarly, a general recurrence formula for $|V_i|[n]$ can be obtained using $V_i(s)V_i^*(s^*) = |V_i|(s)|V_i|(s)$ relationship and obtained expression is presented in (5.32).

$$|V_i|[n] = V_{ire}[n] + \frac{1}{2}\left[\sum_{k=1}^{n-1} V_i[k] V_i^*[n-k] - |V_i|[k]|V_i|[n-k]\right];\ i \in N;\ \text{for } n \geq 1 \quad (5.32)$$

The germ solutions $W_i[0]$ and $|V_i|[0]$ can be obtained by substituting $s = 0$ in their respective equations.

5.5.2.1 Power series expansion of load bus HE equation

The holomorphically embedded equation of load bus as presented in (5.28) can be expanded using (5.15) as follows:

$$\sum_{k=1}^{N} Y_{ik}^{tr(SY)}(V_k[0]+V_k[1]s+V_k[2]s^2+....) = s(P_{Gi}-jQ_{Gi})(W_i^*[0]+W_i^*[1]s+W_i^*[2]s^2+....)$$
$$- sP_{Li}^0\Big[\alpha_p(V_i[0]+V_i[1]s+....)+\big\{\beta_p(|V_i|[0]+|V_i|[1]s+....)+\gamma_p\big\}\big\{W_i^*[0]+W_i^*[1]s+....\big\}\Big]$$
$$+ jsQ_{Li}^0\Big[\alpha_q(V_i[0]+V_i[1]s+....)+\big\{\beta_q(|V_i|[0]+|V_i|[1]s+....)+\gamma_q\big\}\big\{W_i^*[0]+W_i^*[1]s+....\big\}\Big]$$
$$-sY_i^{Shunt}(V_i[0]+V_i[1]s+...)-jsQ_i^{Sh}(W_i^*[0]+W_i^*[1]s+....)-s\sum_{k=1}^{N} Y_{ik}^{tr(Un)}(V_k[0]+V_k[1]s+....)$$
$$; \ i \in PQ; \ \text{for } n \geq 1 \quad (5.33)$$

By comparing the coefficients of s^n on both sides of (5.33), a recurrence relation to calculate the power series coefficients is obtained. The general recurrence formula to calculate the power series coefficients of $V_i[n]$ for $n \geq 1$ can be expressed as follows:

$$\sum_{k=1}^{N} Y_{ik}^{tr(SY)}V_k[n] = (P_{Gi}-jQ_{Gi})W_i^*[n-1]-P_{Li}^0\Bigg[\alpha_pV_i[n-1]+\beta_p\sum_{d=0}^{n-1}|V_i|[d]W_i^*[n-1-d]$$
$$+\gamma_pW_i^*[n-1]\Bigg]+jQ_{Li}^0\Bigg[\alpha_qV_i[n-1]+\beta_q\sum_{d=0}^{n-1}|V_i|[d]W_i^*[n-1-d]+\gamma_qW_i^*[n-1]\Bigg]$$
$$-Y_i^{Shunt}V_i[n-1]-jQ_i^{Sh}W_i^*[n-1]-\sum_{k=1}^{N} Y_{ik}^{tr(Un)}V_k[n-1]; i \in PQ; \ \text{for } n \geq 1 \quad (5.34)$$

$$\sum_{k=1}^{N} Y_{ik}^{tr(SY)}V_k[n] = RHS\_Known\_PQ[n-1]; i \in PQ; \ \text{for } n \geq 1 \quad (5.35)$$

5.5.3 Generator Bus HE Modeling

Any generator bus can be described by its active power balance equation by summing the complex power and its conjugate, and specified voltage magnitude constraint. Mathematically,

$$V_i\sum_{k=1}^{N} Y_{ik}^*V_k^* + V_i^*\sum_{k=1}^{N} Y_{ik}V_k = 2(P_{Gi}-P_{Li}); i \in PV \quad (5.36)$$

$$|V_i|^2 = V_iV_i^* = |V_i^{SP}|^2; i \in PV \quad (5.37)$$

Where, PV and V_i^{SP} is the set of generator buses and specified voltage magnitude of the i^{th} generator bus respectively. By putting the P_{Li} from (5.19), we get

$$V_i \sum_{k=1}^{N} \left(Y_{ik}^{tr(SY)}\right)^* V_k^* + V_i^* \sum_{k=1}^{N} Y_{ik}^{tr(SY)} V_k + |V_i|^2 \Re(2Y_i^{Shunt}) = 2P_{Gi} - 2P_{Li}^0 \Big(\alpha_p |V_i|^2 + \beta_p |V_i| + \gamma_p\Big) - V_i \sum_{k=1}^{N} \left(Y_{ik}^{tr(Un)}\right)^* V_k^* - V_i^* \sum_{k=1}^{N} Y_{ik}^{tr(Un)} V_k \quad (5.38)$$

Equations (5.37) and (5.38) can be expressed as a function of complex parameter s as follows:

$$V_i(s) V_i^*(s^*) = 1 + s\big(|V_i^{SP}|^2 - 1\big);\ i \in PV \quad (5.39)$$

$$V_i(s) \sum_{k=1}^{N} \left(Y_{ik}^{tr(SY)}\right)^* V_k^*(s^*) + V_i^*(s^*) \sum_{k=1}^{N} Y_{ik}^{tr(SY)} V_k(s) + s|V_i|(s)|V_i|(s) \Re(2Y_i^{Shunt}) = 2sP_{Gi} - 2sP_{Li}^0\big(\alpha_p |V_i|(s)|V_i|(s) + \beta_p |V_i|(s) + \gamma_p\big) - sV_i(s) \sum_{k=1}^{N} \left(Y_{ik}^{tr(Un)}\right)^* V_k^*(s^*) - sV_i^*(s^*) \sum_{k=1}^{N} Y_{ik}^{tr(Un)} V_k(s);\ i \in PV \quad (5.40)$$

As a necessary condition for correct way of embedding, the original active power balance equation and the voltage magnitude constraint of the generator bus are retrieved at $s = 1$. The germ solutions are analogous to flat voltage profile start as in conventional NRLF method. Both the germ solutions and flat voltage profile start act as initial conditions for solving the power flow. However, the germ solutions are deterministic in nature. To obtain the correct solution at $s = 1$, the germ solution must be correct. The germ solution can be obtained by simultaneously solving the holomorphically embedded equation of load bus, generator bus and slack bus at $s = 0$. The germ solutions for voltage phasor of the i^{th} bus is $V_i[0] = 1\angle 0$, where $i \in N$.

5.5.3.1 Power series expansion of generator bus HE equation

Let's consider the term $\left(i.e. V_i^*(s^*) \sum_{k=1}^{N} Y_{ik}^{tr(SY)} V_k(s)\right)$ of (5.40). Using (5.15), it can be expanded as follows:

$$V_i^*(s^*) \sum_{k=1}^{N} Y_{ik}^{tr(SY)} V_k(s) = \sum_{k=1}^{N} Y_{ik}^{tr(SY)} (V_k[0] + V_k[1]s + ...)(V_i^*[0] + V_i^*[1]s + ...) \quad (5.41)$$

A generalized recurrence relation can be obtained as follows:

$$V_i^*(s^*)\sum_{k=1}^{N} Y_{ik}^{tr(SY)}V_k(s) = \sum_{k=1}^{N} Y_{ik}^{tr(SY)}\sum_{d=0}^{n} V_k[d]V_i^*[n-d] \tag{5.42}$$

The another term $\left(V_i(s)\sum_{k=1}^{N}(Y_{ik}^{trans})^*V_k^*(s^*)\right)$ of (5.40) is treated in similar manner. Now, consider the remaining terms of (5.40):

$$\begin{aligned}2s|V_i|(s)|V_i|(s)\Re(Y_i^{Shunt}) = 2sP_{Gi} - 2sP_{Li}^0\big(\alpha_p|V_i|(s)|V_i|(s) + \beta_p|V_i|(s) + \gamma_p\big)\\ - sV_i^*(s^*)\sum_{k=1}^{N} Y_{ik}^{tr(Un)}V_k(s) - sV_i(s)\sum_{k=1}^{N}\left(Y_{ik}^{tr(Un)}\right)^*V_k^*(s^*)\end{aligned} \tag{5.43}$$

Using (5.15), equation (5.43) can be expressed as follows:

$$\begin{aligned}&2s(|V_i|[0]+|V_i|[1]s+....)(|V_i|[0]+|V_i|[1]s+....)\Re(Y_i^{Shunt}) = 2sP_{Gi} - 2sP_{Li}^0\Big[\alpha_p(|V_i|[0]+\\ &|V_i|[1]s+....)(|V_i|[0]+|V_i|[1]s+....)+\beta_p(|V_i|[0]+|V_i|[1]s+....)+\gamma_p\Big] - s\sum_{k=1}^{N} Y_{ik}^{tr(Un)}(V_k[0]\\ &+V_k[1]s+....)(V_i^*[0]+V_i^*[1]s+....) - s\sum_{k=1}^{N} Y_{ik}^{tr(Un)}(V_k^*[0]+V_k^*[1]s+....)(V_i[0]+V_i[1]s+....)\end{aligned} \tag{5.44}$$

A recurrence relation for (5.44) can be expressed as follows:

$$\begin{aligned}&2\Re(Y_i^{Shunt})\sum_{d=0}^{n-1}|V_i|[d]|V_i|[n-1-d] = 2\eta_{n1}P_{Gi} - 2P_{Li}^0\Bigg[\alpha_p\sum_{d=0}^{n-1}|V_i|[d]|V_i|[n-1-d]+\eta_{n1}\gamma_p\\ &+\beta_p|V_i|[n-1]\Bigg] - \sum_{k=1}^{N} Y_{ik}^{tr(Un)}\sum_{d=0}^{n-1} V_k[d]V_i^*[n-d-1] - \sum_{k=1}^{N}\left(Y_{ik}^{tr(Un)}\right)^*\sum_{d=0}^{n-1} V_k^*[d]V_i[n-d-1]\end{aligned} \tag{5.45}$$

A generalized recurrence formula for (5.40) can be obtained by taking sum of general recurrence relations of each individual term of (5.40) and it can be written as follows:

$$\sum_{k=1}^{N} Y_{ik}^{tr(SY)}\Big[V_k[0]V_i^*[n]+V_k[n]V_i^*[0]\Big]+\sum_{k=1}^{N}\Big(Y_{ik}^{tr(SY)}\Big)^*\Big[V_k^*[0]V_i[n]+V_k^*[n]V_i[0]\Big] = 2\eta_{n1}P_{Gi}$$
$$-2P_{Li}^0\left[\alpha_p\sum_{d=0}^{n-1}|V_i|[d]|V_i|[n-1-d]+\beta_p|V_i|[n-1]+\eta_{n1}\gamma_p\right]-\sum_{k=1}^{N}Y_{ik}^{tr(SY)}\sum_{d=1}^{n-1}V_k[d]V_i^*[n-d]$$
$$-\sum_{k=1}^{N}\Big(Y_{ik}^{tr(SY)}\Big)^*\sum_{d=1}^{n-1}V_k^*[d]V_i[n-d]-2\Re(Y_i^{Shunt})\sum_{d=0}^{n-1}|V_i|[d]|V_i|[n-1-d]$$
$$-\sum_{k=1}^{N}Y_{ik}^{tr(Un)}\sum_{d=0}^{n-1}V_k[d]V_i^*[n-d-1]-\sum_{k=1}^{N}\Big(Y_{ik}^{tr(Un)}\Big)^*\sum_{d=0}^{n-1}V_k^*[d]V_i[n-d-1] \quad (5.46)$$

$$\sum_{k=1}^{N} Y_{ik}^{tr(SY)}\Big[V_k[0]V_i^*[n]+V_k[n]V_i^*[0]\Big]+\sum_{k=1}^{N}\Big(Y_{ik}^{tr(SY)}\Big)^*\Big[V_k^*[0]V_i[n]+V_k^*[n]V_i[0]\Big] =$$
$$= RHS\_Known\_PV\_P[n-1];\ i\in PV;\ \text{for } n\geq 1 \quad (5.47)$$

Similarly, a recurrence formula needs to be developed for the voltage magnitude constraints of the generator bus. Equation (5.39) can be expanded as follows:

$$\big(V_i[0]+V_i[1]s+V_i[2]s^2+....\big)\big(V_i^*[0]+V_i^*[1]s+V_i^*[2]s^2+....\big)=1+s(|V_i^{sp}|^2-1) \quad (5.48)$$

By comparing the coefficients of s^n, a general recurrence formula of $V_{ire}[n]$ for $n\geq 1$ can be obtained as follows:

$$V_{ire}[n]=\eta_{n1}\frac{|V_i^{SP}|^2-1}{2}-\frac{1}{2}\sum_{d=1}^{n-1}V_i[d]V_i^*[n-d];\ i\in PV;\ \text{for } n\geq 1 \quad (5.49)$$

$$V_{ire}[n]=RHS\_Known\_PV\_V[n-1];\ i\in PV;\ \text{for } n\geq 1 \quad (5.50)$$

Where, $V_{ire}[n]$ represents the n^{th} coefficient of the real part of voltage power series. Equations (5.46) and (5.49) represent a consistent system of equations for the generator bus model that has a unique solution. As discussed in Section 5.4, the next objective is to rearrange (5.25), (5.34), (5.46), and (5.49) such that the resultant equations can be represented as linear matrix equation in explicit form. To represent all equations in explicit form, all known and unknown variables must be shifted to LHS and RHS respectively. For this purpose variables are separated into real and imaginary parts as $Y_{ik}^{tr(SY)}=G_{ik}^{SY}+jB_{ik}^{SY}$, $V_i[n]=V_{ire}+jV_{iim}$. After performing lots of algebraic operations, the linear matrix in explicit form can be represented as in (5.51) for N-bus power system. Where, subscripts r, m, and p denote the slack bus, load bus, and generator bus respectively. Now, the voltage phasors of all buses are calculated using SVD based Padé approximation to handle the degeneracy cases of power series.

$$\begin{bmatrix} & \vdots & \vdots & & \vdots & \vdots & & \vdots & \vdots & \\ \dots & 1 & 0 & \dots & 0 & 0 & \dots & 0 & 0 & \dots \\ \dots & 0 & 1 & \dots & 0 & 0 & \dots & 0 & 0 & \dots \\ & \vdots & \vdots & & \vdots & \vdots & & \vdots & \vdots & \\ \dots & G^{SY}_{mr} & -B^{SY}_{mr} & \dots & G^{SY}_{mm} & -B^{SY}_{mm} & \dots & G^{SY}_{mp} & -B^{SY}_{mp} & \dots \\ \dots & B^{SY}_{mr} & G^{SY}_{mr} & \dots & B^{SY}_{mm} & G^{SY}_{mm} & \dots & B^{SY}_{mp} & G^{SY}_{mp} & \dots \\ & \vdots & \vdots & & \vdots & \vdots & & \vdots & \vdots & \\ \dots & \mu_{pr} & \xi_{pr} & \dots & \mu_{pm} & \xi_{pm} & \dots & \mu_{pp} & \xi_{pp} & \dots \\ \dots & 0 & 0 & \dots & 0 & 0 & \dots & 1 & 0 & \dots \\ & \vdots & \vdots & & \vdots & \vdots & & \vdots & \vdots & \end{bmatrix} \begin{bmatrix} \vdots \\ V_{rre}[n] \\ V_{rim}[n] \\ \vdots \\ V_{mre}[n] \\ V_{mim}[n] \\ \vdots \\ V_{pre}[n] \\ V_{pim}[n] \\ \vdots \end{bmatrix} = \begin{bmatrix} \vdots \\ RHS\_Known\_Slack[n-1] \\ 0 \\ \vdots \\ \Re(RHS\_Known\_PQ[n-1]) \\ \Im(RHS\_Known\_PQ[n-1]) \\ \vdots \\ RHS\_Known\_PV\_P[n-1] \\ RHS\_Known\_PV\_V[n-1] \\ \vdots \end{bmatrix} \tag{5.51}$$

Where,

$$\mu_{ik} = 2\big(G^{SY}_{ik} V_{ire}[0] + B^{SY}_{ik} V_{iim}[0]\big),\ k \neq i \tag{5.52}$$

$$\zeta_{ik} = 2\big(G^{SY}_{ik} V_{iim}[0] - B^{SY}_{ik} V_{ire}[0]\big),\ k \neq i \tag{5.53}$$

$$\mu_{ii} = 2\left[G^{SY}_{ii} V_{ire}[0] + B^{SY}_{ii} V_{iim}[0] + \sum_{k=1}^{N} \big(G^{SY}_{ik} V_{kre}[0] - B^{SY}_{ik} V_{kim}[0]\big)\right] \tag{5.54}$$

$$\zeta_{ii} = 2\left[G^{SY}_{ii} V_{iim}[0] - B^{SY}_{ii} V_{ire}[0] + \sum_{k=1}^{N} \big(G^{SY}_{ik} V_{kim}[0] + B^{SY}_{ik} V_{kre}[0]\big)\right] \tag{5.55}$$

5.6 Results and Discussions

The IEEE 30 and 118-bus test systems are considered with the different loading combination to investigate the potential of the proposed index. Power flow results of HELM is used to compute the value of proposed index. The line and bus data of both systems are taken from [114] and are given in Appendix B. A MATLAB code is developed to perform the test [115]. The results are compared with L-index [19] to prove its suitability and feasibility. The results of simulation are presented in following sections.

5.6.1 IEEE 30-Bus Test System

As mentioned, the IEEE 30-bus test system is considered for investigation of the proposed index. The proposed index and L-index are evaluated for different loading conditions. Results for 1.56 times MVA of the system are shown in Table 5.10 and Figure 5.3. Both the proposed-index and the L-index denote bus 30 as the weakest bus. The proposed index for bus 30 reaches to 0.0086 at the voltage stability limit, but the L-index fails to reach near its critical value 1.0. This can also be observed from Figure 5.3. The strongest load bus in the IEEE 30-bus test system is bus no. 2, for which proposed index is 0.6363 and L-index is 0.2077. The top ten stressed load buses are ranked, and listed in Table 5.10, on the basis of proposed-index. It is observed that the L-index is consistent with the proposed-index except with only small disagreement for buses 25 and 18. It is to be noted here that lower value of L-index and higher value of proposed index is an indication of higher voltage stability margin.

Table 5.10: Ranking of buses for IEEE 30-bus test system

Node No.	L-index	Proposed Index	Node No.	L-Index	Proposed Index
30	0.8935	0.0086	25	0.7580	0.1053
26	0.8234	0.0476	18	0.7581	0.1133
29	0.8214	0.0581	23	0.7518	0.1153
24	0.7708	0.0969	20	0.7520	0.1188
19	0.7700	0.1032	21	0.7287	0.1361

The proposed index is also tested for heavy active loading at different nodes. The real load at different nodes is increased upto the voltage collapse point [34]. The real load of value 2.57 *p.u.* at node 6 makes the node 30 most critical node with proposed index value 0.0037. The L-index with the value 0.9312 identifies the same node as the most critical node. The ranking of nodes are consistent with L-index but L-index falls behind from its

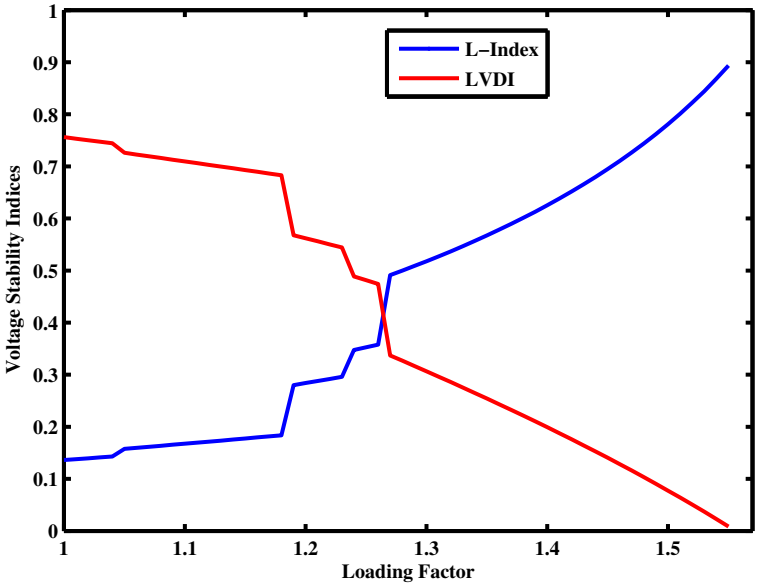

FIGURE 5.3: Variation of voltage stability indices with both real and reactive load for IEEE 30-bus test system

TABLE 5.11: Test results of IEEE 30-bus test system at increased real load of selected nodes

Node Loading ($p.u.$)	Node No.	L-Index	Proposed Index
P = 2.57 at node 6	30	0.9312	0.0037
	29	0.8893	0.0345
	26	0.8776	0.0389
	25	0.8406	0.0745
	24	0.8317	0.0858
	27	0.8275	0.0858
P = 0.83 at node 27	30	0.8806	0.0016
	29	0.8448	0.0322
	27	0.7922	0.0823
	26	0.7328	0.1137
	25	0.7046	0.1486
	24	0.5459	0.3053

critical value at voltage collapse. Similar results are obtained for node 27 with real load of value 0.83 $p.u.$ Simulation are carried out for heavy reactive loading. Node 30 is identified as the most critical node for value of reactive load 2.4 $p.u.$ at node 6 and 0.62 $p.u.$ load at node 27. The results are confirmed by L-index. From Table 5.12, it is observed that the L-index is far behind its critical value 1. Value 0.8114 shows that it is unable to detect voltage instability when the reactive load of value 0.62 $p.u.$ is assigned to node 27.

TABLE 5.12: Test results of IEEE 30-bus test system at increased reactive load of selected nodes

Node Loading (*p.u.*)	Node No.	*L*-Index	Proposed Index
Q=2.4 at node 6	30	0.9599	0.0100
	29	0.8884	0.0426
	26	0.8742	0.0464
	25	0.8019	0.0878
	27	0.7822	0.0979
	24	0.7786	0.1050
Q =0.62 at node 27	30	0.8114	0.0217
	29	0.7511	0.0542
	27	0.6607	0.1090
	26	0.6120	0.1500
	25	0.5637	0.1903
	24	0.4307	0.3558

TABLE 5.13: Test results of IEEE 30-bus test system at increased real and reactive load of selected nodes

Node Loading (*p.u.*)	Node No.	*L*-Index	Proposed Index
P=Q=1.38 at node 6	30	0.9269	0.0071
	29	0.8717	0.0394
	26	0.8588	0.0436
	25	0.8071	0.0822
	27	0.7899	0.0932
	24	0.7939	0.0960
P=Q=0.4 at node 27	30	0.8259	0.0077
	29	0.7762	0.0400
	27	0.7024	0.0936
	26	0.6544	0.1327
	25	0.6164	0.1708
	24	0.4793	0.3346

The node 30 is identified as the most critical node again when both active and reactive load at node 6 and 27 are increased in the same proportion. The results are presented in Table 5.13. When the active and reactive load at node 6 are of value 1.38 *p.u.*, a slight discrepancy in the raking of nodes 27 and 24 has been observed. Otherwise, the proposed index is consistent with *L*-index. From all the observations of different cases, node 30 is identified as the most critical node and the area that include buses 30-29-27-26-25-24 is the weakest area of the system. The strongest node in that area is node 28. Results of simulation proves that the proposed index is more accurate than *L*-index to detect the voltage instability.

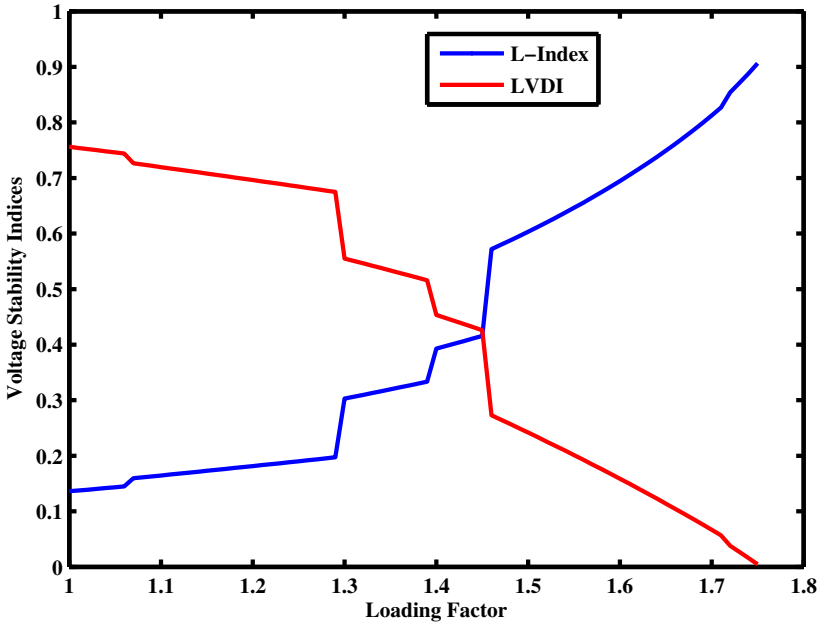

FIGURE 5.4: Variation of voltage stability indices with real load for IEEE 30-bus test system

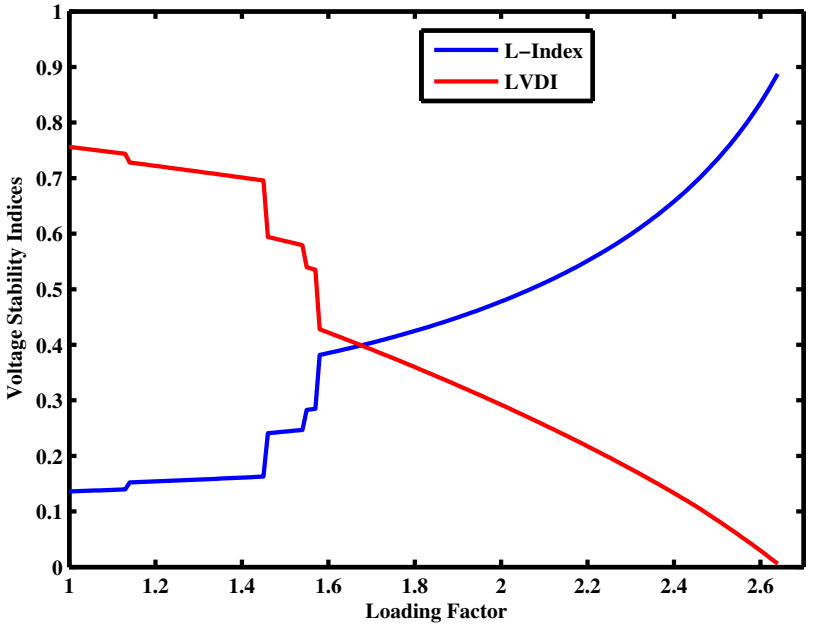

FIGURE 5.5: Variation of voltage stability indices with reactive load for IEEE 30-bus system

5.6.2 IEEE 118-Bus Test System

To prove the effectiveness of the proposed index, the tests are also performed on the larger IEEE 118-bus test system. Literature reveals that the voltage stability is more sensitive to the flow of reactive power [2, 7, 19, 34]. Therefore, the results for single and multiple load change with the reactive load only are presented in this section. To investigate the capability of the proposed index, the reactive load at the selected nodes are increased upto the voltage collapse point. The reactive load at node 95 of value 4.77 *p.u.* makes node 95 the most critical node with proposed-index=0.0371. The $L-$index with the value 0.9117 also identifies this node as the most critical node. The ranking of nodes are consistent with L-index. For reactive load of value 3.05 *p.u.* at node 76, both indices identify node 76 as the most critical node. From Table 5.14, it can be observed that L-index falls behind its critical value 1 at maximum loading point. The reactive load is also increased at nodes 2 and 118 upto the voltage stability limit. Node 118 is identified as the most critical node for the value of reactive load 3.4 *p.u.* at node 118. The results are presented in Table 5.14 and confirmed by L-index.

TABLE 5.14: Test results of IEEE 118-bus test system at increased reactive load of selected nodes

Node Loading (*p.u.*)	Node No.	L-Index	Proposed Index
Q=4.77 at node 95	95	0.9117	0.0371
	96	0.3550	0.4214
	94	0.3495	0.4242
	93	0.2201	0.5820
	82	0.2152	0.5957
Q=3.05 at node 76	76	0.8553	0.0453
	118	0.4917	0.2736
	75	0.2494	0.5428
	74	0.2443	0.5573
	1	0.1580	0.7257
Q=3.4 at node 118	118	0.8260	0.0629
	76	0.5956	0.2001
	75	0.3385	0.4333
	74	0.3090	0.4768
	1	0.1686	0.7109
Q=3.45 at node 2	2	0.8619	0.0573
	1	0.5008	0.2820
	3	0.3569	0.4270
	117	0.3000	0.4975
	12	0.2510	0.5598

TABLE 5.15: Test results of IEEE 118-bus test system at increased reactive load

Loading Multiplier ($p.u.$)	Node No.	L-Index	Proposed Index
$\lambda = 4.255$	76	0.9012	0.0399
	118	0.6982	0.1352
	1	0.5274	0.2309
	95	0.6104	0.2558
	117	0.4889	0.2746
	2	0.4778	0.2874
	82	0.5470	0.2877
	78	0.4981	0.2964
	3	0.4654	0.3014
	74	0.4574	0.3031

Proposed index is also tested for combined reactive loading of the system. Now, the reactive load at all buses of the system is increased upto the level of voltage collapse. As shown in Table 5.15, for the loading factor 4.255, the proposed index for node 76 reaches at 0.0399, which shows that this node is in the critical state. But 0.9012 value of L-index shows that margin is still available *i.e.* L-index could not detect the voltage instability for this case. Also, a slight discrepancy in ranking of buses 1 and 95 is observed from Table 5.15. From the investigation of results presented in Tables 5.10–5.15, it is observed that the proposed index is more versatile and accurate than L-index to detect the voltage instability.

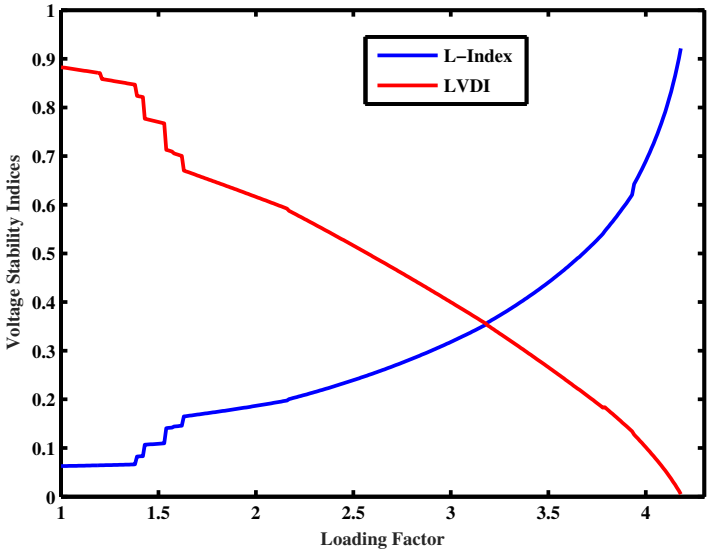

FIGURE 5.6: Variation of voltage stability indices with reactive load for IEEE 118-bus test system

5.7 HE Formulation for Non-uniform Scaling of Loading

The formulation presented in Section 5.5 is only valid for uniform load increase in the system. However, in the voltage stability studies non-uniform load increase in the system is more pragmatic for voltage stability assessment. Therefore, this section proposes a new HE formulation for non-uniform or random scaling of loading in the system. A new random load increase scenario is presented, where the increase in load at each bus is considered proportional to its proximity to voltage collapse. The proposed HE formulation is as follows:

$$V_i(s) = V_i^{SP};\ i \in SB \tag{5.56}$$

$$V_i(s)V_i^*(s^*) = |V_i^{SP}|^2;\ i \in PV \tag{5.57}$$

$$V_i^*(s^*)\sum_{k=1}^{N} Y_{ik}^{tr}V_k(s) + V_i(s)\sum_{k=1}^{N}\left(Y_{ik}^{tr}\right)^* V_k^*(s^*) + 2|V_i|(s)|V_i|(s)\Re(Y_i^{Shunt}) - 2P_{Gi} + 2P_{Li} = 2s\Delta P_{Gi} - 2s\mathbb{k}_i\Delta P_{Li};\ i \in PV \tag{5.58}$$

$$\sum_{k=1}^{N} Y_{ik}^{tr}V_k(s) = W_i^*(s^*)\Big[-P_{Li} + jQ_{Li} + s\mathbb{k}_i(-\Delta P_{Li} + j\Delta Q_{Li})\Big] - Y_i^{Shunt}V_i(s);\ i \in PQ \tag{5.59}$$

Where, $\mathbb{k}_i$ is a proportionality constant and equal to unity minus value of the proposed index of i^{th} bus. The loads are assumed to be ZIP type load as given in (5.19) and (5.20). Now, by substituting $s = 0$ in (5.56), (5.57), (5.58) and (5.59), we can obtain:

$$V_i[0] = V_i^{SP};\ i \in SB \tag{5.60}$$

$$V_i[0]V_i^*[0] = |V_i^{SP}|^2;\ i \in PV \tag{5.61}$$

$$V_i^*[0]\sum_{k=1}^{N} Y_{ik}^{tr}V_k[0] + V_i[0]\sum_{k=1}^{N}\left(Y_{ik}^{tr}\right)^* V_k^*[0] + 2|V_i|[0]|V_i|[0]\Re(Y_i^{Shunt}) - 2P_{Gi} + 2P_{Li}^0\Big[\alpha_p|V_i|[0]|V_i|[0] + \beta_p|V_i|[0] + \gamma_p\Big] = 0;\ i \in PV \tag{5.62}$$

$$\sum_{k=1}^{N} Y_{ik}^{tr}V_k[0] + P_{Li}^0\Big[\alpha_p V_i[0] + \beta_p|V_i|[0]W_i^*[0] + \gamma_p W_i^*[0]\Big] - jQ_{Li}^0\Big[\alpha_q V_i[0] + \beta_q|V_i|[0]W_i^*[0] + \gamma_q W_i^*[0]\Big] + Y_i^{Shunt}V_i[0] = 0;\ i \in PQ \tag{5.63}$$

The germ solutions can be obtained by simultaneously solving (5.60), (5.61), (5.62) and (5.63). Also, at $s = 1$, original equations can be recovered as it is a necessary condition. After expanding (5.60), (5.61), (5.62) and (5.63) using Maclurin series, and comparing the coefficients of s^n, the general recurrence relation of these equations can be obtained, but the dimension of the coefficient matrix of linear algebraic equations is equal to $(2s+5(p+m))\times(2s+5(p+m))$. Although, the elimination of the variables $W_i^*[n]$ and $|V_i|[n]$ from the expressions allows to preserve the order of coefficient matrix equal to $2(s+p+m)$ *i.e.* $2N$. The recurrence relations of $W_i^*[n]$ and $|V_i|[n]$ can be expressed as follows:

$$W_i^*[n] = -\frac{1}{V_i^*[0]}\sum_{d=0}^{n-1} W_i^*[d]V_i^*[n-d] \tag{5.64}$$

$$|V_i|[n] = \frac{1}{2|V_i|[0]}\left[\sum_{d=0}^{n} V_i[d]V_i^*[n-d] - \sum_{d=1}^{n-1}|V_i|[d]|V_i|[n-d]\right] \tag{5.65}$$

Now, the general recurrence formulae for (5.60), (5.61), (5.62) and (5.63) can be expressed as follows:

$$V_i[n] = 0;\ i \in SB;\ \text{for } n \geq 1 \tag{5.66}$$

$$V_i[0]V_i^*[n] + V_i[n]V_i^*[0] = -\sum_{d=1}^{n-1} V_i[d]V_i^*[n-d]\ ; i \in PV;\ \text{for } n \geq 1 \tag{5.67}$$

$$\begin{aligned}
&\sum_{k=1}^{N} Y_{ik}^{tr}V_k[0]V_i^*[n] + \sum_{k=1}^{N} Y_{ik}^{tr}V_k[n]V_i^*[0] + \sum_{k=1}^{N}\left(Y_{ik}^{tr}\right)^* V_k^*[0]V_i[n] + \sum_{k=1}^{N}\left(Y_{ik}^{tr}\right)^* V_k^*[n]V_i[0] \\
&\quad + \left[2\Re(Y_i^{Shunt}) + 2P_{Li}^0\alpha_p + \frac{P_{Li}^0\beta_p}{|V_i|[0]}\right]\left(V_i[0]V_i^*[n] + V_i[n]V_i^*[0]\right) = 2\eta_{n1}\Delta P_{Gi} \\
&-2\Bbbk_i\Delta P_{Li}^0\left[\alpha_p\sum_{d=0}^{n-1}|V_i|[d]|V_i|[n-1-d] + \beta_p|V_i|[n-1] + \eta_{n1}\gamma_p\right] - 2P_{Li}^0\alpha_p\sum_{d=1}^{n-1}|V_i|[d]|V_i|[n-d] \\
&\quad - \left[2\Re(Y_i^{Shunt}) + 2P_{Li}^0\alpha_p + \frac{P_{Li}^0\beta_p}{|V_i|[0]}\right]\left[\sum_{d=1}^{n-1} V_i[d]V_i^*[n-d] - \sum_{d=1}^{n-1}|V_i|[d]V_i|[n-d]\right] \\
&\quad - \sum_{k=1}^{N} Y_{ik}^{tr}\sum_{d=1}^{n-1} V_k[d]V_i^*[n-d] - \sum_{k=1}^{N}(Y_{ik}^{tr})^*\sum_{d=1}^{n-1} V_k^*[d]V_i[n-d] \\
&\quad - 2\Re(Y_i^{Shunt})\sum_{d=1}^{n-1}|V_i|[d]|V_i|[n-d]\ ; i \in PV;\ \text{for } n \geq 1
\end{aligned} \tag{5.68}$$

$$\sum_{k=1}^{N} Y_{ik}^{tr} V_k[n] + \left(P_{Li}^0 \alpha_p - jQ_{Li}^0 \alpha_q + Y_i^{Shunt}\right) V_i[n] - \frac{W_i^*[0]}{V_i^*[0]} \Bigg(P_{Li}^0 \beta_p |V_i|[0] + P_{Li}^0 \gamma_p - jQ_{Li}^0 \beta_q |V_i|[0] - jQ_{Li}^0 \gamma_q \Bigg) V_i^*[n] + \frac{W_i^*[0]}{2|V_i|[0]} \Big(P_{Li}^0 \beta_p - jQ_{Li}^0 \beta_q \Big) \Big(V_i[0] V_i^*[n] + V_i[n] V_i^*[0] \Big) = -\mathbb{k}_i \Delta P_{Li}^0 \Bigg[\alpha_p V_i[n-1] + \beta_p \sum_{d=0}^{n-1} |V_i|[d] W_i^*[n-1-d] + \gamma_p W_i^*[n-1] \Bigg] + j\mathbb{k}_i \Delta Q_{Li}^0 \Bigg[\alpha_q V_i[n-1] + \beta_q \sum_{d=0}^{n-1} |V_i|[d] W_i^*[n-1-d] + \gamma_q W_i^*[n-1] \Bigg] - \Big(P_{Li}^0 \beta_p - jQ_{Li}^0 \beta_q \Big) \sum_{d=1}^{n-1} |V_i|[d] W_i^*[n-d] + \Big(P_{Li}^0 \beta_p |V_i|[0] + P_{Li}^0 \gamma_p - jQ_{Li}^0 \beta_q |V_i|[0] - jQ_{Li}^0 \gamma_q \Big) \left(\frac{1}{V_i^*[0]} \sum_{d=1}^{n-1} W_i^*[k] V_i^*[n-k] \right) - \frac{W_i^*[0]}{2|V_i|[0]} \Big(P_{Li}^0 \beta_p - jQ_{Li}^0 \beta_q \Big) \Bigg[\sum_{d=1}^{n-1} V_i[d] V_i^*[n-d] - \sum_{d=1}^{n-1} |V_i|[d] |V_i|[n-d] \Bigg] ; i \in PQ; \text{ for } n \geq 1 \quad (5.69)$$

As discussed in Section 5.4, the next objective is to rearrange (5.66), (5.67), (5.68), and (5.69) such that the resultant equations can be represented as linear matrix equations in explicit form. To represent all equations in explicit form, all known and unknown variables must be shifted to LHS and RHS respectively. For this purpose variables are splitted into real and imaginary parts as $Y_{ik}^{tr} = G_{ik} + jB_{ik}$, $V_i[n] = V_{ire} + jV_{iim}$. After performing lots of algebraic operations, the linear matrix in explicit form can be represented as in (5.70) for N-bus power system. Where, subscripts r, m, and p denote the slack bus, load bus, and generator bus respectively. Now, the voltage phasor of all buses are calculated using SVD based Padé approximation to handle the degeneracy cases of power series. The RHS of (5.67), (5.68) and (5.69) are denoted as $RHS\_Known\_PV\_V\_D[n-1]$, $RHS\_Known\_PV\_P\_D[n-1]$ and $RHS\_Known\_PQ\_D[n-1]$ respectively.

$$\begin{bmatrix} & \vdots & \vdots & & \vdots & \vdots & & \vdots & \vdots & \\ \dots & 1 & 0 & \dots & 0 & 0 & \dots & 0 & 0 & \dots \\ \dots & 0 & 1 & \dots & 0 & 0 & \dots & 0 & 0 & \dots \\ & \vdots & \vdots & & \vdots & \vdots & & \vdots & \vdots & \\ \dots & \mu_{mr}^{PQ,R} & \xi_{mr}^{PQ,R} & \dots & \mu_{mm}^{PQ,R} & \xi_{mm}^{PQ,R} & \dots & \mu_{mp}^{PQ,R} & \xi_{mp}^{PQ,R} & \dots \\ \dots & \mu_{mr}^{PQ,I} & \xi_{mr}^{PQ,I} & \dots & \mu_{mm}^{PQ,I} & \xi_{mm}^{PQ,I} & \dots & \mu_{mp}^{PQ,I} & \xi_{mp}^{PQ,I} & \dots \\ & \vdots & \vdots & & \vdots & \vdots & & \vdots & \vdots & \\ \dots & \mu_{pr} & \xi_{pr} & \dots & \mu_{pm} & \xi_{pm} & \dots & \mu_{pp} & \xi_{pp} & \dots \\ \dots & 0 & 0 & \dots & 0 & 0 & \dots & 2V_{ire}[0] & 2V_{iim}[0] & \dots \\ & \vdots & \vdots & & \vdots & \vdots & & \vdots & \vdots & \end{bmatrix} \begin{bmatrix} \vdots \\ V_{rre}[n] \\ V_{rim}[n] \\ \vdots \\ V_{mre}[n] \\ V_{mim}[n] \\ \vdots \\ V_{pre}[n] \\ V_{pim}[n] \\ \vdots \end{bmatrix} = \begin{bmatrix} \vdots \\ 0 \\ 0 \\ \vdots \\ \Re(RHS\_Known\_PQ\_D[n-1]) \\ \Im(RHS\_Known\_PQ\_D[n-1]) \\ \vdots \\ RHS\_Known\_PV\_P\_D[n-1] \\ RHS\_Known\_PV\_V\_D[n-1] \\ \vdots \end{bmatrix} \tag{5.70}$$

Where, μ_{ik} and μ_{ik} are same as in (5.52) and (5.53) respectively and others are as follows:

$$\mu_{ii} = 2\big(G_{ii}V_{ire}[0] + B_{ii}V_{iim}[0]\big) + 2\Re\big(Y_i^{Shunt}\big)V_{ire}[0] + \frac{P_{Li}^0\beta_p V_{ire}[0]}{|V_i|[0]} + 2P_{Li}^0\alpha_p V_{ire}[0] + 2\sum_{k=1}^{N}\big(G_{ik}V_{kre}[0] - B_{ik}V_{kim}[0]\big) \tag{5.71}$$

$$\xi_{ii} = 2\big(G_{ii}V_{iim}[0] - B_{ii}V_{ire}[0]\big) + 2\Re\big(Y_i^{Shunt}\big)V_{iim}[0] + \frac{P_{Li}^0\beta_p V_{iim}[0]}{|V_i|[0]} + 2P_{Li}^0\alpha_p V_{iim}[0] + 2\sum_{k=1}^{N}\big(G_{ik}V_{kim}[0] + B_{ik}V_{kre}[0]\big) \tag{5.72}$$

$$\mu_{ik}^{PQ,R} = G_{ik};\ k \neq i \tag{5.73}$$

$$\xi_{ik}^{PQ,R} = -B_{ik};\ k \neq i \tag{5.74}$$

$$\mu_{ii}^{PQ,R} = G_{ii} + P_{Li}^{0}\alpha_p + 2W_{ire}[0]W_{iim}[0]\big(Q_{Li}^{0}\beta_q|V_i|[0] + Q_{Li}^{0}\gamma_q\big) + \Re\big(Y_i^{Shunt}\big) - \big(P_{Li}^{0}\beta_p|V_i|[0] + P_{Li}^{0}\gamma_p\big)\Big\{\big(W_{ire}[0]\big)^2 - \big(W_{iim}[0]\big)^2\Big\} + \frac{V_{ire}[0]}{|V_i|[0]}\big(P_{Li}^{0}\beta_p W_{ire}[0] - Q_{Li}^{0}\beta_q W_{iim}[0]\big) \quad (5.75)$$

$$\xi_{ii}^{PQ,R} = -B_{ii} + Q_{Li}^{0}\alpha_q + 2W_{ire}[0]W_{iim}[0]\big(P_{Li}^{0}\beta_p|V_i|[0] + P_{Li}^{0}\gamma_p\big) - \Im\big(Y_i^{Shunt}\big) + \big(Q_{Li}^{0}\beta_q|V_i|[0] + Q_{Li}^{0}\gamma_q\big)\Big\{\big(W_{ire}[0]\big)^2 - \big(W_{iim}[0]\big)^2\Big\} + \frac{V_{iim}[0]}{|V_i|[0]}\big(P_{Li}^{0}\beta_p W_{ire}[0] - Q_{Li}^{0}\beta_q W_{iim}[0]\big) \quad (5.76)$$

$$\mu_{ik}^{PQ,I} = B_{ik};\ k \neq\ i \quad (5.77)$$

$$\xi_{ik}^{PQ,I} = -G_{ik};\ k \neq\ i \quad (5.78)$$

$$\mu_{ii}^{PQ,I} = B_{ii} - Q_{Li}^{0}\alpha_q - 2W_{ire}[0]W_{iim}[0]\big(P_{Li}^{0}\beta_p|V_i|[0] + P_{Li}^{0}\gamma_p\big) + \Im\big(Y_i^{Shunt}\big) + \big(Q_{Li}^{0}\beta_q|V_i|[0] + Q_{Li}^{0}\gamma_q\big)\Big\{\big(W_{ire}[0]\big)^2 - \big(W_{iim}[0]\big)^2\Big\} - \frac{V_{ire}[0]}{|V_i|[0]}\big(P_{Li}^{0}\beta_p W_{iim}[0] + Q_{Li}^{0}\beta_q W_{ire}[0]\big) \quad (5.79)$$

$$\xi_{ii}^{PQ,I} = G_{ii} + P_{Li}^{0}\alpha_p - 2W_{ire}[0]W_{iim}[0]\big(Q_{Li}^{0}\beta_q|V_i|[0] + Q_{Li}^{0}\gamma_q\big) + \Re\big(Y_i^{shunt}\big) - \big(P_{Li}^{0}\beta_p|V_i|[0] + P_{Li}^{0}\gamma_p\big)\Big\{\big(W_{ire}[0]\big)^2 - \big(W_{iim}[0]\big)^2\Big\} - \frac{V_{iim}[0]}{|V_i|[0]}\big(P_{Li}^{0}\beta_p W_{iim}[0] + Q_{Li}^{0}\beta_q W_{iim}[0]\big) \quad (5.80)$$

5.7.1 Results and Discussions

The proposed index and HE formulation for non-uniform load increase are also investigated for IEEE 30-bus test system and sample results have been presented here. The result of the proposed index for increasing apparent power loading non-uniformly is shown in Table 5.16. At maximum loading point, the value of the proposed index is 0.0041 for bus 30 which shows that it is at the verge of voltage collapse. L-index is equal to 0.8860 for this case and therefore it is unable to detect the voltage collapse condition of the power system. The buses are ranked in the order of criticality on the basis of the proposed index and shown in Table 5.16. The ranking is supported by L-index except for buses 25 and 24. The variation of $LVDI$ and L-index with increase in real and reactive load are presented in Figure 5.7. It is evident from this figure that the proposed index for bus 30 drops to 0.0041 at the voltage stability limit, but the L-index fails to reach near its critical value 1. From Tables 5.10 and 5.16, it can be observed that the ranking of buses are similar for uniform and non-uniform increase in loading except a small discrepancy. From Figures 5.3 and 5.7, it can also be observed that the maximum loadability of the system is decreased (*i.e.* 1.4 p.u.) as expected. Therefore, it can be concluded that if increase in loading is proportional to the degree of criticality of individual buses, the maximum loading limit is reduced. Simulation result for non-uniform apparent power loading shows that the proposed index reaches near its critical value zero at the point of voltage collapse. The simulation results prove the versatility of the proposed index.

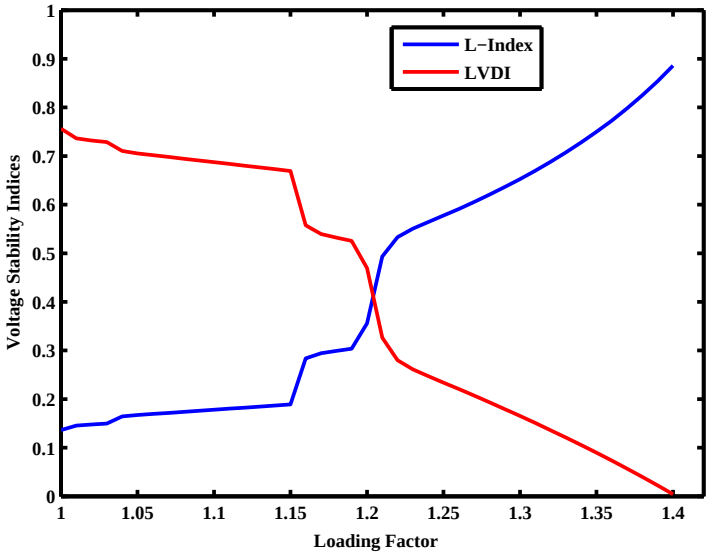

FIGURE 5.7: Variation of voltage stability indices for non-uniform in IEEE 30-bus test system

TABLE 5.16: Ranking of buses of IEEE 30-bus test system for non-uniform loading

Node No.	L-Index	Proposed Index	Node No.	L-Index	Proposed Index
30	0.8860	0.0041	19	0.7450	0.1132
26	0.8221	0.0379	18	0.7341	0.1225
29	0.8162	0.0512	23	0.7291	0.1237
25	0.7475	0.1027	20	0.7272	0.1291
24	0.7480	0.1055	27	0.7055	0.1403

5.8 Summary

In this chapter, a new node based voltage stability index which calculates the voltage and load distance to maximum loading point is proposed and evaluated using extended HELM for ZIP type load. The proposed index is compared with L-index to prove its potential. Numerical results for ZIP type loads are presented to demonstrate the accuracy of the proposed voltage stability index using the extended HELM. It has been proved that the proposed voltage stability index accurately identifies the weak buses in the IEEE-30 and IEEE-118 bus test systems. The proposed approach can be used as a tool in power system planning and operation. The extended version of HELM includes the shunt conductance of steady-state pi-model of VRT and fixed reactive power injections at the buses. As the conventional HELM can be ill-posed for constructing Padé approximations for degeneracy cases of power series, therefore, SVD based Padé approximation is used in this work. A new HE formulation is also proposed for non-uniform scaling of the load in the system.

Chapter 6

Holomorphic Embedded Load-Flow Model of STATCOM

6.1 Introduction

As discussed in Chapter 4, before installing a physical model, performance and effectiveness of the FACTS devices must be checked by developing their models and integrating them in the load-flow methods. Different models of FACTS devices have been proposed in the literature and all of the existing models have been developed using numerical iterative techniques. Most of these models are based on N-R method due to its quadratic convergence property. The N-R method is computationally too expensive due to the repeated evaluation of the Jacobian matrix and the corresponding factorizations that need to be done at each iteration [66, 67]. Existing iterative methods based models suffer from the problem of convergence/spurious solution, if proper initial conditions are not chosen. The problem can be resolved if models are developed using Holomorphic Embedded Load-Flow Method (HELM).

HELM is a novel technique for solving the AC power flow problem [77–79, 93]. It is based on a complex-valued embedding technique specifically devised to exploit the particular algebraic nonlinearities of the power flow problem [118, 121]. In [92], HELM modeling of Thyristor–based FACTS controllers, *i.e.* Static Var Compensator (SVC), Thyristor Controlled Switched Capacitor (TCSC), Thyristor Controlled Voltage Regulator (TCVR), and Thyristor Controlled Phase Angle Regulator (TCPAR) have been presented. In these models, FACTS devices are represented as a variable reactance/tap ratio that modifies the

power balance equations. Models presented in [92] are extension of existing holomorphic based load-flow equation [78] with a minor change in the bus power balance equation. Moreover, various control modes of FACTS devices have not been explored in [92].

A variable reactance/tap ratio based model cannot represent the actual characteristics of voltage source FACTS devices. A Voltage Source Converter (VSC) model is quite complex which requires large number of equations to be incorporated in load-flow, modification of coefficient-matrix equation, and representation of different control modes, *etc.* But so far HELM has not been employed to develop the complex models of VSC based FACTS devices. Considering the modeling of VSC based devices using HELM as a new area of research, this chapter proposes a HELM model of STATCOM. The following paper has been accepted from this chapter:

- Pradeep Singh and Rajive Tiwari, "STATCOM Model using Holomorphic Embedding", *IEEE Access*, vol. 7, pp. 33075-33086, 2019.

6.2 Proposed HELM Model of STATCOM

A STATCOM is normally used to control the bus voltage by reactive power shunt compensation. It consists of an inverter, a coupling transformer, and a DC capacitor as shown in Figure 6.1.

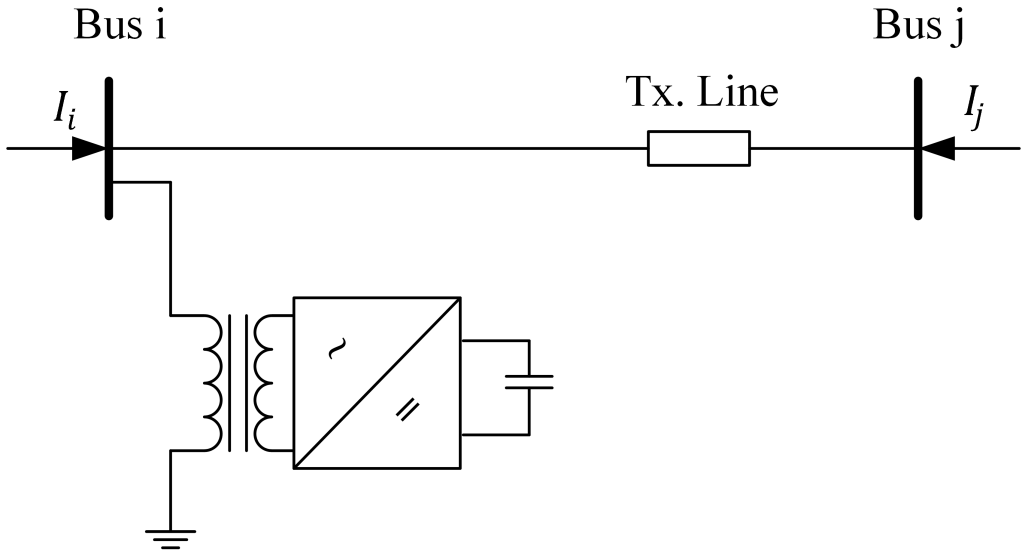

FIGURE 6.1: STATCOM basic structure

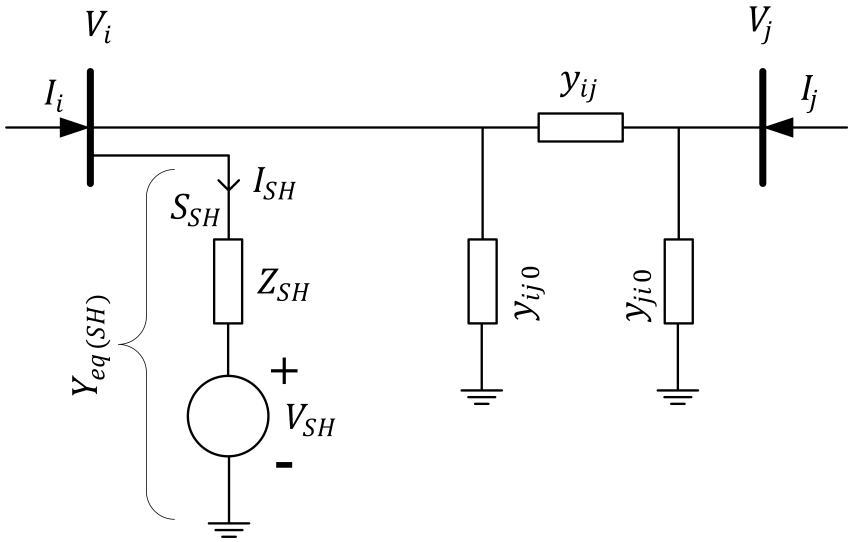

FIGURE 6.2: Equivalent circuit of STATCOM

During the development of the HELM model of STATCOM, it has been assumed that the system and STATCOM are 3-phase balanced and the harmonics generated by STATCOM are negligible. A schematic equivalent circuit diagram of STATCOM at bus i is shown in Figure 6.2. This device acts as a controllable fundamental frequency positive sequence voltage source V_{SH} (bounded between V_{SHmax} and V_{SHmin}) which is used to control the various parameters to the specified values. In Figure 6.2, S_{SH}, Z_{SH}, $Y_{eq(SH)}$, and I_{SH} are the complex power injected by STATCOM at bus i, STATCOM coupling transformer leakage impedance, equivalent admittance of the STATCOM, and complex current injected by STATCOM at bus i respectively.

From Figure 6.2, the power balance equation of STATCOM connected bus i of N-bus power system can be expressed as:

$$\sum_{k=1}^{N} Y_{ik}V_k = \frac{(P_{Gi} - jQ_{Gi}) - (P_{Li} - jQ_{Li})}{V_i^*} - \frac{S_{SH}^*}{V_i^*} \tag{6.1}$$

Where, Y_{ik} and V_i are the $(i,k)^{th}$ element of bus admittance matrix and i^{th} bus voltage respectively. To derive the recurrence formula for STATCOM connected bus, (6.1) must be embedded with a complex parameter s in such a way that the resultant equations satisfy the requirement of embedding. In (6.1), the STATCOM output voltage is treated as a free variable function of s and the proposed holomorphic embedding of (6.1) is expressed as

following:

$$\sum_{k=1}^{N} Y_{ik}^{tr(SY)} V_k(s) = sW_i^*(s^*)\big(P_{Gi}-jQ_{Gi}-P_{Li}+jQ_{Li}\big)-Y_{SH}\big(V_i(s)-V_{SH}(s)\big)-sY_i^{Shunt}V_i(s) - s\sum_{k=1}^{N} Y_{ik}^{tr(Un)} V_k(s);\ i \in ST \quad (6.2)$$

Where, Y_{SH} is the reciprocal of Z_{SH} *i.e.* STATCOM coupling transformer leakage admittance and all other variables are same as defined in Section 5.4. To fulfill the Wirtinger's derivative condition for holomorphic function [121], $W_i^*(s^*)$ is used in (6.2) in place of $W_i^*(s)$; where, $W_i^*(s^*)$ is the reciprocal of $V_i^*(s^*)$. Solution of (6.2) at $s = 0$ offers germ solutions which is given as:

$$\sum_{k=1}^{N} Y_{ik}^{tr(SY)} V_k[0] + Y_{SH}\big(V_i[0] - V_{SH}[0]\big) = 0 \quad (6.3)$$

As the germ solutions for bus voltages are $1\angle 0°$ and the terms multiplied by s are vanished, the germ solution for V_{SH} will be $1\angle 0°$, as per (6.3). For deriving the recurrence formula of (6.2), the STATCOM output voltage is represented by the following power series:

$$V_{SH}(s) = \sum_{n=0}^{\infty} V_{SH}[n]s^n \quad (6.4)$$

By substituting $V_{SH}(s)$ from (6.4) into (6.2) and comparing the coefficients of s^n, the general recurrence formula for $n \geq 1$ is obtained as follows:

$$\sum_{k=1}^{N} Y_{ik}^{tr(SY)} V_k[n] + Y_{SH}V_i[n] - Y_{SH}V_{SH}[n] = \big(P_{Gi} - jQ_{Gi} - P_{Li} + jQ_{Li}\big)W_i^*[n-1] - Y_i^{Shunt}V_i[n-1] - \sum_{k=1}^{N} Y_{ik}^{tr(Un)} V_k[n-1];\ i \in ST;\ \text{for } n \geq 1 \quad (6.5)$$

Where, $V_{SH} = V_{SHre} + jV_{SHim}$ is a complex variable that adds two unknown variable in (6.5). Therefore, to find out the unique solution for unknown variables, two additional equations are required. These additional equations are related to the STATCOM real power exchange constraint and its control mode. In steady-state, only the reactive power is exchanged between the STATCOM and the AC system, and the real power exchange is considered as zero which can be represented as:

$$\Re(V_{SH}I_{SH}^*) = \Re(V_{SH}^*I_{SH}) = 0 \quad (6.6)$$

$$\Re\Big(V_{SH}^{*}Y_{SH}(V_i - V_{SH})\Big) = 0 \tag{6.7}$$

The real and imaginary part of variables are denoted by $\Re$ and $\Im$ respectively. Equation (6.7) can be holomorphically embedded as follows:

$$\Re\left[V_{SH}^{*}(s^{*})Y_{SH}\Big\{V_i(s) - V_{SH}(s)\Big\}\right] = 0 \tag{6.8}$$

A general recurrence formula can be obtained by substituting the STATCOM output voltage and bus voltage power series into (6.8), for $n \geq 1$ in the following way:

$$\Re\Big[Y_{SH}(V_i[n] - V_{SH}[n])\Big] = -\Re\left[Y_{SH}\left\{\sum_{d=1}^{n-1} V_{SH}^{*}[d]V_i[n-d] - \sum_{d=1}^{n-1} V_{SH}^{*}[d]V_{SH}[n-d]\right\}\right] \tag{6.9}$$

It has been recognized that besides the bus voltage magnitude control, STATCOM has the ability to control reactive power flow, current, angle, and impedance *etc.* Mathematical modeling of different control modes is developed and investigated. Various control modes of proposed model are as follows:

6.2.1 Control Mode 1: Voltage Magnitude Control of the STATCOM Connected at Bus 'i'

The i^{th} bus voltage magnitude control constraint is as follows:

$$|V_i| - V_i^{SP} = 0 \tag{6.10}$$

The voltage magnitude control constraint in (6.10) is similar to the PV bus voltage magnitude constraint so the holomorphic embedding proposed in [80] is used in the following way:

$$V_i(s)V_i^{*}(s^{*}) = 1 + s\Big[\big(V_i^{SP}\big)^2 - 1\Big] \tag{6.11}$$

The general recurrence formula for $n \geq 1$ is as follows:

$$V_{ire}[n] = \eta_{n1}\frac{\big(V_i^{SP}\big)^2 - 1}{2} - \frac{1}{2}\sum_{d=1}^{n-1} V_i[d]V_i^{*}[n-d] \tag{6.12}$$

6.2.2 Control Mode 2: Reactive Power Injection Control

Reactive power injected by the STATCOM is controlled to a reactive power injection reference by regulating the STATCOM output voltage phasor. Mathematically, it is expressed as:

$$Q_{SH} - Q_{SH}^{SP} = 0 \tag{6.13}$$

From Figure 6.2

$$\Im\Big[- V_i^*(V_i - V_{SH})Y_{SH}\Big] = Q_{SH}^{SP} \tag{6.14}$$

The proposed holomorphic embedding for (6.14) is expressed as follows::

$$-\Im\Big[Y_{SH}V_i^*(s^*)\big\{V_i(s) - V_{SH}(s)\big\}\Big] = sQ_{SH}^{SP} \tag{6.15}$$

A general recurrence formula for (6.15) for $n \geq 1$ is expressed in the following way:

$$-\Im\Big[Y_{SH}\big(V_i[n]-V_{SH}[n]\big)\Big] = \eta_{n1}Q_{SH}^{SP}+\Im\left[Y_{SH}\left\{\sum_{d=1}^{n-1}V_i^*[d]V_i[n-d]-\sum_{d=1}^{n-1}V_i^*[d]V_{SH}[n-d]\right\}\right] \tag{6.16}$$

Where, $Y_{SH} = g_{SH} + jb_{SH}$ is the admittance of the coupling transformer.

6.2.3 Control Mode 3: Control of Equivalent Shunt Admittance

A STATCOM can be represented as an equivalent fictitious admittance. In this control mode, the STATCOM output voltage phasor V_{SH} is regulated to control the equivalent imaginary admittance to a specified admittance reference. Mathematically, it can be represented as follows:

$$b_{eq(SH)} - b_{eq(SH)}^{SP} = 0 \tag{6.17}$$

$$\Im\left[\frac{Y_{SH}(V_i - V_{SH})}{V_{SH}}\right] = b_{eq(SH)}^{SP} \tag{6.18}$$

The proposed way of embedding for (6.18) is as follows:

$$\Im\left[\frac{Y_{SH}\big\{V_i(s) - V_{SH}(s)\big\}}{V_{SH}(s)}\right] = sb_{eq(SH)}^{SP} \tag{6.19}$$

A general recurrence formula of (6.19) for $n \geq 1$ is obtained in the following way:

$$\Im\Big[Y_{SH}\big(V_i[n]-V_{SH}[n]\big)\Big] = \eta_{n1}b^{SP}_{eq(SH)} - \Im\Bigg[Y_{SH}\Bigg\{\sum_{d=1}^{n-1} V_i[d]W_{SH}[n-d] - \sum_{d=1}^{n-1} V_{SH}[d]W_{SH}[n-d]\Bigg\}\Bigg] \tag{6.20}$$

6.2.4 Control Mode 4: Control of STATCOM Current Magnitude (capacitive mode)

In this control mode, the magnitude of STATCOM current is controlled to a specified current magnitude control reference. To achieve this, STATCOM output voltage phasor is regulated. Mathematically,

$$|I_{SH}| = I^{SP}_{SH} \tag{6.21}$$

Equation (6.21) has two solutions, one for capacitive mode and another one for inductive mode, and solution can arbitrarily converge to any one of the solution. To enforce the capacitive mode, *i.e.* I_{SH} to lead V_{SH} by 90°, equation (6.21) is modified in the following way:

$$I_{SH} = I^{SP}_{SH}\angle(\theta_{SH} + 90^0) = jI^{SP}_{SH}\big(cos\theta_{SH} + jsin\theta_{SH}\big) \tag{6.22}$$

As $V_{SH} = |V_{SH}|(cos\theta_{SH} + jsin\theta_{SH})$ and $I_{SH} = (V_i - V_{SH})Y_{SH}$, substituting V_{SH} and I_{SH} into (6.22), we obtain

$$|V_{SH}|(V_i - V_{SH})Y_{SH} = jI^{SP}_{SH}V_{SH} \tag{6.23}$$

The proposed HE modeling of STATCOM's control constraint in capacitive mode is represented as:

$$Y_{SH}\Big[V_i(s)|V_{SH}|(s) - V_{SH}(s)|V_{SH}|(s)\Big] = jsI^{SP}_{SH}V_{SH}(s) \tag{6.24}$$

The general recurrence formula for control mode 4 is obtained in the following way:

$$Y_{SH}\big(V_i[n] - V_{SH}[n]\big) = -Y_{SH}\Bigg\{\sum_{d=1}^{n-1} V_i[d]|V_{SH}|[n-d] - \sum_{d=1}^{n-1} V_{SH}[d]|V_{SH}|[n-d]\Bigg\} + jI^{SP}_{SH}V_{SH}[n-1] \tag{6.25}$$

Now HE formulation of (6.25) enforces the solution to capacitive compensation mode, *i.e.* I_{SH} leads V_{SH} by 90°, while keeping the current magnitude constant.

6.2.5 Control Mode 5: Control of STATCOM Current Magnitude (inductive mode)

In this control mode, the magnitude of STATCOM current is controlled to a specified current value with current lagging the voltage by 90°. To obtain lagging mode, equation (6.21) is modified as per (6.26):

$$I_{SH} = I_{SH}^{SP}\angle(\theta_{SH} - 90^0) = -jI_{SH}^{SP}\big(cos\theta_{SH} + jsin\theta_{SH}\big) \tag{6.26}$$

Similar to capacitive compensation mode, a general recurrence formula obtained for inductive compensation is described as:

$$Y_{SH}\big(V_i[n] - V_{SH}[n]\big) = -Y_{SH}\left\{\sum_{d=1}^{n-1} V_i[d]|V_{SH}|[n-d] - \sum_{d=1}^{n-1} V_{SH}[d]|V_{SH}|[n-d]\right\} - jI_{SH}^{SP}V_{SH}[n-1] \tag{6.27}$$

Equation (6.27) enforces the solution in inductive compensation mode; *i.e.* I_{SH} lags V_{SH} by 90°, while keeping the current magnitude to specified value.

6.2.6 Control Mode 6: Control of STATCOM Output Voltage Magnitude $|\mathbf{V_{SH}}|$

STATCOM can be used to control the voltage magnitude of V_{SH} to a specified voltage. Mathematically, such a control constraint is described as:

$$|V_{SH}| - V_{SH}^{SP} = 0 \tag{6.28}$$

This control constraint is also similar to PV bus voltage magnitude constraint. Therefore, the general recurrence formula for $n \geq 1$ can be written in a manner similar to [80] in the following way:

$$V_{SHre}[n] = \eta_{n1}\frac{\left\{\left(V_{SH}^{SP}\right)^2 - 1\right\}}{2} - \frac{1}{2}\sum_{d=1}^{n-1} V_{SH}[d]V_{SH}^{*}[n-d] \tag{6.29}$$

6.2.7 Control Mode 7: Remote Bus Voltage Magnitude Control

In this control mode, the STATCOM is used to control the voltage magnitude of remote bus say j to a specified voltage magnitude reference. Mathematically, it is expressed as:

$$|V_j| - V_j^{SP} = 0 \tag{6.30}$$

A general recurrence formula for (6.30) can be expressed in the following way:

$$V_{jre}[n] = \eta_{n1}\frac{\left\{\left(V_j^{SP}\right)^2 - 1\right\}}{2} - \frac{1}{2}\sum_{d=1}^{n-1} V_j[d]V_j^*[n-d] \tag{6.31}$$

6.2.8 Control Mode 8: Local or Remote Reactive Power Flow Control

In this control mode, the STATCOM is used to control the local or remote transmission line reactive power flow to a specified reactive power reference. Mathematically,

$$Q_{jk} - Q_{jk}^{SP} = 0 \tag{6.32}$$

$$\Im\Big[V_j^*\big(V_k - V_j\big)Y_{jk}\Big] = Q_{jk}^{SP} \tag{6.33}$$

The proposed holomorphic embedding of (6.33) is as follows:

$$\Im\Big[V_j^*(s^*)\big\{V_k(s) - V_j(s)\big\}Y_{jk}\Big] = sQ_{jk}^{SP} \tag{6.34}$$

A general recurrence formula for (6.34) for $n \geq 1$ is obtained in the following way:

$$\Im\Big[Y_{jk}\big(V_k[n] - V_j[n]\big)\Big] = \eta_{n1}Q_{jk}^{SP} - \Im\left[Y_{jk}\left\{\sum_{d=1}^{n-1} V_j^*[d]V_k[n-d] - \sum_{d=1}^{n-1} V_j^*[d]V_j[n-d]\right\}\right] \tag{6.35}$$

Now as discussed in Section 5.4, all the system equations must be represented as linear matrix equations in explicit form. To represent equations in explicit form, all known and unknown variables are shifted to LHS and RHS respectively. Let the variables are separated into real and imaginary parts as $Y_{ik}^{tr(SY)} = G_{ik}^{SY} + jB_{ik}^{SY}$, $Y_{SH} = g_{SH} + jb_{SH}$, $V_i[n] = V_{ire}[n] + jV_{iim}[n]$ and $V_{SH}[n] = V_{SHre}[n] + jV_{SHim}[n]$. The linear matrix equations in explicit form are given in (6.36) and (6.37) for N-bus power system, where subscripts r, m, p, q, SH denote the slack bus, load bus, PV bus, STATCOM connected bus and STATCOM output voltage respectively.

$$
\begin{bmatrix}
 & \vdots & \vdots & & \vdots & \vdots & & \vdots & \vdots & & \vdots & \vdots & & \vdots & \vdots & \\
\dots & 1 & 0 & \dots & 0 & 0 & \dots & 0 & 0 & \dots & 0 & 0 & \dots & 0 & 0 & \dots \\
\dots & 0 & 1 & \dots & 0 & 0 & \dots & 0 & 0 & \dots & 0 & 0 & \dots & 0 & 0 & \dots \\
 & \vdots & \vdots & & \vdots & \vdots & & \vdots & \vdots & & \vdots & \vdots & & \vdots & \vdots & \\
\dots & G_{mr}^{SY} & -B_{mr}^{SY} & \dots & G_{mm}^{SY} & -B_{mm}^{SY} & \dots & G_{mp}^{SY} & -B_{mp}^{SY} & \dots & G_{mq}^{SY} & -B_{mq}^{SY} & \dots & 0 & 0 & \dots \\
\dots & B_{mr}^{SY} & G_{mr}^{SY} & \dots & B_{mm}^{SY} & G_{mm}^{SY} & \dots & B_{mp}^{SY} & G_{mp}^{SY} & \dots & B_{mq}^{SY} & G_{mq}^{SY} & \dots & 0 & 0 & \dots \\
 & \vdots & \vdots & & \vdots & \vdots & & \vdots & \vdots & & \vdots & \vdots & & \vdots & \vdots & \\
\dots & \mu_{pr} & \xi_{pr} & \dots & \mu_{pm} & \xi_{pm} & \dots & \mu_{pp} & \xi_{pp} & \dots & \mu_{pq} & \xi_{pq} & \dots & 0 & 0 & \dots \\
\dots & 0 & 0 & \dots & 0 & 0 & \dots & 1 & 0 & \dots & 0 & 0 & \dots & 0 & 0 & \dots \\
 & \vdots & \vdots & & \vdots & \vdots & & \vdots & \vdots & & \vdots & \vdots & & \vdots & \vdots & \\
\dots & G_{qr}^{SY} & -B_{qr}^{SY} & \dots & G_{qm}^{SY} & -B_{qm}^{SY} & \dots & G_{qp}^{SY} & -B_{qp}^{SY} & \dots & (G_{qq}^{SY}+g_{SH}) & -(B_{qq}^{SY}+b_{SH}) & \dots & -g_{SH} & b_{SH} & \dots \\
\dots & B_{qr}^{SY} & G_{qr}^{SY} & \dots & B_{qm}^{SY} & G_{qm}^{SY} & \dots & B_{qp}^{SY} & G_{qp}^{SY} & \dots & (B_{qq}^{SY}+b_{SH}) & (G_{qq}^{SY}+g_{SH}) & \dots & -b_{SH} & -g_{SH} & \dots \\
 & \vdots & \vdots & & \vdots & \vdots & & \vdots & \vdots & & \vdots & \vdots & & \vdots & \vdots & \\
\dots & 0 & 0 & \dots & 0 & 0 & \dots & 0 & 0 & \dots & g_{SH} & -b_{SH} & \dots & -g_{SH} & b_{SH} & \dots \\
\multicolumn{16}{c}{\text{Select row vector from equation (6.37) corresponding to desired control mode}} \\
\dots & \vdots & \vdots & & \vdots & \vdots & & \vdots & \vdots & & \vdots & \vdots & & \vdots & \vdots & \dots
\end{bmatrix}
\begin{bmatrix}
\vdots \\ V_{rre}[n] \\ V_{rim}[n] \\ \vdots \\ V_{mre}[n] \\ V_{mim}[n] \\ \vdots \\ V_{pre}[n] \\ V_{pim}[n] \\ \vdots \\ V_{qre}[n] \\ V_{qim}[n] \\ \vdots \\ V_{SHre}[n] \\ V_{SHim}[n] \\ \vdots
\end{bmatrix}
=
\begin{bmatrix}
\vdots \\ \Re[RHS\_of\_Eq\ (5.25)] \\ 0 \\ \vdots \\ \Re[RHS\_of\_Eq\ (5.34)] \\ \Im[RHS\_of\_Eq\ (5.34)] \\ \vdots \\ \Re[RHS\_of\_Eq\ (5.46)] \\ \Im[RHS\_of\_Eq\ (5.49)] \\ \vdots \\ \Re[RHS\_of\_Eq\ (6.5)] \\ \Im[RHS\_of\_Eq\ (6.5)] \\ \vdots \\ RHS\_of\_Eq\ (6.9) \\ \text{RHS of desired mode from Eq (6.37)} \\ \vdots
\end{bmatrix}
; \text{for } n \geq 1 \quad (6.36)
$$

$$
\begin{bmatrix}
\dots & 0 & 0 & \dots & 0 & 0 & \dots & 0 & 0 & \dots & 1 & 0 & \dots & 0 & 0 & \dots \\
\dots & 0 & 0 & \dots & 0 & 0 & \dots & 0 & 0 & \dots & -b_{SH} & -g_{SH} & \dots & b_{SH} & g_{SH} & \dots \\
\dots & 0 & 0 & \dots & 0 & 0 & \dots & 0 & 0 & \dots & b_{SH} & g_{SH} & \dots & -b_{SH} & -g_{SH} & \dots \\
\dots & 0 & 0 & \dots & 0 & 0 & \dots & 0 & 0 & \dots & b_{SH} & g_{SH} & \dots & -b_{SH} & -g_{SH} & \dots \\
\dots & 0 & 0 & \dots & 0 & 0 & \dots & 0 & 0 & \dots & b_{SH} & g_{SH} & \dots & -b_{SH} & -g_{SH} & \dots \\
\dots & 0 & 0 & \dots & 0 & 0 & \dots & 0 & 0 & \dots & 0 & 0 & \dots & 1 & 0 & \dots \\
\dots & 0 & 0 & \dots & 1 & 0 & \dots & 0 & 0 & \dots & 0 & 0 & \dots & 0 & 0 & \dots \\
\dots & 0 & 0 & \dots & 0 & 0 & \dots & B_{qp}^{SY} & G_{qp}^{SY} & \dots & -B_{qp}^{SY} & -G_{qp}^{SY} & \dots & 0 & 0 & \dots
\end{bmatrix}
\begin{bmatrix}
\vdots \\ V_{rre}[n] \\ V_{rim}[n] \\ \vdots \\ V_{mre}[n] \\ V_{mim}[n] \\ \vdots \\ V_{pre}[n] \\ V_{pim}[n] \\ \vdots \\ V_{qre}[n] \\ V_{qim}[n] \\ \vdots \\ V_{SHre}[n] \\ V_{SHim}[n] \\ \vdots
\end{bmatrix}
=
\begin{bmatrix}
RHS\_of\_Eq\ (6.12) \\ RHS\_of\_Eq\ (6.16) \\ RHS\_of\_Eq\ (6.20) \\ RHS\_of\_Eq\ (6.25) \\ RHS\_of\_Eq\ (6.27) \\ RHS\_of\_Eq\ (6.29) \\ RHS\_of\_Eq\ (6.31) \\ RHS\_of\_Eq\ (6.35)
\end{bmatrix}
; \text{for } n \geq 1 \quad (6.37)
$$

6.3 Results and Discussions

To validate the proposed HELM model of STATCOM and explore the multi-control capabilities of the STATCOM, numerical studies have been carried out on the IEEE 30 and 118-bus test systems. The impedance of STATCOM coupling transformer is assumed as $Z_{SH} = 0.1 + j0.1$ *p.u.* In order to validate the proposed model of STATCOM and its multi-control capabilities in power flow studies, cases 1-9 on the IEEE 30 and 118-bus test systems have been carried out.

6.3.1 IEEE 30-Bus Test system

Case 1 is the base case without STATCOM. In IEEE 30-bus test system the STATCOM is installed at bus 12 for cases 2-9 [122]. In cases 2-9, eight different control modes has been investigated. The number of iteration (NI) and number of terms (NT) are measure of convergence for models based on N-R method and HELM respectively. The results of different control modes are shown in Table 6.1.

Specified values of parameters and number of terms (NT) for each control mode are shown in third and last column respectively, in Table 6.1. Desired parameters obtained for different control modes are shown in bold letters. It is evident from this table that proposed model of STATCOM is able to control the voltage of bus no. 12 to the specified value 1 *p.u.* as per the control mode 1. Investigation of control mode 2 from this table proves that absorbed shunt power is equal to control reference 1 *p.u.* Since the proposed model is acting in inductive mode, voltage of STATCOM connected bus 12 is 0.7954 *p.u.*, which is minimum among all the considered cases. System losses are also maximum for this case. The proposed model can also act like a controllable admittance which can be verified from control mode 3 of this table. In controlled shunt current injection modes 4 (leading) and 5 (lagging), the STATCOM current is controlled to specified value 0.2 *p.u.* Case 7 of the table demonstrates the capability of proposed model to control the output voltage of STATCOM to specified value 1 *p.u.* which is shown in 6^{th} column of the table with bold letters. Voltage of the bus 12 in this case is 1.0177 *p.u.* As the STATCOM voltage is lower than bus voltage, the STATCOM acts in inductive mode and absorbs reactive power of 0.3563 *p.u.* Voltage of the bus 17 was 1.0392 *p.u.* without STATCOM which was controlled to specified value 1 *p.u.* as per case 8. The reactive power control of a transmission line using STATCOM is significant. In case 9, the STATCOM controls the reactive power flow of transmission line 12-13 from -0.1026 *p.u.* to a specified value 0.0

p.u. The transmission line flow capacity can be increased by forcing the reactive power flow through transmission line to zero. This control mode may be attractive in electricity market environments, as re-dispatching active power becomes much more expensive than controlling reactive power. The system losses for different cases are also compared and shown in the Table 6.1.

Studies have also been carried out with the device limit constraints to prove robustness of proposed model and results are presented in Table 6.2. Whenever the limit constraints are violated, the controlled mode is relaxed. The symbols LLV/ULV denote the lower and upper limit violation. Limits of STATCOM output voltage V_{SH} are selected as 0.9-1.1 *p.u.* For base case, when the specified voltage of bus 12 is considered as 0.9 *p.u.* and constraints are not enforced, lower limit of V_{SH} is violated. When limit constraints are imposed, control mode is released. Voltage of bus 12 is 0.9375 *p.u.* while V_{SH} is maintained to lower limit 0.9 *p.u.* To test the case of upper limit violation, loading is increased to 1.65 times the base case load and V_{12}^{SP} is considered as 1.06 *p.u.* Voltage V_{SH} is 1.1050 *p.u.* in unconstrained condition that violates the upper limit. When limits are imposed, V_{SH} is maintained to upper limit 1.1 *p.u.* while V_{12}^{SP} is observed to be 1.0567 *p.u.*

TABLE 6.1: Numerical results of proposed model with different control mode on the IEEE 30-bus test system

Case No.	Control Mode	Control Reference ($p.u.$)	Different Bus Voltages ($p.u.$)	Reactive Power Flows ($p.u.$)	STATCOM Parameters ($p.u.$)	System Losses P_{loss} (MW) Q_{loss} $(MVAr)$	NT
1	None	NA	$V_9 = 1.0511\angle -14.43^\circ$ $V_{11} = 1.0820\angle -14.43^\circ$ $V_{12} = 1.0574\angle -15.30^\circ$ $V_{13} = 1.0710\angle -15.30^\circ$ $V_{17} = 1.0392\angle -16.18^\circ$	$Q_{9-11} = -0.1564$ $Q_{12-13} = -0.1026$	NA	$P_{loss} = 17.60$ $Q_{loss} = 23.02$	8
2	1	$V_{12}^{SP} = 1$	$V_9 = 1.0380\angle -14.78^\circ$ $V_{11} = 1.082\angle -14.78^\circ$ $\mathbf{V_{12} = 1\angle -15.28^\circ}$ $V_{13} = 1.0325\angle -15.28^\circ$ $V_{17} = 1.0095\angle -16.64^\circ$	$Q_{9-11} = -0.2195$ $Q_{12-13} = -0.2324$	$\lvert V_{SH}\rvert = 0.9772$ $\theta_{SH} = -13.99^\circ$ $Q_{SH} = -0.4501$ $b_{eq(SH)} = -0.4607$ $I_{SH} = -0.4502$	$P_{loss} = 18.19$ $Q_{loss} = 25.87$	8
3	2	$Q_{SH}^{SP} = -1$	$V_9 = 0.9305\angle -16.52^\circ$ $V_{11} = 0.9813\angle -16.52^\circ$ $V_{12} = 0.7954\angle -16.85^\circ$ $V_{13} = 0.8356\angle -16.85^\circ$ $V_{17} = 0.8666\angle -19.26^\circ$	$Q_{9-11} = -0.2275$ $Q_{12-13} = -0.2284$	$\lvert V_{SH}\rvert = 0.7299$ $\theta_{SH} = -12.30^\circ$ $\mathbf{Q_{SH} = -1}$ $b_{eq(SH)} = -1.7275$ $I_{SH} = -1.2608$	$P_{loss} = 24.98$ $Q_{loss} = 64.15$	14

Continued on next page

Table 6.1 – *Continued from previous page*

Case No.	Control Mode	Control Reference ($p.u.$)	Different Bus Voltages ($p.u.$)	Reactive Power Flows ($p.u.$)	STATCOM Parameters ($p.u.$)	System Losses P_{loss} (MW) Q_{loss} $(MVAr)$	NT
4	3	$b_{eq(SH)}^{SP} = -0.1$	$V_9 = 1.0492\angle -14.47°$ $V_{11} = 1.0820\angle -14.47°$ $V_{12} = 1.0492\angle -15.28°$ $V_{13} = 1.0710\angle -15.28°$ $V_{17} = 1.0349\angle -16.23°$	$Q_{9-11} = -0.1655$ $Q_{12-13} = -0.1635$	$\lvert V_{SH}\rvert = 1.0439$ $\theta_{SH} = -14.99\ °$ $Q_{SH} = -0.1095$ $\mathbf{b_{eq(SH)} = -0.1}$ $I_{SH} = -0.1044$	$P_{loss} = 17.63$ $Q_{loss} = 23.23$	8
5	4	$I_{SH}^{SP} = 0.2$ (Capacitive)	$V_9 = 1.0546\angle -14.37°$ $V_{11} = 1.0820\angle -14.37°$ $V_{12} = 1.0731\angle -15.37°$ $V_{13} = 1.0710\angle -15.37°$ $V_{17} = 1.0473\angle -16.11°$	$Q_{9-11} = -0.1388$ $Q_{12-13} = 0.0164$	$\lvert V_{SH}\rvert = 1.0831$ $\theta_{SH} = -15.91°$ $Q_{SH} = 0.2146$ $b_{eq(SH)} = 0.1847$ $\mathbf{I_{SH} = 0.2}$	$P_{loss} = 17.61$ $Q_{loss} = 23.28$	8
6	5	$I_{SH}^{SP} = 0.2$ (Inductive)	$V_9 = 1.0475\angle -14.51°$ $V_{11} = 1.082\angle -14.51°$ $V_{12} = 1.0416\angle -15.27°$ $V_{13} = 1.0710\angle -15.27°$ $V_{17} = 1.0310\angle -16.29°$	$Q_{9-11} = -0.1739$ $Q_{12-13} = -0.2187$	$\lvert V_{SH}\rvert = 1.0316$ $\theta_{SH} = -14.72°$ $Q_{SH} = -0.2083$ $b_{eq(SH)} = -0.1939$ $\mathbf{I_{SH} = -0.2}$	$P_{loss} = 17.68$ $Q_{loss} = 23.65$	8

Continued on next page

Table 6.1 – *Continued from previous page*

Case No.	Control Mode	Control Reference ($p.u.$)	Different Bus Voltages ($p.u.$)	Reactive Power Flows ($p.u.$)	STATCOM Parameters ($p.u.$)	System Losses P_{loss} (MW) Q_{loss} $(MVAr)$	NT
7	6	$V_{SH}^{SP} = 1$	$V_9 = 1.0420\angle -14.66^\circ$ $V_{11} = 1.0820\angle -14.66^\circ$ $V_{12} = 1.0177\angle -15.26^\circ$ $V_{13} = 1.0497\angle -15.26^\circ$ $V_{17} = 1.0186\angle -16.48^\circ$	$Q_{9-11} = -0.2002$ $Q_{12-13} = -0.2327$	$\mathbf{\lvert V_{SH}\rvert = 1}$ $\theta_{SH} = -14.28^\circ$ $Q_{SH} = -0.3563$ $b_{eq(SH)} = -0.3502$ $I_{SH} = -0.3502$	$P_{loss} = 17.93$ $Q_{loss} = 24.66$	8
8	7	$V_{17}^{SP} = 1$	$V_9 = 1.0329\angle -14.90^\circ$ $V_{11} = 1.0792\angle -14.90^\circ$ $V_{12} = 0.9829\angle -15.32^\circ$ $V_{13} = 1.0160\angle -15.32^\circ$ $\mathbf{V_{17} = 1\angle -16.81^\circ}$	$Q_{9-11} = -0.2297$ $Q_{12-13} = -0.2322$	$\lvert V_{SH}\rvert = 0.9554$ $\theta_{SH} = -13.73^\circ$ $Q_{SH} = -0.5333$ $b_{eq(SH)} = -0.5682$ $I_{SH} = -0.5428$	$P_{loss} = 18.51$ $Q_{loss} = 27.37$	8
9	8	$Q_{13-12}^{SP} = 0.0$	$V_9 = 1.0541\angle -14.38^\circ$ $V_{11} = 1.0820\angle -14.38^\circ$ $V_{12} = 1.0710\angle -15.36^\circ$ $V_{13} = 1.0710\angle -15.36^\circ$ $V_{17} = 1.0462\angle -16.12^\circ$	$Q_{9-11} = -0.1412$ $\mathbf{Q_{12-13} = 0.0}$	$\lvert V_{SH}\rvert = 1.0796$ $\theta_{SH} = -15.82^\circ$ $Q_{SH} = 0.1850$ $b_{eq(SH)} = 0.16$ $I_{SH} = 0.1728$	$P_{loss} = 17.60$ $Q_{loss} = 23.20$	8

TABLE 6.2: Power flows results of case 2 for the IEEE 30-bus test system with/without constraint $0.9 \leq |V_{SH}| \leq 1.1$

Specified Parameters	Limits	LLV/ULV	NT	Power Flow Results $(p.u.)$
$V_{12}^{SP} = 0.9\ (p.u.)$	Not Imposed	NA	10	$V_{12} = 0.9\angle -15.76^{\circ}$ $V_{SH} = 0.8550\angle -12.97^{\circ}$ $S_{12-13} = 0 - j0.2308$ $P_{loss} = 0.2060$ $Q_{loss} = 0.3911$
	Imposed	LLV	8	$V_{12} = 0.9375\angle -15.52^{\circ}$ $V_{SH} = 0.9\angle -13.27^{\circ}$ $S_{12-13} = 0 - j0.2314$ $P_{loss} = 0.1951$ $Q_{loss} = 0.3285$
$V_{12}^{SP} = 1.06\ (p.u.)$	Not Imposed	NA	12	$V_{12} = 1.06\angle -30.81^{\circ}$ $V_{SH} = 1.1050\angle -33.30^{\circ}$ $S_{12-13} = 0 - j0.0833$ $P_{loss} = 0.6560$ $Q_{loss} = 2.1783$
	Imposed	ULV	14	$V_{12} = 1.0567\angle -30.82^{\circ}$ $V_{SH} = 1.1\angle -33.22^{\circ}$ $S_{12-13} = 0 - j0.1082$ $P_{loss} = 0.6570$ $Q_{loss} = 2.1811$

6.3.1.1 Effect of initial conditions

The proposed model not only have multi-control capabilities but also have excellent convergence characteristics. To demonstrate the unique feature of the proposed model, the model is tested under various system/operating conditions and compared with conventional N-R method based model. The results of control mode 1 are shown to demonstrate the effect of initial conditions. As shown in Table 6.3, the solution of conventional model depends on initial conditions. As initial conditions are changed, solutions are also affected. It is verified from this table that the line flows, bus voltages, and line losses are different for diverse value of initial conditions. It shows that conventional model converges on spurious solutions. It is also seen from this table that the improper choice of initial conditions diverged the solution in many cases which indicates that there is no guarantee of convergence. Number of iterations are also affected by the initial conditions. It varies from 6 to 10 for different initial conditions.

TABLE 6.3: Effect of initial conditions on Conventional N-R based model and proposed HELM model of STATCOM

STATCOM Model	Initial Conditions/Germ Solution		NI/NT	Different Bus Voltages *(p.u.)*	Power Flows of Different Lines *(p.u.)*	System Losses P_{loss} (MW) Q_{loss} $(MVAR)$
	V_{SH} *(p.u.)*	θ_{SH} (Degree)				
Conventional N-R based Model	1	0	6	$V_9 = 1.037\angle -14.832°$ $V_{11} = 1.082\angle -14.832°$ $V_{12} = 1\angle -15.335°$ $V_{13} = 1.031\angle -15.335°$ $V_{17} = 1.009\angle -16.693°$	$Q_{9-11} = -0.22495$ $P_{27-30} = 0.07097$ $Q_{27-30} = 0.01672$ $P_{29-30} = 0.03705$ $Q_{29-30} = 0.00608$	$P_{loss} = 18.228$ $Q_{loss} = 28.628$
	1	8	7	$V_9 = 1.037\angle -14.832°$ $V_{11} = 1.082\angle -14.832°$ $V_{12} = 1\angle -15.335°$ $V_{13} = 1.031\angle -15.335°$ $V_{17} = 1.009\angle -16.693°$	$Q_{9-11} = -0.22495$ $P_{27-30} = 0.07097$ $Q_{27-30} = 0.01672$ $P_{29-30} = 0.03705$ $Q_{29-30} = 0.00608$	$P_{loss} = 18.228$ $Q_{loss} = 28.628$
	1.1	15	8	$V_9 = 1.037\angle -14.832°$ $V_{11} = 1.082\angle -14.832°$ $V_{12} = 1\angle -15.335°$ $V_{13} = 1.031\angle -15.335°$ $V_{17} = 1.009\angle -16.693°$	$Q_{9-11} = -0.22495$ $P_{27-30} = 0.07097$ $Q_{27-30} = 0.01672$ $P_{29-30} = 0.03705$ $Q_{29-30} = 0.00608$	$P_{loss} = 18.228$ $Q_{loss} = 28.628$
	0.9	-39	8	$V_9 = 1.037\angle -14.832°$ $V_{11} = 1.082\angle -14.832°$ $V_{12} = 1\angle -15.335°$ $V_{13} = 1.031\angle -15.335°$ $V_{17} = 1.009\angle -16.693°$	$Q_{9-11} = -0.22495$ $P_{27-30} = 0.07097$ $Q_{27-30} = 0.01672$ $P_{29-30} = 0.03705$ $Q_{29-30} = 0.00608$	$P_{loss} = 18.228$ $Q_{loss} = 28.628$
	0.9	-40	Diverged	NA	NA	NA
	1.1	-40	10	$V_9 = 1.041\angle -14.819°$ $V_{11} = 1.082\angle -14.819°$ $V_{12} = 1\angle -15.275°$ $V_{13} = 1.031\angle -15.275°$ $V_{17} = 1.012\angle -16.669°$	$Q_{9-11} = -0.20591$ $P_{27-30} = 0.06192$ $Q_{27-30} = 0.01672$ $P_{29-30} = 0.03704$ $Q_{29-30} = 0.00607$	$P_{loss} = 18.244$ $Q_{loss} = 28.099$
	1.1	-41	Diverged	NA	NA	NA
Proposed Model	1	0	8	$V_9 = 1.038\angle -14.7812°$ $V_{11} = 1.082\angle -14.7812°$ $V_{12} = 1\angle -15.2824°$ $V_{13} = 1.0325\angle -15.2824°$ $V_{17} = 1.0095\angle -16.6432°$	$Q_{9-11} = -0.2195$ $P_{27-30} = 0.0710$ $Q_{27-30} = 0.0167$ $P_{29-30} = 0.0370$ $Q_{29-30} = 0.0061$	$P_{loss} = 18.19$ $Q_{loss} = 25.87$

Conversely, in the proposed HELM model of STATCOM the initial conditions or germ solutions are deterministic. The solution is unique and took 8 number of terms to converge. As the STATCOM is a shunt connected device, the better choice is $V_{SH} = 1\angle 0°$ known from the past experience. But, in the proposed model initial parameters are deterministic. The aim of this section is to illustrate the difference between the choice and deterministic nature of initial conditions. This problem is more serious when SSSC is connected in series and better choice of the initial condition is not $V_{SE} = 1\angle 0°$. Also, rigorous analysis is needed to evaluate the initial parameters for each system. But, in the HE approach, the initial parameters are deterministic and remain same for each system condition.

Robustness of the proposed method is also reflected by the fact that convergence characteristics of proposed model are insensitive to the impedance of coupling transformer. From Table 6.4, it can be observed that the NT is not sensitive to the coupling transformer impedance. For base case, NT of proposed model is found to be 8 while NI of conventional N-R method based model varied for different values of impedance. In some of the cases, solution is diverged which proves weakness of the N-R based models. The model is also tested under heavy loading conditions and similar results are observed from Table 6.4. Repetition of the results for different operating conditions confirm that convergence characteristics of the proposed model are unaffected by the value of coupling transformer impedance. From various simulation results it is verified that the proposed HELM model of STATCOM is a reliable model which provide the solution under all the conditions if solution exists.

TABLE 6.4: Effect of STATCOM coupling transformer leakage impedance (30-bus)

Z_{SH} $(p.u.)$	Base Case		Heavy Loading	
	Conventional N-R based Model (NI)	Proposed Model (NT)	Conventional N-R based Model (NI)	Proposed Model (NT)
0.1+j0.1	6	8	11	12
0.01+j0.01	6	8	12	12
0.001+j0.001	Diverged	8	Diverged	12
0.0001+j0.0001	Diverged	8	Diverged	12

6.3.2 IEEE 118-Bus Test System

The proposed model of STATCOM and its multi-control capabilities have also been investigated on IEEE 118-bus test system. Case 1 is the base case without STATCOM. The different STATCOM are installed at buses 21, 45 and 94 for cases 2-9 [122]. In cases 2-9, different control modes have been investigated. The results of different control modes are shown in Table 6.5. Specified values of parameters and number of terms (NT) for each case are shown in third and last column respectively, in Table 6.5. Desired parameters obtained for different cases are shown in bold letters. It is evident from this table that proposed model of STATCOM is able to control the voltage of buses 21, 45 and 94 to the specified value 1 *p.u.* as per the case 2. Investigation of case 3 from this table proves that absorbed shunt power are equal to control reference 1 *p.u.* Since proposed model is acting in inductive mode, voltage of STATCOM connected buses 21, 45 and 94 are 0.7343, 0.8519 and 0.9085 *p.u.* respectively, which is minimum among all the considered cases. Proposed model can also acts like a controllable admittance which can be verified from case 4 of this table. In controlled shunt current injection case 5 (leading) and 6 (lagging), the STATCOM current is controlled to specified value 0.2 *p.u.* Case 7 of the table demonstrates the capability of proposed model to control the output voltage of STATCOMs to specified value 1 *p.u.* which is shown in 3^{th} column of the table with bold letters. Voltage of the buses 21, 45 and 94 in this case are 0.9883, 0.9946 and 0.9939 *p.u.* respectively. As the STATCOM voltages are lower than bus voltage, the STATCOM acts in inductive mode and absorbs reactive power of 0.0232, 0.8793 and 0.3465 *p.u.* respectively. Voltage of the buses 23, 43 and 94 were 0.9997, 0.9788 and 0.9909 *p.u.* respectively without STATCOMs which were controlled to specified value 1 *p.u.* as per case 8. In case 9, all three STATCOM work in different control mode and from Table 6.5 it can be observed that all three specified parameters have been achieved. The system losses for different cases are also shown in the Table 6.5.

TABLE 6.5: Numerical results of proposed model with different control mode on the IEEE 118-bus test system

Case No.	Control Reference ($p.u.$)	Power Flow Solutions ($p.u.$)	System Losses P_{loss} (MW) Q_{loss} $(MVAR)$	NT
1	NA	$V_{20} = 0.9581\angle -17.81°$, $V_{21} = 0.9587\angle -16.22°$, $V_{23} = 0.9997\angle -8.75°$ $V_{43} = 0.9788\angle -18.54°$, $V_{45} = 0.9870\angle -14.23°$, $V_{46} = 1.0050\angle -11.42°$ $V_{92} = 0.9930\angle 3.84°$, $V_{94} = 0.9909\angle -1.31°$, $V_{100} = 1.0170\angle -1.92°$ $Q_{20-21} = 0.0496$, $Q_{45-46} = -0.0310$, $Q_{94-100} = -0.4884$	$P_{loss} = 132.43$ $Q_{loss} = 560.95$	10
2	$V_{21}^{SP} = 1$ $V_{45}^{SP} = 1$ $V_{94}^{SP} = 1$	$V_{20} = 0.9839\angle -18.08°$, $\mathbf{V_{21} = 1\angle -16.75°}$, $V_{23} = 1.0033\angle -8.88°$ $V_{43} = 0.9836\angle -18.59°$, $\mathbf{V_{45} = 1\angle -14.45°}$, $V_{46} = 1.0050\angle -11.44°$ $V_{92} = 0.9945\angle 3.77°$, $\mathbf{V_{94} = 1\angle -1.49°}$, $V_{100} = 1.0170\angle -1.94°$ $V_{SH}^{21} = 1.0162\angle -17.68°$, $V_{SH}^{45} = 1.0093\angle -14.98°$, $V_{SH}^{94} = 1.0172\angle -2.49°$ $Q_{20-21} = 0.0496$, $Q_{45-46} = -0.0310$, $Q_{94-100} = -0.4884$, $Q_{SH}^{21} = 0.3269$ $Q_{SH}^{45} = 0.1873$, $Q_{SH}^{94} = 0.3465$, $b_{eq(SH)}^{21} = 0.3217$, $b_{eq(SH)}^{45} = 0.1856$ $b_{eq(SH)}^{94} = 0.3407$, $I_{SH}^{21} = 0.3270$, $I_{SH}^{45} = 0.1873$, $I_{SH}^{94} = 0.3465$	$P_{loss} = 132.28$ $Q_{loss} = 563.11$	10

Continued on next page

Table 6.5 – *Continued from previous page*

Case No.	Control Reference ($p.u.$)	Power Flow Solutions ($p.u.$)	System Losses P_{loss} (MW) Q_{loss} $(MVAr)$	NT
3	$Q_{SH}^{SP(21)} = -1$ $Q_{SH}^{SP(45)} = -1$ $Q_{SH}^{SP(94)} = -1$	$V_{20} = 0.8615\angle -18.78°$, $V_{21} = 0.7995\angle -16.46°$, $V_{23} = 0.9860\angle -9.51°$ $V_{43} = 0.9517\angle -19.37°$, $V_{45} = 0.9087\angle -14.05°$, $V_{46} = 1.0050\angle -12.13°$ $V_{92} = 0.9876\angle 3.49°$, $V_{94} = 0.9619\angle -1.39°$, $V_{100} = 1.0156\angle -2.42°$ $V_{SH}^{21} = 0.7343\angle -11.96°$, $V_{SH}^{45} = 0.8519\angle -10.57°$, $V_{SH}^{94} = 0.9085\angle 1.71°$ $Q_{20-21} = 0.6669$, $Q_{45-46} = -0.5429$, $Q_{94-100} = 0.1015$, $\mathbf{Q_{SH}^{21}} = \mathbf{-1}$ $\mathbf{Q_{SH}^{45}} = \mathbf{-1}$, $\mathbf{Q_{SH}^{94}} = \mathbf{-1}$, $b_{eq(SH)}^{21} = -1.7085$, $b_{eq(SH)}^{45} = -1.2943$ $b_{eq(SH)}^{94} = -1.1460$, $I_{SH}^{21} = -1.2546$, $I_{SH}^{45} = -1.1025$, $I_{SH}^{94} = -1.0411$	$P_{loss} = 145.25$ $Q_{loss} = 499.36$	10
4	$b_{eq(SH)}^{SP(21)} = -0.1$ $b_{eq(SH)}^{SP(45)} = -0.1$ $b_{eq(SH)}^{SP(94)} = -0.1$	$V_{20} = 0.9511\angle -17.77°$, $V_{21} = 0.9471\angle -16.12°$, $V_{23} = 0.9988\angle -8.74°$ $V_{43} = 0.9765\angle -18.54°$, $V_{45} = 0.9803\angle -14.14°$, $V_{46} = 1.0050\angle -11.42°$ $V_{92} = 0.9930\angle 3.84°$, $V_{94} = 0.9884\angle -1.28°$, $V_{100} = 1.0170\angle -1.92°$ $V_{SH}^{21} = 0.9424\angle -15.84°$, $V_{SH}^{45} = 0.9754\angle -13.85°$, $V_{SH}^{94} = 0.9834\angle -0.99°$ $Q_{20-21} = 0.1011$, $Q_{45-46} = -0.0796$, $Q_{94-100} = 0.0984$, $Q_{SH}^{21} = -0.0892$ $Q_{SH}^{45} = -0.0956$, $Q_{SH}^{94} = -0.0972$, $\mathbf{b_{eq(SH)}^{21}} = \mathbf{-0.1}$, $\mathbf{b_{eq(SH)}^{45}} = \mathbf{-0.1}$ $\mathbf{b_{eq(SH)}^{94}} = \mathbf{-0.1}$, $I_{SH}^{21} = -0.0942$, $I_{SH}^{45} = -0.0975$, $I_{SH}^{94} = -0.0983$	$P_{loss} = 132.69$ $Q_{loss} = 559.34$	10

Continued on next page

Table 6.5 – *Continued from previous page*

Case No.	Control Reference ($p.u.$)	Power Flow Solutions ($p.u.$)	System Losses P_{loss} (MW) Q_{loss} $(MVAr)$	NT
5	$I_{SH}^{SP(21)} = 0.2$ $I_{SH}^{SP(45)} = 0.2$ $I_{SH}^{SP(94)} = 0.2$	$V_{20} = 0.9739\angle -17.96°$, $V_{21} = 0.9840\angle -16.52°$, $V_{23} = 1.0019\angle -8.82°$ $V_{43} = 0.9839\angle -18.59°$, $V_{45} = 1.0009\angle -14.46°$, $V_{46} = 1.0050\angle -11.44°$ $V_{92} = 0.9936\angle 3.81°$, $V_{94} = 0.9960\angle -1.41°$, $V_{100} = 1.0170\angle -1.92°$ $V_{SH}^{21} = 0.9940\angle -17.10°$, $V_{SH}^{45} = 1.0108\angle -15.03°$, $V_{SH}^{94} = 1.0060\angle -1.98°$ $Q_{20-21} = -0.0592$, $Q_{45-46} = 0.0709$, $Q_{94-100} = 0.0986$, $Q_{SH}^{21} = 0.1968$ $Q_{SH}^{45} = 0.2002$, $Q_{SH}^{94} = 0.1992$, $b_{eq(SH)}^{21} = 0.2012$, $b_{eq(SH)}^{45} = 0.1979$ $b_{eq(SH)}^{94} = 0.1988$, $\mathbf{I_{SH}^{21} = 0.2}$, $\mathbf{I_{SH}^{45} = 0.2}$, $\mathbf{I_{SH}^{94} = 0.2}$	$P_{loss} = 132.25$ $Q_{loss} = 562.79$	10
6	$I_{SH}^{SP(21)} = -0.2$ $I_{SH}^{SP(45)} = -0.2$ $I_{SH}^{SP(94)} = -0.2$	$V_{20} = 0.9437\angle -17.76°$, $V_{21} = 0.9343\angle -16.03°$, $V_{23} = 0.9977\angle -8.74°$ $V_{43} = 0.9740\angle -18.55°$, $V_{45} = 0.9731\angle -14.05°$, $V_{46} = 1.0050\angle -11.44°$ $V_{92} = 0.9930\angle 3.83°$, $V_{94} = 0.9858\angle -1.25°$, $V_{100} = 1.0170\angle 1.94°$ $V_{SH}^{21} = 0.9243\angle -15.42°$, $V_{SH}^{45} = 0.9631\angle -13.46°$, $V_{SH}^{94} = 0.9758\angle -0.67°$ $Q_{20-21} = 0.1591$, $Q_{45-46} = -0.1300$, $Q_{94-100} = 0.0985$, $Q_{SH}^{21} = -0.1868$ $Q_{SH}^{45} = -0.1946$, $Q_{SH}^{94} = -0.1972$, $b_{eq(SH)}^{21} = -0.2164$, $b_{eq(SH)}^{45} = -0.2077$ $b_{eq(SH)}^{94} = -0.2050$, $\mathbf{I_{SH}^{21} = -0.2}$, $\mathbf{I_{SH}^{45} = -0.2}$, $\mathbf{I_{SH}^{94} = -0.2}$	$P_{loss} = 133.12$ $Q_{loss} = 557.02$	10

Continued on next page

Table 6.5 – *Continued from previous page*

Case No.	Control Reference ($p.u.$)	Power Flow Solutions ($p.u.$)	System Losses P_{loss} (MW) Q_{loss} $(MVAr)$	NT
7	$V_{SH}^{SP(21)} = 1$ $V_{SH}^{SP(45)} = 1$ $V_{SH}^{SP(94)} = 1$	$V_{20} = 0.9766\angle -17.98°$, $V_{21} = 0.9883\angle -16.56°$, $V_{23} = 1.0023\angle -8.84°$ $V_{43} = 0.9816\angle -18.56°$, $V_{45} = 0.9946\angle -14.35°$, $V_{46} = 1.0050\angle -11.42°$ $V_{92} = 0.9931\angle 3.83°$, $V_{94} = 0.9939\angle -1.37°$, $V_{100} = 1.0170\angle -1.92°$ $\mathbf{V_{SH}^{21} = 1\angle -17.26°}$, $\mathbf{V_{SH}^{45} = 1\angle -14.66°}$, $\mathbf{V_{SH}^{94} = 1\angle 1.72°}$ $Q_{20-21} = -0.0784$, $Q_{45-46} = 0.0241$, $Q_{94-100} = 0.0986$, $Q_{SH}^{21} = 0.2317$ $Q_{SH}^{45} = 0.1082$, $Q_{SH}^{94} = 0.1211$, $b_{eq(SH)}^{21} = 0.2345$, $b_{eq(SH)}^{45} = 0.1088$ $b_{eq(SH)}^{94} = 0.1218$, $I_{SH}^{21} = 0.2345$, $I_{SH}^{45} = 0.1088$, $I_{SH}^{94} = 0.1218$	$P_{loss} = 132.28$ $Q_{loss} = 562.48$	10
8	$V_{23}^{SP} = 1$ $V_{43}^{SP} = 1$ $V_{94}^{SP} = 1$	$V_{20} = 0.9601\angle -17.89°$, $V_{21} = 0.9618\angle -16.33°$, $\mathbf{V_{23} = 1\angle -8.82°}$ $\mathbf{V_{43} = 1\angle -18.92°}$, $V_{45} = 1.0444\angle -15.48°$, $V_{46} = 1.0050\angle -11.71°$ $V_{92} = 0.9945\angle 3.74°$, $\mathbf{V_{94} = 1\angle -1.52°}$, $V_{100} = 1.0170\angle -1.96°$ $V_{SH}^{21} = 0.9630\angle -16.39°$, $V_{SH}^{45} = 1.0857\angle -17.79°$, $V_{SH}^{94} = 1.0172\angle -2.51°$ $Q_{20-21} = 0.0371$, $Q_{45-46} = 0.4147$, $Q_{94-100} = 0.0986$, $Q_{SH}^{21} = 0.0232$ $Q_{SH}^{45} = 0.8793$, $Q_{SH}^{94} = 0.3465$, $b_{eq(SH)}^{21} = 0.0250$, $b_{eq(SH)}^{45} = 0.7760$ $b_{eq(SH)}^{94} = 0.3407$, $I_{SH}^{21} = 0.0241$, $I_{SH}^{45} = 0.8425$, $I_{SH}^{94} = 0.3466$	$P_{loss} = 133.89$ $Q_{loss} = 557.79$	12

Continued on next page

Table 6.5 – *Continued from previous page*

Case No.	Control Reference $(p.u.)$	Power Flow Solutions $(p.u.)$	System Losses $P_{loss}\ (MW)$ $Q_{loss}\ (MVAr)$	NT
9	$Q_{SH}^{SP(21)} = -0.4$ $V_{45}^{SP} = 1$ $I_{SH}^{SP(94)} = 0.1$	$V_{20} = 0.9265\angle -17.76°$, $V_{21} = 0.9049\angle -15.86°$, $V_{23} = 0.9952\angle -8.74°$ $V_{43} = 0.9834\angle -18.67°$, $\mathbf{V_{45} = 1\angle -14.49°}$, $V_{46} = 1.0050\angle -11.48°$ $V_{92} = 0.9930\angle 3.82°$, $V_{94} = 0.9934\angle -1.37°$, $V_{100} = 1.0170\angle -1.93°$ $V_{SH}^{21} = 0.8825\angle -14.46°$, $V_{SH}^{45} = 1.0094\angle -15.03°$, $V_{SH}^{94} = 0.9983\angle -1.66°$ $Q_{20-21} = 0.2884$, $Q_{45-46} = 0.0648$, $Q_{94-100} = 0.0987$, $\mathbf{Q_{SH}^{21} = -0.4}$ $Q_{SH}^{45} = 0.1883$, $Q_{SH}^{94} = 0.0993$, $b_{eq(SH)}^{21} = -0.5010$, $b_{eq(SH)}^{45} = 0.1866$ $b_{eq(SH)}^{94} = 0.1002$, $I_{SH}^{21} = -0.4422$, $I_{SH}^{45} = 0.1883$, $\mathbf{I_{SH}^{94} = 0.1}$	$P_{loss} = 133.41$ $Q_{loss} = 555.39$	10

TABLE 6.6: Power flows results of case 2 for the IEEE 118-bus test system with/without constraint $0.9 \leq |V_{SH}| \leq 1.1$

Specified Parameters	Limits	LLV/ULV	NT	Power Flow Results $(p.u.)$
$V_{12}^{SP} = V_{45}^{SP} = V_{94}^{SP} = 0.9\ (p.u.)$	Not Imposed	NA	10	$V_{21} = 0.9\angle -16.45^\circ$ $V_{45} = 0.9\angle -14.07^\circ$ $V_{94} = 0.9\angle -2.85^\circ$ $V_{SH}^{21} = 0.8756\angle -14.92^\circ$ $V_{SH}^{45} = 0.8367\angle -10.17^\circ$ $V_{SH}^{94} = 0.7470\angle -10.17^\circ$ $P_{loss} = 1.4890$ $Q_{loss} = 4.9086$
	Imposed	LLV	10	$V_{21} = 0.9172\angle -16.08^\circ$ $V_{45} = 0.9366\angle -13.81^\circ$ $V_{94} = 0.9586\angle -1.29^\circ$ $V_{SH}^{21} = 0.9\angle -15.01^\circ$ $V_{SH}^{45} = 0.9\angle -11.62^\circ$ $V_{SH}^{94} = 0.9\angle 2.11^\circ$ $P_{loss} = 1.3707$ $Q_{loss} = 5.3968$
$V_{12}^{SP} = V_{45}^{SP} = V_{94}^{SP} = 1.07\ (p.u.)$	Not Imposed	NA	10	$V_{21} = 1.07\angle -18.54^\circ$ $V_{45} = 1.07\angle -16.66^\circ$ $V_{94} = 1.07\angle -5.71^\circ$ $V_{SH}^{21} = 1.1130\angle -20.89^\circ$ $V_{SH}^{45} = 1.1294\angle -19.93^\circ$ $V_{SH}^{94} = 1.2130\angle -13.99^\circ$ $P_{loss} = 1.4374$ $Q_{loss} = 5.2806$
	Imposed	ULV	10	$V_{21} = 1.0605\angle -17.99^\circ$ $V_{45} = 1.0529\angle -15.85^\circ$ $V_{94} = 1.0296\angle -2.67^\circ$ $V_{SH}^{21} = 1.1\angle -20.17^\circ$ $V_{SH}^{45} = 1.1\angle -18.47^\circ$ $V_{SH}^{94} = 1.1\angle -6.74^\circ$ $P_{loss} = 1.3651$ $Q_{loss} = 5.5114$

The studies have also been carried out for IEEE 118-bus test system with the device limit constraints to prove robustness of proposed model and results are presented in Table 6.6. Whenever the limit constraints are violated, the controlled mode is relaxed. Lower and upper limits of output voltage for all the three STATCOMs are considered 0.9 and 1.1

p.u. respectively. For base case, when the specified voltage of buses 21, 45 and 94 are considered as 0.9 *p.u.* and constraints are not enforced, lower limits of V_{SH} are violated. When limit constraints are imposed, control mode are released. Voltage of buses 21, 45 and 94 are 0.9172, 0.9366 and 0.9586 *p.u.* respectively, while STATCOMs output voltage are maintained to lower limit 0.9 *p.u.* To test the case of upper limit violation, V_{21}^{SP}, V_{45}^{SP} and V_{94}^{SP} are considered as 1.07 *p.u.* Voltages V_{SH}^{21}, V_{SH}^{45} and V_{SH}^{94} are 1.1130, 1.1294 and 1.2130 *p.u.* respectively in unconstrained condition that violates the upper limits. When limits are imposed, V_{SH}^{21}, V_{SH}^{45} and V_{SH}^{94} are maintained to upper limit 1.1 *p.u.*, while V_{21}^{SP}, V_{45}^{SP} and V_{94}^{SP} are observed to be 1.0605, 1.0529 and 1.0296 *p.u.* respectively.

Proposed model not only have multi-control capabilities but also have excellent convergence characteristics. To demonstrate the unique feature of the proposed model, the model is tested under various operating conditions. The convergence characteristics of the proposed model w.r.t. to the impedance of coupling transformers (*i.e.* STATCOM 1, 2 and 3) have been presented in Table 6.7 for IEEE 118-bus test system to prove robustness of the proposed model. From Table 6.7, it can be observed that the NT is not sensitive to the coupling transformer impedance. For base case, NT of proposed model is found to be 10. The proposed model is also tested under heavy loading conditions and similar results are observed from Table 6.7. Repetitions of the results for different operating conditions confirm that convergence characteristics of proposed model are unaffected by the value of coupling transformer impedance. From various simulation results it is verified that the proposed HELM model of STATCOM is a reliable model which provide the solution under all the conditions if solution exists.

Table 6.7: Effect of STATCOM coupling transformer leakage impedance (118-bus)

Z_{SH} (*p.u.*)	Proposed Model (NT)	
	Base Case	Heavy Loading
0.1+j0.1	10	14
0.01+j0.01	10	14
0.001+j0.001	10	14
0.0001+j0.0001	10	14

6.4 Summary

In this chapter, HELM model of STATCOM is proposed. The proposed model is developed using Holomorphic Embedding technique in place of conventional N-R technique to

overcome the problem of convergence. The proposed model has following features:

- Various control modes to control different parameters.
- Non-iterative approach based model.
- Clear indication if solution doesn't exist.
- Initial conditions are deterministic in nature.
- Always converges, even for ill conditioned power system if solution exists.
- Robust and reliable.
- Complexity of Jacobian matrix and its factorization is not present.

The multi-control capability of HELM model of STATCOM is investigated on IEEE 30-bus and 118-bus test systems and compared with conventional model. The convergence characteristics of proposed model are also tested for different values of impedance of coupling transformer. Simulation results of various system/operating conditions prove that the proposed model offers unique solution. Convergence characteristics of the proposed model are not affected by change in initial conditions of the system which proves the reliability and robustness of the model.

Chapter 7

Optimal Allocation of STATCOM to Improve Power System Performance

7.1 Introduction

Nowadays, the electrical power system is experiencing new challenges due to various Technical, Economical and Environmental (TEE) constraints, which result in stressed operating conditions. The stressed operating conditions may lead the system to voltage instability and loss of economy, if corrective control actions are not taken [19]. The insufficient reactive power, heavy loading on the transmission line and power shipping across long distances play a vital role in consequent blackouts and voltage collapse. The FACTS devices have been utilized for adequate operation of existing power system infrastructures by controlling the power flow over designated transmission routes. FACTS devices are also used to enhance voltage stability margin and the system security. As the FACTS devices control the power flow in transmission lines, the system losses can be reduced *i.e.* the efficiency of the system can be improved [101, 102, 105]. Each FACTS device has its own advantages and limitations, and zone of application. The most effective use of FACTS devices depends on the locations and sizes of these devices [95]. Therefore, the FACTS devices should be optimally allocated to extract the maximum possible benefits. The optimal allocation of FACTS devices can improve the power system performance in terms of better node voltage profile, reduce system losses and power flows, and better power quality and reliability of power supply [98, 105, 106]. The optimal allocation problem of FACTS devices involves

the determination of their optimal number, location and size in the power system and it is a non-linear complex combinatorial optimization problem which is subjected to various equality and non-equality constraints.

As discussed in Chapter 2, various techniques have been used to optimally allocate the FACTS devices in the transmission system which can be classified into three broad categories: classical optimization methods, evolutionary computation techniques, and index based methods. Generally, analytical methods sometimes fail to determine optimal solution in an efficient manner and also suffer from slow convergence. On the other hand, meta-heuristics methods can determine optimal solution of complex optimization problems. A number of successful attempts have been made in the literature to solve the optimal allocation problem of STATCOM. Each optimization technique has its own advantages and weaknesses in terms of computational time, accuracy, and simplicity. But the challenging task is to tune the parameters which guide the algorithm to reach the solution, and care should be taken to avoid the local minima and slow convergence. For an enormously large search space, these algorithms show premature convergence as they stuck into local minima. Several researchers have made attempt to squeeze the search space by fixing or restricting the optimal candidate node location for STATCOM using indices based approaches. However, these approaches don't provide a true picture of whole power system but only offer a rough idea about the optimal candidate node location which can lead to a sub-optimal solution. The existing Sine Cosine Algorithm (SCA) has proved its potential in solving complex optimization problem, however the exploration and exploitation potential of SCA needs to be enhanced. Hence, some modifications are required to be incorporated to achieve better performance.

In this chapter, the problem of optimal allocation of HELM model of STATCOM is formulated by considering multiple objectives of conflicting nature *viz.* maximum node voltage deviation minimization, cost minimization and node severity to voltage instability minimization. In this chapter, the fuzzy approach is used to transform multiple objectives into a single objective function. As the Fuzzy framework [111, 112] offers a means to combine the objectives which are conflicting in nature and also ensures minimum degree of satisfaction among the different objectives. This formulated multi-objective problem is solved by proposing an Improved SCA, *i.e.* ISCA. Some modifications are suggested in this algorithm to enhance its exploration and exploitation capacity. To investigate the potential of proposed ISCA, it has been tested on 23 benchmark test functions and also compared with standard Ant Lion Optimizer (ALO), Grey Wolf Optimizer (GWO), Moth-flame Optimization (MFO), Particle Swarm Optimization (PSO), Whale Optimization Algorithm

(WOA) and Sine Cosine Algorithm (SCA). This section also explores the application potential of ISCA for FACTS allocation problem. The proposed method is investigated on benchmark IEEE 30 and 118-bus test systems, and application results obtained are analyzed and compared with standard GWO and SCA algorithm. The following papers have been accepted from this chapter:

- Pradeep Singh, Rajive Tiwari, Mukesh Kumar Shah, Khaleequr Rehman Niazi, Nand Kishor Meena and Saurabh Ratra, "Voltage stability index and APFC for performance improvement of modern power systems with intense renewables", *The Journal of Engineering*, IET 2018.
- Pradeep Singh and Rajive Tiwari, "Optimal Allocation of STATCOM using Improved Sine Cosine Optimization Algorithm", 8^{th} *IEEE India International Conference on Power Electronics (IICPE-2018).*

7.2 Overview of Fuzzy Logic

Fuzzy sets theory was developed by Lotfi Zadeh [112]. Fuzzy sets can be defined as:
"If X is a collection of objects denoted by x, then a fuzzy set $\widetilde{A}$ in X is a set of ordered pairs:

$$\widetilde{A} = \left\{ \left(x, \mu_{\widetilde{A}}(x)\right) \middle|\ x \ \epsilon \ X \right\} \tag{7.1}$$

Where, $\mu_{\widetilde{A}}(x)$ is called the membership function of x in $\widetilde{A}$ that maps X to the membership space M (*i.e.* $M = [0, 1]$). The range of the membership function is a subset of the non-negative real numbers and whose supremum is finite". The fuzzy approach is used to convert the multi-objective problem to single objective problem. In fuzzy domain, each objective is linked with a membership function and these membership functions indicate the degree of satisfaction of the objectives. There are various fuzzy membership function such as trapezoidal fuzzy membership function, triangular fuzzy membership function, sinusoidal fuzzy membership function *etc.* The overall degree of fuzzy satisfaction may be evaluated using different composition operations. Any one composition from 'Max-min composition', 'Max-weighted addition composition', 'Max-product composition' and 'Max-geometric mean composition' can be used to calculate the overall degree of fuzzy satisfaction. But, if the 'max-min composition' is adopted, it can't differentiate between the solutions, when one membership value is less than other membership values for the same option *i.e.* may not provide best compromising solution. The overall degree of fuzzy satisfaction will not be zero in case of 'max-weighted addition composition' until and unless

all operational constraints violate. However, the 'max-product composition' provides the best compromising solution but it doesn't convey information about the nearness of the solution to the ideal solution. Therefore, in the proposed work 'max-geometric mean composition' is used as it gives the best compromising solution without violation of any operational constraints. It can be defined as follows:

$$\mu F = \left(\mu f_1 \times \mu f_2 \times ..... \times \mu f_n\right)^{\frac{1}{n}} \tag{7.2}$$

Where, μf_1, μf_2,.....,μf_n are the fuzzy membership values of their respective objectives f_1, f_2,.....,f_n. n is the number of objectives and μF is the degree of overall fuzzy satisfaction.

7.3 Improved Sine Cosine Algorithm (ISCA)

SCA starts the optimization process with the numerous random sets of solutions as it is a population-based optimization technique [123]. These random sets of solutions are recurrently evaluated by an objective function and improved by some set of rules. In the stochastic methods, there is no guarantee to get a solution in a single run, but the probability of finding minima or maxima will be increased with enough number of random sets and effective set of rules [98, 106, 123]. As discussed in the literature, there are two important phases of the optimization process, *i.e.* exploration and exploitation. In the exploration phase, the sets of random solutions are abruptly changed with a high rate of randomness to enter into the promising area in the search space. In the next phase *i.e.* exploitation phase, there is a very gradual change in the random sets of solutions as compared to the exploration phase.

In this research work, the following improvement is suggested for the position update:

$$X_z^{i+1} = \begin{cases} X_z^i + C_1 sin(r_1)|r_2 P_z^i - X_z^i|; r_3 < 0.5 \\ X_z^i + C_1 cos(r_1)|r_2 P_z^i - X_z^i|; r_3 \geq 0.5 \end{cases} \tag{7.3}$$

Where, X_z^i and P_z^i are the position of current and destination points in z^{th} dimension in i^{th} iteration respectively. Symbol $||$ is used to denote absolute value. r_1, r_2, and r_3 are random numbers between $[0, 2\pi]$, $[0, 1]$, and $[0, 1]$ respectively. The random number r_1 decides the magnitude of displacement towards or outwards the destination. The random number r_2 works as a weighting factor for destination position in order to stochastically magnify ($r_2 > 1$) or mollify ($r_2 < 1$) the influence of destination point in defining the distance. The random number r_3 arbitrarily picks sine and cosine component of (7.3).

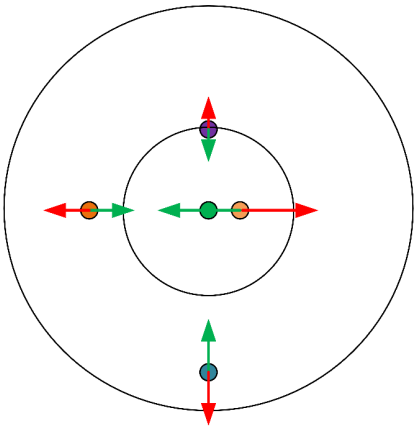

FIGURE 7.1: Effect of Sine and Cosine terms of (7.3) on the next position

Figure 7.1 demonstrates the effect of (7.3) on the next position. In Figure 7.1, the destination position is denoted by the green color dot and different sets of solutions are denoted by other color dots. How far the movements away and towards the destination is denoted by the length of red and green colored arrows respectively. For exploration of the search space, the algorithm should search the search space outside the space between the corresponding position and destination position. This can be achieved by the range of sine and cosine wave or it can be achieved by selecting the range of random number r_1. Because its magnitude mainly participate in deciding the length of the arrow. Therefore, this mechanism assures the exploration of the search space. The cyclic pattern of the sine and cosine components permit a solution to be re-positioned around another solution. This feature is responsible for the proper exploitation of the promising area. To ensure the convergence of the algorithm or to find out promising area, there should be a balance between the exploration and exploitation phase. For this purpose, equation (7.4) is proposed for adaptive change in the range of sine and cosine wave as follows:

$$C_1 = \alpha * cos\left[90^\circ - 90^\circ\left(\frac{it - it_{max}}{it_{max}}\right)\right] * cos\left[60^\circ - 60^\circ\left(\frac{it - it_{max}}{it_{max}}\right)\right] \tag{7.4}$$

Where, it and it_{max} are the current and maximum number of iterations, and α is a constant which is considered equal to 2. The plot of (7.4) shows the variation of C_1 with increase in the number of iterations. From Figure 7.2, it can be easily observed that at starting, the higher value of C_1 allows the more exploration of the search space. As the number of iterations reach towards the maximum number of iterations, the lower value of C_1 allows more exploitation. To confirm the effectiveness of the ISCA algorithm, a wide range of test problem and optimal allocation problem for HELM model of STATCOM have been investigated in Section 7.5.

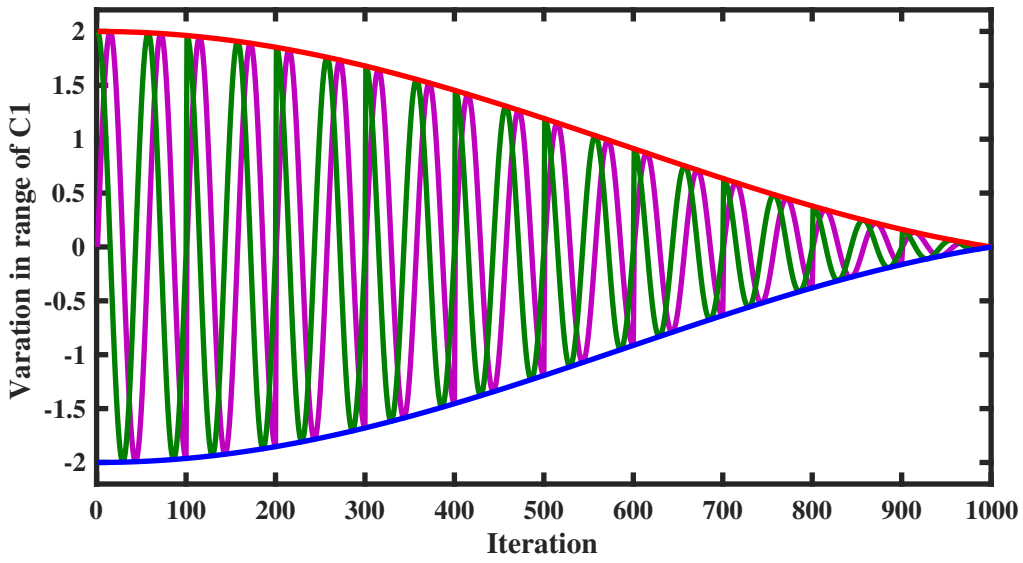

FIGURE 7.2: Pattern for range of Sine and Cosine on the course of iteration

7.4 Fuzzified Multi-Objective Problem Formulation

In this section, a fuzzified multi-objective problem for multiple STATCOM allocation with three objectives is formulated. The considered objective functions and fuzzy membership functions are discussed in the following sections.

7.4.1 Objective Functions and their Fuzzy Membership Functions

In practice, during the planning and operation of the power system more than one objectives are required to achieve. Therefore, the following three objectives are considered for STATCOM allocation problem.

1) *Minimization of Maximum Node Voltage Deviation:* The node voltage deviation is considered as an objective as it is the measure of voltage quality of the system nodes and it is essential to provide regulated node voltage profile across the system. This objective can be expressed as follows:

$$min\ f_1 = \max_{i \in PQ} |1 - V_i| \tag{7.5}$$

Where, PQ and V_i are the set of load buses and the magnitude of i^{th} load bus voltage respectively.

2) *Minimization of Node Severity to Voltage Collapse:* The minimization of the first objective is not a sufficient measure to define the security level of the power system. Therefore, to accommodate the voltage stability security, the minimization of $L-$index is also considered as an objective function. The lower value of $L-$index indicates that more voltage stability margin is available, *i.e.* the system is more secure. The value of $L-$index for any load bus can be calculated as follows:

$$L_k = \left| 1 - \frac{\sum_{i \in PV} F_{ki} V_i}{V_k} \right| \tag{7.6}$$

Where, PV is the set of generator buses and the objective function can be expressed as:

$$min\ f_2 = max(L_k);\ k\ \in\ PQ \tag{7.7}$$

3) *Minimization of Cost of STATCOM:* This objective function is considered to minimize the cost/size of the optimally located STATCOM and can be expressed as follows [124]:

$$min\ f_3 = 0.0003\eth^2 - 0.3051\eth + 127.38 \text{ US \$/kVAR} \tag{7.8}$$

Where, $\eth$ is the installed capacity of the STATCOM in $MVAR$. A linear membership function may reject the moderate value solution, therefore, a quarter cosine membership function is used to calculate the membership value for these objectives. This membership function selects the high and moderate value solutions and rejects the low-value solutions. It can be expressed as follows:

$$\mu f_j = \begin{cases} 1; & f_j \leq f_{j,min} \\ cos\left[\frac{\pi}{2} * \frac{(f_j - f_{j,min})}{(f_{j,max} - f_{j,min})}\right]; & f_{j,min} < f_j < f_{j,max} \\ 0; & f_j \geq f_{j,max} \end{cases} \tag{7.9}$$

Where, μf_j is the membership function value of the f_j objective, while $f_{j,min}$ and $f_{j,max}$ are lower and upper limits of the j^{th} objective. Multiple objectives of conflicting nature can only be satisfied simultaneously by compromising among them. As discussed in Section 7.2, the 'max-geometric mean composition' is used to obtain the overall degree of fuzzy satisfaction for the fuzzy membership functions. From (7.2), it can be expressed as:

$$\mu F = (\mu f_1 \times \mu f_2 \times \mu f_3)^{1/3} \tag{7.10}$$

The system with a maximum degree of overall fuzzy satisfaction, μF, will give the best

compromising solution. Therefore, the formulated optimization problem can be expressed as:

$$min\ f = \frac{1}{1+\mu F} \tag{7.11}$$

The function f is selected as the fitness function for the proposed ISCA since it provides best compromising solution without the violation of any operating constraints.

7.4.2 Constraints

The objective functions formulated in (7.5), (7.7) and (7.8) are subjected to the following equality and inequality constraints:

$$\begin{aligned} P_i &= V_i \sum_{k=1}^{N} V_k Y_{ik} cos(\theta_{ik} + \delta_k - \delta_i); \forall i \\ Q_i &= V_i \sum_{k=1}^{N} V_k Y_{ik} sin(\theta_{ik} + \delta_k - \delta_i); \forall i \end{aligned} \tag{7.12}$$

$$\begin{aligned} P_G^{min} \leq P_G \leq P_G^{max} \\ Q_G^{min} \leq Q_G \leq Q_G^{max} \end{aligned} \tag{7.13}$$

The constraints expressed in (7.12) represents the bus power balance equality constraints. Equation (7.13) is the set of inequality constraints, which are active and reactive power generation capability of generators. STATCOMs are allocated on the basis of individuals and fitness of every individual of the population is computed using (7.11) by running holomorphic embedded load-flow method (HELM).

7.5 Simulation Results and Discussions

The proposed algorithm is tested over numerous test functions which include unimodal, multimodal and composite test functions [123]. As the unimodal test functions family has only global minima or maxima, therefore, it is suitable for testing the speed and convergence time of an algorithm. Multi-modal test functions family has many local minima, therefore, it is suitable to check the capability of an algorithm to avoid/pass the local minima and exploration of search space. The composite test functions are the combination of unimodal and multimodal with different properties. In this research work, to solve different test functions a total number of 30 search agents are deployed to find out global minima in course of 500 iterations. The single run results may be attractive

Table 7.1: Results on benchmark functions

F	avg						
	ALO	GWO	MFO	PSO	WOA	SCA	ISCA
F1	1.00E+00	1.42E-108	1.62E-21	2.68E-34	1.46E-146	3.49E-17	2.81E-16
F2	1.97E-01	1.21E-66	1.00E+00	8.58E-21	5.31E-108	1.20E-18	5.22E-17
F3	3.76E-08	1.49E-56	1.00E+00	1.45E-14	7.54E-02	7.65E-12	1.35E-14
F4	1.48E-04	4.46E-37	4.92E-01	6.50E-10	1.00E+00	4.31E-07	9.72E-09
F5	5.15E-03	7.12E-04	1.00E+00	4.35E-04	6.55E-04	7.83E-04	7.27E-04
F6	7.91E-09	2.70E-06	1.62E-29	1.80E-32	1.81E-04	1.00E+00	5.81E-01
F7	1.00E+00	2.49E-02	4.89E-01	2.36E-01	7.46E-02	1.51E-01	1.73E-02
F8	6.81E-01	7.67E-01	9.24E-01	7.17E-01	1.00E+00	6.31E-01	5.86E-01
F9	7.84E-01	7.25E-03	1.00E+00	1.44E-01	0.00E+00	3.30E-02	0.00E+00
F10	1.00E+00	5.26E-14	5.88E-01	5.77E-14	3.87E-14	5.37E-13	1.81E-12
F11	1.00E+00	8.04E-02	7.57E-01	6.97E-01	3.07E-01	2.21E-01	0.00E+00
F12	1.00E+00	3.54E-03	1.91E-01	5.12E-32	1.89E-03	7.50E-02	4.66E-02
F13	8.61E-03	4.11E-02	8.61E-03	4.57E-32	3.82E-02	1.00E+00	5.09E-01
F14	3.10E-01	1.00E+00	4.97E-01	2.88E-33	4.89E-01	3.80E-01	2.12E-01
F15	5.91E-01	1.00E+00	2.86E-01	1.55E-01	1.48E-01	1.55E-01	9.08E-02
F16	1.00E+00	1.00E+00	1.00E+00	1.00E+00	1.00E+00	1.00E+00	1.00E+00
F17	9.96E-01	9.96E-01	9.96E-01	9.96E-01	9.96E-01	1.00E+00	9.96E-01
F18	1.00E+00	1.00E+00	1.00E+00	1.00E+00	1.00E+00	1.00E+00	1.00E+00
F19	1.00E+00	9.99E-01	1.00E+00	1.00E+00	9.99E-01	9.98E-01	9.97E-01
F20	9.96E-01	9.92E-01	9.85E-01	1.00E+00	9.94E-01	9.07E-01	6.78E-01
F21	7.54E-01	1.00E+00	6.77E-01	8.41E-01	8.92E-01	2.59E-01	6.26E-02
F22	7.18E-01	1.00E+00	6.59E-01	8.86E-01	8.26E-01	2.85E-01	7.74E-02
F23	6.94E-01	1.00E+00	7.82E-01	9.83E-01	7.70E-01	4.09E-01	1.30E-01
Sum	14.73492378	10.91272853	15.3311656	9.657058056	10.61297778	9.504588952	6.984930021
F	std						
	ALO	GWO	MFO	PSO	WOA	SCA	ISCA
F1	1.00E+00	1.30E-107	1.25E-20	1.77E-33	2.26E-145	4.73E-16	1.13E-15
F2	1.32E-01	4.71E-67	1.00E+00	6.02E-21	3.37E-108	7.07E-19	7.18E-18
F3	8.96E-09	8.38E-57	1.00E+00	7.18E-15	3.02E-02	3.88E-12	2.62E-15
F4	5.11E-05	4.19E-37	2.59E-01	5.19E-10	1.00E+00	5.46E-07	2.19E-09
F5	5.63E-03	1.98E-05	1.00E+00	5.88E-05	4.37E-05	1.11E-05	8.48E-06
F6	6.18E-09	2.51E-06	1.81E-28	1.82E-31	2.60E-04	1.00E+00	1.92E-01
F7	1.00E+00	2.75E-02	5.10E-01	2.12E-01	1.42E-01	2.36E-01	8.79E-03
F8	6.51E-01	5.56E-01	6.57E-01	6.72E-01	1.00E+00	2.35E-01	7.77E-02
F9	5.04E-01	6.81E-02	1.00E+00	1.11E-01	0.00E+00	2.17E-01	0.00E+00
F10	1.00E+00	3.41E-15	8.32E-01	4.43E-15	7.17E-15	4.93E-13	4.32E-13
F11	6.20E-01	1.08E-01	6.02E-01	1.00E+00	7.25E-01	6.80E-01	0.00E+00
F12	1.00E+00	5.60E-03	3.02E-01	3.47E-34	3.27E-03	1.97E-02	4.23E-03
F13	4.62E-02	3.77E-01	4.62E-02	3.06E-33	2.66E-01	1.00E+00	2.77E-01
F14	1.42E-01	1.00E+00	5.90E-01	7.09E-35	6.71E-01	2.24E-01	6.01E-08
F15	7.55E-01	1.00E+00	3.96E-01	2.01E-02	5.35E-02	4.44E-02	9.52E-03
F16	1.98E-09	1.89E-04	1.95E-11	1.89E-11	9.08E-07	4.48E-01	1.00E+00
F17	1.91E-11	2.83E-04	0.00E+00	0.00E+00	1.29E-03	1.00E+00	1.73E-02
F18	1.15E-08	4.25E-01	1.21E-10	6.14E-11	5.34E-01	1.00E+00	1.35E-02
F19	8.77E-12	1.00E+00	7.95E-13	7.95E-13	7.34E-01	3.68E-01	2.80E-01
F20	1.31E-01	1.44E-01	1.37E-01	1.29E-01	1.91E-01	5.01E-01	1.00E+00
F21	9.73E-01	5.40E-01	1.00E+00	7.83E-01	7.47E-01	6.15E-01	5.05E-02
F22	8.95E-01	7.50E-05	1.00E+00	6.70E-01	7.54E-01	6.42E-01	4.74E-02
F23	9.85E-01	2.78E-01	1.00E+00	3.83E-01	9.81E-01	4.42E-01	2.22E-01
Sum	9.840298236	5.529580465	11.33071302	3.979590987	7.834520692	8.673003442	3.199493786

but unreliable due to its stochastic nature, therefore, each algorithm is run 30 times and statistical results were compiled and presented in Table 7.1 to check and compare the performance of the ISCA. The results are also compared with different algorithms. The results in Table 7.1 show that the ISCA performs better as compared to other considered optimization algorithms on the majority of unimodal test functions, multi-modal test functions and composite test functions. Better performance on the unimodal test functions shows that the ISCA has a high exploitation and convergence. The overall performance can also be compared using the last row of Table 7.1, as it presents the summation of average and standard deviation on all test function of all algorithms. The least value of average and standard deviation summation in the last row of Table 7.1 clearly indicates that the ISCA performs better as compared to other algorithms. From Table 7.1, it is proved that ISCA has potential to find out the global minima of the test functions. But, the real problem is challenging due to unknown search space and location of global minima along with a large number of equality and inequality constraints. Therefore, it is necessary to investigate the performance of ISCA in solving the real challenging problem. In this chapter, applicability of the proposed ISCA algorithm is investigated for optimum allocation of STATCOM on standard IEEE test systems and compared with established methods to prove its application potential.

7.5.1 STATCOM Allocation using SCA, GWO and Proposed ISCA

This section presents the ISCA for optimal placement of HELM model of STATCOM on standard IEEE 30 and 118-bus test systems. For investigation purpose, various cases are considered and solved using the proposed ISCA. In this work, the shunt reactive power control mode is considered as presented in Section 6.2.2. The control parameters used in the considered optimization techniques are as follows: number of search agents are 50 and maximum number of iteration are 100. The problem is formulated in MATLAB environment [115] and simulated on Intel(R) Core(TM) i3-4150 CPU 3.50 GHz processor with 4-GB RAM. The loading factor is denoted by λ and in this research work it is considered equal to 1.3 *p.u.*. The results of simulation studies are summarized below:

7.5.1.1 IEEE 30-Bus Test System

This case study deals with the determination of optimal locations and sizes of multiple STATCOMs in IEEE-30 bus test system. It consists of 30 buses, 41 transmission lines, 2 synchronous generators and 4 synchronous condensers. The objective considered here is

the minimization of maximum node voltage deviation, L-index and cost of the STATCOM. The formulated multi-objective problem has been solved using proposed ISCA, and the simulation results have been compared with GWO and SCA. Table 7.2 presents the optimal locations and sizes of STATCOMs along with the values of different objectives. It is observed from the comparison that the proposed ISCA provides the most compromising solution for the formulated problem as compared to existing GWO and SCA algorithms. From the comparative study of value of overall objective function, it is also noted that as the complexity of the system increases, the proposed ISCA provides better value of overall objective function. The bus voltage profile of the system both without and with STATCOMs is shown in Figure 7.3. A significant improvement in the node voltage profile of the system is observed with the installation of STATCOMs. From Table 7.2, it can also be observed that the best compromising solution is obtained with two STATCOMs. The total active power loss in the system without STATCOM, with one STATCOM, two STATCOMs, and three STATCOMs are 33.09 MW, 32.65 MW, 32.53 MW, 32.38 MW respectively. The total reactive power loss in the system without STATCOM, with one STATCOM, two STATCOMs, and three STATCOMs are 85.80 MVAR, 80.63 MVAR, 80.32 MVAR, 79.69 MVAR respectively. The cost of installation of one STATCOM, two STATCOMs, and three STATCOMs are 4626240, 4798500 and 6042090 US$. The values of L-index for all the three cases are presented in Figure 7.4. The reduction in values of L-index indicates the voltage stability enhancement by the installation of STATCOMs. The convergence characteristics of GWO, SCA, and ISCA for optimal allocation of two STATCOMs are shown in Figure 7.5. It can be observed that ISCA achieves the optimal solution in a lesser number of iterations without trapping in a local optima. Therefore, ISCA performs better as compared to other considered optimization techniques.

Table 7.2: Comparison results for simultaneous allocation of STATCOMs (30-bus)

No. of ST	Methods	Optimal STATCOM nodes (sizes in *MVAR*)	Values of objective functions			
			f_1	f_2	f_3	f
1	GWO	28 (40)	1	0.9806	0.9707	0.5041
	SCA	28 (40)	1	0.9806	0.9707	0.5041
	ISCA	28 (40)	1	0.9806	0.9707	0.5041
2	GWO	7 (30), 27 (10)	1	0.9848	0.9685	0.5039
	SCA	6 (30), 25 (10)	1	0.9836	0.9685	0.5040
	ISCA	27 (10), 28 (30)	1	0.9848	0.9685	0.5039
3	GWO	7 (30), 24 (10), 27 (10)	0.9994	0.9862	0.9502	0.5055
	SCA	4 (30), 21 (10), 25 (10)	0.9946	0.9849	0.9502	0.5060
	ISCA	6 (20), 26 (10), 28 (10)	1	0.9837	0.9670	0.5042

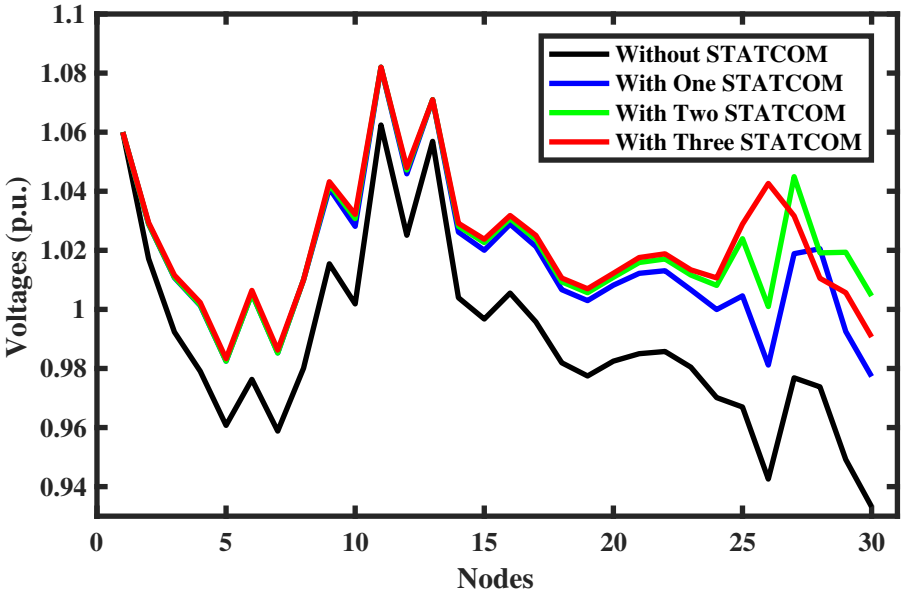

FIGURE 7.3: Node voltage profile of IEEE 30-bus test system

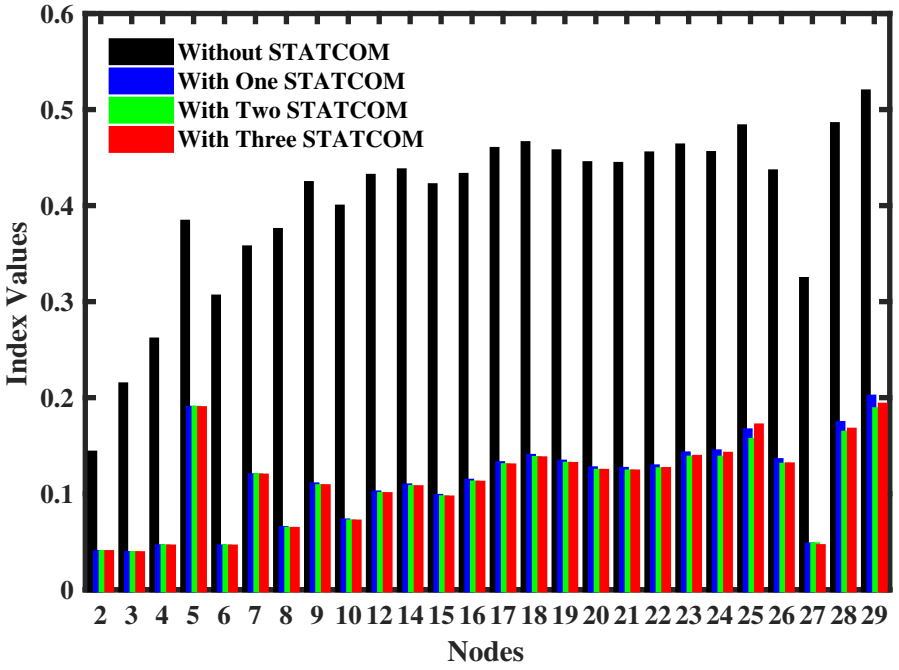

FIGURE 7.4: Values of L-index at different load buses of IEEE 30-bus test system

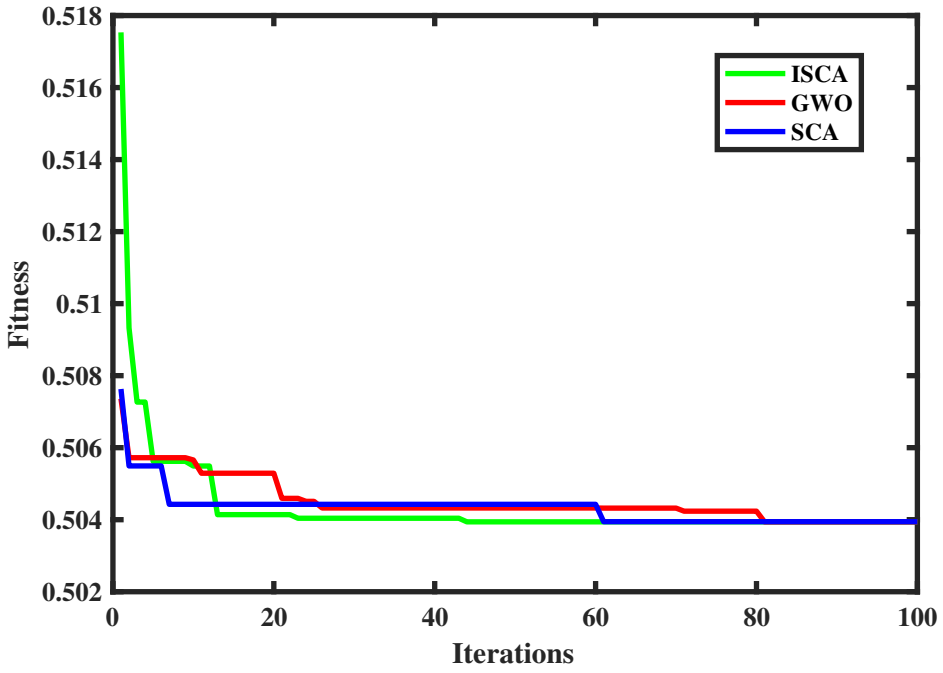

FIGURE 7.5: Convergence characteristics of GWO, SCA and ISCA for placement of two STATCOMs in IEEE 30-bus test system

7.5.1.2 IEEE 118-Bus Test System

This section deals with the determination of optimal locations and sizes of multiple STATCOMs in IEEE-118 bus test system. As discussed earlier, the objective is the simultaneous minimization of maximum node voltage deviation, L-index and cost of the STATCOM. The formulated multi-objective problem has been solved using proposed ISCA, and the simulation results have been compared with GWO and SCA. Table 7.3 presents the optimal locations and sizes of STATCOMs along with the values of different objectives. It is observed from the comparison that the proposed ISCA provides the most compromising solution for the formulated problem as compared to existing GWO and SCA algorithm. From Table 7.3, it can also be observed that the best compromising solution is obtained with two STATCOMs. The total active power loss in the system without STATCOM, with one STATCOM, two STATCOMs, and three STATCOMs are 484.53 MW, 479.25 MW, 479.49 MW, 479.04 MW respectively. The total reactive power loss in the system without STATCOM, with one STATCOM, two STATCOMs, and three STATCOMs are 1498.01 MVAR, 1469.29 MVAR, 1472.56 MVAR, 1464.97 MVAR respectively. The cost of installation of with one STATCOM, two STATCOMs, and three STATCOMs are 9211590, 9634950 and 17392740 US$ respectively. The values of L-index for all three cases are

presented in Figure 7.7. The reduction in values of L-index indicates the voltage stability enhancement by the installation of STATCOMs. Further, the convergence curves of GWO, SCA, and ISCA for optimal allocation of two STATCOM are shown in Figure 7.6. It can be observed that ISCA achieves the optimal solution without getting trapped in local minima. Therefore, ISCA performs better as compared to other considered optimization techniques.

TABLE 7.3: Comparison results for simultaneous allocation of STATCOMs (118-bus)

No. of ST	Methods	Optimal STATCOM nodes (sizes in *MVAR*)	Values of objective functions			
			f_1	f_2	f_3	f
1	GWO	75 (90)	0.3290	0.9643	0.8856	0.6042
	SCA	76 (100)	0.2575	0.9646	0.8660	0.6253
	ISCA	118 (100)	0.4742	0.9758	0.8660	0.5756
2	GWO	78 (10), 118 (80)	0.4730	0.9747	0.8751	0.5751
	SCA	118 (80), 11 (20)	0.4776	0.9745	0.8434	0.5773
	ISCA	74 (30), 118 (50)	0.4723	0.9646	0.8859	0.5750
3	GWO	60 (40), 118 (90), 64 (30)	0.4837	0.9752	0.6123	0.6021
	SCA	94 (20), 118 (50), 106 (10)	0.2505	0.9635	0.8831	0.6260
	ISCA	57 (10), 81 (50), 118 (100)	0.4797	0.9758	0.6335	0.5999

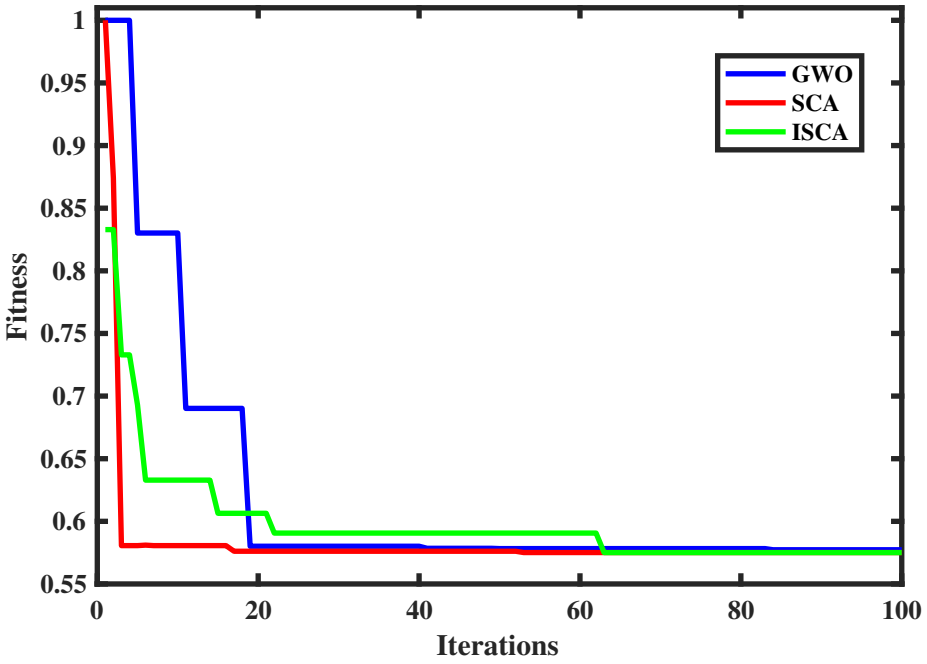

FIGURE 7.6: Convergence characteristics of GWO, SCA and ISCA for placement of two STATCOMs in IEEE 118-bus test system

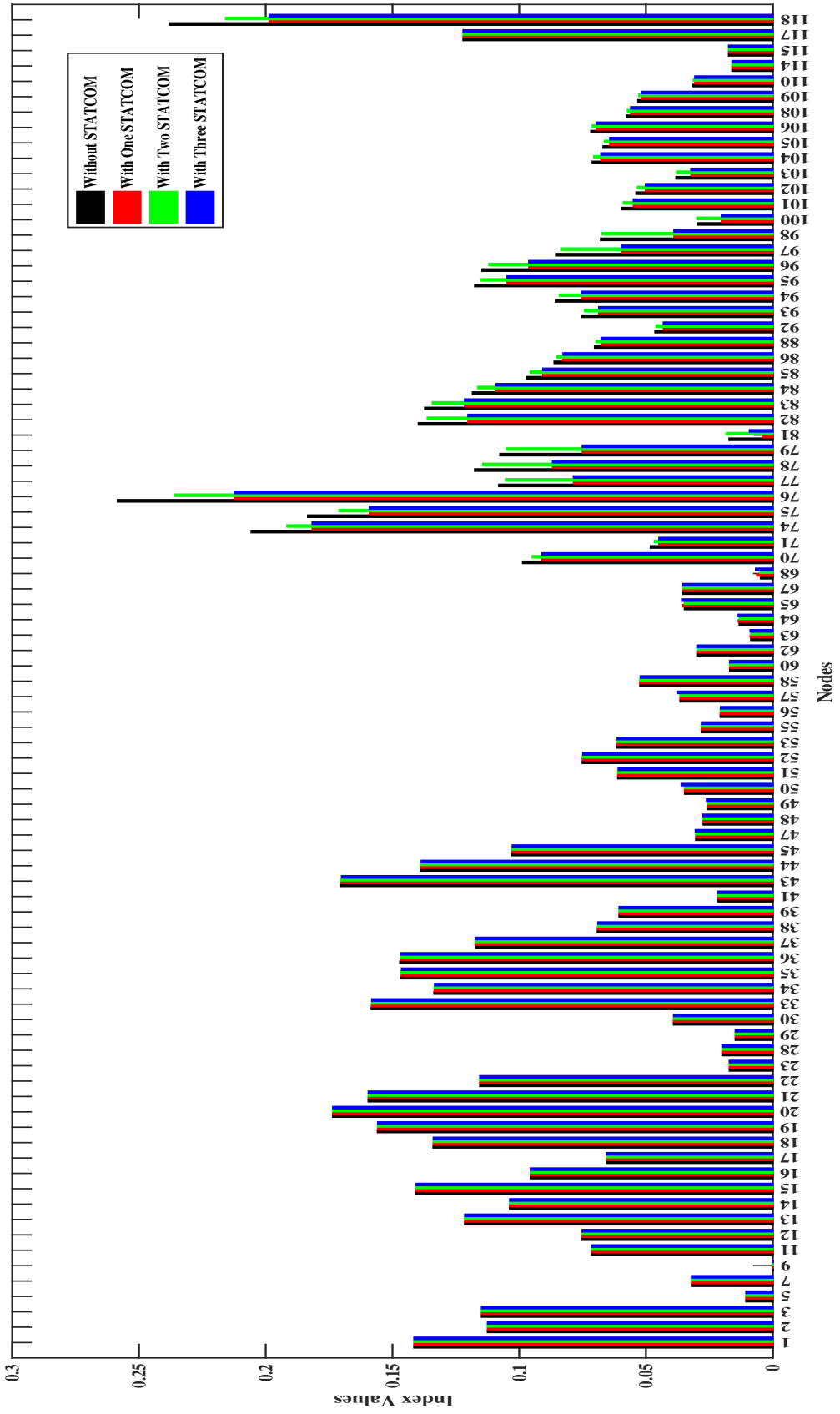

FIGURE 7.7: Values of L-index at different load buses of IEEE 118-bus test system

7.6 Summary

In this chapter, a multi-objective optimization problem framework using fuzzy membership function is formulated for optimal allocation of STATCOMs. The population-based optimization algorithms SCA and GWO are explored to optimize the formulated problem. Some improvements are also suggested to overcome the limitations of SCA. In order to validate the effectiveness of the proposed ISCA, it is tested on 23 standard test functions and also on the IEEE 30 and 118-bus test systems for different cases to optimize the formulated problem. The effect of suggested modification is demonstrated by various different parameters. The obtained results reveal that the proposed ISCA provides more promising results for complex multi-objective optimization problem. The performance of ISCA is found reasonably good when the simulation results are compared with considered optimization techniques.

Chapter 8

Conclusions and Future Scope

The aim of this chapter is to recapitulate the key contributions and findings of the research work of this thesis and to suggest some scope for future research work in this area. The focus of this thesis work are voltage stability assessment and FACTS modeling.

8.1 Conclusions

In Chapter 2, a brief literature survey concerning different aspects of voltage stability assessment, FACTS devices and their modeling, and optimal allocation of FACTS devices have been presented and research objectives have been framed on the basis of critical review of the literature. From the literature survey, it has been found that most of the voltage stability indices are based upon the approximate model of transmission line where line capacitance and resistance are neglected. In [34], the transmission line is considered as equivalent pi-model where line parameters were assumed as lumped parameters. Prediction of the current state of a power system based on these indices was erroneous due to the assumptions considered during development of these indices. Moreover, the accurate loading margins can't be estimated by [29, 41] due to negligence of various parameters.

Considering these limitations and shortcomings of the existing indices, a new voltage stability index namely *DPVSI* has been developed for voltage stability assessment in Chapter 3. The novelty of this index is that it is based on distributed parameters of the transmission line which is a meticulous representation of power system leading to precise indication of voltage stability state. Stressed condition of a line can be monitored and reactive loading margin can be calculated online using the proposed index. The work also

contributes to assess local and global voltage stability of the power system. In this work, index value of individual line is indicative of local voltage stability while maximum value of the index reflects the global voltage stability. Application potential of the work is explored on IEEE test systems. Followings conclusions can be drawn from this chapter:

- It is based on the distributed parameters of the transmission line and also takes into accounts the effect of the relative direction of active and reactive powers flow through the transmission line. The line resistance and shunt admittance are also considered during development stage of the proposed index. Therefore, the proposed index provides more accurate and promising results.
- The proposed index is capable to indicate the local as well as global voltage stability state of the power system.
- The proposed index is suitable to identify the weak lines in the power system and it can estimate the available reactive loading margin.
- Assessment of viability of new lines from voltage stability point of view at the planning stage can be done using proposed index.
- It is also suitable for online assessment of voltage stability state of the power system. Therefore, it can assist the system operator to undertake improved preventive actions before system collapse.

Advances in the high power solid-state switches have led to the development of FACTS controllers that provide capability of flexible control of stressed power network [44, 45]. In the literature, lots of devices have been proposed and modeled by the researchers. But due to high cost and proneness to failures, existing FACTS devices are still limited in practice. Although, an electromagnetic device *i.e.* ST provides cost effective solution but it can't generate reactive power. There is a pressing need to develop new approach which increases the reliability and reduces the cost simultaneously. Therefore, a new member to FACTS family termed as APFC for fast, reliable and cost effective solution of power flow control has been proposed in Chapter 4. It is an amalgamation of a large capacity ST and small capacity DPFC. The proposed APFC can regulate the bus voltage, active and reactive power flow through the transmission line simultaneously. The APFC can also be operated as shunt or series compensator independently. The major contributions of APFC are:

- Robustness of ST and elimination of common DC-link, increases reliability and security.

- Cost effectiveness since size of DC battery/capacitor required to supply reactive power is reduced as now reactive power can be exchanged through SEN transformer.
- Fast response and continuous control of power flow.
- Common excitation winding of DPFC and ST, eliminates the need of additional transformer, thereby saving the cost.

An accurate steady-state model, which can represent all the operational and functional features of the device is required to investigate its possible benefits. At the same time, model should not deteriorate the convergence characteristics of load-flow method. The well recognized modeling approaches for FACTS devices, especially VSM and PIM have their own pros and cons. In the model of FACTS devices [44–46, 53, 55, 57, 58, 61–64, 66, 67, 71, 72, 116] developed so far, converter losses are also not accounted. Therefore, this chapter also developed a hybrid approach to model the APFC. The proposed model is incorporated into the standard NRLF method for studying its viability and practicability. The model is tested on standard IEEE bus systems and results of simulation proved its excellent convergence characteristics. The main advantages of the proposed mathematical approach are:

- Symmetry of admittance matrix is preserved.
- Better convergence characteristics.
- Provide valuable information of both series and shunt state variables.
- More precise as converter losses are also incorporated.

In Chapter 5, a comprehensive study on various line and node based voltage stability indicators under different loading conditions on two different test cases has been presented. It is observed that the node based voltage stability indicator performs better in assessment of voltage stability state than the line based voltage stability indicators. The line based voltage stability indices mislead in identifying weak nodes. Considering the demerits of the line based indices, a new node based voltage stability index which estimates the voltage and load distance to maximum loading point is proposed and compared with L-index. The traditional iterative numerical techniques are core to solve power flow problem. But, these existing iterative methods have the following drawbacks:

- They have multiple solutions of state variables, and only one of them corresponds to the real operating state of the power system.

- There is no guarantee of convergence.
- Convergence characteristics depend upon the choice of initial conditions.
- May converge to spurious solutions.

A new load-flow technique known as HELM has been developed by Trias to circumvent the aforesaid problems. The key advantages of HELM are the non-iterative process, deterministic initial seed and clear indication if solution doesn't exist. But, the existing formulation of HELM requires some modifications. Therefore, in Chapter 5, extended version of HELM has been proposed, which includes the shunt conductance of steady-state pi-model of VRT and fixed reactive power injection at a bus. As conventional HELM method can be ill-posed for constructing Padé approximations for degeneracy cases of power series, therefore, SVD based Padé approximation is used in this work. Moreover, a new HE formulation is proposed for non-uniform scaling of the load in the power system. Numerical results for ZIP type loads are presented to demonstrate the accuracy of the proposed voltage stability index and evaluated using the extended HELM. It has been observed that the proposed voltage stability index accurately identifies the weak buses in the IEEE test systems. Consequently, the proposed approach can be used as a tool in power system planning and operation.

The non-linear algebraic equations become more complex when FACTS devices are incorporated in the load-flow program. The load-flow doesn't converge for ill-conditioned power systems. Therefore, there is a pressing need to develop a model of FACTS device which converges under all the operating/system conditions. Considering this an HELM model of STATCOM has been proposed in Chapter 6. The proposed model is developed using holomorphic embedding technique in place of conventional N-R technique to overcome the problem of convergence. The multi-control capability of HELM model of STATCOM is investigated on IEEE test system and compared with conventional model. The convergence characteristics of proposed model are also tested for different values of impedance of coupling transformer. Simulation results of various system/operating conditions prove that the proposed model offers unique solution. Convergence characteristics of the proposed model are not affected by change in initial conditions of the system which proves the reliability and robustness of the model. The proposed model has following features:

- Various control modes to control different parameters.
- Non-iterative approach based model.

- Clear indication if the solution doesn't exist.
- Initial conditions are deterministic in nature.
- Always converge, even for ill conditioned power system if the solution exists.
- Robust and reliable.
- Complexity of Jacobian matrix and its factorization is not present.

The FACTS devices have been utilized for efficient use of existing system infrastructure by controlling the power flow over designated transmission routes [94, 97, 98, 106]. FACTS devices are also used to enhance voltage stability margin and system security. Therefore, the FACTS devices should be optimally allocated to extract the maximum possible benefits. The optimal allocation of FACTS devices can improve the power system performance in terms of better node voltage profile, reduce system losses and power flows, and better power quality and reliability of power supply [98, 105, 106]. Therefore, an optimization framework framework using fuzzy membership function is developed for optimal allocation of HELM model of STATCOM in Chapter 7. The population-based optimization algorithms SCA and GWO are used to optimize the formulated problem. Some improvements are also suggested to overcome the limitations of SCA. In order to validate the effectiveness of the proposed ISCA, it is tested on 23 standard test functions as well as on the IEEE test systems for different cases. The obtained results reveal that the proposed ISCA provides more promising results for complex multi-objective optimization problem.

8.2 Major Contributions

The major contributions of this thesis work are as follows:

- A new line based voltage stability index has been developed for monitoring critical conditions of transmission lines.
- A new FACTS device namely Amalgam Power Flow Controller (APFC) has been developed to mitigate the high cost and low reliability problem.
- A new mathematical approach to model the FACTS devices (Hybrid Approach based Model-HABM) has been developed.

- A new node based voltage stability index has been developed to accurately identify the weak nodes of the power system, which evaluates the load and voltage distance from the SNB point.
- Some improvements in standard HELM has been suggested to explore the applicability of HE method.
- HELM model of STATCOM has been developed to circumvent the convergence problem and need of better initial seed.
- Some modifications in standard Sine Cosine Algorithm (SCA) have been suggested to enhance its exploration and exploitation capability.
- A new multi-objective Fuzzified-SCA, GWO and ISCA approaches have been formulated for optimal allocation problem of HELM model of STATCOM.

8.3 Future Scope

Based on the research carried out in this thesis, the future research directions that appear from this thesis are summarized below:

- Research should be conducted to develop such a line based voltage stability index, which is not affected by the topological changes of the power system.
- The proposed voltage stability index may be investigated for dynamic voltage stability analysis.
- An efficient approach based on the combination of Dragonfly Optimization (DFO) algorithm and Support Vector Regression (SVR) should be developed for on-line voltage stability assessment. The DFO algorithm enhance the performance of SVR model significantly by helping in selection of SVR parameters setting, as the performance of the SVR model extremely depends on careful selection of its parameters. In this approach, the voltage magnitudes of the Phasor Measurement Unit (PMU) buses can be adopted as the input data for the hybrid DFO-SVR model, while the minimum values of Voltage Stability Index (VSI) can be taken as the output vector. Using the data provided by PMUs as the input variables can make the approach capable of assessing the voltage stability in a real time manner, which can assist the operators to adopt the required measures to avert large blackouts. The predictive

ability of the proposed hybrid model can be investigated through the various IEEE test-bus systems.

- The dynamic and hardware models of APFC should be developed to investigate its dynamic performance. The suitable strategy to inject series voltages from different series devices should be developed.
- Research should be conducted to develop the HELM model of other types of FACTS devices.
- The suitability of ISCA optimization algorithm should be tested on another real engineering complex problems.
- In the formulated multi-objective problem, more objectives such as generation cost, depreciation cost of FACTS devices and amount of load shedding may be included.
- Optimal locations of the dynamic Volts-Ampere-Reactive (VAR) sources can be determined for addressing the Fault-Induced Delayed Voltage Recovery (FIDVR) issues in the voltage stability analysis and assessment methodology. A time domain dynamic simulations, sensitivity analysis can be performed to assess the need for dynamic VAR sources. The objective of this study can be to determine the optimal installation of dynamic VAR sources while satisfying the requirement of voltage stability margin and transient voltage dip under a set of criteria. New insights can be presented on the effect of FACTS controls on the reactive power compensation, which supports voltage recovery.

Appendix A

Existing Line and Node based Voltage Stability Indices

A.1 Existing Line and Node based Voltage Stability Indices

Some of the established line voltage stability indices *FVSI* [41], L_{mn} [29], *POR* [40], *MLI* [35], L_s [37], *LQP* [31], *LCPI* [34] and node based voltage stability indices *L*-index [19], *AVSI* are discussed in the following sections:

A.1.1 Fast Voltage Stability Index *(FVSI)*

The fast voltage stability index named *FVSI* has been developed by Musirin *et al.* [41]. It is formulated from two bus representation of a system as shown in Figure A.1. The *FVSI* is defined as :

$$FVSI = \frac{4Z^2Q_j}{V_i^2X} \leq 1 \tag{A.1}$$

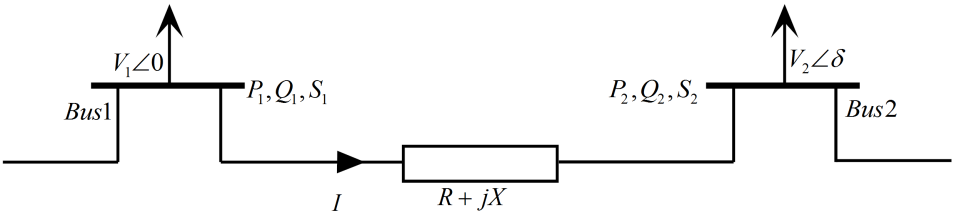

FIGURE A.1: 2-bus power system model

Where, Z is the line impedance, X is the line reactance, V_i is the bus voltage at the sending end, and P_j and Q_j are the active and reactive power flowing through the transmission line respectively. *FVSI* of a line near to unity indicates that the line is close to its stability limit. The shortcoming of this index is that when $Q_j \leq 0$, it indicates that the respective line and thus the system is always secure at that particular condition. Moreover, transmission line shunt capacitance has been ignored and account only the effect of reactive power flows through the transmission line.

A.1.2 Line Stability Index ($\mathbf{L_{mn}}$)

Moghavvemi and Omar derived the line stability index represented as L_{mn}, with the line flow data. The line stability index, as derived by [29], is defined as:

$$L_{mn} = \frac{4Q_j X}{\left(V_i sin(\theta - \delta)\right)^2} \leq 1 \tag{A.2}$$

Where, θ is the impedance angle of line and $\delta = \delta_i - \delta_j$ is the phase difference of sending and receiving end bus voltages, while all other variables are same as explained in Section A.1.1. To maintain the voltage stability, the value of L_{mn} should be less than unity. This index also suffer from the same problem as *FVSI*.

A.1.3 Line Porosity Coefficient Index *(POR)*

The line's porosity coefficient index namely *POR* for voltage stability assessment of power system has been developed in [40]. Mathematically, *POR* can be expressed as:

$$POR = \frac{X^S}{X^{line}} > 1 \tag{A.3}$$

Where, X^S is the reactance of porosity and X^{line} is the transmission line reactance. To maintain the voltage stability, the value of *POR* should be greater than unity. The main problem of this index is that its upper limit is not bounded.

A.1.4 Maximum Loadability Index *(MLI)*

The maximum lodability index denoted as *MLI* is proposed by Venkatesh *et al.* [35]. It is based on quadratic equation of voltage. It can be formulated as follows:

$$MLI = \frac{V_i^2\Big[-(r_{ij}P_{ij} + x_{ij}Q_{ij}) + \sqrt{(r_{ij}^2 + x_{ij}^2)(P_{ij}^2 + Q_{ij}^2)}\Big]}{2(x_{ij}P_{ij} - r_{ij}Q_{ij})^2} > 1 \tag{A.4}$$

Where, P_{ij} and Q_{ij} are real and reactive power flowing through the line, r_{ij} and x_{ij} are resistance and reactance of line and V_i is sending end voltage. *MLI* should be greater than one to maintain the stability of the system. The main discrepancy of this index is that it loses mathematical robustness when power factor angle equals to the line impedance angle because denominator term becomes zero. Moreover, the shunt admittance has been neglected.

A.1.5 Line Lodability Index ($\mathbf{L_s}$)

The line loadability index (L_s) is proposed by Yu *et al.*, evaluates the voltage stability and available loading margin of transmission line [37]. The line with minimal L_s is considered to be weakest transmission line and corresponding bus is weakest bus. The L_s is defined as:

$$L_s = \frac{V_i^2}{2\Big[r_{ij}P_{ij} + x_{ij}Q_{ij} + \sqrt{(r_{ij}^2 + x_{ij}^2)(P_{ij}^2 + Q_{ij}^2)}\Big]} \leq 1 \tag{A.5}$$

All the variables are same as explained in Section A.1.4. L_s should be greater than unity to maintain the voltage stability of the system. But the shunt admittance has been ignored.

A.1.6 Line Stability Factor *(LQP)*

The line stability factor (LQP) is proposed by Mohamed *et al.* [31] is defined as follows:

$$LQP = 4\left(\frac{x_{ij}}{V_i^2}\right)\left(\frac{x_{ij}P_i^2}{V_i^2} + Q_j\right) \leq 1 \tag{A.6}$$

Where, P_i is real power flowing through the transmission line while other variables are same as explained in earlier sections. To maintain the voltage stability, LQP should be less than unity. In this index, the line resistance and shunt admittance have not been considered.

A.1.7 Line Collapse Proximity Index *(LCPI)*

The line collapse proximity index *(LCPI)* is proposed by Rajive *et al.* [34]. In order to account all the parameters of the transmission line, the formulation of $LCPI$ considered the shunt admittance of the line. The magnitude and relative direction of active and reactive power flows is also considered to accurately predict the voltage collapse. It is formulated in terms of A, B, C and D parameters of the transmission line and it can be defined as:

$$LCPI = \frac{4Acos\alpha(P_jBcos\beta) + Q_jBsin\beta}{(V_icos\delta)^2} \leq 1 \tag{A.7}$$

Where, A, B, α, β are the elements of T parameters of the transmission line. $LCPI$ should be less than unity to maintain stability.

A.1.8 *L*-Index

The L-index is proposed by Kessel *et al.* [19]. It is quantitative measure for estimation of margin between current state of system and voltage instability. The L-index is defined as:

$$L = \max_{j=\alpha_L}\{L_j\} = \max_{j=\alpha_L}\left|1 - \sum_{i\in\alpha_G} F_{ij}\frac{V_i}{V_j}\right| \leq 1 \tag{A.8}$$

Where, F_{ij} is a sub-matrix of admittance matrix, which provide relationship between generator and load buses. α_L is the set of consumer nodes and α_G is the set of generator nodes. The L-index should be less than unity to maintain stability.

A.1.9 Area based Voltage Stability Index *(AVSI)*

The area based voltage stability index ($AVSI$) is proposed by Pradeep *et al.* It is based on area under the curve of quadratic equation and can be expressed as:

$$AVSI = \frac{A}{2A_0} \geq 0 \tag{A.9}$$

Where, A and A_0 are the area under the curve at particular loading condition and no-load condition respectively. The area enclosed by curve decreases as the power system move towards the SNB point. This index should be greater than zero to maintain system stability.

Appendix B

Transmission Test Systems

B.1 Study System–1

It is the IEEE 30-bus benchmark test system with total real and reactive power demand of 283.40 MW and 126.20 $MVAR$ respectively. Other parameters used for load-flow studies are given below.

TABLE B.1: Bus Data of IEEE 30-bus Test System

Bus	Bus	Voltage	Angle	Load		Generator				Injected
No.	Type	Magnitude ($p.u.$)	(Degree)	MW	$MVAR$	MW	$MVAR$	Q_{min}	Q_{max}	$MVAR$
1	1	1.060	0	0.000	0.000	0.000	0	0.000	0.000	0.000
2	2	1.043	0	21.70	12.70	40.00	0	-40.0	50.00	0.000
3	3	1.000	0	2.400	1.200	0.000	0	0.000	0.000	0.000
4	3	1.060	0	7.600	1.600	0.000	0	0.000	0.000	0.000
5	2	1.010	0	94.20	19.00	0.000	0	-40.0	40.00	0.000
6	3	1.000	0	0.000	0.000	0.000	0	0.000	0.000	0.000
7	3	1.000	0	22.80	10.90	0.000	0	0.000	0.000	0.000
8	2	1.010	0	30.00	30.00	0.000	0	-10.0	60.00	0.000
9	3	1.000	0	0.000	0.000	0.000	0	0.000	0.000	0.000
10	3	1.000	0	5.800	2.000	0.000	0	-6.00	24.00	19.00
11	2	1.082	0	0.000	0.000	0.000	0	0.000	0.000	0.000
12	3	1.000	0	11.20	7.500	0.000	0	0.000	0.000	0.000
13	2	1.071	0	0.000	0.000	0.000	0	-6.00	24.00	0.000
14	3	1.000	0	6.200	1.600	0.000	0	0.000	0.000	0.000
15	3	1.000	0	8.200	2.500	0.000	0	0.000	0.000	0.000
16	3	1.000	0	3.500	1.800	0.000	0	0.000	0.000	0.000
17	3	1.000	0	9.000	5.800	0.000	0	0.000	0.000	0.000
18	3	1.000	0	3.200	0.900	0.000	0	0.000	0.000	0.000
19	3	1.000	0	9.500	3.400	0.000	0	0.000	0.000	0.000
20	3	1.000	0	2.200	0.700	0.000	0	0.000	0.000	0.000
21	3	1.000	0	17.50	11.20	0.000	0	0.000	0.000	0.000
22	3	1.000	0	0.000	0.000	0.000	0	0.000	0.000	0.000
23	3	1.000	0	3.200	1.600	0.000	0	0.000	0.000	0.000
24	3	1.000	0	8.700	6.700	0.000	0	0.000	0.000	4.300
25	3	1.000	0	0.000	0.000	0.000	0	0.000	0.000	0.000
26	3	1.000	0	3.500	2.300	0.000	0	0.000	0.000	0.000
27	3	1.000	0	0.000	0.000	0.000	0	0.000	0.000	0.000
28	3	1.000	0	0.000	0.000	0.000	0	0.000	0.000	0.000
29	3	1.000	0	2.400	0.900	0.000	0	0.000	0.000	0.000
30	3	1.000	0	10.60	1.900	0.000	0	0.000	0.000	0.000

TABLE B.2: Line Data of IEEE 30-bus Test System

From Bus	To Bus	Line Impedance		Half Line Charging	Tap
		Resistance ($p.u.$)	Reactance ($p.u.$)	Susceptance ($p.u.$)	Ratio
1	2	0.0192	0.0575	0.0264	1.0000
1	3	0.0452	0.1852	0.0204	1.0000
2	4	0.0570	0.1737	0.0184	1.0000
3	4	0.0132	0.0379	0.0042	1.0000
2	5	0.0472	0.1983	0.0209	1.0000
2	6	0.0581	0.1763	0.0187	1.0000
4	6	0.0119	0.0414	0.0045	1.0000
5	7	0.0460	0.1160	0.0102	1.0000
6	7	0.0267	0.0820	0.0085	1.0000
6	8	0.0120	0.0420	0.0045	1.0000
6	9	0.0000	0.2080	0.0000	0.9780
6	10	0.0000	0.5560	0.0000	0.9690
9	11	0.0000	0.2080	0.0000	1.0000
9	10	0.0000	0.1100	0.0000	1.0000
4	12	0.0000	0.2560	0.0000	0.9320
12	13	0.0000	0.1400	0.0000	1.0000
12	14	0.1231	0.2559	0.0000	1.0000
12	15	0.0662	0.1304	0.0000	1.0000
12	16	0.0945	0.1987	0.0000	1.0000
14	15	0.2210	0.1997	0.0000	1.0000
16	17	0.0824	0.1923	0.0000	1.0000
15	18	0.1073	0.2185	0.0000	1.0000
18	19	0.0639	0.1292	0.0000	1.0000
19	20	0.0340	0.0680	0.0000	1.0000
10	20	0.0936	0.2090	0.0000	1.0000
10	17	0.0324	0.0845	0.0000	1.0000
10	21	0.0348	0.0749	0.0000	1.0000
10	22	0.0727	0.1499	0.0000	1.0000
21	22	0.0116	0.0236	0.0000	1.0000
15	23	0.1000	0.2020	0.0000	1.0000
22	24	0.1150	0.1790	0.0000	1.0000
23	24	0.1320	0.2700	0.0000	1.0000
24	25	0.1885	0.3292	0.0000	1.0000
25	26	0.2544	0.3800	0.0000	1.0000
25	27	0.1093	0.2087	0.0000	1.0000
28	27	0.0000	0.3960	0.0000	0.9680
27	29	0.2198	0.4153	0.0000	1.0000
27	30	0.3202	0.6027	0.0000	1.0000
29	30	0.2399	0.4533	0.0000	1.0000
8	28	0.0636	0.2000	0.0214	1.0000
6	28	0.0169	0.0599	0.0650	1.0000

B.2 Study System–2

It is the IEEE 118-bus test system with total real and reactive power demand of 4242 MW and 1438 $MVAR$ respectively. Other parameters used for load-flow studies are given below.

TABLE B.3: Bus Data of IEEE 118-bus Test System

Bus No.	Bus Type	Voltage Magnitude ($p.u.$)	Angle (Degree)	Load		Generator				Injected $MVAR$
				MW	$MVAR$	MW	$MVAR$	Q_{min}	Q_{max}	
1	2	0.955	0	51.00	27.00	0.000	0	15.000	-5.0000	0.00
2	3	1.000	0	20.00	9.000	0.000	0	0.0000	0.0000	0.00
3	3	1.000	0	39.00	10.00	0.000	0	0.0000	0.0000	0.00
4	2	0.998	0	39.00	12.00	0.000	0	300.00	-300.00	0.00
5	3	1.000	0	0.000	0.000	0.000	0	0.0000	0.0000	-40.0
6	2	0.990	0	52.00	22.00	0.000	0	50.000	-13.000	0.00
7	3	1.000	0	19.00	2.000	0.000	0	0.0000	0.0000	0.00
8	2	1.015	0	28.00	0.000	0.000	0	300.00	-300.00	0.00
9	3	1.000	0	0.000	0.000	0.000	0	0.0000	0.0000	0.00
10	2	1.050	0	0.000	0.000	450.0	0	200.00	-147.00	0.00
11	3	1.000	0	70.00	23.00	0.000	0	0.0000	0.0000	0.00
12	2	0.990	0	47.00	10.00	85.00	0	120.00	-35.000	0.00
13	3	1.000	0	34.00	16.00	0.000	0	0.0000	0.0000	0.00

Continued on next page...

Table B.3 – continued from previous page.

Bus No.	Bus Type	Voltage Magnitude ($p.u.$)	Angle (Degree)	Load		Generator				Injected $MVAR$
				MW	$MVAR$	MW	$MVAR$	Q_{min}	Q_{max}	
14	3	1.000	0	14.00	1.000	0.000	0	0.0000	0.0000	0.00
15	2	0.970	0	90.00	30.00	0.000	0	30.000	-10.000	0.00
16	3	1.000	0	25.00	10.00	0.000	0	0.0000	0.0000	0.00
17	3	1.000	0	11.00	3.000	0.000	0	0.0000	0.0000	0.00
18	2	0.973	0	60.00	34.00	0.000	0	50.000	-16.000	0.00
19	2	0.963	0	45.00	25.00	0.000	0	24.000	-8.0000	0.00
20	3	1.000	0	18.00	3.000	0.000	0	0.0000	0.0000	0.00
21	3	1.000	0	14.00	8.000	0.000	0	0.0000	0.0000	0.00
22	3	1.000	0	10.00	5.000	0.000	0	0.0000	0.0000	0.00
23	3	1.000	0	7.000	3.000	0.000	0	0.0000	0.0000	0.00
24	2	0.992	0	13.00	0.000	0.000	0	300.00	-300.00	0.00
25	2	1.050	0	0.000	0.000	220.0	0	140.00	-47.000	0.00
26	2	1.015	0	0.000	0.000	314.0	0	1000.0	-1000.0	0.00
27	2	0.968	0	71.00	13.00	0.000	0	300.00	-300.00	0.00
28	3	1.000	0	17.00	7.000	0.000	0	0.0000	0.0000	0.00
29	3	1.000	0	24.00	4.000	0.000	0	0.0000	0.0000	0.00
30	3	1.000	0	0.000	0.000	0.000	0	0.0000	0.0000	0.00
31	2	0.967	0	43.00	27.00	7.000	0	300.00	-300.00	0.00
32	2	0.964	0	59.00	23.00	0.000	0	42.000	-14.000	0.00
33	3	1.000	0	23.00	9.000	0.000	0	0.0000	0.0000	0.00
34	2	0.986	0	59.00	26.00	0.000	0	24.000	-8.0000	14.0
35	3	1.000	0	33.00	9.000	0.000	0	0.0000	0.0000	0.00
36	2	0.980	0	31.00	17.00	0.000	0	24.000	-8.0000	0.00
37	3	1.000	0	0.000	0.000	0.000	0	0.0000	0.0000	-25.0
38	3	1.000	0	0.000	0.000	0.000	0	0.0000	0.0000	0.00
39	3	1.000	0	27.00	11.00	0.000	0	0.0000	0.0000	0.00
40	2	0.970	0	66.00	23.00	0.000	0	300.00	-300.00	0.00
41	3	1.000	0	37.00	10.00	0.000	0	0.0000	0.0000	0.00
42	2	0.985	0	96.00	23.00	0.000	0	300.00	-300.00	0.00
43	3	1.000	0	18.00	7.000	0.000	0	0.0000	0.0000	0.00
44	3	1.000	0	16.00	8.000	0.000	0	0.0000	0.0000	10.0
45	3	1.000	0	53.00	22.00	0.000	0	0.0000	0.0000	10.0
46	2	1.005	0	28.00	10.00	19.00	0	100.00	-100.00	10.0
47	3	1.000	0	34.00	0.000	0.000	0	0.0000	0.0000	0.00
48	3	1.000	0	20.00	11.00	0.000	0	0.0000	0.0000	15.0
49	2	1.025	0	87.00	30.00	204.0	0	210.00	-85.000	0.00
50	3	1.000	0	17.00	4.000	0.000	0	0.0000	0.0000	0.00
51	3	1.000	0	17.00	8.000	0.000	0	0.0000	0.0000	0.00
52	3	1.000	0	18.00	5.000	0.000	0	0.0000	0.0000	0.00
53	3	1.000	0	23.00	11.00	0.000	0	0.0000	0.0000	0.00
54	2	0.955	0	113.0	32.00	48.00	0	300.00	-300.00	0.00
55	2	0.952	0	63.00	22.00	0.000	0	23.000	-8.0000	0.00
56	2	0.954	0	84.00	18.00	0.000	0	15.000	-8.0000	0.00
57	3	1.000	0	12.00	3.000	0.000	0	0.0000	0.0000	0.00
58	3	1.000	0	12.00	3.000	0.000	0	0.0000	0.0000	0.00
59	2	0.985	0	277.0	113.0	155.0	0	180.00	-60.000	0.00
60	3	1.000	0	78.00	3.000	0.000	0	0.0000	0.0000	0.00
61	2	0.995	0	0.000	0.000	160.0	0	300.00	-100.00	0.00
62	2	0.998	0	77.00	14.00	0.000	0	20.000	-20.000	0.00
63	3	1.000	0	0.000	0.000	0.000	0	0.0000	0.0000	0.00
64	3	1.000	0	0.000	0.000	0.000	0	0.0000	0.0000	0.00
65	2	1.005	0	0.000	0.000	391.0	0	200.00	-67.000	0.00
66	2	1.050	0	39.00	18.00	392.0	0	200.00	-67.000	0.00
67	3	1.000	0	28.00	7.000	0.000	0	0.0000	0.0000	0.00
68	3	1.000	0	0.000	0.000	0.000	0	0.0000	0.0000	0.00
69	1	1.035	0	0.000	0.000	516.4	0	300.00	-300.00	0.00
70	2	0.984	0	66.00	20.00	0.000	0	32.000	-10.000	0.00
71	3	1.000	0	0.000	0.000	0.000	0	0.0000	0.0000	0.00
72	2	0.980	0	12.00	0.000	0.000	0	100.00	-100.00	0.00
73	2	0.991	0	6.000	0.000	0.000	0	100.00	-100.00	0.00
74	2	0.958	0	68.00	27.00	0.000	0	9.0000	-6.0000	12.0
75	3	1.000	0	47.00	11.00	0.000	0	0.0000	0.0000	0.00
76	2	0.943	0	68.00	36.00	0.000	0	23.000	-8.0000	0.00
77	2	1.006	0	61.00	28.00	0.000	0	70.000	-20.000	0.00
78	3	1.000	0	71.00	26.00	0.000	0	0.0000	0.0000	0.00
79	3	1.000	0	39.00	32.00	0.000	0	0.0000	0.0000	20.0

Continued on next page...

Table B.3 – continued from previous page.

Bus No.	Bus Type	Voltage Magnitude ($p.u.$)	Angle (Degree)	Load		Generator				Injected $MVAR$
				MW	$MVAR$	MW	$MVAR$	Q_{min}	Q_{max}	
80	2	1.040	0	130.0	26.00	477.0	0	280.00	-165.00	0.00
81	3	1.000	0	0.000	0.000	0.000	0	0.0000	0.0000	0.00
82	3	1.000	0	54.00	27.00	0.000	0	0.0000	0.0000	20.0
83	3	1.000	0	20.00	10.00	0.000	0	0.0000	0.0000	10.0
84	3	1.000	0	11.00	7.000	0.000	0	0.0000	0.0000	0.00
85	2	0.985	0	24.00	15.00	0.000	0	23.000	-8.0000	0.00
86	3	1.000	0	21.00	10.00	0.000	0	0.0000	0.0000	0.00
87	2	1.015	0	0.000	0.000	4.000	0	1000.0	-100.00	0.00
88	3	1.000	0	48.00	10.00	0.000	0	0.0000	0.0000	0.00
89	2	1.005	0	0.000	0.000	607.0	0	300.00	-210.00	0.00
90	2	0.985	0	163.0	42.00	0.000	0	300.00	-300.00	0.00
91	2	0.980	0	10.00	0.000	0.000	0	100.00	-100.00	0.00
92	2	0.993	0	65.00	10.00	0.000	0	9.0000	-3.0000	0.00
93	3	1.000	0	12.00	7.000	0.000	0	0.0000	0.0000	0.00
94	3	1.000	0	30.00	16.00	0.000	0	0.0000	0.0000	0.00
95	3	1.000	0	42.00	31.00	0.000	0	0.0000	0.0000	0.00
96	3	1.000	0	38.00	15.00	0.000	0	0.0000	0.0000	0.00
97	3	1.000	0	15.00	9.000	0.000	0	0.0000	0.0000	0.00
98	3	1.000	0	34.00	8.000	0.000	0	0.0000	0.0000	0.00
99	2	1.010	0	42.00	0.000	0.000	0	100.00	-100.00	0.00
100	2	1.017	0	37.00	18.00	252.0	0	155.00	-50.000	0.00
101	3	1.000	0	22.00	15.00	0.000	0	0.0000	0.0000	0.00
102	3	1.000	0	5.000	3.000	0.000	0	0.0000	0.0000	0.00
103	2	1.001	0	23.00	16.00	40.00	0	40.000	-15.000	0.00
104	2	0.971	0	38.00	25.00	0.000	0	23.000	-8.0000	0.00
105	2	0.965	0	31.00	26.00	0.000	0	23.000	-8.0000	20.0
106	3	1.000	0	43.00	16.00	0.000	0	0.0000	0.0000	0.00
107	2	0.952	0	50.00	12.00	0.000	0	200.00	-200.00	6.00
108	3	1.000	0	2.000	1.000	0.000	0	0.0000	0.0000	0.00
109	3	1.000	0	8.000	3.000	0.000	0	0.0000	0.0000	0.00
110	2	0.973	0	39.00	30.00	0.000	0	23.000	-8.0000	6.00
111	2	0.980	0	0.000	0.000	36.00	0	1000.0	-100.00	0.00
112	2	0.975	0	68.00	13.00	0.000	0	1000.0	-100.00	0.00
113	2	0.993	0	6.000	0.000	0.000	0	200.00	-100.00	0.00
114	3	1.000	0	8.000	3.000	0.000	0	0.0000	0.0000	0.00
115	3	1.000	0	22.00	7.000	0.000	0	0.0000	0.0000	0.00
116	2	1.005	0	184.0	0.000	0.000	0	1000.0	-1000.0	0.00
117	3	1.000	0	20.00	8.000	0.000	0	0.0000	0.0000	0.00
118	3	1.000	0	33.00	15.00	0.000	0	0.0000	0.0000	0.00

TABLE B.4: Line Data of IEEE 118-bus Test System

From Bus	To Bus	Line Impedance		Half Line Charging Susceptance ($p.u.$)	Tap Ratio
		Resistance ($p.u.$)	Reactance ($p.u.$)		
1	2	0.03030	0.09990	0.01270	1.0000
1	3	0.01290	0.04240	0.00541	1.0000
4	5	0.00176	0.00798	0.00105	1.0000
3	5	0.02410	0.10800	0.01420	1.0000
5	6	0.01190	0.05400	0.00713	1.0000
6	7	0.00459	0.02080	0.00275	1.0000
8	9	0.00244	0.03050	0.58100	1.0000
8	5	0.00000	0.02670	0.00000	0.9850
9	10	0.00258	0.03220	0.61500	1.0000
4	11	0.02090	0.06880	0.00874	1.0000
5	11	0.02030	0.06820	0.00869	1.0000
11	12	0.00595	0.01960	0.00251	1.0000
2	12	0.01870	0.06160	0.00786	1.0000
3	12	0.04840	0.16000	0.02030	1.0000
7	12	0.00862	0.03400	0.00437	1.0000
11	13	0.02225	0.07310	0.00938	1.0000

Continued on next page...

Table B.4 – continued from previous page.

From Bus	To Bus	Line Impedance		Half Line Charging Susceptance ($p.u.$)	Tap Ratio
		Resistance ($p.u.$)	Reactance ($p.u.$)		
12	14	0.02150	0.07070	0.00908	1.0000
13	15	0.07440	0.24440	0.03134	1.0000
14	15	0.05950	0.19500	0.02510	1.0000
12	16	0.02120	0.08340	0.01070	1.0000
15	17	0.01320	0.04370	0.02220	1.0000
16	17	0.04540	0.18010	0.02330	1.0000
17	18	0.01230	0.05050	0.00649	1.0000
18	19	0.01119	0.04930	0.00571	1.0000
19	20	0.02520	0.11700	0.01490	1.0000
15	19	0.01200	0.03940	0.00505	1.0000
20	21	0.01830	0.08490	0.01080	1.0000
21	22	0.02090	0.09700	0.01230	1.0000
22	23	0.03420	0.15900	0.02020	1.0000
23	24	0.01350	0.04920	0.02490	1.0000
23	25	0.01560	0.08000	0.04320	1.0000
26	25	0.00000	0.03820	0.00000	0.9600
25	27	0.03180	0.16300	0.08820	1.0000
27	28	0.01913	0.08550	0.01080	1.0000
28	29	0.02370	0.09430	0.01190	1.0000
30	17	0.00000	0.03880	0.00000	0.9600
8	30	0.00431	0.05040	0.25700	1.0000
26	30	0.00799	0.08600	0.45400	1.0000
17	31	0.04740	0.15630	0.01995	1.0000
29	31	0.01080	0.03310	0.00415	1.0000
23	32	0.03170	0.11530	0.05865	1.0000
31	32	0.02980	0.09850	0.01255	1.0000
27	32	0.02290	0.07550	0.00963	1.0000
15	33	0.03800	0.12440	0.01597	1.0000
19	34	0.07520	0.24700	0.03160	1.0000
35	36	0.00224	0.01020	0.00134	1.0000
35	37	0.01100	0.04970	0.00659	1.0000
33	37	0.04150	0.14200	0.01830	1.0000
34	36	0.00871	0.02680	0.00284	1.0000
34	37	0.00256	0.00940	0.00492	1.0000
38	37	0.00000	0.03750	0.00000	0.9350
37	39	0.03210	0.10600	0.01350	1.0000
37	40	0.05930	0.16800	0.02100	1.0000
30	38	0.00464	0.05400	0.21100	1.0000
39	40	0.01840	0.06050	0.00776	1.0000
40	41	0.01450	0.04870	0.00611	1.0000
40	42	0.05550	0.18300	0.02330	1.0000
41	42	0.04100	0.13500	0.01720	1.0000
43	44	0.06080	0.24540	0.03034	1.0000
34	43	0.04130	0.16810	0.02113	1.0000
44	45	0.02240	0.09010	0.01120	1.0000
45	46	0.04000	0.13560	0.01660	1.0000
46	47	0.03800	0.12700	0.01580	1.0000
46	48	0.06010	0.18900	0.02360	1.0000
47	49	0.01910	0.06250	0.00802	1.0000
42	49	0.07150	0.32300	0.04300	1.0000
42	49	0.07150	0.32300	0.04300	1.0000
45	49	0.06840	0.18600	0.02220	1.0000
48	49	0.01790	0.05050	0.00629	1.0000
49	50	0.02670	0.07520	0.00937	1.0000
49	51	0.04860	0.13700	0.01710	1.0000
51	52	0.02030	0.05880	0.00698	1.0000
52	53	0.04050	0.16350	0.02029	1.0000
53	54	0.02630	0.12200	0.01550	1.0000
49	54	0.07300	0.28900	0.03690	1.0000
49	54	0.08690	0.29100	0.03650	1.0000
54	55	0.01690	0.07070	0.01010	1.0000
54	56	0.00275	0.00955	0.00366	1.0000
55	56	0.00488	0.01510	0.00187	1.0000
56	57	0.03430	0.09660	0.01210	1.0000
50	57	0.04740	0.13400	0.01660	1.0000
56	58	0.03430	0.09660	0.01210	1.0000

Continued on next page...

Table B.4 – continued from previous page.

From Bus	To Bus	Line Impedance		Half Line Charging Susceptance ($p.u.$)	Tap Ratio
		Resistance ($p.u.$)	Reactance ($p.u.$)		
51	58	0.02550	0.07190	0.00894	1.0000
54	59	0.05030	0.22930	0.02990	1.0000
56	59	0.08250	0.25100	0.02845	1.0000
56	59	0.08030	0.23900	0.02680	1.0000
55	59	0.04739	0.21580	0.02823	1.0000
59	60	0.03170	0.14500	0.01880	1.0000
59	61	0.03280	0.15000	0.01940	1.0000
60	61	0.00264	0.01350	0.00728	1.0000
60	62	0.01230	0.05610	0.00734	1.0000
61	62	0.00824	0.03760	0.00490	1.0000
63	59	0.00000	0.03860	0.00000	0.9600
63	64	0.00172	0.02000	0.10800	1.0000
64	61	0.00000	0.02680	0.00000	0.9850
38	65	0.00901	0.09860	0.52300	1.0000
64	65	0.00269	0.03020	0.19000	1.0000
49	66	0.01800	0.09190	0.01240	1.0000
49	66	0.01800	0.09190	0.01240	1.0000
62	66	0.04820	0.21800	0.02890	1.0000
62	67	0.02580	0.11700	0.01550	1.0000
65	66	0.00000	0.03700	0.00000	0.9350
66	67	0.02240	0.10150	0.01341	1.0000
65	68	0.00138	0.01600	0.31900	1.0000
47	69	0.08440	0.27780	0.03546	1.0000
49	69	0.09850	0.32400	0.04140	1.0000
68	69	0.00000	0.03700	0.00000	0.9350
69	70	0.03000	0.12700	0.06100	1.0000
24	70	0.00221	0.41150	0.05099	1.0000
70	71	0.00882	0.03550	0.00439	1.0000
24	72	0.04880	0.19600	0.02440	1.0000
71	72	0.04460	0.18000	0.02222	1.0000
71	73	0.00866	0.04540	0.00589	1.0000
70	74	0.04010	0.13230	0.01684	1.0000
70	75	0.04280	0.14100	0.01800	1.0000
69	75	0.04050	0.12200	0.06200	1.0000
74	75	0.01230	0.04060	0.00517	1.0000
76	77	0.04440	0.14800	0.01840	1.0000
69	77	0.03090	0.10100	0.05190	1.0000
75	77	0.06010	0.19990	0.02489	1.0000
77	78	0.00376	0.01240	0.00632	1.0000
78	79	0.00546	0.02440	0.00324	1.0000
77	80	0.01700	0.04850	0.02360	1.0000
77	80	0.02940	0.10500	0.01140	1.0000
79	80	0.01560	0.07040	0.00935	1.0000
68	81	0.00175	0.02020	0.40400	1.0000
81	80	0.00000	0.03700	0.00000	0.9350
77	82	0.02980	0.08530	0.04087	1.0000
82	83	0.01120	0.03665	0.01898	1.0000
83	84	0.06250	0.13200	0.01290	1.0000
83	85	0.04300	0.14800	0.01740	1.0000
84	85	0.03020	0.06410	0.00617	1.0000
85	86	0.03500	0.12300	0.01380	1.0000
86	87	0.02828	0.20740	0.02225	1.0000
85	88	0.02000	0.10200	0.01380	1.0000
85	89	0.02390	0.17300	0.02350	1.0000
88	89	0.01390	0.07120	0.00967	1.0000
89	90	0.05180	0.18800	0.02640	1.0000
89	90	0.02380	0.09970	0.05300	1.0000
90	91	0.02540	0.08360	0.01070	1.0000
89	92	0.00990	0.05050	0.02740	1.0000
89	92	0.03930	0.15810	0.02070	1.0000
91	92	0.03870	0.12720	0.01634	1.0000
92	93	0.02580	0.08480	0.01090	1.0000
92	94	0.04810	0.15800	0.02030	1.0000
93	94	0.02230	0.07320	0.00938	1.0000
94	95	0.01320	0.04340	0.00555	1.0000
80	96	0.03560	0.18200	0.02470	1.0000

Continued on next page...

Table B.4 – continued from previous page.

From Bus	To Bus	Line Impedance		Half Line Charging Susceptance ($p.u.$)	Tap Ratio
		Resistance ($p.u.$)	Reactance ($p.u.$)		
82	96	0.01620	0.05300	0.02720	1.0000
94	96	0.02690	0.08690	0.01150	1.0000
80	97	0.01830	0.09340	0.01270	1.0000
80	98	0.02380	0.10800	0.01430	1.0000
80	99	0.04540	0.20600	0.02730	1.0000
92	100	0.06480	0.29500	0.02360	1.0000
94	100	0.01780	0.05800	0.03020	1.0000
95	96	0.01710	0.05470	0.00737	1.0000
96	97	0.01730	0.08850	0.01200	1.0000
98	100	0.03970	0.17900	0.02380	1.0000
99	100	0.01800	0.08130	0.01080	1.0000
100	101	0.02770	0.12620	0.01640	1.0000
92	102	0.01230	0.05590	0.00732	1.0000
101	102	0.02460	0.11200	0.01470	1.0000
100	103	0.01600	0.05250	0.02680	1.0000
100	104	0.04510	0.20400	0.02705	1.0000
103	104	0.04660	0.15840	0.02035	1.0000
103	105	0.05350	0.16250	0.02040	1.0000
100	106	0.06050	0.22900	0.03100	1.0000
104	105	0.00994	0.03780	0.00493	1.0000
105	106	0.01400	0.05470	0.00717	1.0000
105	107	0.05300	0.18300	0.02360	1.0000
105	108	0.02610	0.07030	0.00922	1.0000
106	107	0.05300	0.18300	0.02360	1.0000
108	109	0.01050	0.02880	0.00380	1.0000
103	110	0.03906	0.18130	0.02305	1.0000
109	110	0.02780	0.07620	0.01010	1.0000
110	111	0.02200	0.07550	0.01000	1.0000
110	112	0.02470	0.06400	0.03100	1.0000
17	113	0.00913	0.03010	0.00384	1.0000
32	113	0.06150	0.20300	0.02590	1.0000
32	114	0.01350	0.06120	0.00814	1.0000
27	115	0.01640	0.07410	0.00986	1.0000
114	115	0.00230	0.01040	0.00138	1.0000
68	116	0.00034	0.00405	0.08200	1.0000
12	117	0.03290	0.14000	0.01790	1.0000
75	118	0.01450	0.04810	0.00599	1.0000
76	118	0.01640	0.05440	0.00678	1.0000

Bibliography

[1] P. Kundur, J. Paserba, V. Ajjarapu, G. Andersson, A. Bose, C. Canizares, N. Hatziargyriou, D. Hill, A. Stankovic, C. Taylor *et al.*, "Definition and classification of power system stability," *IEEE Transactions on Power Systems*, vol. 19, no. 2, pp. 1387–1401, 2004.

[2] C. W. Taylor, *Power system voltage stability*. McGraw-Hill, 1994, vol. 1.

[3] P. Kundur, *Power system stability and control*. McGraw-Hill, 1994, vol. 7.

[4] V. Ajjarapu, *Computational techniques for voltage stability assessment and control*. Springer Science and Business Media, 2007.

[5] E. W. Kimbark, *Power system stability*. John Wiley and Sons, 1995, vol. 1.

[6] V. A. Venikov, V. A. Stroev, V. I. Idelchick, and V. I. Tarasov, "Estimation of electrical power system steady-state stability in load flow calculations," *IEEE Transactions on Power Apparatus and Systems*, vol. 94, no. 3, pp. 1034–1041, 1975.

[7] J. A. Momoh, "A knowledge-based support system for voltage collapse detection and prevention," Electric Power Research Institute, Palo Alto, CA (USA); Howard University, Washington, DC (USA). Department of Electrical Engineering, Tech. Rep., 1991.

[8] S. Abe, Y. Fukunaga, A. Isono, and B. Kondo, "Power system voltage stability," *IEEE Transactions on Power Apparatus and Systems*, no. 10, pp. 3830–3840, 1982.

[9] V. Ajjarapu and C. Christy, "The continuation power flow: a tool for steady state voltage stability analysis," *IEEE Transactions on Power Systems*, vol. 7, no. 1, pp. 416–423, 1992.

[10] Y. H. Hong, C. T. Pan, and W. W. Lin, "Fast calculation of a voltage stability index of power systems," *IEEE Transactions on Power Systems*, vol. 12, no. 4, pp. 1555–1560, 1997.

[11] N. Amjady and M. H. Velayati, "Dynamic voltage stability prediction of power systems by a new feature selection technique and probabilistic neural network," *European Transactions on Electrical Power*, vol. 21, no. 1, pp. 312–328, 2011.

[12] D. Devaraj, J. Preetha-Roselyn, and R. Uma-Rani, "Artificial neural network model for voltage security based contingency ranking," *Applied Soft Computing*, vol. 7, pp. 722–727, 2007.

[13] C. Reis and F. P. M. Barbosa, "A comparison of voltage stability indices," in *IEEE Mediterranean Electrotechnical Conference, MELECON*. IEEE, 2006, pp. 1007–1010.

[14] R. B. Prada and J. D. Santos, "Load modelling in static voltage stability indices calculation," *European Transactions on Electrical Power*, vol. 9, no. 5, pp. 305–308, 1999.

[15] B. Wu, Y. Zhang, and M. J. Chen, "Probabilistic approach to voltage stability analysis with load uncertainty considered," *European Transactions on Electrical Power*, vol. 19, no. 2, pp. 209–224, 2009.

[16] B. Gao, G. K. Morison, and P. Kundur, "Voltage stability evaluation using modal analysis," *IEEE Transactions on Power Systems*, vol. 7, no. 4, pp. 1529–1542, 1992.

[17] P. A. Lof, T. Smed, G. Andersson, and D. J. Hill, "Fast calculation of a voltage stability index," *IEEE Transactions on Power Systems*, vol. 7, no. 1, pp. 54–64, 1992.

[18] F. W. Mohn and A. C. Z. D. Souza, "Tracing PV and QV curves with the help of a CRIC continuation method," *IEEE Transactions on Power Systems*, vol. 21, no. 3, pp. 1115–1122, 2006.

[19] P. Kessel and H. Glavitsch, "Estimating the voltage stability of a power system," *IEEE Transactions on Power Delivery*, vol. 1, no. 3, pp. 346–354, 1986.

[20] J. Hongjie, Y. Xiaodan, and Y. Yixin, "An improved voltage stability index and its application," *Electrical Power and Energy Systems*, vol. 27, p. 567–574, 2005.

[21] Y. Wang, W. Li, and J. Lu, "A new node voltage stability index based on local voltage phasors," *Electric Power Systems Research*, vol. 79, pp. 265–271, 2009.

[22] Y. Wang, C. Wang, F. Lin, W. Li, L. Y. Wang, and J. Zhao, "A new transfer impedance based system equivalent model for voltage stability analysis," *Electrical Power and Energy Systems*, vol. 62, pp. 38–44, 2014.

[23] T. Moger and T. Dhadbanjan, "A novel index for identification of weak nodes for reactive compensation to improve voltage stability," *IET- Generation, Transmission and Distribution*, vol. 9, no. 14, pp. 1826–1834, 2015.

[24] F. Gubina and B. Strmčnik, "Voltage collapse proximity index determination using voltage phasors approach," *IEEE Transactions on Power Systems*, vol. 10, no. 2, pp. 788–794, 1995.

[25] S. Perez-Londono, L. F. Rodriguez, and G. Olivar, "A simplified voltage stability index (SVSI)," *International Journal of Electrical Power & Energy Systems*, vol. 63, pp. 806–813, 2014.

[26] M. M. M. Kamel, A. A. Karrar, and A. H. Eltom, "Development and application of a new voltage stability index for on-line monitoring and shedding," *IEEE Transactions on Power Systems*, vol. 33, no. 2, pp. 1231–1241, 2017.

[27] G. B. Jasmon, L. H. Callistus, and C. Lee, "Prediction of voltage collapse in power systems using a reduced system model," in *International Conference on Control*. IET, 1991, pp. 32–36.

[28] M. Moghavvemi and F. M. Omar, "A line outage study for prediction of static voltage collapse," *IEEE Power Engineering Review*, vol. 18, no. 8, pp. 52–54, 1998.

[29] ——, "Technique for contingency monitoring and voltage collapse prediction," *IEE Proceedings-Generation Transmission Distribution*, vol. 145, no. 6, pp. 634–640, 1998.

[30] I. Musirin and T. K. A. Rahman, "Novel fast voltage stability index (FVSI) for voltage stability analysis in power transmission system," in *Student Conference on Research and Development.* IEEE, 2002, pp. 265–268.

[31] A. Mohamed, G. B. Jasmon, and S. Yusoff, "A static voltage collapse indicator using line stability factors," *Journal of Industrial Technology*, vol. 7, no. 1, pp. 73–85, 1989.

[32] A. Yazdanpanah-Goharrizi and R. Asghari, "A novel line stability index (NLSI) for voltage stability assessment of power systems," *WSEAS International Conference on Power Systems*, no. 15-17, pp. 164–167, 2007.

[33] M. Moghavvemi and O. Faruque, "Real-time contingency evaluation and ranking technique," *IEE Proceedings-Generation, Transmission and Distribution*, vol. 145, no. 5, pp. 517–524, 1998.

[34] R. Tiwari, K. R. Niazi, and V. Gupta, "Line collapse proximity index for prediction of voltage collapse in power systems," *International Journal of Electrical Power & Energy Systems*, vol. 41, no. 1, pp. 105–111, 2012.

[35] B. Venkatesh, R. Ranjan, and H. Gooi, "Optimal reconfiguration of radial distribution systems to maximize loadability," *IEEE Transactions on Power Systems*, vol. 19, no. 1, pp. 260–266, 2004.

[36] M. Moghavvemi and M. Faruque, "Technique for assessment of voltage stability in ill-conditioned radial distribution network," *IEEE Power Engineering Review*, vol. 21, no. 1, pp. 58–60, 2001.

[37] J. Yu, W. Li, and W. Yan, "Letter to the editor: a new line loadability index for radial distribution systems," *Electric Power Components and Systems*, vol. 36, no. 11, pp. 1245–1252, 2008.

[38] R. Ranjan and D. Das, "Voltage stability analysis of radial distribution networks," *Electric Power Components and Systems*, vol. 31, no. 5, pp. 501–511, 2003.

[39] L. Baozhu and L. Bolong, "A novel static voltage stability index based on equilibrium solution region of branch power flow," in *Third International Conference on Electric Utility Deregulation and Restructuring and Power Technologies, DRPT 2008.* IEEE, 2008, pp. 809–814.

[40] S. S. Halilčević and I. Softić, "The line and node voltage stability index presented through the porosity of high-voltage transmission lines," *Electric Power Components and Systems*, vol. 44, no. 16, pp. 1865–1876, 2016.

[41] I. Musirin and T. K. A. Rahman, "On-line voltage stability based contingency ranking using fast voltage stability index (FVSI)," *Proceedings IEEE/PES Transmission Distribution and Exhibition Conference*, pp. 1118–1123, 2002.

[42] A. M. Chebbo, M. R. Irving, and M. J. H. Sterling, "Voltage collapse proximity indicator: behaviour and implications," *IEE Proceedings-C (Generation, Transmission and Distribution)*, vol. 139, no. 3, pp. 241–252, 1992.

[43] N. G. Hingorani, L. Gyugyi, and M. El-Hawary, *Understanding FACTS: Concepts and Technology of Flexible AC Transmission Systems*. IEEE Press New York, 2000, vol. 1.

[44] A. Rajabi-Ghahnavieh, M. Fotuhi-Firuzabad, M. Shahidehpour, and R. Feuillet, "UPFC for enhancing power system reliability," *IEEE Transactions on Power Delivery*, vol. 25, no. 4, pp. 2881–2890, 2010.

[45] H. Cai, Z. Qu, and D. Gan, "Determination of the power transfer capacity of a UPFC with consideration of the system and equipment constraints and of installation locations," *IEE Proceedings- Generation, Transmission and Distribution*, vol. 149, no. 1, pp. 114–120, 2002.

[46] Z. Yuan, S. W. de Haan, J. B. Ferreira, and D. Cvoric, "A FACTS device: distributed power-flow controller (DPFC)," *IEEE Transactions on Power Electronics*, vol. 25, no. 10, pp. 2564–2572, 2010.

[47] X. P. Zhang, C. Rehtanz, and B. Pal, *Flexible AC Transmission Systems: modelling and control*. Springer Science & Business Media, 2012.

[48] K. K. Sen and M. L. Sen, "Comparison of the "SEN" transformer with the unified power flow controller," *IEEE Transactions on Power Delivery*, vol. 18, no. 4, pp. 1523–1533, 2003.

[49] S. Bhowmick, B. Das, and N. Kumar, "An indirect model of SSSC for reducing complexity of coding in Newton power flow algorithm," *Electric Power Systems Research*, vol. 77, no. 10, pp. 1432–1441, 2007.

[50] M. O. Faruque and V. Dinavahi, "A tap-changing algorithm for the implementation of "SEN" transformer," *IEEE Transactions on Power Delivery*, vol. 22, no. 3, pp. 1750–1757, 2007.

[51] B. Asghari, M. O. Faruque, and V. Dinavahi, "Detailed real-time transient model of the "SEN" transformer," *IEEE Transactions on Power Delivery*, vol. 23, no. 3, pp. 1513–1521, 2008.

[52] M. Noroozian, L. Ängquist, M. Ghandhari, and G. Andersson, "Use of UPFC for optimal power flow control," *IEEE Transactions on Power Delivery*, vol. 12, no. 4, pp. 1629–1634, 1997.

[53] A. Nabavi-Niaki and M. R. Iravani, "Steady-state and dynamic models of unified power flow controller (UPFC) for power system studies," *IEEE Transactions on Power Systems*, vol. 11, no. 4, pp. 1937–1943, 1996.

[54] D. J. Gotham and G. Heydt, "Power flow control and power flow studies for systems with FACTS devices," *IEEE Transactions on Power Systems*, vol. 13, no. 1, pp. 60–65, 1998.

[55] C. R. Fuerte-Esquivel and E. Acha, "Unified Power Flow Controller: a critical comparison of Newton-Raphson UPFC algorithms in power flow studies," in *IEE Proceedings- Generation, Transmission and Distribution*, vol. 144, no. 5. IET, 1997, pp. 437–444.

[56] A. J. F. Keri, A. S. Mehraban, X. Lombard, A. Eiriachy, and A. A. Edris, "Unified Power Flow Controller (UPFC): modeling and analysis," *IEEE Transactions on Power Delivery*, vol. 14, no. 2, pp. 648–654, 1999.

[57] C. R. Fuerte-Esquivel, E. Acha, and H. Ambriz-Perez, "A comprehensive Newton-Raphson UPFC model for the quadratic power flow solution of practical power networks," *IEEE Transactions on Power Systems*, vol. 15, no. 1, pp. 102–109, 2000.

[58] M. I. Alomoush, "Exact Pi-model of UPFC-inserted transmission lines in power flow studies," *IEEE Power Engineering Review*, vol. 22, no. 12, pp. 54–56, 2002.

[59] M. Zarghami and M. L. Crow, "The existence of multiple equilibria in the UPFC power injection model," *IEEE Transactions on Power Systems*, vol. 22, no. 4, pp. 2280–2282, 2007.

[60] G. Radman and R. S. Raje, "Power flow model/calculation for power systems with multiple FACTS controllers," *Electric Power Systems Research*, vol. 77, no. 12, pp. 1521–1531, 2007.

[61] S. Bhowmick, B. Das, and N. Kumar, "An indirect UPFC model to enhance reusability of Newton power-flow codes," *IEEE Transactions on Power Delivery*, vol. 23, no. 4, pp. 2079–2088, 2008.

[62] R. Tiwari, K. R. Niazi, and V. Gupta, "Variable series impedance model of a unified power flow controller for load flow analysis," *Electric Power Components and Systems*, vol. 40, no. 1, pp. 74–92, 2011.

[63] M. Pereira and L. C. Zanetta, "A current based model for load flow studies with UPFC," *IEEE Transactions on Power Systems*, vol. 28, no. 2, pp. 677–682, 2013.

[64] X. Wei, J. H. Chow, B. Fardanesh, and A. A. Edris, "A common modeling framework of voltage-sourced converters for load flow, sensitivity, and dispatch analysis," *IEEE Transactions on Power Systems*, vol. 19, no. 2, pp. 934–941, 2004.

[65] S. An, J. Condren, and T. W. Gedra, "An ideal transformer UPFC model, OPF first-order sensitivities, and application to screening for optimal UPFC locations," *IEEE Transactions on Power Systems*, vol. 22, no. 1, pp. 68–75, 2007.

[66] Y. Zhang, Y. Zhang, and C. Chen, "A novel power injection model of IPFC for power flow analysis inclusive of practical constraints," *IEEE Transactions on Power Systems*, vol. 21, no. 4, pp. 1550–1556, 2006.

[67] X. Jiang, X. Fang, J. H. Chow, A. A. Edris, E. Uzunovic, M. Parisi, and L. Hopkins, "A novel approach for modeling voltage-sourced converter-based FACTS controllers," *IEEE Transactions on Power Delivery*, vol. 23, no. 4, pp. 2591–2598, 2008.

[68] M. I. Alomoush, "Derivation of UPFC DC load flow model with examples of its use in restructured power systems," *IEEE Transactions on Power Systems*, vol. 18, no. 3, pp. 1173–1180, 2003.

[69] S. Yang, Y. Liu, X. Wang, D. Gunasekaran, U. Karki, and F. Z. Peng, "Modulation and control of transformerless UPFC," *IEEE Transactions on Power Electronics*, vol. 31, no. 2, pp. 1050–1063, 2016.

[70] K. K. Sen and M. L. Sen, "Introducing the family of "SEN" transformers: a set of power flow controlling transformers," *IEEE Transactions on Power Delivery*, vol. 18, no. 1, pp. 149–157, 2003.

[71] J. Yuan, L. Liu, W. Fei, L. Chen, B. Chen, and B. Chen, "Hybrid electromagnetic unified power flow controller: A novel flexible and effective approach to control power flow," *IEEE Transactions on Power Delivery*, 2016.

[72] K. K. Sen and E. J. Stacey, "UPFC-Unified Power Flow Controller: theory, modeling, and applications," *IEEE Transactions on Power Delivery*, vol. 13, no. 4, pp. 1453–1460, 1998.

[73] L. Wu, J. Qin, M. Saeedifard, O. Wasynczuk, and K. Shenai, "Efficiency evaluation of the modular multilevel converter based on Si and SiC switching devices for medium/high-voltage applications," *IEEE Transactions on Electron Devices*, vol. 62, no. 2, pp. 286–293, 2015.

[74] S. Madhusoodhanan, K. Mainali, A. K. Tripathi, A. Kadavelugu, D. Patel, and S. Bhattacharya, "Power loss analysis of medium-voltage three-phase converters using 15-kV/40-A SiC N-IGBT," *IEEE Journal of Emerging and Selected Topics in Power Electronics*, vol. 4, no. 3, pp. 902–917, 2016.

[75] P. Sauer, "Explicit load flow series and functions," *IEEE Transactions on Power Apparatus and Systems*, no. 8, pp. 3754–3763, 1981.

[76] H. Chen and L. Chung, "Load flow solution for ill-conditioned by homotopy continuation method," *International Journal of Power and Energy Systems*, vol. 28, no. 1, p. 99, 2008.

[77] A. Trias, "The holomorphic embedding load flow method," in *IEEE Power and Energy Society General Meeting*. IEEE, 2012, pp. 1–8.

[78] S. Rao, Y. Feng, D. J. Tylavsky, and M. K. Subramanian, "The holomorphic embedding method applied to the power-flow problem," *IEEE Transactions on Power Systems*, vol. 31, no. 5, pp. 3816–3828, 2016.

[79] S. D. Rao, D. J. Tylavsky, and Y. Feng, "Estimating the saddle-node bifurcation point of static power systems using the holomorphic embedding method," *International Journal of Electrical Power & Energy Systems*, vol. 84, pp. 1–12, 2017.

[80] M. K. Subramanian, Y. Feng, and D. Tylavsky, "PV bus modeling in a holomorphically embedded power-flow formulation," in *North American Power Symposium (NAPS)*. IEEE, 2013, pp. 1–6.

[81] M. K. Subramanian, "Application of holomorphic embedding to the power-flow problem," Master's thesis, Arizona State University, 2014.

[82] I. Wallace, D. Roberts, A. Grothey, and K. McKinnon, "Alternative PV bus modelling with the holomorphic embedding load flow method," *arXiv preprint arXiv:1607.00163*, 2016.

[83] B. Schmidt, "Implementation and evaluation of the holomorphic embedding load flow method," Master's thesis, Master Thesis, 2015.

[84] Y. Feng and D. Tylavsky, "A novel method to converge to the unstable equilibrium point for a two-bus system," in *North American Power Symposium (NAPS)*. IEEE, 2013, pp. 1–6.

[85] A. J. Sarnari and R. Živanović, "Robust Padé approximation for the holomorphic embedding load flow," in *Australasian Universities Power Engineering Conference (AUPEC)*. IEEE, 2016, pp. 1–6.

[86] B. Wang, C. Liu, and K. Sun, "Multi-stage holomorphic embedding method for calculating the power-voltage curve," *IEEE Transactions on Power Systems*, vol. 33, no. 1, pp. 1127–1129, 2018.

[87] S. S. Baghsorkhi and S. P. Suetin, "Embedding AC power flow with voltage control in the complex plane: The case of analytic continuation via Padé approximants," *arXiv preprint arXiv:1504.03249*, 2015.

[88] Y. Zhu and D. Tylavsky, "Bivariate holomorphic embedding applied to the power flow problem," in *North American Power Symposium (NAPS)*. IEEE, 2016, pp. 1–6.

[89] H. D. Chiang, T. Wang, and H. Sheng, "A novel fast and flexible holomorphic embedding method for power flow problems," *IEEE Transactions on Power Systems*, vol. 33, no. 3, pp. 2551–2562, 2018.

[90] C. Liu, B. Wang, F. Hu, K. Sun, and C. L. Bak, "Real-time voltage stability assessment for load areas based on the holomorphic embedding method," *arXiv preprint arXiv:1702.01464*, 2017.

[91] A. Trias and J. L. Marín, "The holomorphic embedding load flow method for DC power systems and nonlinear DC circuits," *IEEE Transactions on Circuits and Systems I: Regular Papers*, vol. 63, no. 2, pp. 322–333, 2016.

[92] M. B. Kejani and E. Gholipour, "Holomorphic embedding load-flow modeling of thyristor-based FACTS controllers," *IEEE Transactions on Power Systems*, vol. 32, no. 6, pp. 4871–4879, 2017.

[93] C. Liu, B. Wang, F. Hu, K. Sun, and C. L. Bak, "Online voltage stability assessment for load areas based on the holomorphic embedding method," *IEEE Transactions on Power Systems*, vol. 33, no. 4, pp. 3720–3734, 2018.

[94] P. Singh and R. Tiwari, "Amalgam power flow controller: A novel flexible, reliable, and cost-effective solution to control power flow," *IEEE Transactions on Power Systems*, vol. 33, no. 3, pp. 2842–2853, 2018.

[95] D. Varghese and V. Janamala, "Optimal location and parameters of GUPFC for transmission loss minimization using PSO algorithm," in *Innovations in Power and Advanced Computing Technologies (i-PACT)*. IEEE, 2017, pp. 1–6.

[96] G. Y. Yang, G. Hovland, R. Majumder, and Z. Y. Dong, "TCSC allocation based on line flow based equations via mixed-integer programming," *IEEE Transactions on Power Systems*, vol. 22, no. 4, pp. 2262–2269, 2007.

[97] A. Kapetanaki, V. Levi, M. Buhari, and J. A. Schachter, "Maximization of wind energy utilization through corrective scheduling and FACTS deployment," *IEEE Transactions on Power Systems*, vol. 32, no. 6, pp. 4764–4773, 2017.

[98] N. K. Sharma, A. Ghosh, and R. K. Varma, "A novel placement strategy for FACTS controllers," *IEEE Transactions on Power Delivery*, vol. 18, no. 3, pp. 982–987, 2003.

[99] Y. Mansour, W. Xu, F. Alvarado, and C. Rinzin, "SVC placement using critical modes of voltage instability," in *Conference Proceedings- Power Industry Computer Application Conference*. IEEE, 1993, pp. 131–137.

[100] X. Chen, N. Pahalawaththa, U. Annakkage, and C. Kumble, "Controlled series compensation for improving the stability of multi-machine power systems," *IEE Proceedings-Generation, Transmission and Distribution*, vol. 142, no. 4, pp. 361–366, 1995.

[101] E. Ghahremani and I. Kamwa, "Optimal placement of multiple-type FACTS devices to maximize power system loadability using a generic graphical user interface," *IEEE Transactions on Power Systems*, vol. 28, no. 2, pp. 764–778, 2013.

[102] N. Yorino, E. E. Araby, H. Sasaki, and S. Harada, "A new formulation for FACTS allocation for security enhancement against voltage collapse," *IEEE Transactions on Power Systems*, vol. 18, no. 1, pp. 3–10, 2003.

[103] S. Singh and A. David, "Congestion management by optimising FACTS device location," in *International Conference on Electric Utility Deregulation and Restructuring and Power Technologies, DRPT 2000*. IEEE, 2000, pp. 23–28.

[104] S. Gerbex, R. Cherkaoui, and A. J. Germond, "Optimal location of multi-type FACTS devices in a power system by means of genetic algorithms," *IEEE Transactions on Power Systems*, vol. 16, no. 3, pp. 537–544, 2001.

[105] S. Panda and N. P. Padhy, "Optimal location and controller design of STATCOM for power system stability improvement using PSO," *Journal of the Franklin Institute*, vol. 345, no. 2, pp. 166–181, 2008.

[106] C. Duan, W. Fang, L. Jiang, and S. Niu, "FACTS devices allocation via sparse optimization," *IEEE Transactions on Power Systems*, vol. 31, no. 2, pp. 1308–1319, 2016.

[107] S. Ranganathan, M. S. Kalavathi *et al.*, "Self-adaptive firefly algorithm based multi-objectives for multi-type FACTS placement," *IET Generation, Transmission and Distribution*, vol. 10, no. 11, pp. 2576–2584, 2016.

[108] L. Ippolito and P. Siano, "Selection of optimal number and location of thyristor-controlled phase shifters using genetic based algorithms," in *IEE Proceedings- Generation, Transmission and Distribution*, vol. 151, no. 5. IET, 2004, pp. 630–637.

[109] J. Hao, L. B. Shi, and C. Chen, "Optimising location of unified power flow controllers by means of improved evolutionary programming," in *IEE Proceedings- Generation, Transmission and Distribution*, vol. 151, no. 6. IET, 2004, pp. 705–712.

[110] C. M. Huang and Y. C. Huang, "Hybrid optimisation method for optimal power flow using flexible AC transmission system devices," *IET- Generation, Transmission and Distribution*, vol. 8, no. 12, pp. 2036–2045, 2014.

[111] J. S. R. Jang, C. T. Sun, and E. Mizutani, "Neuro-fuzzy and soft computing: a computational approach to learning and machine intelligence." Prentice-Hall, 1997.

[112] L. A. Zadeh, "Fuzzy sets," in *Fuzzy Sets, Fuzzy Logic, And Fuzzy Systems: Selected Papers by Lotfi A Zadeh*. World Scientific, 1996, pp. 394–432.

[113] D. H. A. Lee, "Voltage stability assessment using equivalent nodal analysis," *IEEE Transactions on Power Systems*, vol. 31, no. 1, pp. 454–463, 2016.

[114] R. Christie, "Power system test archive," *University of Washington*, 1999.

[115] "MATLAB Release 2010, The Mathworks Inc., Natick, Massachusetts, United States."

[116] C. Schauder and H. Mehta, "Vector analysis and control of advanced static VAR compensators," in *IEE Proceedings C-Generation, Transmission and Distribution*, vol. 140, no. 4. IET, 1993, pp. 299–306.

[117] Z. Yuan, "Distributed power flow controller," Ph.D. dissertation, 2010.

[118] A. Trias, "Fundamentals of the holomorphic embedding load-flow method," *arXiv preprint arXiv:1509.02421*, 2015.

[119] J. Nuttall, "The convergence of Padé approximants to functions with branch points," *Padé and Rational Approximation*, pp. 101–109, 2013.

[120] P. Gonnet, S. Guttel, and L. N. Trefethen, "Robust Padé approximation via SVD," *SIAM review*, vol. 55, no. 1, pp. 101–117, 2013.

[121] S. D. Rao, "Exploration of a scalable holomorphic embedding method formulation for power system analysis applications," Ph.D. dissertation, Arizona State University, 2017.

[122] X. P. Zhang, E. Handschin, and M. Yao, "Multi-control functional static synchronous compensator (STATCOM) in power system steady-state operations," *Electric Power Systems Research*, vol. 72, no. 3, pp. 269–278, 2004.

[123] S. Mirjalili, "SCA: A Sine Cosine Algorithm for solving optimization problems," *Knowledge-Based Systems*, vol. 96, pp. 120–133, 2016.

[124] R. S. Wibowo, N. Yorino, M. Eghbal, Y. Zoka, and Y. Sasaki, "FACTS devices allocation with control coordination considering congestion relief and voltage stability," *IEEE Transactions on Power Systems*, vol. 26, no. 4, pp. 2302–2310, 2011.

Publications

Following papers have been published/accepted/under review out of this thesis work.

International Journals

1. P. Singh and R. Tiwari, "STATCOM Model using Holomorphic Embedding", *IEEE Access*, vol. 7, pp. 33075-33086, 2019.
2. P. Singh and R. Tiwari, "Amalgam Power Flow Controller: A Novel Flexible, Reliable, and Cost-Effective Solution to Control Power Flow", *IEEE Transactions on Power Systems*, vol. 33, no. 3, pp. 2842-2853, May 2018.
3. P. Singh and R. Tiwari, "Distributed Parameter-based Voltage Stability Index for Identification of Critical Lines and Voltage Stability Margin in Power System", *Cogent Engineering, Taylor & Francis*, vol. 5, no. 1, pp. 1-20, 2018.
4. P. Singh, R. Tiwari, M. K. Shah, K. R. Niazi, N. K. Meena and S. Ratra, "Voltage Stability Index and APFC for Performance Improvement of Modern Power Systems with Intense Renewables", *The Journal of Engineering*, IET 2018.
5. P. Singh and R. Tiwari, "Extended Holomorphic Embedded Load-Flow and Voltage Stability Assessment of Power Systems", *Electric Power Systems Research*. (Under Review)

International Conferences

1. P. Singh and R. Tiwari, "Optimal Allocation of STATCOM using Improved Sine Cosine Optimization Algorithm," 8^{th} *IEEE India International Conference on Power Electronics (IICPE-2018).*
2. P. Singh, J. Singh and R. Tiwari, "Performance Evaluation and Quality Analysis of Line and Node based Voltage Stability Indices for the Determination of the Voltage Instability Point," *Intelligent Computing Techniques for Smart Energy Systems (ICTSES'18).*

Brief bio-data

Pradeep Singh received his Bachelor of Engineering degree (2009) in Electrical Engineering from Maharashi Dayanand University, Rohtak and his Master's degree in Power System (2013) from Rajasthan Technical University, Kota. Presently, he is a research scholar in the Department of Electrical Engineering, Malaviya National Institute of Technology Jaipur. His area of research includes assessment of voltage stability, FACTS devices and power-flow methods.